Table of Contents

List of Figures

List of Tables

List of Symbols and Abbreviations

θ	Contact angle (°)
γ_{SV}	Interfacial tension of the solid-vapor interface (mN/m)
γ_{LS}	Interfacial tension of the solid-liquid interface (mN/m)
γ_{LV}	Interfacial tension of the liquid-vapor interface (mN/m)
K	Penetration and spreading rate constant
PAH	Polycyclic aromatic hydrocarbon
V	Volume (cm^3)
I	Current (A)
D	Density (g/cm^3)
SEM	Scanning electron microscope
XPS	X-ray photoelectron spectroscopy
FT-IR	Fourier transform infrared spectroscopy
OM	Optical microscopy
TGA	Thermogravimetric analysis
GAD	Green anode density (g/cm^3)
BAD	Baked anode density (g/cm^3)
GER	Electrical resistivity of green anode (μΩm)
BER	Electrical resistivity of baked anode (μΩm)
QI	Quinoline insolubles (wt %)
TI	Toluene insolubles (wt %)
SP	Softening point (°C)
CV	Coking value (wt %)
Eb	Binding energy (eV)
SD	Standard deviation
Py	pyridine/imine
NR_3	amine
N+	ammonium

PR	pyrrole
Tv	Vibro-compaction time
S	Standard conditions

CHAPTER 1

INTRODUCTION

1.1 Background

The production of primary aluminum is carried out in electrolytic cells. Alumina (Al_2O_3) is dissolved in a bath of molten cryolite (Na_3AlF_6) at approximately 960 °C, and aluminum (produced through the electrolysis of alumina) is collected on the cathode surface placed at the bottom of the bath (Figure 1.1). Carbon anodes, immersed in the molten electrolyte, are used in the reduction process and thus are consumed during the electrolysis. The anodes need to be replaced approximately every 14-28 days depending on the anode quality, and the operation parameters of the cell [1]. This electrolytic process is represented by the following reaction (1-1):

$$2Al_2O_3 + 3C \rightarrow 4Al + 3\,CO_2 \qquad (1\text{-}1)$$

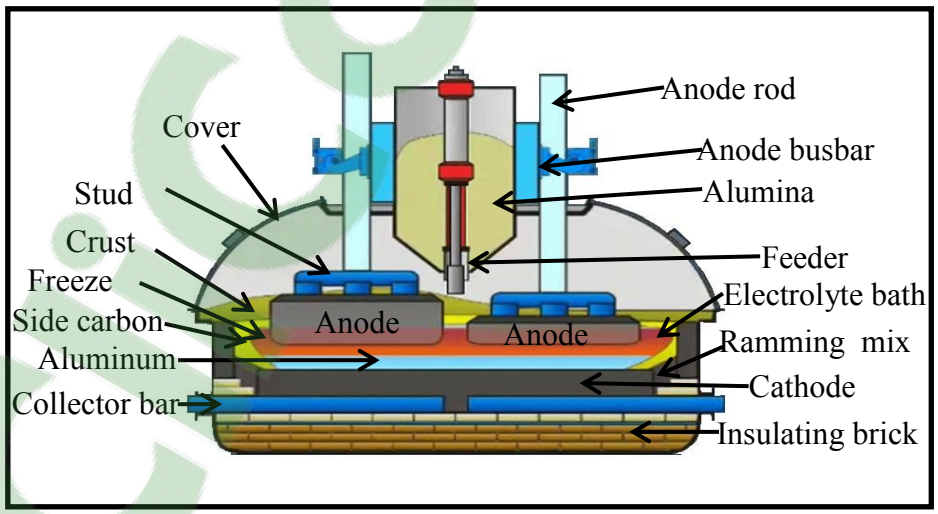

Figure 1.1: Schematic view of an electrolysis cell with prebaked anodes.

Prebaked carbon anodes consist of approximately 65 % petroleum coke, 20 % recycled anodes and butts (about 85 % dry aggregates), and 15 % coal tar pitch (binder) [1]. The production of anodes involves the mixing of raw materials, the compaction of the resulting paste, and the baking of green anodes to fabricate baked anodes with appropriate properties.

The carbon anode quality is a function of practical and economic constraints within a plant and is influenced by the quality of raw materials and the process conditions [1]. Variations in raw material properties pose a big challenge in controlling and improving the quality of anodes.

1.2 Statement of the Problem

Coal tar pitch is one of the raw materials for carbon anodes, and the pitch properties have an important influence on the anode properties [1]. Pitches may have significant differences in their chemical composition and physical properties depending on their origins. This, in turn, determines their behavior during pyrolysis (baking) and the characteristics of the resultant products [2]. The pitch properties used as indicators of pitch quality are: softening point, coking value, pitch density, C/H ratio, quinoline insolubles (QI), toluene insolubles (TI), viscosity, volatile content, and impurity content [1]. Moreover, the structure of carbonized coke and the interface between coke and pitch formed during anode manufacturing have a significant influence on the anode properties. Different pitches need to be analyzed, and the conditions that help produce better quality anodes have to be determined.

1.3 Objectives

The global objective is to study the effect of pitch properties on anode properties. It is difficult to estimate the anode quality without plant trial or an experimental study. The plant trials are costly and time consuming; thus, an experimental lab study is a viable option. In this project, tests with different pitches were carried out, and anodes made from these pitches were analyzed. This was complemented by the analysis of available industrial data.

There are three specific objectives of the project. The first objective is to identify the correlation between the wettability of a given coke by various pitches with different QI contents and to study the properties of the anodes made with these pitches. This study involved the investigation of a number of pitches and anodes made from them. The chemical and physical properties of different coal tar pitches were measured in order to study the effect of pitch properties on anode properties. Then, the relation between anode properties and pitch properties were studied in detail.

The second objective is to compare the differences in texture and topography of carbonized pitch as well as the interface between pitch and aggregate particles in anodes, which were produced in the laboratory using an anode recipe similar to those typically found in industry. Moreover, an attempt was made to relate the nature of the carbonized pitch with the characteristics of the pitch, especially with its QI content. Finally, the anode properties were correlated with the pitch properties. The conditions that give better quality anodes were determined.

The third objective is to determine the kinetics of devolatilization taking place during anode baking. Such results can be used to quantify the energy available from the volatiles and the rate of volatile release during baking in order to compare pitches with different properties and anodes produced with different pitch percentages, but baked under the same conditions.

1.4 Scope

The thesis contains five chapters and six appendixes. Chapter 1 introduces the general subject, the background, the statement of the problem, the objectives and the scope. Chapter 2 presents the previous works reported on anode technology focusing on the influence of pitch properties and the impact of the wettability of coke by pitch on the anode properties.

Chapter 3 provides information on the raw materials, the methodology, and the experimental systems used in this research. It also gives a description of the techniques used for the characterization of anode samples, e.g., Scanning Electron Microscope (SEM), Optical Microscope (OM), X-ray Photoelectron Spectroscopy (XPS), Fourier Transform Infrared (FT-IR) spectroscopy, etc.

Chapter 4 presents the results and discussion on the study of the effect of pitch properties on anode properties starting with the wettability of coke by various pitches. The investigation of the properties of laboratory anodes (density, air/CO_2 reactivity, and electrical resistivity) as well as some of the production parameters (pitch type, pitch content, and anode production conditions such as vibro-compaction time, kneading temperature, and pitch and/or coke preheating temperature) is presented which show the

relationship between pitch properties and carbon anode properties. Also, a new method for the etching of baked anodes has been developed in this study. In addition, the above work was complemented by the analysis of available industrial data.

Chapter 5 gives conclusions of the current study and recommendations for future work. Some details of the different parts of this study are given in the appendices.

CHAPTER 2

LITERATURE REVIEW

Carbon anodes for the production of aluminum are manufactured using coal tar pitch as binder and dry aggregates as the filler material. Pitch is present in the anode in the form of binder matrix [1]. Good binding between dry aggregates and pitch results in dense anodes, and thereby greatly affects the final anode properties [1]. Pitch properties have an influence on anode properties. Pitches may have significant differences in their chemical composition depending on their origin. This, in turn, determines their behavior during pyrolysis (baking) and the characteristics of the resultant products (baked anodes) [1]. The properties, which are used as indicators of pitch quality, are: softening point, coking value, density, C/H ratio, quinoline insolubles (QI), toluene insolubles (TI), viscosity, and impurity content [1]. The anode properties that define its quality are CO_2 and air reactivity, baked density, air permeability, mechanical strength, electrical resistivity, chemical purity, and thermal shock resistance. Most properties of pitch are interrelated [1, 3-7] and affect the properties of the anodes [1, 3, 4, 7-12]. Pitch properties QI and softening point as well as the wettability of coke by pitch are of great importance.

2.1 Pitch properties

Prebaked carbon anodes consist of petroleum coke, recycled butts, and coal tar pitch. The raw materials might have significantly different properties depending on their origin. It is important to identify the relationship between the properties of raw materials and carbon anodes. The role of binder pitch is to cover the coke particle surface, penetrate

into the pores, and fill the void space between the particles. Good wetting of coke by pitch helps coat and bind coke particles and penetrate into the pores. A good understanding of the raw material properties will help produce anodes of good quality (good physical, electrical, mechanical properties and good resistance to air and CO_2 reactivities) [1, 13].

Pitch quality is determined by its physical and chemical properties. The important properties of pitch as the binder in carbon anodes are: 1) strong bonding to aggregate; 2) satisfactory wetting characteristics; 3) high coking value yielding a strong coke structure; 4) low ash and sulphur; 5) less volatile emission during anode baking; and 6) formation of an oxidation resistant binder matrix [1].

Pitch is obtained as a residue during the distillation of coal tar in coke oven at 1100 °C. Coal tar is a by-product produced during the production of metallurgical coke. Pitch is a complex mixture of mainly polycyclic aromatic and heterocyclic compounds. Different functional groups could also be attached to the rings. The chemical compounds in pitch have a broad molecular weight distribution [1, 14]. Composition and properties of pitch are dependent on the processing conditions and the tar feedstock [1]. Coal tar pitch has more aromatic groups than aliphatic groups and the ratio of H_{ar}/H_{al} (aromatic hydrogen/aliphatic hydrogen) is greater than 3 [1]. Aliphatic functional groups usually exist as cyclic structure or attached as branches to the cyclic structure in coal tar pitch. For petroleum pitch, aliphatic chains predominantly exist. There is no PAH and no QI in petroleum pitch [1]. The viscosity of petroleum pitch changes less with temperature. The binding pitch used in the production of prebaked anodes is usually coal tar pitch.

The factors that influence the chemical and physical properties of coal tar pitch are: carbonization process of the parent coal (coal pyrolysis) and crude tar, tar characteristics and composition, tar distillation method, distillation efficiency, and additional treatment of pitch [1]. Pitch properties used as the indicators of pitch quality are softening point (SP), coking value (CV), pitch density and C/H ratio, quinoline insolubles (QI), toluene insolubles (TI), viscosity, impurity content, and wettability of pitch by coke [1]. A statistical analysis of the pitch properties was made to quantify the relationship between different pitch properties. No significant relationship was found between softening point and quinoline insoluble content, distillation conditions or sulfur content of the pitches. The properties of great importance for anode manufacturing are coking value, viscosity/softening point, and density [1]. The ranges of these properties generally used are summarized in Table 2.1. The data show that the typical pitch used around the year 2000 had a mean Mettler softening point of 112 °C and 10 % primary quinoline insolubles. Liquid pitch is usually added to the aggregate at a temperature around 190 °C (nearly 80 °C higher than the mean Mettler softening point). It was reported that just over one third of the plants used more than one pitch supplier [1].

Table 2.1: Pitch Specifications [1].

Variable	Min.	Max.	Mean
Mettler softening point (°C)	99	125	112
Primary QI content (%)	6	16.3	10
Liquid pitch addition temperature (°C)	160	220	190

2.1.1 Softening point (SP)

It was reported that, with increasing softening point, apparent density and crushing strength increase, and electrical resistivity and porosity decrease for the anode [8]. Pitch with a high softening point improved anode properties since its increased coking value results in denser anodes. The ability of a binder to retain a dense structure helps attain a high apparent density, and the development of continuous inter-particulate bridges contributes to low electrical resistivity [8]. It was also reported that, with increasing softening point, a decrease in baking loss was observed, resulting in an increase in baked apparent density [1]. Its higher coking value beneficially influences the anode quality. However, increasing softening point of pitch requires adjustment in anode production conditions [12]. Prebaked anodes are typically made using pitches with a Mettler softening point between 100 °C and 120 °C. The softening point-viscosity relationship is important for anode manufacturing. It was published in the literature that a higher softening point is accompanied by an increase in the aromaticity index, density, and coking value [1].

2.1.2 Coking value

One of the most important pitch properties for anode quality is the coking value [1]. A reasonable coking value is essential for pitch quality [1, 3]. Coking value is the residual carbon retained in the form of carbonized pitch after baking. Some of the pitch is lost during baking due to volatile release. It was shown that the coking value increases with increasing softening point. Pitch density as well as its QI content and aromaticity contribute to the coking value [1].

2.1.3 Pitch Density

It was reported that, with increasing pitch density, the anode properties such as apparent density and crushing strength increase, and electrical resistivity and porosity decrease [8]. A high pitch density yields better anode properties and accounts for better compressive strength for the manufacture of electrodes [8]. Pitch density can be an indicator of pitch coking value, and denser pitches have a higher coking value and aromaticity [1]. It has been reported that the quality of carbon anodes is related directly to the aromaticity of the binder pitch. The aromaticity of tars and pitches is closely related to the QI content [1]. Low aromaticity is associated with more rapid structural changes upon exposure to high temperatures [15]. Typical pitch density is 1.30-1.32 g/cm^3. Pitch aromaticity and carbon to hydrogen ratio increase with increasing pitch density.

2.1.4 Quinoline insolubles (QI)

Pitch can be characterised by its solubility in selected solvents such as quinoline, toluene, and benzene. Quinoline insolubles (QI) are the solid carbon particles remaining from pitch after its dissolution in quinoline [1].

Two types of quinoline insolubles exist: primary QI and secondary QI [1, 16, 17]. The primary QI particles which are formed in the coke oven can be beneficial for anode quality [1]. The primary QI [7] can be grouped as normal primary QI and carbon black/carry-over. The size of normal primary QI particles (Figure 2.1 (a)) is about 1µm. The size for carbon black particles (5-500 µm) (Figure 2.1 (c)) are larger because of the agglomeration of small particles. Limited quantity of primary QI in binder pitch increases bond strength and mechanical strength and protects the underlying filler from both air-burn

and CO_2 oxidation [18]. Large quantities of primary QI and carbon black can reduce the binding capacity of pitch. The absence of primary QI causes high anisotropy of the binder-coke bridges [1] and generates higher flow conditions which gives inferior strength [7]. Primary QI is necessary for optimized properties of binder pitch, a limited amount is necessary [7]. Secondary QI particles (Figure 2.1 (b)) are formed during the thermal treatment of pitch at a temperature greater than 400 °C. They are anisotropic and can be classified as mesophase (> 4 µm) and mesogens (2 - 4 µm). The size of secondary QI particles is greater than those of normal primary QI [19]. The C/H ratios of secondary QI (< 3) are less than those of primary QI (> 3.5) [1, 7]. A substantial proportion of mesophase (> 4 µm) blocks the micropores of coke and prevents binder pitch and fine particles infiltrating into the pores of the filler coke. This is detrimental to anode density and adversely affects the mechanical strength and reactivity [20].

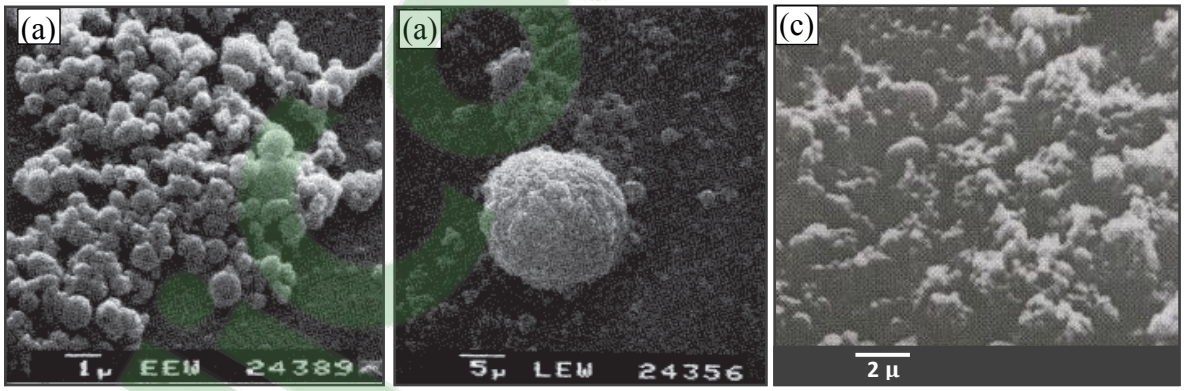

Figure 2.1: Quinoline insoluble components extracted from coal tar pitches: (a) Primary QI particles [7], (b) Secondary QI spheres [7], (c) Carbon black particles [16].

It has been shown that baked anode properties can deteriorate at very high and very low levels of QI [1]. There are differences of opinion among the researchers on the role of

QI. Some researchers reported that QI particles are not binding agents like pitch; but, they act as particulate filler material [1, 3]. Thus, part of pitch is used to wet the primary QI. Therefore, more pitch is necessary in the anode recipe when high QI pitches are used, and this leads to improved anode properties [8]. However, other researchers indicated that the primary QI prevents mesophase from coalescing during the baking of anodes, and thus promotes the formation of fine-mosaic texture in the carbon bridges, resulting in high mechanical strength and low oxidation reactivity [6, 35]. As the coking value of the QI content is higher than other compounds in the pitch [1, 3], the presence of QI influences the coking value and the pitch density. Pitches with high QI have higher coking values and higher densities than those with low QI [7]. High QI has no impact on air and CO_2 reactivities as long as the alkaline metal content in the anode is low [9].

There are conflicting results in the literature. Within the range of 0 % to 20 % of QI, some authors found that increasing QI increased the density [8, 21], mechanical strength [8, 9, 21-23], electrical resistivity [9, 21], air reactivity [17, 20] of anodes while others reported a decrease in density [7], mechanical strength [17], air permeability [24], electrical resistivity [8], porosity [8] or found no effect on the density [11, 17], mechanical strength [7], electrical resistivity [17], and oxidation reactivity [24, 25] of anodes.

It has been reported that the binder pitches containing 6-8.5 % QI can provide optimum wetting behavior, producing high-performance baked anodes [7]. However, it was reported by other researchers that the specimens which had the highest apparent density and crushing strength and the lowest electrical resistivity and total porosity were made with pitches which had more than 10 % QI [8]. It was also reported that the anode properties

were favorable at the QI levels less than 13 % [12]. Some researchers have shown that low primary QI pitches (1 % < QI content < 5 %) performed (resulted in anode properties) similar to the high primary QI pitches (5 % < QI content < 20 %) [7, 21, 24, 26]. Some studies showed that, by reducing the primary QI levels from greater than 10 % to less than 5 %, the anode mechanical properties (strength) were reduced, but still remained acceptable with decreasing primary QI until the minimum primary QI level was reached. Another author confirmed the minimum primary QI level of less than 2 %, but suggested further study. Below the minimum primary QI level, unacceptable anode properties were obtained [27]. Medium to high primary QI content correlates directly with superior anode quality. Nevertheless, low QI content pitches were also used successfully with appropriate process adaptations [11, 24].

As can be seen from the above summary, there is not an agreement in the literature on the optimum QI level of pitch required to have a good quality anode. This is probably due to the fact that it is not only the level of QI, but also the particle size of QI as well as the structure of coke used affect the anode properties. One objective of the current work is to study the correlation between the wettability of a given coke by various pitches with different QI contents and the properties of anodes made with these pitches.

2.1.5 Toluene insolubles (TI)

The toluene insolubles content influences the pitch binding ability. β-resins are the fraction obtained by the difference between the toluene insolubles and the quinoline insolubles (TI-QI), and this contributes to the coking value and the bond formation between the filler particles [4]. It is reported that increase in β-resin improves the aromaticity and

the coking value of pitch and can have some effect on its viscosity and wetting characteristics [5]. However, it is also reported that β-resins do not have a marked correlation with the anode properties (apparent density, crushing strength, electrical resistivity, porosity) [8].

2.1.6 Viscosity

The viscosity is an indicator of the pitch fluidity which is strongly dependent on temperature. It is measured in the range of 150 °C to 260 °C depending on the pitch softening point. Viscosity is analogous to softening point; a low viscosity pitch has a low softening point [3]. Viscosity of pitch decreases with increase in temperature and affects wetting [1].

2.1.7 Impurity content

The ash content is an indicator of the total impurities in a pitch. The sulfur content can be used to determine the sulfur emissions that may occur during anode baking or electrolysis [1]. Different impurities have a significant effect on anode reactivity. It was also found in the literature that sodium and calcium act as catalysts to accelerate the CO_2 reactivity whereas sulfur acts as an inhibitor. Impurities such as vanadium, nickel, and sodium have an impact on air reactivity [28].

2.2 Wettability of coke by pitch

Wettability of coke by pitch is one of the important parameters which determine the quality of binding between coke and pitch [29]. Low wettability of a pitch-coke system indicates that a poor bond formation is expected between the binder and the coke particles

after baking. This can result in a high electrical resistivity, poor mechanical properties, and high CO_2 reactivity [1].

Wetting can be physical due to intermolecular interactions (adhesive and cohesive forces) between solid (coke) and liquid (pitch) or can be chemical due to reactions at the solid-liquid interface. Since petroleum coke, anode butt, and coal tar pitch contain complimentary functional groups, there is a possibility that the functional groups on coke and butt surfaces interact with those present in pitch [14]. The interaction between coke and pitch depends on the properties of both pitch (i.e., chemical composition, surface tension, contact angle, viscosity, primary QI, mesophase content, etc.) and coke (i.e., particle size, structure, texture, surface roughness, chemical functional groups on the surface, porosity, etc.) [14, 30, 31]. Aggregate particles are held in place by bonds formed with pitch depending on pitch physical and chemical properties. Bonding quality also depends on shape, size, and chemical and structural properties of aggregate particles. Angular-shaped particles can stay in place and can adhere better to carbonised coke [32, 33]. The modification of pitch and/or coke may alter the coke wettability by pitch.

The degree of wettability of a solid by a liquid can be described in terms of the angle formed between them when they are brought into contact. The contact angle is a measure of the ability of a liquid to spread on the solid surface and penetrate through it if the solid is porous [14, 29, 30, 34-36]. It is reported in the literature that the sessile-drop technique, during which the change in contact angle with time is monitored under an inert gas atmosphere, can be used successfully for wettability studies [14, 29, 30, 34-36]. The contact angle is a function of temperature and decreases with increasing temperature above

the pitch softening point [1, 6]. The pitch softening point-viscosity relationship is important for anode manufacturing [1]. Viscosity is analogous to softening point, a low viscosity pitch has a low softening point [3]. The relatively high pitch viscosity prevents substantially its penetration into the pores of the larger aggregate fraction at lower mixing temperatures [1].

The wettability of coke by pitch is determined by measuring the contact angle of a pitch droplet on a solid coke bed surface [1] as mentioned above. The relationship between the interfacial tension and the contact angle for a liquid drop on a solid surface is expressed by Young's equation (Equation 2-1):

$$\gamma_{LV} \cos\theta = \gamma_{SV} - \gamma_{LS} \tag{2-1}$$

where γ_{SV} is the interfacial tension of the solid-vapor interface, γ_{LS} is the interfacial tension of the solid-liquid interface, γ_{LV} is the interfacial tension of the liquid-vapor interface, and θ is the contact angle. γ_{LV} is also known as the surface tension. These three phases meet at a point called the triple point. The force balance given by the Young equation at the triple point determines the wettability of solid phase by liquid phase in the presence of vapor phase. Figure 2.2 shows possible contact angles between a liquid pitch drop and a solid coke bed.

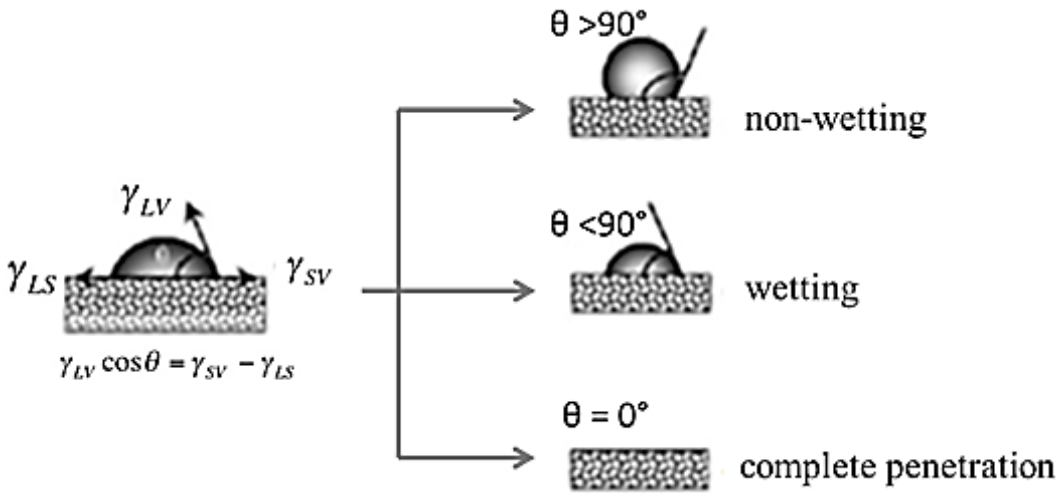

Figure 2.2: Contact angle for a pitch on a coke bed [37].

If θ > 90º, the liquid–solid system is non–wetting; if θ < 90º, the system is wetting.θ =0º indicates complete wetting (Figure 2.2).

In a wettability model, reported in the literature to describe the dynamic contact angle, a parameter (K) was introduced for measuring adhesive wettability [38], between a liquid and a solid [39, 40]. For an ideal liquid-solid system, the penetration and spreading rate depends on the contact angle at a particular time and can be expressed as:

$$\frac{d\theta}{dt} = -K\theta \qquad (2\text{-}2)$$

where K can be considered as the spreading and penetration constant, which represents how fast a liquid can spread on a solid surface and penetrate into the solid. A higher K value indicates that the contact angle reaches equilibrium more rapidly and the liquid spreads and penetrates into the solid faster [39, 40]. By knowing the K value, the interaction of solid with liquid can be quantified.

A term to limit the decrease of the contact angle is added to Equation (2-2) as follows [39, 40]:

$$\frac{d\theta}{dt} = -K\theta \times (1 - \frac{\theta_i - \theta}{\theta_i - \theta_e}) \quad (2\text{-}3)$$

where θ_i represents the initial contact angle, and θ_e represents the apparent equilibrium contact angle. When there is no equilibrium, a reference angle can be assigned for θ_e, which permits the relative comparison of different solid-liquid systems. Rearranging Equation (2-3), the following equation is obtained:

$$\frac{d\theta}{dt} = K\theta \times (\frac{\theta_e - \theta}{\theta_i - \theta_e}) \quad (2\text{-}4)$$

After integration, the equation can be expressed as:

$$\theta = \frac{\theta_i \theta_e}{\theta_i + (\theta_e - \theta_i)\exp[K(\frac{\theta_e}{\theta_e - \theta_i})t]} \quad (2\text{-}5)$$

K-value of the liquid-solid system can be determined by curve-fitting the experimental data to the equation below:

$$\frac{\theta_e - \theta_i}{\theta_e} \ln \frac{\theta - \theta_e}{\theta} = Kt - \frac{\theta_e - \theta_i}{\theta_e} \ln \frac{\theta_i - \theta_e}{\theta_i} \quad (2\text{-}6)$$

Equation (2-6) shows that if $[((\theta_e - \theta_i)/\theta_e) \ln((\theta - \theta_e)/\theta))]$ is plotted against t (time), the corresponding slope of the line will give the K-value. Equilibrium is not reached in all systems; and that is the case for the pitch-coke systems. In such cases, calculating the K values at a certain time and comparing them allow the evaluation of different pitch-coke systems on a relative basis. Thus, the equilibrium angle is replaced by a reference angle.

2.3 Anode properties

Two types of anodes (Soderberg and prebaked) are used in the electrolytic cells [1]. Raw material is continuously fed in Soderberg anodes, and it produces a lot of fume containing PAH (polycyclic aromatic hydrocarbons). Prebaked anodes need to be replaced at regular time intervals. The advantage of prebaked anodes is that they are compacted and it is easy to maintain their quality (compared to Soderberg anode). This leads to lower carbon consumption as well as makes it easier to control the fumes produced during the baking of anodes [1]. Due to technical and environmental reasons, prebaked anodes are commonly used in the aluminum reduction process, especially in modern smelters. High density and consistent quality anodes are important in the electrolytic process.

Anode quality is a function of a number of practical and economic constraints [1]. High-quality of carbon anodes have a significant impact on decreasing the aluminum production cost [1]. High resistance to oxidation minimises excess carbon consumption. High density and low permeability reduce anode consumption and dusting, and thereby increase the anode life in the cell. Sufficient mechanical strength contributes to structural integrity and makes the handling easier. Low electrical resistance results in less power consumption and improves energy efficiency and economy. High elemental purity helps avoid liquid aluminum contamination and excess anode consumption [1].

Anode fabrication comprises of the following production steps [1, 13]:

1) Raw material storage and handling: The dry aggregate (coke, butt, recycled anodes) is crushed, screened, and sized to prepare for subsequent processing steps.

2) Paste production (mixing of dry aggregate with pitch): The optimum amount of binder varies depending on process parameters, binder characteristics, aggregate surface area (available porosity and sizing), aggregate particle size distribution, and required paste density [1, 13].

Overpitching leads to large quantity of volatile release, and excess pitch may cause the anode to stick to the mould during compaction. High amount of pitch also results in anode slumping, extreme shrinkage, stub hole deformation, crack formation (due to volatile release), and sticking of packing material to the anodes during baking. Underpitching causes high anode porosity, poor mechanical properties, low apparent density, poor oxidation resistance, and high electrical resistivity [1, 13].

Mixing temperature of the aggregate and binder is usually between 150-180 °C because mixing is carried out at a temperature 50-60 °C higher than the softening point of the binder pitch to ensure that the pitch viscosity is sufficiently low for pitch to enter into the coke particle pores and voids by surface tension and capillary effects. This allows binder pitch to uniformly coat the aggregate particles giving a well-wetted paste for compaction. Preheating temperature for aggregate materials is usually 110-165 °C, which is higher than the binder pitch softening point to prevent the solidification of pitch. Insufficient preheating of the feed or insufficient mixing time can result in poor mixing leading to lower anode quality [1, 13]. Two different types of mixers are used: kneaders and batch mixers. Kneading is more intensive than batch mixing. The green density of the paste mixed with a kneader is higher than that prepared in a batch mixer (such as sigma

blade mixer). However, traditional batch mixers have more flexibility to increase the plant capacity as all that is necessary is to add an additional mixer [1, 13].

3) Paste compaction. There are two common methods for the forming of green anodes: pressing and vibratory compaction. Vibratory forming is more suitable for anodes exceeding ~ 700 kg, and as anodes are becoming larger and larger, this technique is being extensively used. Anode density gradients are reduced with vibratory forming. This helps increase the thermal shock (cracking) resistance of an anode [1, 13].

4) Anode baking. After compaction, the green anode is cooled and then baked to convert the binder pitch to carbonized pitch. During the baking process, the binder pitch undergoes pyrolysis, and subsequently, structural changes and polymerization take place forming a solid carbon composite [17, 18].

- 0-200 °C: thermal expansion, binder wets filler and penetrates into the coarse pores;
- 150-350 °C: redistribution of pitch into voids, further pitch impregnation into the aggregate;
- 350-450 °C: shrinkage, release of light pitch volatile;
- 450-600 °C: carbonization, formation of carbon bridge;
- 600-900 °C: release of low molecular weight volatiles due to the cracking of heavy molecules;
- 900-1200 °C: crystalline re-orientation, carbonized binder pitch and calcined aggregate materials stabilize during the soaking period.

During the anode baking process, the thermal decomposition of binder pitch results in the release of volatiles and the formation of carbonized pitch. Some reactions occur as follows [39]:

- Condensation reaction: two molecules or moieties (functional groups) combine to form a larger molecule, together with the loss of a small molecule (such as H_2O, HCl, amine ($-NH_2$)).
- Re-arrangement reaction: a substituent moves from one atom to another atom in the same molecule.
- Polymerization reaction: monomer molecules react to form large molecules (polymer chains).

The process of pitch carbonization is accompanied by marked chemical and physical changes in the binder phase. If the anode is heated rapidly, pores and cracks can form in anodes due to fast release of volatiles as well as pitch expansion and flow. High porosity decreases the density and increases the electrical resistivity of anodes. Consequently, control of heating rate, especially in the critical pitch devolatilization period, is important to prevent crack formation and mechanical problems in baked anodes [1, 13].

2.3.1 Density of anode

Typical industrial anodes have a green density (GAD) in the range of 1.55-1.65 g/cm^3, a baked density (BAD) between 1.50-1.60 g/cm^3, and a baking loss or volatile loss of around 4.5-6 % [1, 13].

Low baked density implies high porosity which leads to low mechanical strength, high elasticity, low thermal conductivity, and high permeability [1, 13]. It is well known that high gas permeability results in high anode consumption. Thus, high porosity increases the air and CO_2 reactivities and electrical resistivity [1, 13].

High baked density reduces air permeability and extends anode life [1, 13]. However, extremely high density leads to thermal shock problem. The baked density depends on the raw materials, aggregate granulometry, mixing and forming conditions, process parameters, and pitch content.

Anode quality improves when the baked anode density is high. However, too high a green density may result in excessive cracking during baking. Apparent density of anode samples (cores) were measured using the ASTM D5502-00 standard [41].

2.3.2 Electrical resistivity (ER) of anode

High electrical resistance brings about high power consumption and reduces efficiency and economy. Typical industrial anodes have electrical resistivities of 50-60 μΩm [1, 13]. The electrical resistivity of baked anodes is lower compared to that of green anodes. A decrease in electrical resistivity of a baked anode results in an increase in its thermal conductivity. However, high thermal conductivity increases the anode surface temperature in the cell, causing excess carbon consumption (air-burn, dust formation) [1, 13]. The electrical resistivity is related to both anode density and cracks in the anode. Denser green anodes have fewer cracks as they contain low porosity. However, excessively high green anode density can lead to crack formation during baking and increase the resistivity.

It is also possible that the following phenomena could occur. During baking, pressure of volatiles trapped in the anode results in cracking. The resulting baked anodes may have high density and cracks. Thus, denser baked anodes do not necessarily have fewer cracks and may have high electrical resistivity. The ASTM D6120-97 standard was used to measure the electrical resistivity of anode samples (cores) [42].

2.3.3 CO_2/air reactivity of anode

During the production of aluminium by the electrolytic reduction of alumina, carbon anodes are predominantly consumed according to Equation (1-1) [1, 13]. A certain quantity of CO is also produced when CO_2 further reacts with anode carbon; this increases anode consumption. Also, air diffuses through the alumina layer covering the top of the anode and reacts with the carbon anode; this is another cause of anode over-consumption. Excess carbon consumption occurs due to (a) air burn (air reactivity); (b) carboxy attack (CO_2 reactivity); and (c) dusting (selective oxidation). These are also grouped into chemical consumption and physical consumption. In chemical consumption, air and CO_2 react with the anode and carbon is consumed due to the reaction [1, 13]. For physical consumption, a part of the coke or pitch detaches from the anode and falls into the electrolytic cell. The inherent cause of physical consumption can be certain selective reactions of air/CO_2 with carbon in baked anodes due to their different degrees of interaction with carbonized pitch and coke. This reactivity imbalance between carbonized pitch and coke weakens the bond structure, and the physical loss of pitch and coke occurs. This process is called dusting.

Air reactivity of an anode depends on permeability and takes place at temperatures of 450-800 °C (temperature on the top of anode). It is reported that the air reactivity is

reduced with increasing calcination temperature of coke [43]. Reaction of oxygen on the anode surfaces exposed to air is called air burn:

$$O_2 + C \rightarrow CO_2 \text{ (favoured at lower temperatures)} \quad (2\text{-}7)$$

$$O_2 + 2C \rightarrow 2CO \text{ (favoured at higher temperatures)} \quad (2\text{-}8)$$

CO_2 reactivity is also permeability-dependent (permeability is intimately linked to porosity) and takes place at bath temperature (950-970 °C) [43]. Permeability is an index that indicates the ease with which a fluid flows through a porous solid [6]. Low baked density implies high porosity which leads to low mechanical strength, high elasticity, low thermal conductivity, and high permeability [1, 13]. This also explains the importance of porosity on the reactivities [1]. Reaction of CO_2 with the anode carbon (also called carboxy attack) is given by the following equation:

$$CO_2 + C \rightarrow 2CO \quad (2\text{-}9)$$

As a result, the excess consumption of carbon increases the cost of aluminum production as well as the CO_2 and CO (greenhouse gas) emissions. The excess consumption is also dependent on the chemical composition and the structure of raw materials used in anode production as well as the production parameters and the baking conditions of the anode [1, 13].

Figure 2.3 (a) shows the temperature distribution in a relatively new anode in the electrolysis cell and the regions where air and CO_2 reactions take place. The CO_2 reactivity is selective and reacts with carbon atoms in reactive sites [43]. The CO_2 bubbles produced during the reaction can increase the resistance between the anode and the electrolyte. Diffusion of the gas into the anode body can lead to internal reaction occurring in the pores.

Raw material properties, production process, pitch content, and baking parameters are the important factors that can have an influence on the gas permeability of the carbon anode; and this, in turn, has an impact on anode reactivity [1, 13]. Figure 2.3 (b) shows dust formation during air/CO_2 reactivity [43]. Sadler (1990) [1, 13] studied the subsurface carboxy reactivity and used macroscopic analysis of anode butts to confirm that internal attack is selective, preferentially attacking the regions of binder and coke fines (Figure 2.3 (b)) [1, 13].

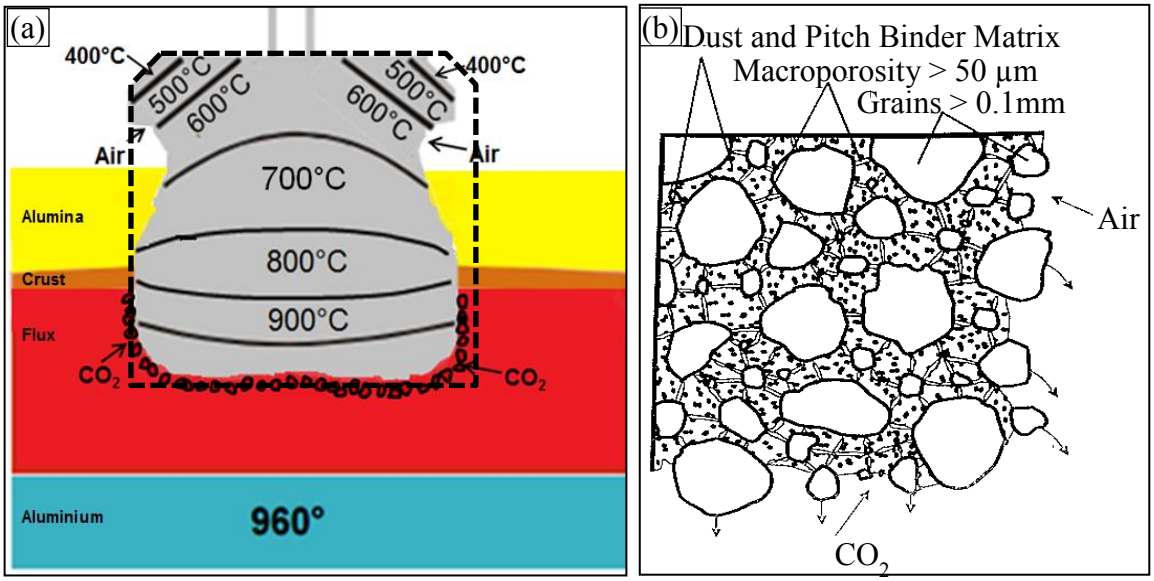

Figure 2.3: (a) Anode behavior in a reduction cell [1, 13], (b) Dust formation during air/CO_2 reactivity [43].

ASTM-D6558-00a [44] for CO_2 reactivity and ASTM-D6559-00a [45] for air reactivity are the standard test methods for baked carbon anode samples.

2.3.4 Kinetic analysis of anode baking

The green anodes are baked in the baking furnace with a certain heating rate up to about 1100-1200 °C. During baking, a part of binder pitch volatilizes, and the rest carbonizes forming a link between the dry aggregate particles (petroleum coke, recycled butts, and rejected green and baked anodes) [1, 13]. The volatiles released during baking provide a part of the energy required for anode baking in the furnace. The effects of baking conditions (heating rate, baking temperature, and soaking time) on some of the anode properties (air permeability, air and CO_2 reactivities) were studied, and the determination of the kinetic expressions for devolatilization were described [46, 47].

The source of pitch and the pitch content (percentage) have an impact on anode quality. Therefore, the study on the rate of volatile release is important. Also, pitch properties and pitch content leading to good anode quality for a given baking condition need to be determined. To our knowledge, there is no recent study on the measurement of devolatilization kinetics of green anodes with different pitches and different pitch contents. This study provides the kinetic data necessary to quantify the energy available from the volatiles and the rate of volatile release for pitches with different properties and different pitch contents under the same baking conditions.

2.3.5 Anode structure characterization

Some researchers showed that good quality carbon anodes are made from relatively anisotropic coke particles which give better anode strength and relatively isotropic carbonized pitch with low impurity since the mechanical strength of an anode is associated

with the presence of disordered texture of carbonized pitch [25, 33]. A controlled degree of disorder and relatively isotropic carbonized pitch seems to give better anode properties.

Carbonized pitch can have two types of structure: anisotropic and isotropic. Structure of carbonized pitch depends on binder pitch composition and how the pitch is pyrolyzed. It was reported that disordered (up to a certain extent) carbonized pitch produces stronger carbonized pitch matrix with more opportunity for chemical bonding with coke particles in addition to physical bonding. Moreover, disordered carbonized pitch has less open porosity which helps protect underlying aggregate materials from air/CO_2 oxidation better than ordered carbonized pitch [48, 49].

Coke has a wide variety of microstructures, which can be grouped into anisotropic, isotropic, and amorphous [50]. The structure of coke affects the anode mechanical properties. Anisotropic (e.g., streak coke) coke is softer and can be graphitized easily (Figure 2.4 (a)). However, isotropic or amorphous (e.g., spherulitic coke) coke is relatively more difficult to graphitize or not graphitizable at all (Figure 2.4 (b), has a high coefficient of thermal expansion, is more susceptible to cracking due to thermal shock, and has a detrimental influence on anode thermo-mechanical properties [30, 31].

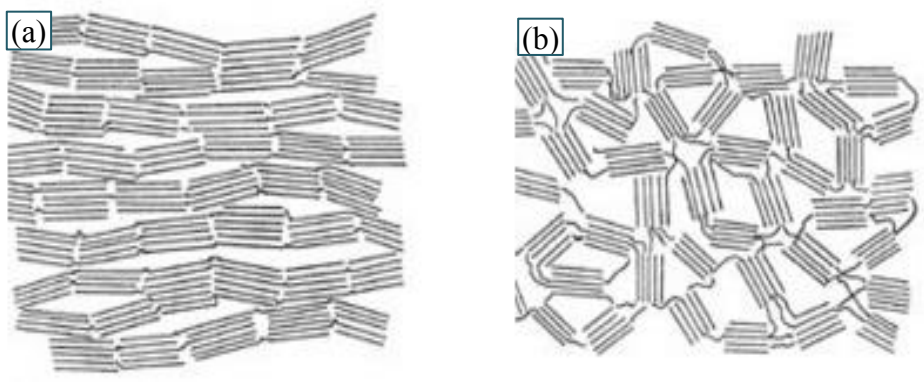

Figure 2.4: Coke structures:(a) Anisotropic, graphitizable, (b) Isotropic, non-graphitizable.

Different authors studied the structures of coke and/or pitch using the scanning electron microscopy (SEM) and optical microscopy (OM) techniques. They found that the variations in composition as well as the physical properties of coke and pitch are accompanied by differences in their microstructures [14, 16, 30, 34-36, 51]. Moreover, during the heating process, pitch undergoes pyrolysis; the thermal decomposition of pitch results in the release of volatiles and the formation of carbonized pitch. Changes in the operational conditions during pitch carbonization (baking) also generate differences in the structure of the resultant carbon material [52].

The structure of carbonized pitch and the interface between coke and pitch formed in the anode manufactured have a significant influence on the anode properties. It is known that pitch quantity and its distribution in an anode are two of the key factors which control the anode properties such as density, electrical resistivity, permeability, and CO_2/air reactivities [53, 54].

A number of studies have been reported in the literature on the characterization of carbonized pitch, cokes, and carbon surfaces using optical microscopy (OM) and

SEM [16, 25, 34, 51, 54, 55]. The proportions of the various textural components were determined by applying a point-counting technique using the SEM images of the etched surfaces, and the mechanical properties of the carbon anodes were correlated with the textural composition of binder pitch [34, 51]. Hays et al. [51] fabricated baked laboratory carbon anodes using fine petroleum coke (+75-150 µm) as aggregate and four coal tar pitches with different types of QI as binder. However, they did not study the commercial carbon anodes which contain approximately 65 % petroleum coke, 20 % recycled anode and butt particles with a wide range of size distribution. One of the objectives of the current work was to compare the differences in the texture and topography of carbonized pitch as well as the interface between pitch and particles in anodes which were produced in the laboratory using an anode recipe similar to that of industry. Moreover, a further attempt was made to relate the nature of the carbonized pitch with the characteristics of the pitch and especially its QI content.

Due to the similar hardness and compositions of coke and carbonized pitch present in baked anodes, it is difficult to identify them and their interface after polishing the surface of a baked anode sample. It was reported that the structure within the texture can be studied by creating a topography using various etchants (e.g. etching the surfaces with atomic oxygen and chromic acid), as the preferential reaction with carbon materials is different depending on different etchants [55]. The etchant preferentially attacks the carbonized pitch without significantly affecting the coke. This way, carbonized pitch could be distinguished from the other carbon particles (coke, butt, etc.). The carbonized pitch has three textural components: lamellar, intermediate, and granular (Figure 2.5). The textural composition of

the carbonized pitch is dependent on the character of the pitch and the type of QI components present [16, 51]. It was reported that primary QI and carbon black reduce lamellar and intermediate textures. Granular structure can be associated with primary QI and carbon black. However, if the granular structure is coarse, it is more related to primary QI. A small amount of primary QI produces intermediate texture. Chromic acid is toxic and carcinogenic. For this reason, chromic acid oxidation is not preferable for use in the laboratory and in the plant. A new method for etching the anodes was developed during this research work and is explained in the methodology section.

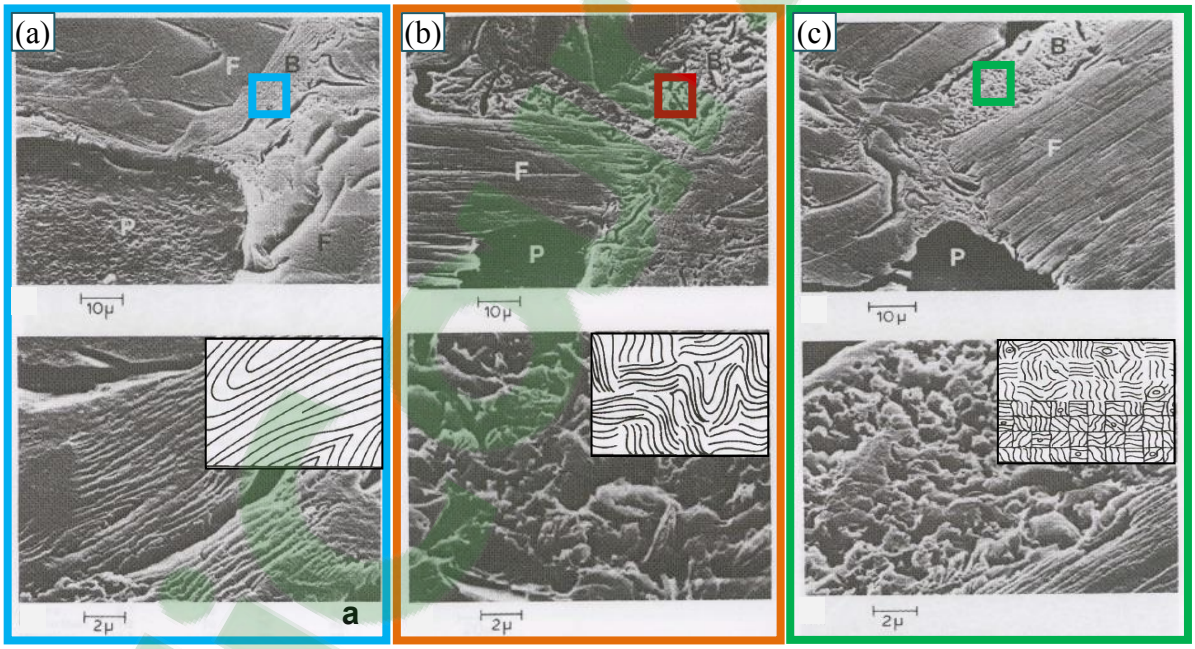

Figure 2.5: Scanning electron micrographs showing the three components of carbonized pitch: (a) Lamellar, (b) Intermediate, and (c) Granular. (F: coke particle, P: pore, B: carbonized pitch).

CHAPTER 3

EXPERIMENTAL

Different pitches were examined to understand the relationship between pitch properties and carbon anode properties. A methodology to study the effect of pitch properties on anode properties is illustrated in the Figure 3.1.

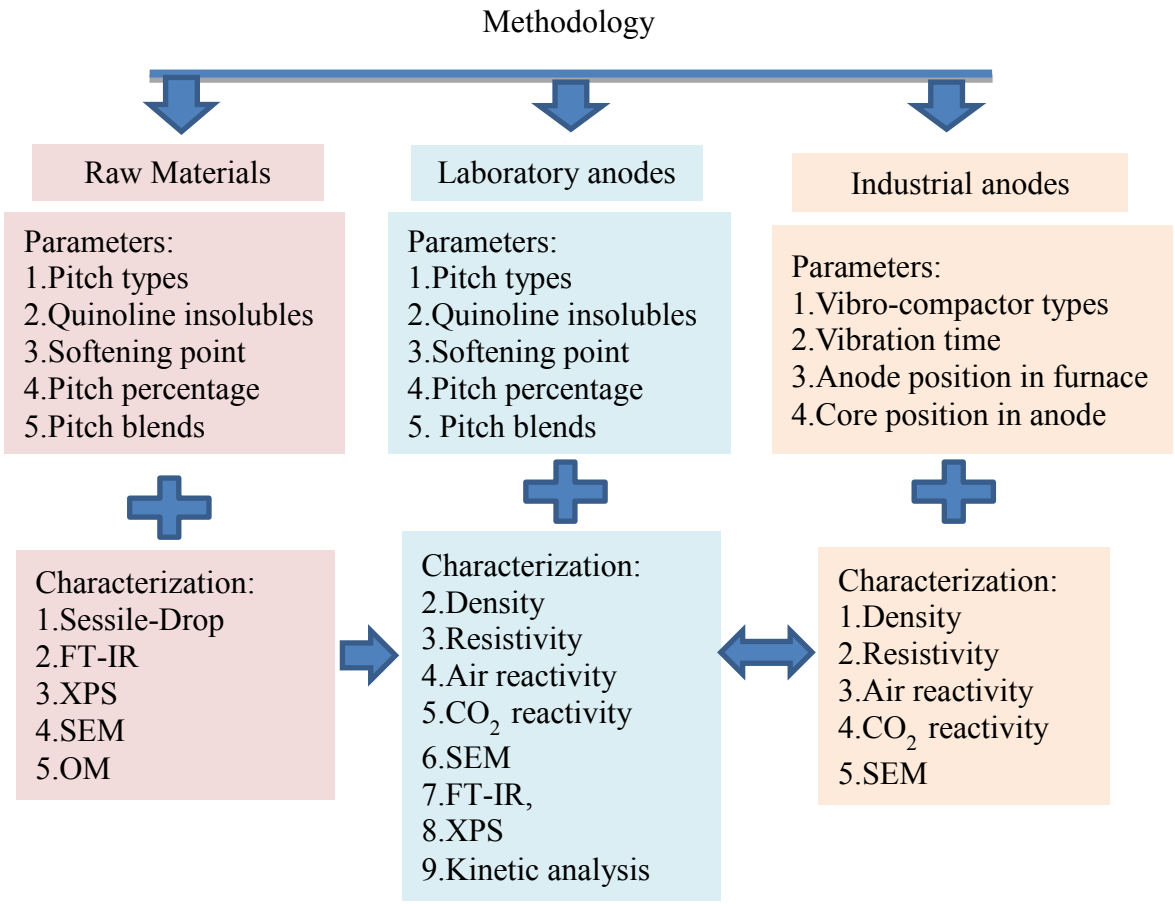

Figure 3.1: Methodology to study the effect of pitch properties on anode properties.

3.1 Raw materials

3.1.1 Properties of raw materials used to produce anodes in the laboratory (UQAC)

The wettability of coke by pitch was determined using a sessile-drop system (see Section 3.3.1) at 170 °C. Six coal-tar pitches with different properties and one petroleum coke were used in this study. Table 3.1 summarizes the properties of the pitches as well as the coke. Two types of coke samples were prepared from the same coke using two different sample preparation methods (Figure 3.2). One of them was directly sieved, and -125+100 µm particles were collected. This coke is identified as "as received". For the second coke sample, the coke particles were crushed in a hammer mill. Then, the crushed coke particles were sieved, and -125+100 µm fraction was collected. This coke is identified as "crushed coke". The coke samples were sieved for 2 minutes with the 125 µm sieve to remove the larger particles and for 4 minutes with the 100 µm sieve to remove the smaller particles.

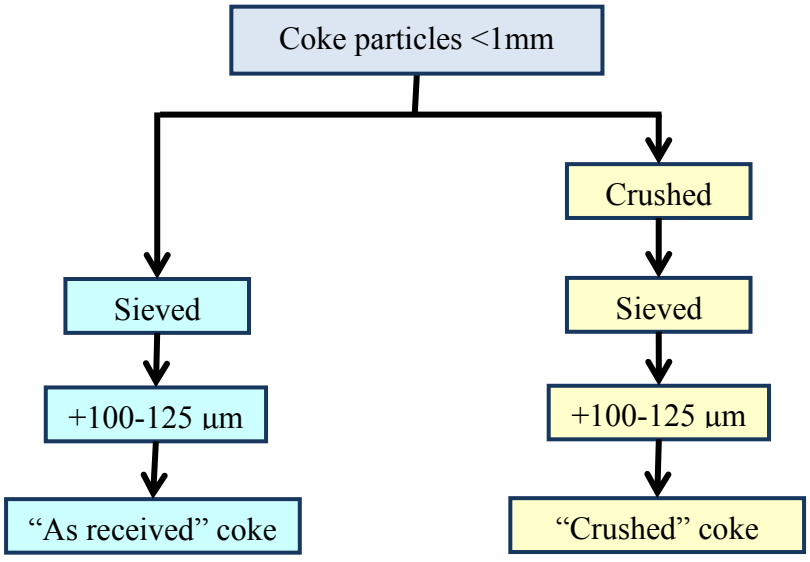

Figure 3.2: Preparation of coke samples for wettability tests by two different techniques.

Wetting tests were performed with the pitches with different QI contents and their blends using the sessile-drop technique. The effect of coke particle size on the wettability of pitch-coke system was also studied. The analysis of the pitch drops that formed on the coke beds during the wettability tests were carried out with OM and SEM to investigate the pitch-coke interface. A wetting test was performed for a pitch with a higher softening point as well. The test temperature was selected as 180 °C based on the softening point. Pitch blends used for wetting tests are discussed in Section 3.2.1.1.

Each wetting experiment was repeated twice, and the contact angle was taken as the average of these two results. If the contact angle at a particular time varied by more than 5º, then the test was repeated. After the experiments, the pitch-coke drops were cut vertically and studied with an optical microscope. Different pitches were also analyzed with FT-IR and XPS.

Table 3.1: Properties of the coal tar pitches and the calcined petroleum coke.

Pitch type	Atomic percentages (%)				SP*	QI*	TI*	Beta resin*	CV*
	C	O	N	S					
Pitch-1	96.6	1.9	1.2	0.3	118.4	3.4	25.9	22.5	58.9
Pitch-2	96.9	1.7	1.1	0.2	119.6	6.9	29.1	22.2	59.1
Pitch-3	97.9	1.0	0.7	0.3	118.0	10.8	33.0	22.2	61.2
Pitch-4	98.1	1.2	0.5	0.2	121.5	7.5	29.6	22.1	59.9
Pitch-5	97.6	1.2	0.9	0.3	119.4	5.1	28.0	22.9	59.6
Pitch-6	97.2	1.6	1.0	0.3	129.6	4.1	27.9	23.8	62.3
Coke	95.9	2.5	0.6	1.0	-	-	-	-	-

*SP: Softening point (°C) (Mettler), QI:Quinoline insolubles (wt %), TI: Toluene insolubles (wt %), Beta resin = TI – Q.I (wt %), CV: Coking value (wt %) (Alcan).

3.1.2 Analysis of industrial anode samples

The industrial anode samples were taken from four industrial green anodes produced using four different vibro-compactors (Vibro-A, Vibro-B, Vibro-C and Vibro-D) in 2011. Their fabrication parameters were the same. Cylindrical cores of 50 mm diameter were taken from the same positions of the four anodes (Figure 3.3). From the top of the anode, cylindrical samples of 50 mm height were cut for air reactivity tests. From the bottom of the anodes, cylindrical samples of 50 mm height were cut for CO_2 reactivity tests. These cores were baked in the baking furnace at UQAC laboratory under standard baking conditions. The identification of the samples for air and CO_2 reactivities are shown in Table 3.2.

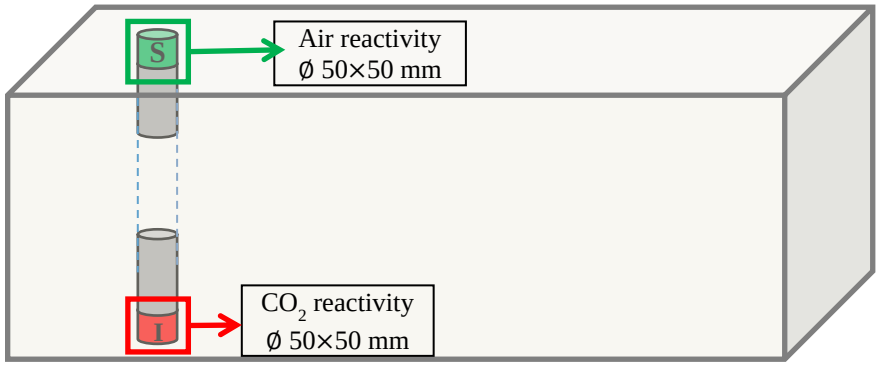

Figure 3.3: Position of samples in four industrial anodes for air reactivity and CO_2 reactivity tests.

Table 3.2: Identification of samples used for air and CO_2 reactivity tests.

	Vibro-A	Vibro-B	Vibro-C	Vibro-D
Samples for air reactivity	S-1	S-2	S-3	S-4
Samples for CO_2 reactivity	I-1	I-2	I-3	I-4

Later in 2013, five industrial anodes (Anode-18, Anode-27, Anode-28, Anode-31, and Anode-32) were fabricated under controlled conditions, and the anodes were baked in the industrial baking furnace (Tv s vibro-compacted anodes in one pit and Tv+7 s vibro-compacted anodes in another pit). The fabrication parameters for the five anodes are given in Table 3.3. The positions in the pit of the baking furnace can be seen in Figure 3.4.

Table 3.3: Fabrication parameters for the five anodes.

Anode no.	Vibro-compactor	Vibration time	Position in the pit*
18	D	Tv s	R1-C1
27	C	Tv+7 s	R1-C3
28	C	Tv+7 s	R3-C3
31	D	Tv+7 s	R1-C1
32	D	Tv+7 s	R2-C2

Tv s represents the standard vibration time, Tv+7 s indicates a 7 s longer vibration time than the standard one.

*R represents row and C represents column in the pit (Figure 3.4).

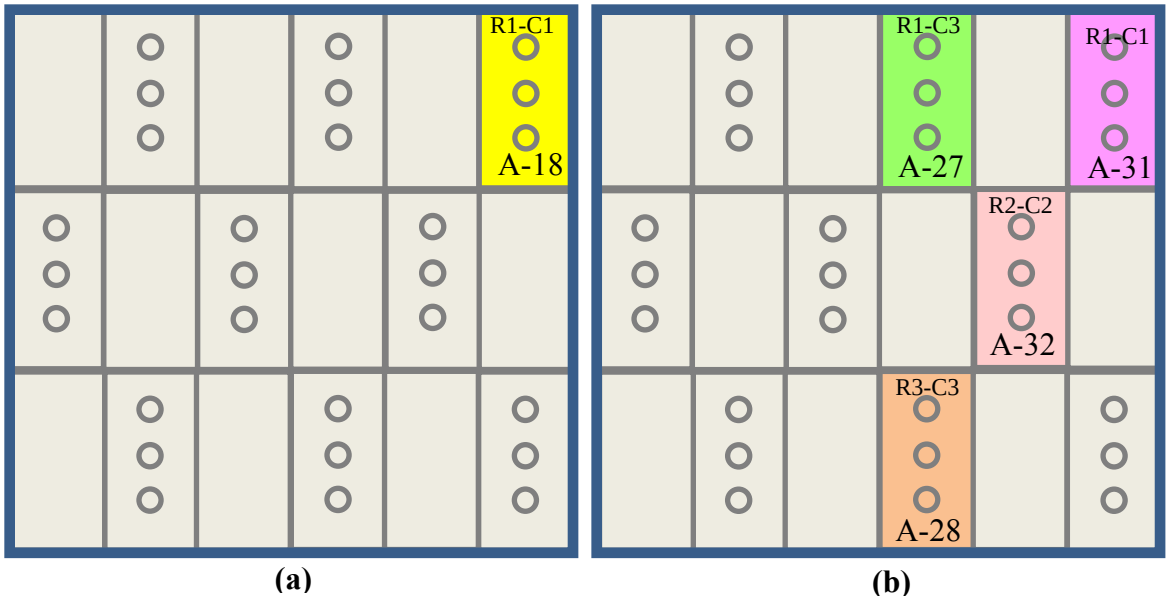

Figure 3.4: Anode positions in the pit (a) Anodes with vibro-compaction time Tv s, (b) Anodes with vibro-compaction time Tv+7 s.

The anodes were cored (cylindrical samples of 50 mm diameter) along the anode height at 25 different positions (Figure 3.5 (a)). Cylindrical samples of 50 mm height cut from the top of the cores 11 and 25 (Figure 3.5 (b)) were used for air reactivity tests. Cylindrical samples of 50 mm height cut from the bottom of the cores 12 and 24 (Figure 3.5 (c)) were used for CO_2 reactivity tests.

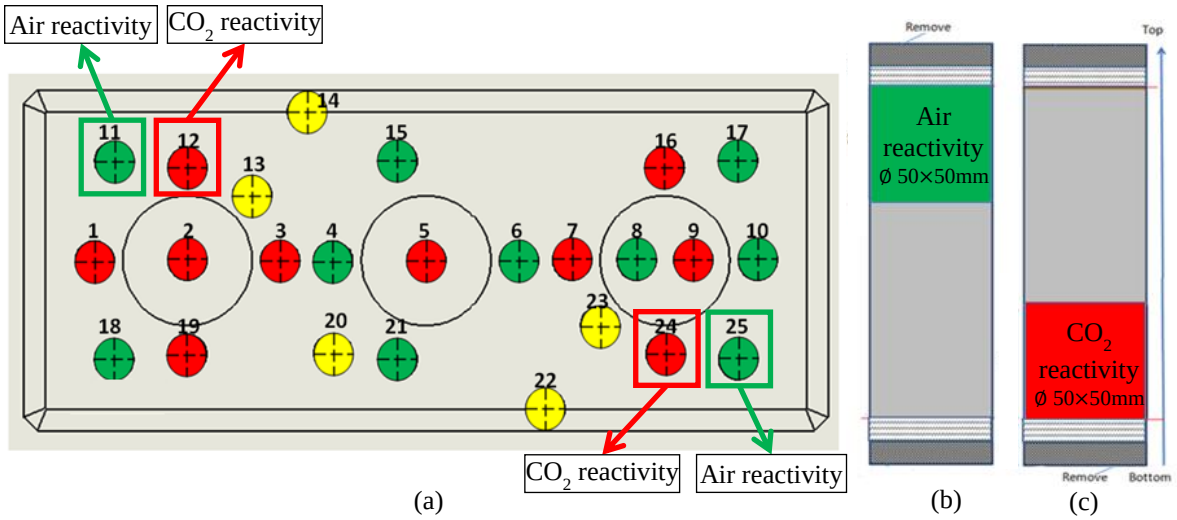

Figure 3.5: (a) Position of the cores in anode, (b) Position of samples in an anode core used for air reactivity test, (c) Position of samples in an anode core used for CO_2 reactivity test.

3.2 Experiments

3.2.1 Wetting tests

3.2.1.1 Wetting tests with different pitches and their blends

In this study, the six coal tar pitches with different properties were grounded to fine particles using a ceramic mortar and pestle. Grinding was done manually. The blends of different pitches were produced by mixing the corresponding pitches in different percentages, and the mixture was kept in the furnace at 170 °C for 10 min to get the final blend. The preparation of the blends was carried out under nitrogen atmosphere to protect the pitch from oxidation. Table 3.4 shows the pitches and their blends used for the wetting tests.

Table 3.4: Pitch blends used for the wetting tests.

Blend No.	1	2	3	4	5	6	7	8	9	10	11	12	13	14	15	16
Pitch-1 (%)	25	75	-	-	-	-	-	-	-	-	-	-	25	75	-	-
Pitch-2 (%)	75	25	75	25	75	25	75	25	75	25	-	-	-	-	-	-
Pitch-3 (%)	-	-	25	75	-	-	-	-	-	-	25	75	75	25	75	25
Pitch-4 (%)	-	-	-	-	25	75	-	-	-	-	-	-	-	-	-	-
Pitch-5 (%)	-	-	-	-	-	-	25	75	-	-	-	-	-	-	25	75
Pitch-6 (%)	-	-	-	-	-	-	-	-	25	75	75	25	-	-	-	-

3.2.1.2 Wetting test with the higher softening-point pitch at higher temperature

In this part, the interaction between the higher softening point pitch and the calcined petroleum coke (-125+100 μm; as received) was studied using the sessile-drop system (see Section 3.3.1) at 180 °C. Pitch-6 (higher softening point pitch), Pitch-2 and their two blends (25 % Pitch-6 and 75 % Pitch-2; 75 % Pitch-6 and 25 % Pitch-2) were tested.

3.2.1.3 Wetting tests using two different coke preparation techniques

Five coal-tar pitches (Pitch-1, Pitch-2, Pitch-3, Pitch-4, and Pitch-5) and the calcined petroleum coke given in Table 3.1 were used in this study. The coke samples were prepared with the two different techniques as explained in Section 3.1.1, and their structure was studied using SEM. The “as received” coke samples and the “crushed” coke samples were uniformly dispersed on a conductive tape on a specimen plate and vacuum-dried for one day at room temperature prior to the SEM analysis (Figure 3.6 (a)). The SEM analysis was done using JEOL-JSM-6480LV with secondary electron scattering, using an accelerating voltage of 20 kV. Also, the sessile-drops were cut vertically after the wetting

experiments and analyzed by the optical microscopy to understand the wetting mechanism (Figure 3.6 (b)).

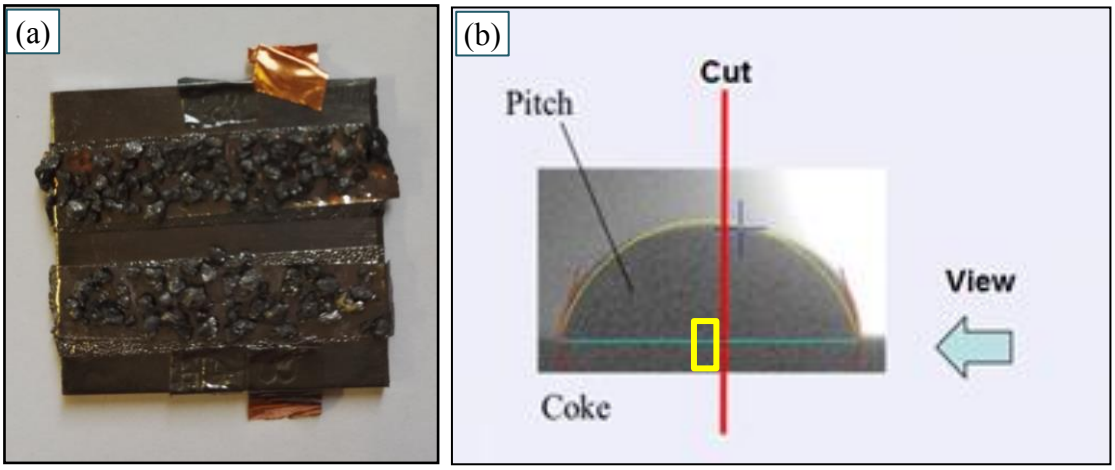

Figure 3.6: (a) The coke particles prepared by the two techniques. (b) The section (yellow region) of the coke-pitch drop analysed.

3.2.2 Laboratory anode manufacture and characterization

As shown in Table 3.5, anodes were fabricated in the laboratory using the standard dry aggregate recipe under standard conditions (S) similar to those used in industry with three standard pitches (Pitch-2, Pitch-3, and Pitch-4) (Anode 2, Anode 6, and Anode 7) as well as with three low QI pitches (Pitch-1, Pitch-5, and Pitch-6) (Anode 5, Anode 9, and Anode 10). The standard pitch percentage was taken as 15 %. Anodes were produced using three other pitch percentages (Anode 1, Anode 3, and Anode 4) with Pitch-2 as well as with the best-wetting pitch blend (MP12: blend of 75 % Pitch-1 and 25 % Pitch-2) (Anode 13) and the least-wetting pitch blend (MP35: blend of 25 % Pitch-3 and 75 % Pitch-5) (Anode 13). Three anodes (Anode 8, Anode 11, and Anode 12) were produced using different mixing and forming parameters. In this project, some properties of carbon anodes (density, CO_2 and air reactivities, and electrical resistivity) were also measured. Moreover, the

texture and the topography of carbonized pitch as well as the interface between pitch and aggregate particles in different carbon anodes were also investigated. In addition, the kinetic analysis was carried out in order to compare the anodes with different pitches and different pitch contents.

Table 3.5: Anode manufacture and characterization in the laboratory.

Anode	Pitch type	Pitch percentage (%)	Pitch preheating (ºC)	Mixing (ºC)	Compaction time (s)	Kinetic analysis	Characterization
1	Pitch-2	13 %	S	S	Tv	√	√
2	Pitch-2	15 %	S	S	Tv	√	√
3	Pitch-2	17 %	S	S	Tv	√	√
4	Pitch-2	20 %	S	S	Tv	-	√
5	Pitch-1	15 %	S	S	Tv	-	√
6	Pitch-3	15 %	S	S	Tv	√	√
7	Pitch-4	15 %	S	S	Tv	√	√
8	Pitch-5	15 %	S	S	Tv - 5	-	√
9	Pitch-5	15 %	S	S	Tv	-	√
10	Pitch-6	15 %	S	S	Tv	-	√
11	Pitch-6	15 %	S + 10	S	Tv	-	√
12	Pitch-6	15 %	S + 10	S + 10	Tv	-	√
13	MP12	15 %	S	S	Tv	-	√
14	MP35	15 %	S	S	Tv	-	√

The density and the electrical resistivity of all green anodes were measured before coring. From each anode, four cores were taken (Figure 3.7). The density and the electrical

resistivity of all the anode cores studied were measured before and after baking. The green anode cores were baked under the conditions similar to those used in industry.

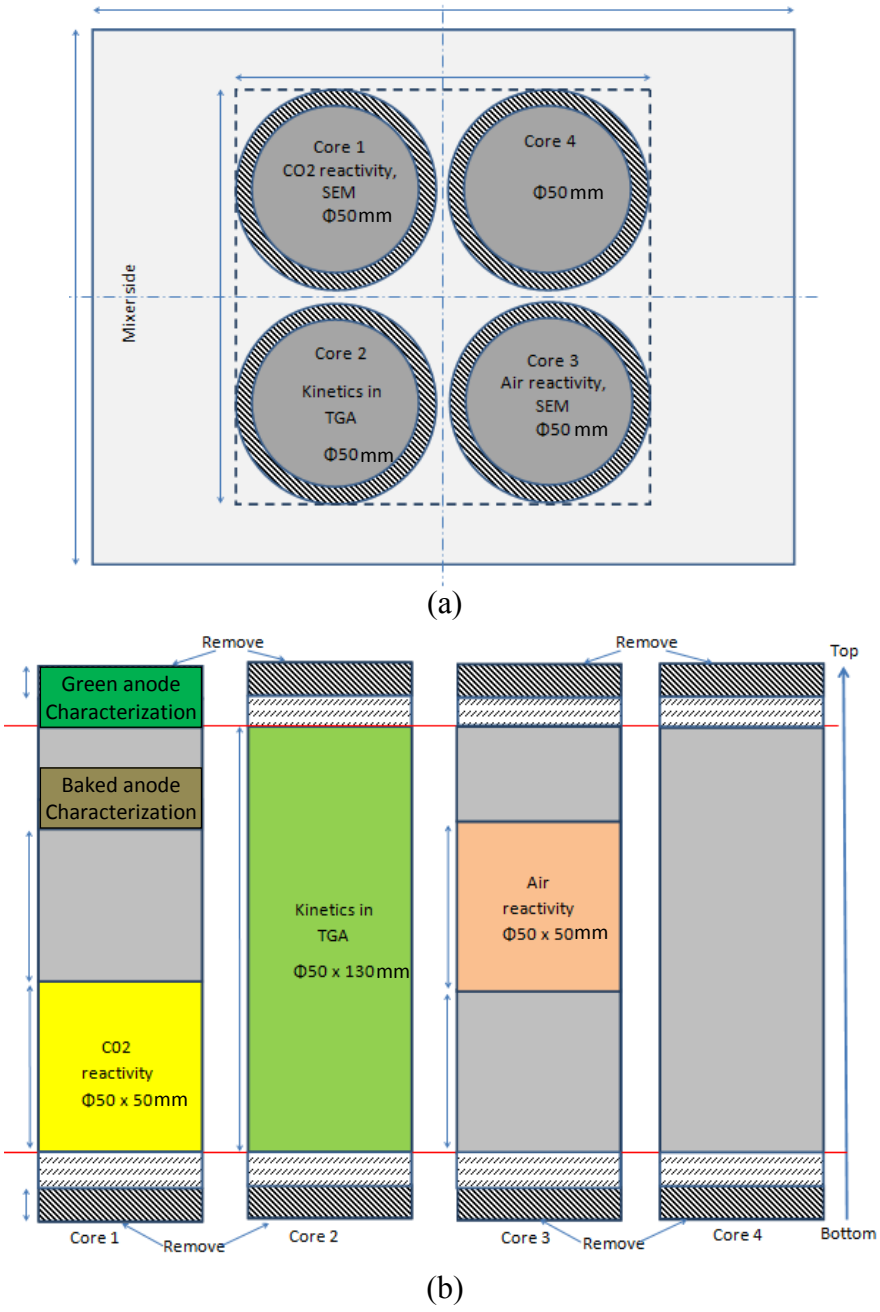

Figure 3.7: (a) Core positions in laboratory anodes. (b) Position of samples used for different tests in anodes cores.

The detailed analysis of green and baked anode samples from Core 1 (structure, coke/pitch interface) was carried out with the optical microscope and SEM. The structure and the coke/pitch interfaces of different anode samples baked under different baking conditions (heating rate, soaking temperature) were also analyzed using the optical microscope and SEM. In addition, a few anode samples made with Pitch-2,were baked under the same conditions (at a standard heating rate similar to that used in industry), but baking was stopped at different temperatures (200 °C, 300 °C, 400 °C, 600 °C, 800 °C, 1050 °C). The samples were analyzed using optical microscopy in order to see the change in the structure of anode during baking. These anodes were prepared during another study that focused on the crack formation during baking [56]. However, their structures and coke/pitch interfaces were analyzed during this study. It is difficult to identify the carbonized pitch and petroleum coke in baked anodes using optical microscopy and SEM. With the objective of facilitating these analyses, a new method (anode etching) was developed in this study since there was no atomic oxygen etching apparatus available in the laboratory. The polished surfaces were ultrasonically cleaned and then dried in the oven at 80 °C for 17 h to remove moisture. Afterwards, they were exposed to air at 525°C for 20 min. This method was chosen primarily because of the difference in the extent of reaction of pitch and coke in anode samples with air; and it was proven to be simple and effective for etching these samples.

Core 1 and Core 3 (Figure 3.7) were baked in the laboratory furnace using the standard heating rate. Sections of Core 1 and Core 3 were used for the CO_2 and air reactivity tests, respectively. The study of CO_2 (ASTM D 6558-00a) and air (ASTM D

6559-00a) reactivities for baked anode cores with different pitches (three standard pitches, three low QI pitches, and two pitch blends) were carried out in the thermogravimetric analyzer (TGA).

Core 2 (Figure 3.7) from the anodes was baked using the standard heating rate to 1100 °C with a soaking time of 8 h in TGA. The weight loss of the samples due to volatile release was continuously recorded with respect to time and temperature. The instantaneous concentrations of volatiles (hydrogen and methane) were measured with the gas chromatograph (GC). Then, the kinetic analysis of pyrolysis was carried out using the data obtained with TGA and GC.

3.2.3 Analysis of industrial anodes

Air and CO_2 reactivities of the small cores taken from industrial anodes (Anode 18, Anode 27, Anode 28, Anode 31, Anode 32) produced during the 2013 measurement campaign as well as from four anodes manufactured in 2011 were measured using TGA at UQAC and analyzed. The anode reactivities were correlated with the anode production and baking parameters (vibro-compaction, compaction time, and positions in the baking furnace). A detailed structural analysis of the samples was carried out with SEM.

3.3 Experimental systems

3.3.1 Sessile-drop system

The wettability of coke by pitch was determined using a sessile-drop system at 170 ºC, which is the typical mixer temperature used in industry. The sessile-drop system consists of a tube furnace, a pitch injection system, a graphite crucible, a digital video

camera, and a vacuum pump (Figure 3.8). The coke sample was placed in the graphite crucible and compacted in order to have a smooth coke bed surface. The injection chamber holds the solid pitch sample. This chamber has a small hole which is placed just above the coke substrate during the experiment. The air in the system was first purged with nitrogen, and then the experiments were conducted under nitrogen atmosphere. In order to decrease oxygen and humidity contents of nitrogen, the gas was passed through a number of traps before it enters the system. There are two entry lines for nitrogen. The main line is directly connected to the furnace tube for maintaining the inert atmosphere inside the tube. The other line that connects the injection chamber to the inert gas supply carries the nitrogen gas necessary for slightly pressurizing this chamber in order to force the molten pitch droplet out onto the surface of the coke substrate. A video of the drop was captured, and the images were saved in a computer. To measure the contact angle, the FTA 32 software was used.

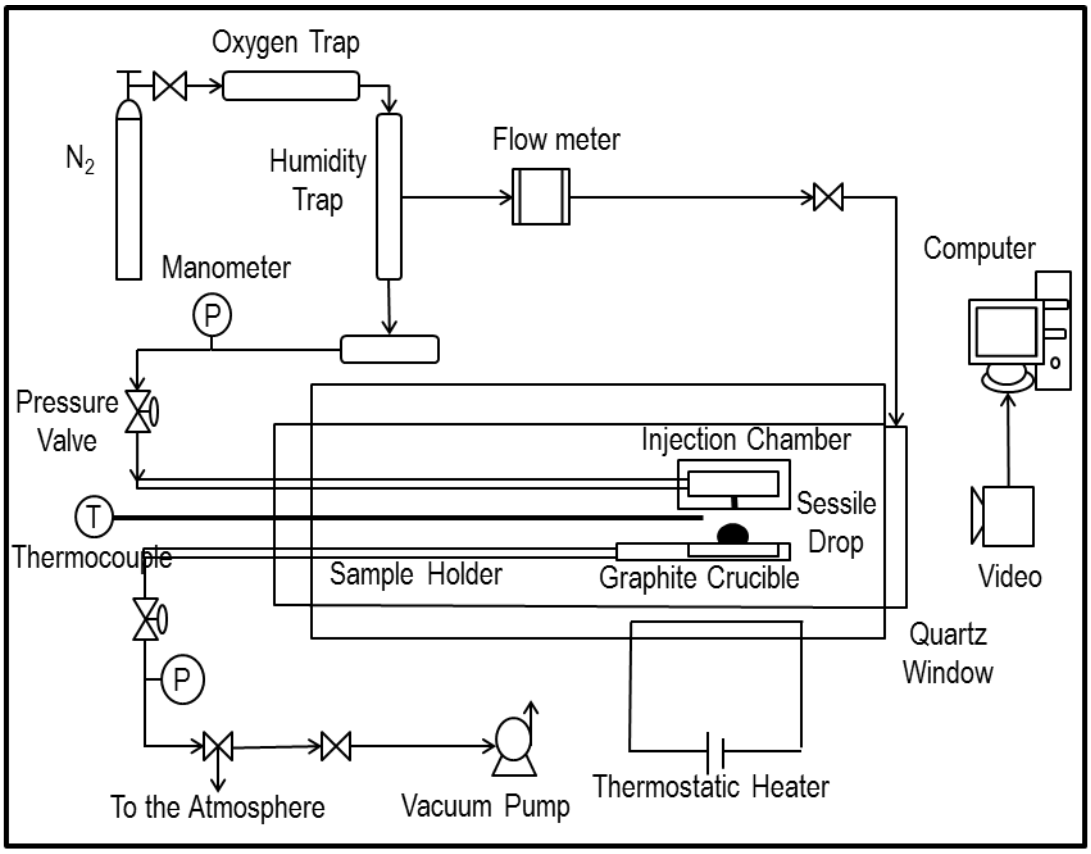

Figure 3.8: Schematic diagram of the sessile-drop set-up at UQAC [57].

Ideal conditions for a wetting test are: (1) a well-compacted coke bed to ensure low bed porosity and smooth top surface; (2) utilization of fine coke particles as it is difficult to obtain a smooth surface with large coke particles, which also have large pores resulting in a large quantity of pitch penetration; (3) use of inert atmosphere as the oxygen may react with pitch, and (4) control the similar pitch drop size (volume and diameter of the pitch drop) for each test.

3.3.2 Laboratory anode fabrication and anode sample preparation

The equipment for laboratory anode fabrication and anode sample preparation is presented in Figure 3.9. The sieve shaker at UQAC, shown in Figure 3.9 (a), was used in order to prepare a desired dry aggregate (coke, butt, and recycled anodes) particle size distribution, and then different fractions of coarse, medium, and fine dry aggregates were weighed according to the recipe. The dry aggregate was preheated to a certain temperature and was mixed for a specific time with the measured quantity of pitch in the mixer shown in Figure 3.9 (b) to prepare the anode paste. Anode forming (green anode) was carried out in a vibro-compactor (Figure 3.9 (c)). The density and the electrical resistivity of green anodes were measured after cooling them naturally to room temperature. From each anode, cylindrical samples with a specific length were cut for detailed analysis using the coring equipment (Figure 3.9 (d)). The cylindrical green anode samples were baked in an electrically-heated laboratory furnace manufactured by Pyradia (Model No-B07D02029021SVCCH), illustrated in Figure 3.9 (e).

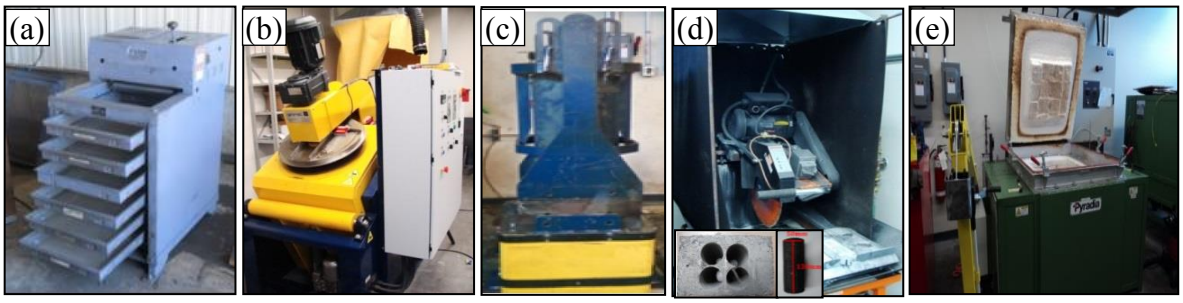

Figure 3.9: (a) Sieving system, (b) Mixer, (c) Vibro-compactor, (d) Set-up for anode coring, (e) Baking furnace.

3.3.3 Density and resistivity measurements of anodes and anode samples

Anodes (as block) were weighed using a balance shown in Figure 3.10 (a). The dimensions (length, width, and height) of anodes were measured using a digital slide caliper shown in Figure 3.10 (b). A tri-square (Figure 3.10 (c)) was used to reduce the chance of error during the measurements. Electrical resistivity of the laboratory anodes were measured with the set-up (called SERMA) [58, 59] shown in Figure 3.10 (d). The voltage drops at a number of points between the top and bottom surfaces of the anode blocks were measured using a 5-A current.

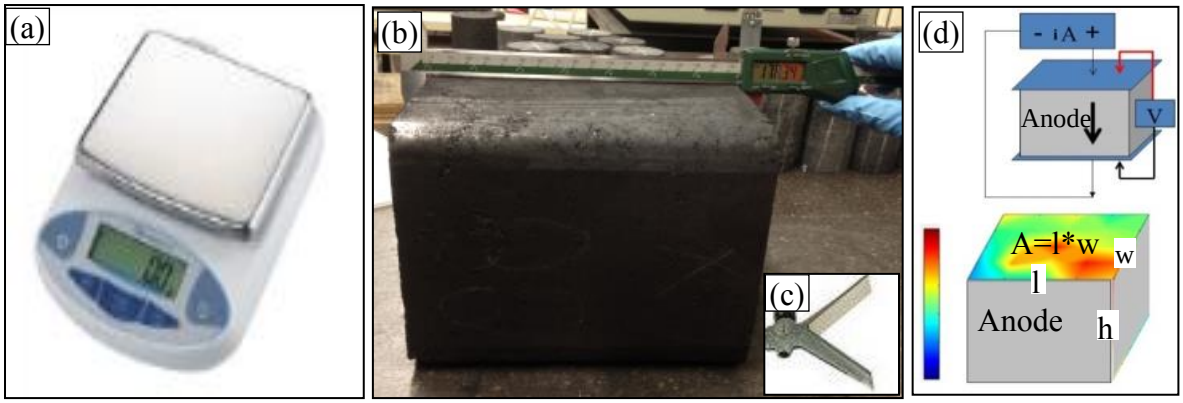

Figure 3.10: Density and resistivity measurements of anodes: (a) Balance, (b) Digital slide caliper, (c) Tri-square, and (d) Set-up for the electrical resistivity measurement of anodes at UQAC.

The density of anode blocks was calculated using Equation (3-1):

$$\rho = \frac{m}{l \times h \times w} \tag{3-1}$$

where ρ = density (g/cm^3); l = length (cm); w = width (cm); h = height (cm); m= mass of the anode (g).

The electrical resistivity of anode blocks was calculated from Equations (3-2) and (3-3):

$$A = l \times w \tag{3-2}$$

where A = area (cm^2); l = length (cm); w = width (cm);

$$ER = \frac{V \times A}{I \times h} \quad (3\text{-}3)$$

where ER = electrical resistivity (μΩm); V = average voltage drop (mV); I = current (A); h = height (cm).

Anode samples (cylindrical cores: Φ50 mm × 130 mm) were dried, and then weighed with a balance shown in Figure 3.11 (a). The diameter and length of anode core samples were measured using the digital slide caliper shown in Figure 3.11 (b). The apparent density of anode samples (cores) were measured using the ASTM D5502-00 standard [41]. The electrical resistivity of the anode samples were measured with the set-up shown in Figure 3.11 (c) according to the ASTM D6120-97 standard [42].

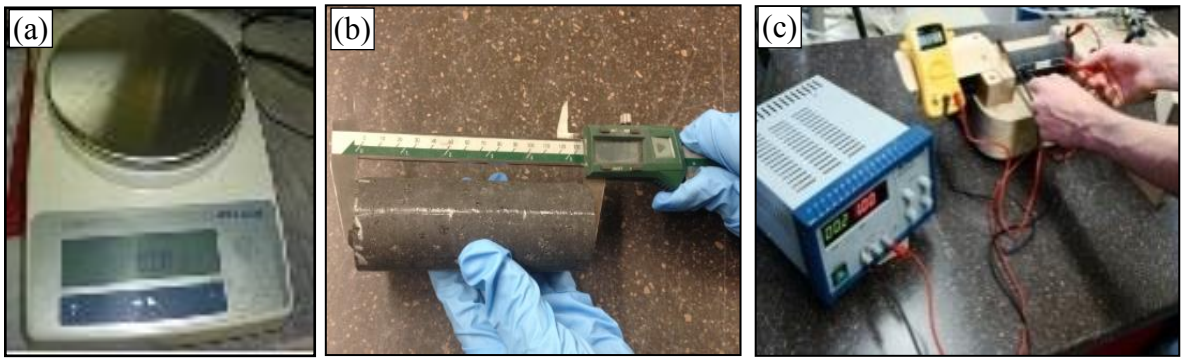

Figure 3.11: Density and resistivity measurements of cylindrical anode samples: (a) Balance, (b) Slide caliper, (c) Set-up for the electrical resistivity measurement of anode samples at UQAC.

The density of cylindrical anode core was calculated with Equations (3-4) and (3-5):

$$V = \pi h \frac{d^2}{4} \quad (3\text{-}4)$$

where V = volume (cm^3); h = height (cm); d = diameter (cm);

$$\rho = \frac{m}{V} \quad (3\text{-}5)$$

where ρ = density (g/cm^3); m = mass (g);

The electrical resistivity of the anode sample was calculated with Equations (3-6) and (3-7):

$$A_c = \pi \frac{d^2}{4} \quad (3\text{-}6)$$

where A_c = cross-sectional area (cm^2); l = length (cm);

$$ER = \frac{V \times A}{I \times L} \quad (3\text{-}7)$$

where ER = electrical resistivity (μΩm); V = average voltage drop (mV); I = current (A); L = distance between contact points of the cored sample (10 cm).

3.3.4 Scanning electron microscope

The scanning electron microscope (Figure 3.12) helps visualize the topography of the surface and the size of particles. The sample is scanned with a focused beam of electrons. These electrons interact with atoms, and secondary electrons are emitted by the atoms excited with the electron beam. The SEM analyses were done using JEOL-JSM-6480LV with secondary electron scattering, using an accelerating voltage of 20 kV.

As discussed previously, the coke samples prepared with two different techniques were investigated using SEM. The “as received” coke particles and the “crushed” coke particles were uniformly dispersed on a conductive tape fixed on a specimen plate (Figure 3.6 (a)) and vacuum-dried for one day at room temperature prior to the SEM analysis.

For green anode sample preparation, the sample was set in a mould using epoxy-resin; then the anode sample surface was polished and cleaned in an ultrasonic bath. The sample was dried in an oven to remove the moisture. Then, it was coated with gold.

Due to the difficulty in identifying the carbonized pitch and petroleum coke in baked anodes using optical microscopy and SEM directly, a new method for anode etching was developed as explained above. SEM analyses were done after the etching of samples.

Figure 3.12: Scanning electron microscope at UQAC.

3.3.5 Optical microscope

The optical microscope (Figure 3.13) uses visible light and a system of lenses to magnify images of small samples. The optical microscope allows the examination of a larger surface area compared to that for the SEM technique.

The solidified pitch-coke sessile-drops were cut vertically (Figure 3.6 (b)) and polished to obtain smooth and flat surfaces containing the interface between coke particles and pitch. These surfaces were investigated using the Nikon Eclipse ME600P optical microscope and analyzed with the image analysis software Clemex Vision 4.0. This

allowed the visualization of pitch penetration through the coke particles as well as the interface of pitch and coke in the drop samples.

Figure 3.13: Optical microscope at UQAC.

3.3.6 FT-IR spectroscopy Analysis

Fourier transform infrared (FT-IR) spectroscopy (Figure 3.14) is a powerful tool to detect different functional groups based on bond energies. FT-IR can also detect different hybridization of carbon present in CH bonds and identify aromatic and aliphatic hydrocarbons, which are difficult to analyze using XPS. The chemical structures of calcined petroleum coke and five coal tar pitches were qualitatively examined by FT-IR spectroscopy at room temperature. The main objective was to identify the complimentary functionality between pitch and coke as well as to compare the chemical functionalities of different pitches. IR spectra were collected in the wavenumber range of 500-4000 cm^{-1}, and all the spectra were recorded at 4 cm^{-1} resolution. Each time, 64 scans were carried out

prior to the Fourier transformation. All spectra were collected using the KBr technique (the ratio of sample and KBr was 1:100). The spectrum version 5.0.1 software was used, and the result was taken as the average of two experiments. The IR spectra for each experimental set were transformed into the absorbance spectra.

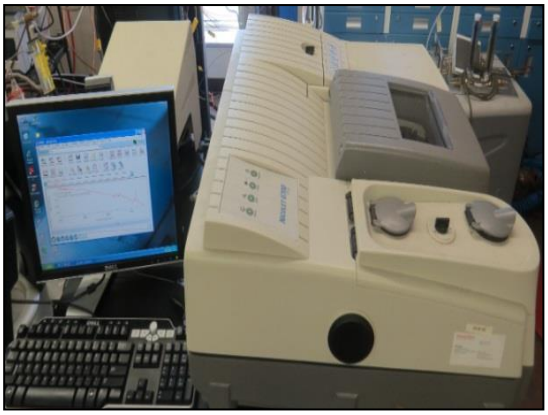

Figure 3.14: Fourier transform infrared spectroscope at UQAC.

3.3.7 XPS Analysis

The quantitative chemical analysis of the elements and functional groups on the surface of coal tar pitch and calcined petroleum coke samples were investigated using X-ray photoelectron spectroscopy (XPS) (Figure 3.15). XPS analysis provides information on the distribution of different atoms and the nature of corresponding bonds on the surface based on their electronic binding energy. In this study, the samples were ground to -125 µm and analyzed with AXIS Ultra XPS spectrometer (Kratos Analytica) using Mono-chromate Al K[α] (hν=1486.6 eV) source at a power of 210 W at the Alberta Centre for Surface Engineering and Science (ACSES), University of Alberta. The analysis of the spectra was performed using the CasaXPS software at UQAC. The analysed surface depth of the sample was 2-5 nm. Quantitative analysis of the XPS high resolution spectra allows

the determination of the chemical nature of elements present on the surface such as C, O, and N.

Figure 3.15: X-ray photoelectron spectroscopy at the University of Alberta.

3.3.8 Thermogravimetric analysis

Thermogravimetric analysis (Figure 3.16) is a method of thermal analysis in which the change in weight of a material is measured as a function of temperature or as a function of time. Gas chromatograph (GC) can be used to separate the components of the effluent gas mixture. The thermogravimetric analyzer connected to the GC was used to analyze the devolatilization kinetics of green anode samples during baking. The thermogravimetric analysis system at UQAC consists of a tube furnace (made of 'Carbolite'), a gas chromatograph, a gas condenser system, a computer for weight loss recording, a line heater system, a vacuum pump for fume removal, a balance (Mettler Toledo model XS2002S), and a temperature programmer. Anode sample is suspended into the vertical tube of the furnace from a balance. The weight loss of the anode sample is continuously recorded with respected to time and temperature by a computer. A thermocouple is placed in the centre of the tube to measure the furnace temperature and is connected to the temperature

programmer. Condensers are used to condense the volatiles coming from the furnace. There is an entry line for the carrier gas (nitrogen). There are two outlet lines for the gas produced from the furnace. One line is connected to a vacuum pump through condensers for the removal of the major part of volatiles. The other line is connected to the GC system (for kinetic analysis). The GC system consists of a gas injection system, entry lines for the carrier gas (nitrogen) and air, a computer for integrator, and a suction pump. The gas (volatile) is passed through humidity traps and injected into the GC system. Line heater is used to prevent condensation of volatiles (tar) as they can block the lines.

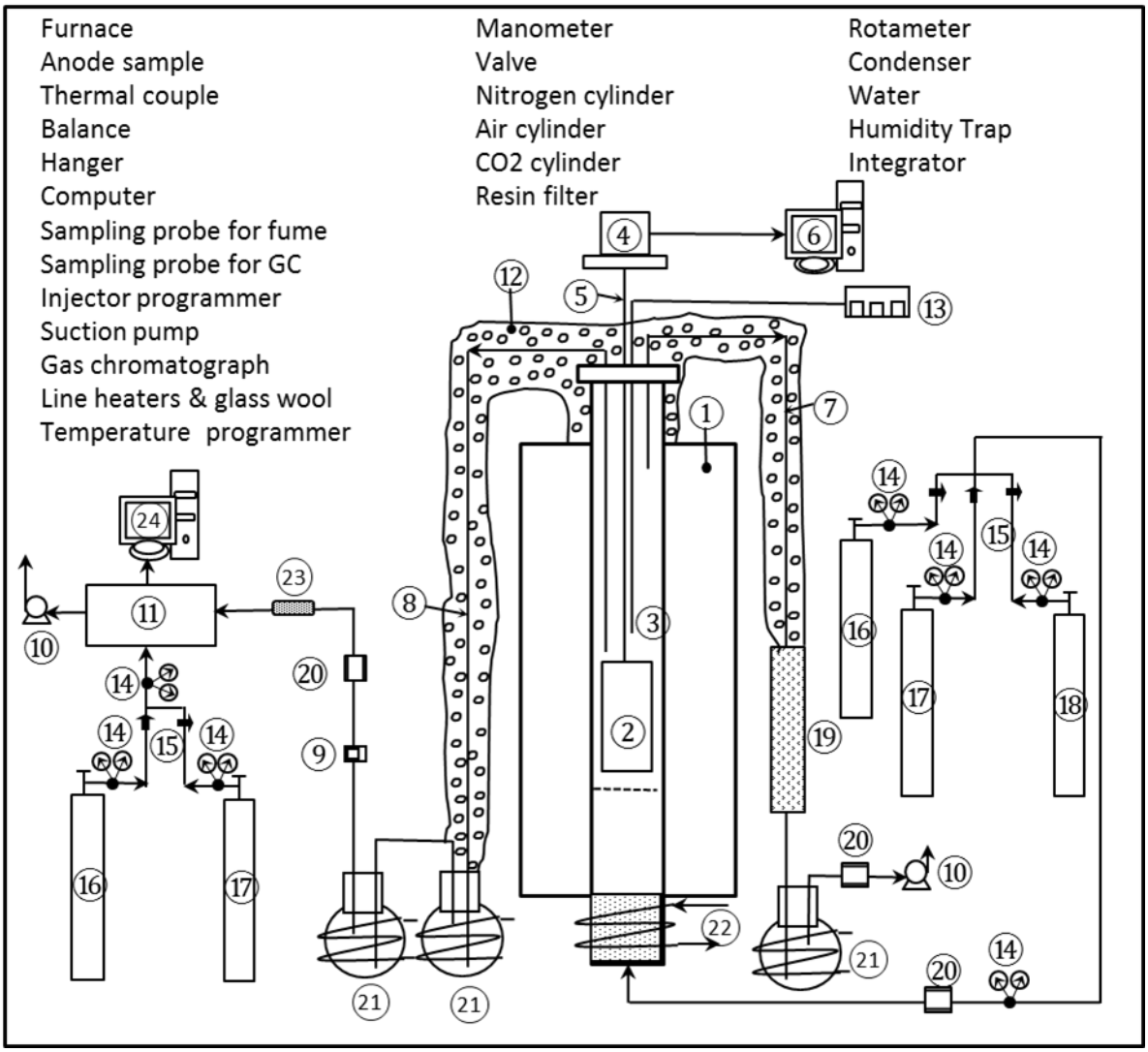

Figure 3.16: A schematic diagram of the thermogravimetric analyzer at UQAC.

3.3.8.1 Air and CO_2 reactivities of anode samples

In this study, anode samples (Φ50 mm × 50 mm) were used to measure the reactivity. The diameter of the TGA furnace tube was 80 mm. The gas (air or CO_2) flow rate was calculated with [44, 45] Equations 3-8 and 3-9:

$$\text{Ratio} = \frac{\text{Tube ID}^2 - \text{Sample OD}^2}{\text{Ref Tube ID}^2 - \text{Ref SampleOD}^2} = \frac{80^2 - 50^2}{100^2 - 50^2} = 0.52 \qquad (3\text{-}8)$$

$$\text{Flow rate } = (250\ \text{L/h}) * 0.52 = 130\ \text{L/h} = 2.16\ \text{L/min} \quad (3\text{-}9)$$

The velocity around the sample depends on the internal diameter of the furnace and the external diameter of the sample. The flowrate was adjusted to maintain a constant gas velocity at 0.71 cm/min around the sample.

The procedure followed for air (ASTM-D6558) or CO_2 (ASTM-D6558-00a) reactivity measurement is given below [44, 45]:

1) The furnace was preheated to 525 ºC for air reactivity, and 960 ºC for CO_2 reactivity;
2) An inert atmosphere was maintained inside the tube of the furnace using N_2 at 2.16 L/min;
3) The mass of the sample was weighed and recorded to the nearest 0.01g as Wi;
4) The sample diameter (d) and the sample height (h) were measured to the nearest 0.001 cm, and the surface area for the reaction was calculated;
5) The balance was tared;
6) A container was placed at the bottom of the tube of the furnace;
7) The sample was tied using a Kanthal wire and suspended in the furnace from the balance;
8) The sample was preheated under N_2 atmosphere for 30 min;
9) The gas flow to the furnace was switched from N_2 to air/CO_2 after 30 min. The flowrate of gas (air/CO_2) was maintained at 2.16 L/min; ;
10) The weight of the sample was recorded every minute during the test. The test duration for air reactivity was 3 h 30 min (30 min N_2 flow + 180 min air flow = 210

min), and for CO_2 reactivity 7 h 30 min (30 min N_2 flow + 420 min CO_2 flow= 450 min);

11) The sample was removed from the reaction chamber as soon as possible after the test as the dusting could be affected. Care was taken so that the sample did not hit the furnace wall during removal, which could result in the dislodging of particles and change in the mass of the dust;
12) The loose dust on the sample surface was collected and weighed ($W_{\text{add dust}}$);
13) The dust collection container was removed from the tube and placed in a desiccator until it cooled down;
14) The loose dust collected was added to the dust collected in the dust collection container and was weighed (W_d);
15) Calculation:

$$A = (\pi dh + \frac{2\pi d^2}{4})/100 \quad (3\text{-}10)$$

where A = area of exposed surface (cm^2); h=height of anode sample (mm); d=diameter of anode sample (mm);

$$TRc = \frac{1000[W_{30} - (W_i - W_{\text{add dust}})]}{7A} \quad (3\text{-}11)$$

where TRc = total air/CO_2 reactivity rate (mg/cm^2-hr); A = area of exposed surface (cm^2); W_{30} = the sample weight (g) after 30 min from the start of the test; W_i = sample weight (g) at 210 min for air reactivity test or sample weight (g) at 450 min for CO_2 reactivity test; $W_{\text{add dust}}$ = weight (g) of loose dust collected from the sample surface after the test.

$$IRc = \frac{1000(W_{30} - W_{60})}{0.5A} \quad (3\text{-}12)$$

where IRc = initial air/CO_2 reactivity rate (mg/cm^2-hr); A = area of exposed surface (cm^2); W_{30} = sample weight (g) after 30 min of test; W_{60} = sample weight (g) at 60 min of test.

$$FRc = \frac{1000[W_j - (W_i - W_{add\ dust})]}{0.5A} \quad (3\text{-}13)$$

where FRc = final air/CO_2 reactivity rate (mg/cm^2-hr); A = area of exposed surface (cm^2); W_j = sample weight (g) after 180 min for air reactivity test, or sample weight (g) after 420 min for CO_2 reactivity test; W_i = sample weight (g) at 210 min for air reactivity test, or sample weight (g) at 450 min for CO_2 reactivity test; $W_{add\ dust}$ =weight (g) of loose dust collected from sample surface after test.

$$DRc = \frac{1000W_d}{7A} \quad (3\text{-}14)$$

where DRc = dusting (air/CO_2 reactivity) rate (mg/cm^2-hr); A = area of exposed surface (cm^2); W_d = weight (g) of total dust collected during the test.

3.3.8.2 Thermogravimetric study of the devolatilization kinetics of green anodes

The thermogravimetric analyser was used to study the devolatilization kinetics of green anode samples (cylindrical cores ∅ 50 mm×130 mm) made with three different pitches (different QI value) (Pitch-2, Pitch-3, and Pitch-4; pitch percentage: 15 %) and two different pitch percentages (13 %, and 17 %) with Pitch-2. The cores were baked using the standard heating rate up to 1100 °C in TGA and kept at the maximum temperature for 8 h (soaking time). During baking, the weight loss of the samples due to volatile release was recorded with respect to time and temperature for a specified time interval. Also, the instantaneous volatile concentrations (hydrogen and methane) were measured with GC. Then, the kinetic analysis of the samples was carried out using the GC and TGA data.

In this study, a model developed by Kocaefe et al. [46, 47, 60] was used, which is described below. The following procedure is taken from the article[46]:

The rate of n^{th} order reaction is given as (Levenspiel, 1999) [61]:

$$\frac{dX_i}{dt} = k_i C_0^{(n-1)}(1 - X_i)^n \tag{3-15}$$

where X_i = conversion of volatile component i, k_i = reaction rate constant for gas i (s^{-1}·concentration^{1-n}), n = reaction order, t = time (s).

With the heating rate defined as h=dT/dt, the reaction rate can be expressed as:

$$\frac{dX_i}{dt} = \left(\frac{dX_i}{dT}\right)\left(\frac{dT}{dt}\right) = \left(\frac{dX_i}{dT}\right)h \tag{3-16}$$

where X_i = conversion of volatile component i, t =time (s), T = absolute temperature of sample (K), h = heating rate (K/s).

The Arrhenius law is given by:

$$k_i = k_{i0}\exp(-E_i/RT) \tag{3-17}$$

where E_i = activation energy for gas i (J/mol), k_i = reaction rate constant for component i (s^{-1}·concentration^{1-n}), k_{i0} = pre-exponential factor for component i (s^{-1}·concentration^{1-n}), R = universal gas constant (8.314 J/mol·K), T = absolute temperature of sample (K),

Combining the above equations (Equations (3-16) and (3-17)) and then taking the logarithms, Equation 3-18 can be obtained:

$$\ln\left(\frac{dX_i/dt}{(1-X_i)^n}\right) = -\frac{E_i}{RT} + \ln\left(\frac{k_{i0,app}}{h}\right) \tag{3-18}$$

The apparent pre-exponential factor is defined as:

$$k_{i0,app} = k_{i0} C_0^{(n-1)} \tag{3-19}$$

where $k_{i0,app}$ = apparent pre-exponential factor for gas i (s^{-1}), k_{i0} = pre-exponential factor for gas i (s^{-1}·concentration^{1-n}), n = reaction order, R^2 = correlation coefficient.

When the right hand side of Equation (3-19) is plotted as a function of 1/T, a line is obtained if the right "n" value is chosen (this corresponds to the "n" value that gives the highest correlation factor, R^2). The activation energy (E_i) of a component "i" and its apparent pre-exponential factor ($k_{i0,app}$) can be obtained from the slope and the intercept of the line, respectively [46].

The methodology for the kinetic analysis developed by Kocaefe et al., and the following procedure is taken from the article [46]:

a) The weight loss data obtained from the thermogravimetric analyser was converted to per 100 g anode basis in order to account for the slight weight differences among the anodes samples. Then, the derivative of this curve was taken, which gives the instantaneous total weight loss due to condensable gas, hydrogen, and methane release.

b) Instantaneous concentrations of hydrogen and methane measured in ppm with the gas chromatograph (as a function of time during the experiment) were first converted to g per 100 g of anode sample using the carrier gas flowrate.

c) The instantaneous condensable gas concentration in g per 100 g of anode sample was obtained from the difference between the derivative of instantaneous total weight loss data and the sum of instantaneous hydrogen and methane concentrations.

d) Then, the instantaneous concentration curves of the three volatile components were integrated numerically in order to calculate their cumulative values as a function of time.

These data correspond to the cumulative weight loss (in g/100g) released for each of the volatile components (condensable gas, hydrogen, and methane).

e) The conversion vs. temperature curves for condensable gas, hydrogen, and methane were determined by dividing the cumulative weight loss of the components at any given time to its final weight loss value.

f) Once the conversion vs. temperature curves were obtained, the activation energies and apparent pre-exponential factors were calculated from Equation 3-18.

CHAPTER 4

RESULTS AND DISCUSSIONS

4.1 Effect of pitch and coke properties on the wettability of pitch-coke systems

4.1.1 Wettability of coke by different pure pitches

The wettability behavior of pitch, as the binder in anodes, affects the properties of anodes. Pitches show significant differences in their chemical composition and physical behavior depending on their origins. Five different coal tar pitches with similar softening points (Pitch-1, Pitch-2, Pitch-3, Pitch-4, and Pitch-5) were studied to understand the interaction between different pitches and one calcined petroleum coke using the sessile-drop test. Figure 4.1 shows the wetting test results for five pure pitches with different properties. Contact angle decreases with increasing time. Smaller contact angle means better wettability. It can be seen that the initial contact angles differ by around 10º between different pitches while the duration for complete penetration/spreading are significantly different. Pitch-1 took the least time (most penetrating) and Pitch-5 took the most time (least penetrating) for complete penetration/spreading. It can also be observed that the contact angle values of these pitches at 60 s follow the trend: Pitch-4 >Pitch-5> Pitch-3 > Pitch-2 > Pitch-1. The time was chosen as 60 s as the typical kneading time for coke and pitch in anode plants is usually around 60 s. The kneading time indicates the mixing time of coke and pitch. Thus, according to the results at 60 s, Pitch-5 and Pitch-4 show similar contact angles, and the wettability of coke by pitch, in descending order, is as follows: Pitch-1 > Pitch-2 > Pitch-3 > Pitch-5 > Pitch-4. It can be seen that, before 60 s, the

wettability of pitch by coke is in the following decreasing order: Pitch-1 > Pitch-2 ≈ Pitch-3 > Pitch-5 > Pitch-4. After 60 s, the wettability of Pitch-5 reduces compared to that of Pitch-4. It was reported in the literature that the interaction between coke and pitch depends on the properties of both pitch (i.e., chemical composition and surface functional groups, surface tension, viscosity, QI, mesophase content, etc.) and coke (e.g. particle size, structure, texture, chemical composition and functional groups on the surface, porosity, etc.) [14, 30, 31]. In order to investigate the mechanism of pitch/coke interactions, the chemical properties of coke and pitch were studied using FT-IR and XPS. The pitches with different QI content were characterized with optical microscopy. Furthermore, the pitch-coke interfaces were investigated using SEM.

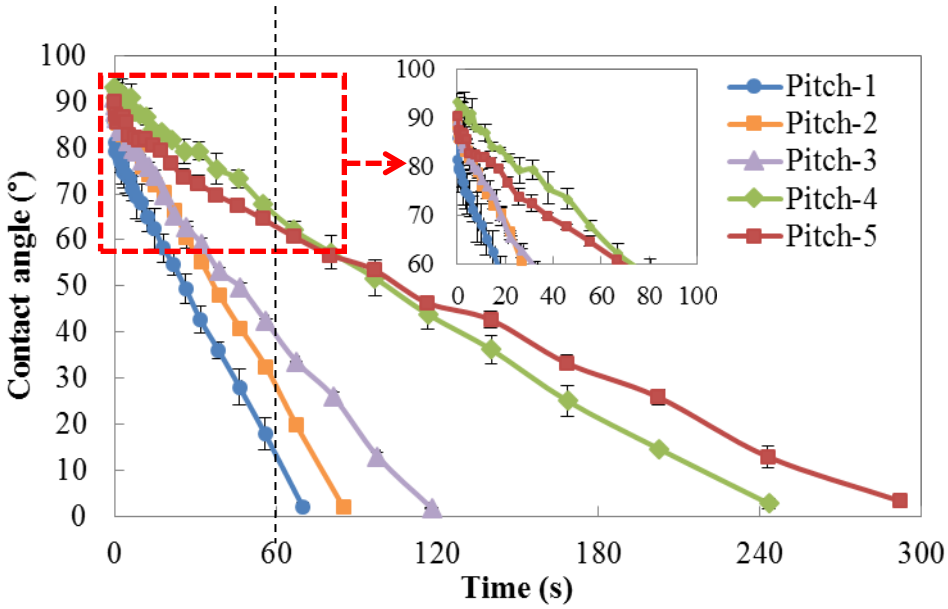

Figure 4.1: Contact angles of different pure pitches.

4.1.1.1 FT-IR analysis

The qualitative analysis of the chemical groups in pitch and coke can be carried out using FT-IR. From the FT-IR spectra shown in Figure 4.2, it can be observed that there are similar chemical functionalities in the five different coal tar pitches. The band at 750 cm^{-1} is due to the ortho-substituted aromatic ring vibrations [14, 62]. The region of 700-900 cm^{-1} includes various bonds related to the aromatic out-of-plane vibration and C-H bending with different degrees of substitution [14, 62]. The regions between 2800-2980 cm^{-1} and 1480-1370 cm^{-1} are for aliphatic hydrogen (stretching vibrations) due to the $–CH_2$- and $–CH_3$ structures for the coal tar pitches [14]. The band at 3000-3100 cm^{-1} relates to aromatic hydrogen (stretching vibrations) [62]. The band at 1600 cm^{-1} is due to aromatic C=C stretching vibrations. The weak band at about 1720 cm^{-1} is for C=O. The band at 1000-1200 cm^{-1} relates to C-O group, which could be assigned to alcohol/phenols/ether. Presence of both C=O and C-O can indicate the presence of carboxylic acid or ester [62]. A wide peak around 3428 cm^{-1} is for free moisture. Multiple peaks in the region of 1200-1300 cm^{-1} are due to C-O /C-N vibrations [14]. All the pitches contain the above chemical functional groups. However, it is difficult to identify the differences in chemical groups between the pitches.

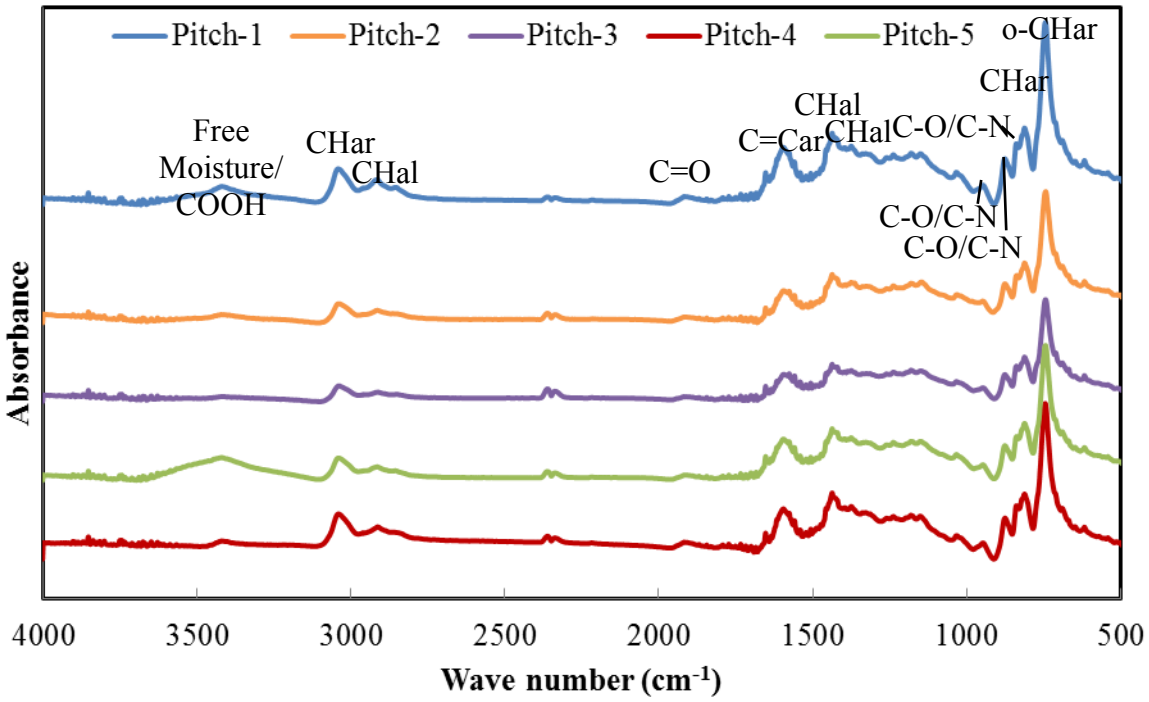

Figure 4.2: FT-IR spectra of five different coal tar pitches.

Figure 4.3 shows the FT-IR spectra of the calcined petroleum coke used in the wetting test. The band at region of 3400-3600 cm^{-1} is related to free moisture/ phenol/carboxylic acid [36]. The band at 3452 cm^{-1} is due to N-H groups in carbazole/secondary amine/OH stretching vibrations. The band at 3000-3100 cm^{-1} is due to aromatic hydrogen stretching vibrations. The region between 3000 and 2700 cm^{-1} are due to C-H stretching vibrations of alkyl substituents and methylene groups in hydro aromatic compounds [36]. A peak near 750 cm^{-1} shows the ortho-substitution of the aromatic ring. Amines (C-N) or ethers (C-O-C) are found in the region around 1100 cm^{-1}. Band corresponding to aromatic C=C bond can be seen near 1500 cm^{-1}. Carbonyl (C=O) group can be found in the region around 1800 cm^{-1}. Two peaks near 1200 cm^{-1} and 1350 cm^{-1} are

due to corresponding C-O stretching vibration in ester/ether/acid and C-O-C vibrations in esters/carboxylic acid/ether [36].

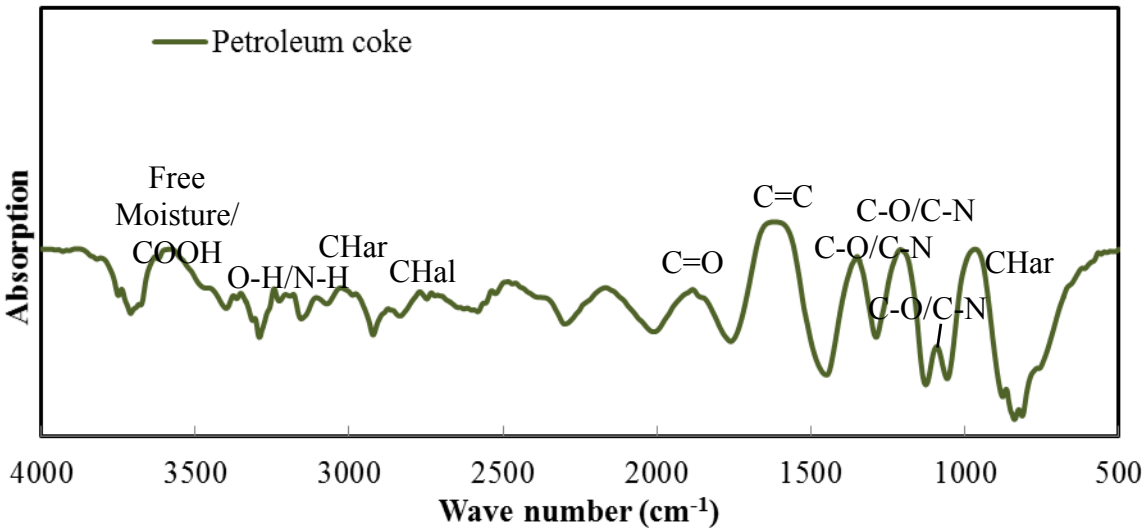

Figure 4.3: FT-IR spectra of calcined petroleum coke.

There are usually three kinds of chemical interaction possible between coke and pitch samples [39]. The first one is hydrogen bond between a hydrogen atom attached to a highly electronegative atom (O, N) and another electronegative atom (O, N). Thus, the hydrogen of O-H group can form a hydrogen bond with functional groups containing oxygen (hydroxyl, ether, and carboxylic groups) or nitrogen atoms (amine). The second type is the acid-base interaction. In this case, acidic functional groups (carboxylic, phenolic, pyrrole) can interact with basic functional groups (amine, pyridine). The third type of interaction is electrostatic in nature. In this case, the negatively charged pi electron cloud of aromatic rings can form electrostatic bonds with positively charged centers (for example quaternary ammonium ion). Coal tar pitch and petroleum coke contain O-H, C-N, COOH, aromatic rings, etc. Thus, this indicates that the petroleum coke and the coal tar pitch contain complimentary functional groups, and it is possible that the functional groups on

the coke surfaces might interact with the complementary functional groups present in pitches.

4.1.1.2 XPS analysis

Using XPS, the quantity of functional groups, close to the surface, can be found. Figure 4.4 (a) shows an example of the survey spectra obtained by XPS scan for Pitch-2. The most prominent peak at 284.3 eV was designated as C1s, other notable peaks were the O1s peak at 533 eV and N1s peak at 400 eV. The relative positions of these peaks can be used to determine the chemical nature of these atoms. High resolution scans and peak fit for C1s region was shown in Figure 4.4 (b). It can give quantitative information about the different functions groups based on the deconvolution of C1s binding energies. Deconvolution of Figure 4.4 (b) reveals three peaks located at 284.3 eV, 285.1 eV, and 286 eV which form the C1s peak. The dominant peak at 284.3 eV is associated with the C=C bond of aromatic structures. The 285.1 eV peak corresponds to C-C bond of aliphatic structures. An approximation was made that the binding energy corresponding to the range of 285.5 eV to 289 eV with a peak at 286 eV corresponds to a number of functional groups C-N/C-O/C-S/C=O/C-SO_2/COOH. The deconvolution of O1s and N1s is presented in Appendix 1. However, the deconvolution of O1s and N1s did not show any direct correlation with the wetting property of pitch.

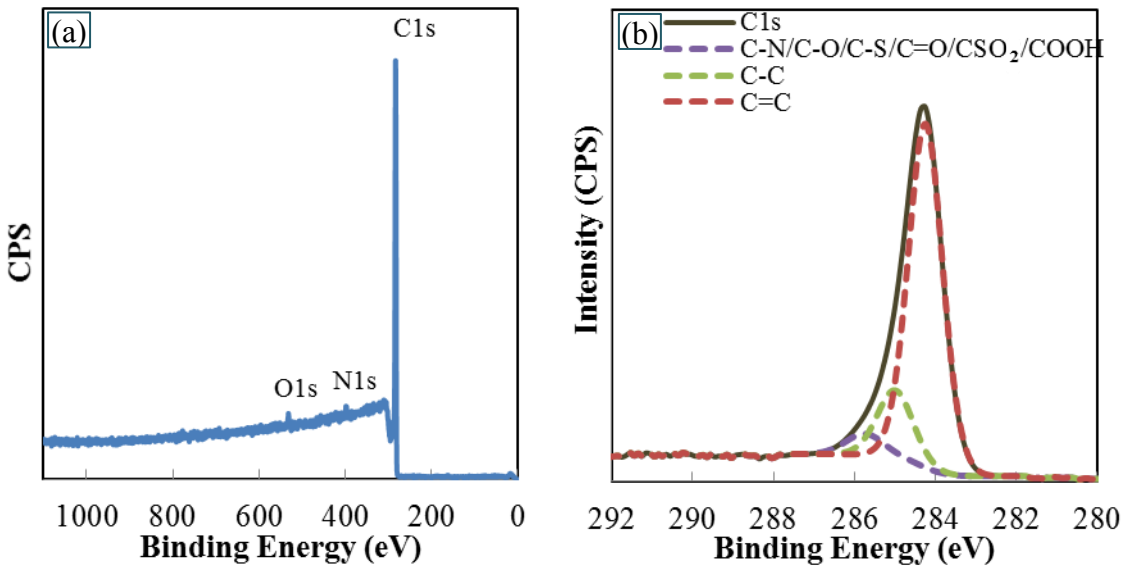

Figure 4.4: XPS spectra of Pitch-2 (a) Survey spectra, (b) De-convoluted C1s spectra.

Table 4.1 summarizes the atomic percentages of different components of the raw materials for the survey spectra and the de-convoluted C1s spectrum. From Figure 4.1, it can be seen that the contact angle at 60 s is decreasing as follows: Pitch-4 > Pitch-5 > Pitch-3 > Pitch-2 > Pitch-1. The relationship between contact angle at 60 s and heteroatom (O, N, and S) contents for different pitches are presented in Figure 4.5 (a).

Except for Pitch-5, the contact angle at 60 s increased with decreasing heteroatom (O, N and S) contents in pitch, and it was observed that there exists a good linear correlation between contact angle at 60 s and heteroatoms (O, N and S) contents for different pitches (Figure 4.5 (b)). The results indicate that except for Pitch-5, the wettability of pitch-coke system increases with increase in heteroatom (O, N, and S) contents in pitch at 60 s. As the percentages of O, N, and S increase, the possibility for the formation of bonds between the functional groups of coke and pitch increases.

The results show that the heteroatoms (O, N, and S) of pitches contribute to the wettability of coke. Usually, the higher is the heteroatom content, the higher is the wetting property of pitch. However, Pitch-5 did not follow the same trend. At 60 s, Pitch-5 and Pitch-4 showed similar contact angles. After 80 s, the wettability of Pitch-5 became less compared to that of Pitch-4 (see Figure 4.1). It is possible that there are other factors which influence the wetting property of Pitch-4 and Pitch-5. This will be explained in detail in the part where the SEM analysis of pitch-coke interface is presented. From the results of the deconvolution of C1s for different pitch samples, it was also observed that the tendency of the contents of CN/CO/CS/C=O/CSO_2/COOH groups for different pitches agrees with that of heteroatoms (O, N and S) shown in Table 4.1 and Figure 4.5 (c).

Table 4.1: Atomic percentages of different components and carbon (C1s) functional groups of the raw materials.

Material	C (at %)*	Carbon (C1s) functional groups (%)			O (at %)	N (at %)	S (at %)
		C=C	C-C	CN/CO/CS/C=O/CSO_2/COOH			
Pitch-1	96.62	81.42	13.00	5.58	1.89	1.21	0.29
Pitch-2	96.93	78.66	15.96	5.38	1.74	1.07	0.25
Pitch-3	97.88	79.41	16.74	3.85	1.15	0.7	0.26
Pitch-4	98.08	75.01	21.03	3.69	1.21	0.51	0.2
Pitch-5	97.61	81.29	14.42	4.29	1.18	0.94	0.27
Coke	95.89	80.54	12.21	7.25	2.53	0.60	0.98

*at %: atomic %

There exists a good linear correlation between the contents of CN/CO/CS/C=O/CSO_2/COOH groups and heteroatom (O, N, and S) contents for different

pitches (Figure 4.5 (c)). It was observed that the contents of CN/CO/CS/C=O/CSO_2/COOH groups increase with increase in heteroatom (O, N, and S) contents. The results also indicate that the wetting property of pitch increases with increase in CN/CO/CS/C=O/CSO_2/COOH, which confirms that heteroatoms of pitch contribute to its wetting property.

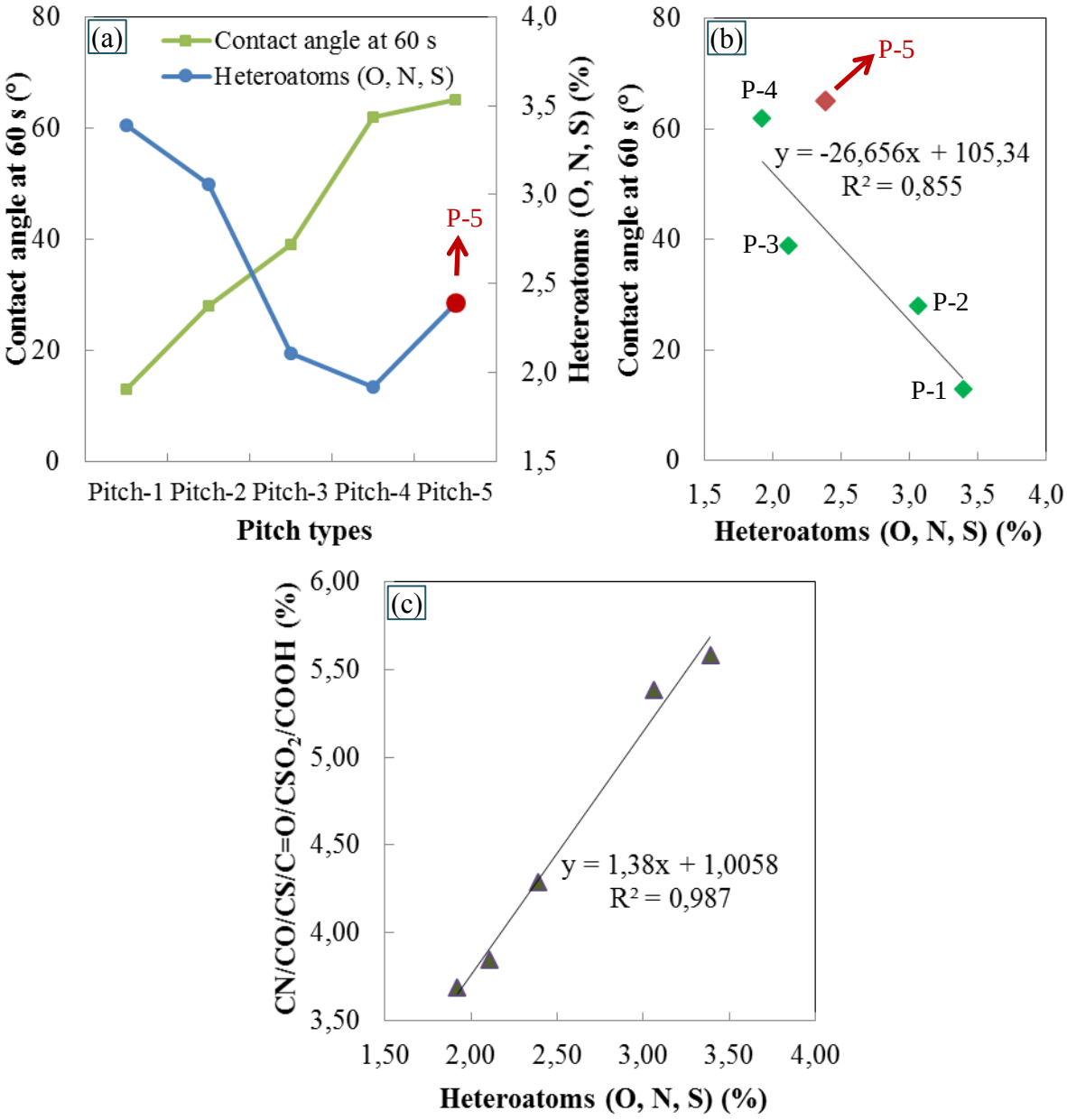

Figure 4.5: (a) Relationship between contact angle at 60 s and heteroatom (O, N, and S) contents, (b) Correlation between contact angle at 60 s and heteroatom (O, N and S) contents, (c) Correlation between the contents of CN/CO/CS/C=O/CSO_2/COOH groups and heteroatom (O, N, and S) contents for different pitches.

4.1.1.3 Optical microscopy analysis

Table 3.1 compares the properties of different pitches. Even though the SP, TI, and CV of the pitches are close, there is a difference in the wettability of the same coke by these pitches. Since the only major difference between the properties of different pitches is the % QI, it is important to analyze the effect of QI level as well as the QI particle size distribution on wetting. As it was reported in the literature, the QI can be divided into two categories: primary QI and secondary QI [1, 11, 17, 21, 24]. The primary QI particles which are formed in the coke oven can be beneficial for anode quality [1]. The primary QI can be grouped as normal primary QI and carbon black/carry-over. The size of normal primary QI particles is about 1µm. The size for carbon black particles (5-500 µm) is larger because of the agglomeration of small particles. Secondary QI particles are formed during the thermal treatment of pitch at temperatures greater than 400 °C. They are anisotropic and can be classified as mesophase (> 4 µm) and mesogens (2 - 4 µm) [7]. Optical microscopy is an important tool to visualize the particles in pitches. Figure 4.6 (a-e) shows the images of five pitches, as received. It is possible to observe the solid particles in all the pitches. It can be seen that pitch contains a lot of particles; some of them stay isolated, some are agglomerated.

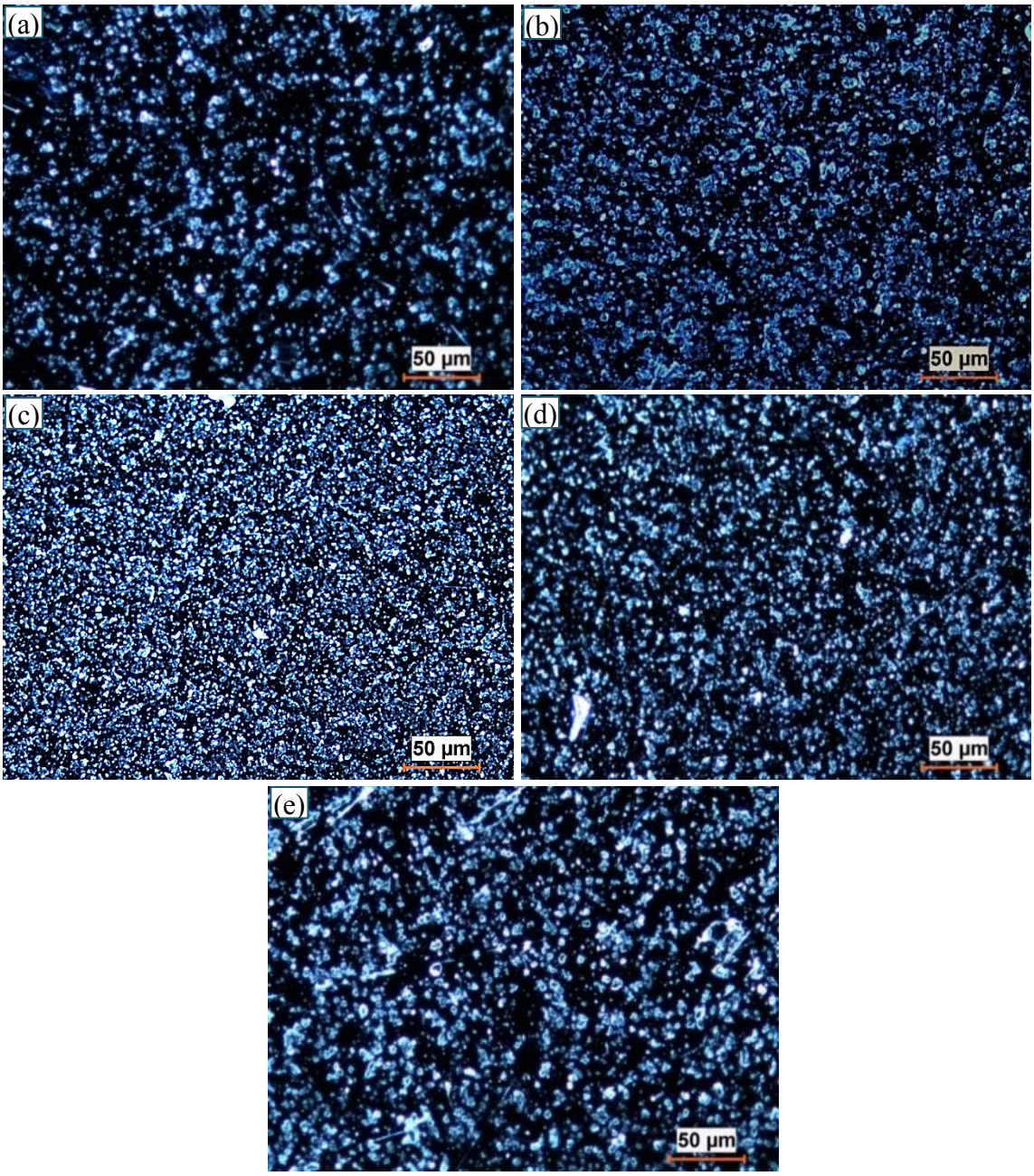

Figure 4.6: Optical microscopy images of (a) Pitch-1, (b) Pitch-2, (c) Pitch-3, (d) Pitch-4, and (e) Pitch-5.

The area percentages of solid particles in pitch presented in Figure 4.6 (a-e) were calculated by the image analysis software of Clemex. The area percentages of solid particles in these five pitches ranged from 11.7 % to 41.8 %, and the value of area

percentage of Pitch-1, Pitch-2, Pitch-3, Pitch-4, and Pitch-5 are 11.7 %, 21.9 %, 41.8 %, 18.5 %, and 14.0 %, respectively. It was observed that there exists a good linear relation between the QI content and the area percentage of solid particles in pitch as shown in Figure 4.7 (a).

It was reported that a typical C/H ratio for coal tar pitch is 1.8, and primary QI material has a C/H ratio of more than 3.5 while secondary QI has a C/H ratio of less than 3 [1] . Typical pitch densities range from 1.3 g/cm^3 to 1.32 g/cm^3 [1]. A larger value of C/H ratio results in higher density. It shows that the density of primary QI is greater than the other components in pitch. It was reported by Turner et al. [20] that QI particles have a relatively large influence on pitch density as their density ranges from 2.0 g/cm^3 to 2.2 g/cm^3.

If the area corresponding to solid particles in pitch is A_{sp} and that for the rest of pitch is A_{rp}, then the percentage of solid particles in pitch by area can be expressed as:

$$a = \frac{A_{sp}}{A_{sp}+A_{rp}} \times 100 \quad (4\text{-}1)$$

The image analysis gives results in area percentage of solid particles in pitch. However, it is more convenient to express the content in terms of weight percentage because it can be used to compare with the QI particle content of pitch given in weight percentage.

If the ρ_p = pitch density, ρ_{sp}= solid particles density, then the weight percentage of solid particles (W_s) in pitches can be expressed as:

$$Ws = \frac{A_{sp}\rho_{sp}}{(A_{sp}+A_{rp})\rho_p} \times 100 = \frac{\rho_{sp}}{\rho_p} \times a \quad (4\text{-}2)$$

Though this calculation of weight percentage has some approximations, it gives a representative weight percent of the solid particles in a pitch sample.

If all the solid particles are QI particles and assuming that the pitch and QI particle densities in this study are 1.31 g/cm^3 and 2.1 g/cm^3, respectively, the calculated values of solid particle area and the corresponding solid particle content in different pitches are presented in Table 4.2.

Table 4.2: Solid particle area and the corresponding solid particle content in different pitches.

Pitch types	Pitch-1	Pitch-2	Pitch-3	Pitch-4	Pitch-5
Area percentage of solid particles in pitch (a)	11.7	21.9	41.8	18.5	14.0
Solid particle content (W_s)	28.0	42.5	65.4	38.0	31.5

The relationship between the QI content and the solid particle content depending on area percentage of solid particles in optical microscope image of pitch is shown in Figure 4.7 (b). The weight percentage of solid particles in these five pitches range from 28.0 % to 65.4 % (see Table 4.2). However, the real weight percentages of QI content in these five pitches range from 3.4 % to 10.8 % (see Table 3.1), which are significantly lower than the values calculated from the image analysis. This indicates that not all the solid particles seen as white dots in optical microscopy images of pitch are QI particles. It may contain certain particles shown as solid in optical microscopy images, but soluble in quinoline or they are in liquid form at 170 °C. However, there exists a linear relation between the QI content and the solid particles, which is discussed below.

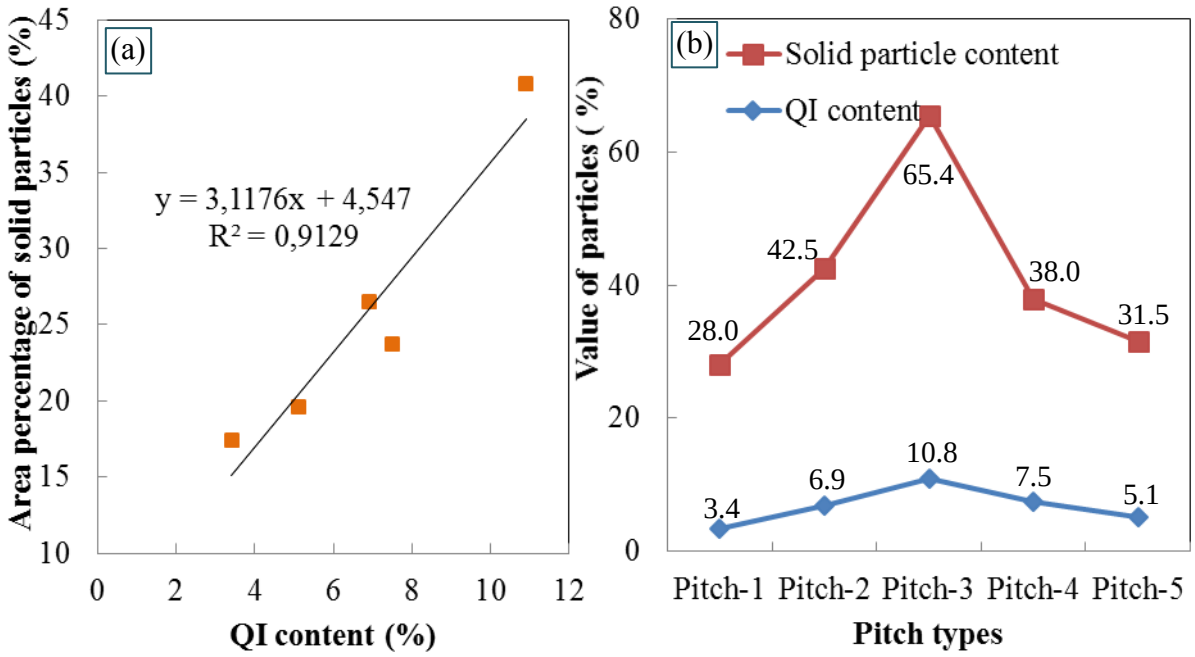

Figure 4.7: (a) Correlation between QI content and area percentage of solid particles in optical microscopy image of pitch, (b) Relationship between QI content and solid particle content determined based on the area percentage of solid particles in optical microscopy image of pitch.

The particles sizes (maximum length) were determined using the image analysis software of Clemex. Figure 4.8 (a) shows the comparison of the number of solid particles in five different pitches using the image analysis technique. This technique may help relate the number of solid particles to the QI content of the different pitches. The solid particles in Pitch-3 show the highest number while Pitch-1 has the lowest number. The number of solid particles in pitches gives a linear relation with the QI content of the corresponding pitches (see Figure 4.8 (b)). The number of particles increases with increasing QI content; however, no direct relationship was found between the QI content of the pitch and the wettability of coke by this pitch (see Figure 4.1 and Table 3.1).

Figure 4.8 (c) shows the particle size distribution in different pitches. The size of most particles is about 1µm. As the size of primary QI is about 1µm [7] and the size of the secondary QI particles is greater than that of normal primary QI [18], it is possible that most of the particles represent primary QI. It is difficult to identify the types of all particles; based on published articles the particle size 2 - 4 µm might be mesogens [7], and the particle size > 4 µm might be mesophase [7] or carbon black [16] (which forms as a result of the agglomeration of small particles). As the pitches were not heat-treated, the presence of mesophase is unlikely [7]. The different solid particle sizes (1-10 µm) are grouped into two regions: small particle-size region (1-3 µm) and big particle size region (4-10 µm). As can be seen in Figure 4.8 (d), in the small particle-size region, the particle count (%) of Pitch-5 is the lowest; however, in the big particle-size region, the particle count (%) of Pitch-5 is the highest. It means that the number of big particles (size 4-10 µm) of Pitch-5 is the highest among these pitches. This may have contributed to the wetting test results obtained above (Pitch-5 being the lowest wetting even though the atomic percentages of O, N, S are reasonably high). Large particles of Pitch-5, after 60 s, may have blocked the pores of coke particles as well as the bed of coke particles preventing the penetration of pitch. Pitch-4 did not show any significant difference in particle size compared to the other pitches except for Pitch-5. The reason for the low wettability of Pitch-4 thus may be due to the low quantity of hetero-atoms as indicated by the XPS results.

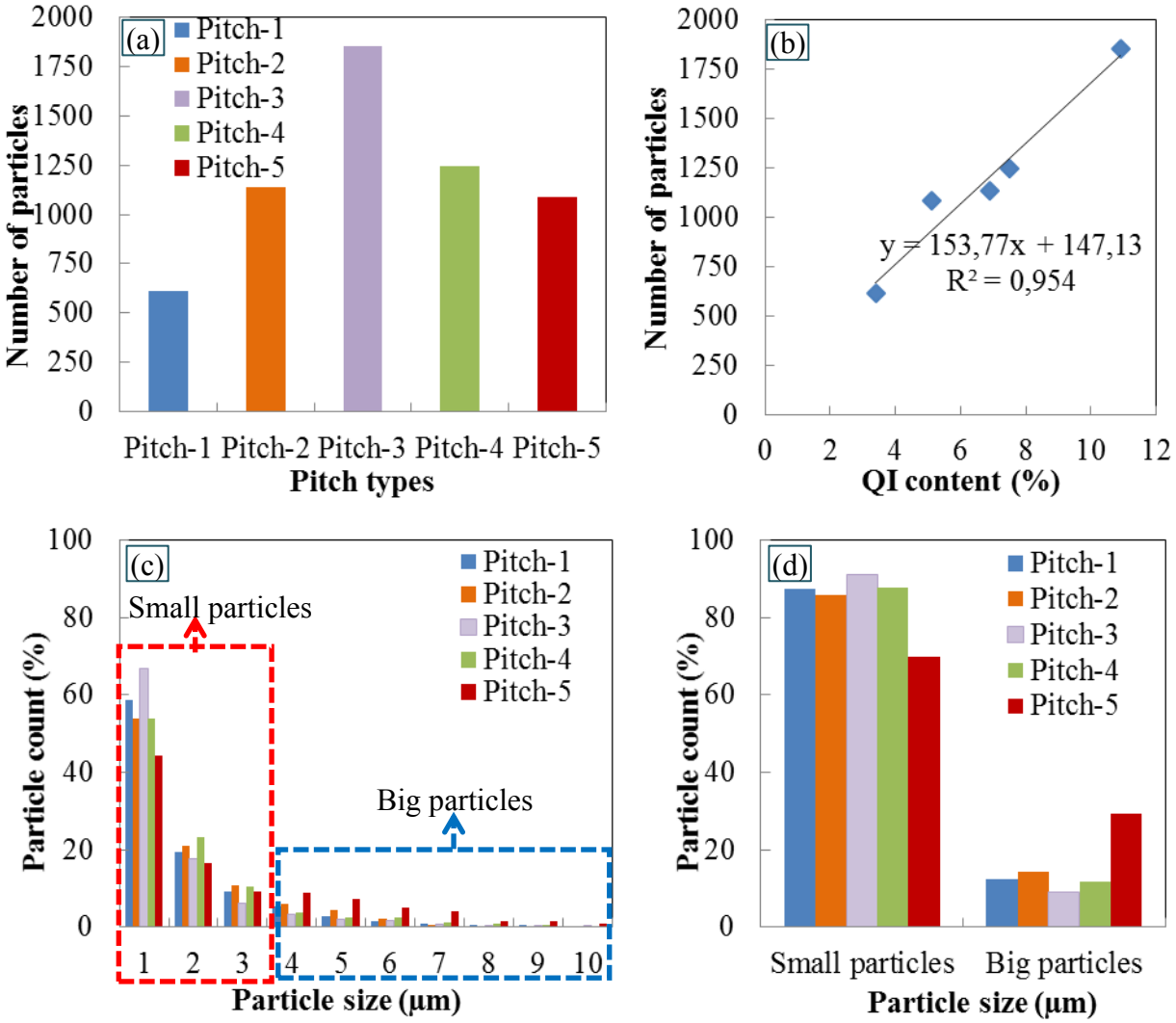

Figure 4.8: (a) Number of particles in five different pitches, (b) Relation between the number of particles and the QI content, (c) Particle size distribution in different pitches, (d) Comparison of particle size distribution.

4.1.1.4 SEM analysis

The analysis of the pitch-coke interface was done with the scanning electron microscopy (SEM) at high magnification. For the analysis, the sessile drop samples obtained from the contact angle experiments were used. It should be noted in this case that the pitch-coke drop used had been heated to 170 ºC whereas the FT-IR and XPS analyses of

pitches and coke as well as the optical microscopy analysis of pitches were carried out on samples at room temperature without prior heating. Thus, the results obtained with the optical microscopy may not be agree with the results obtained using SEM because of the heating of the pitch which may have altered the coke-pitch interactions and the pitch structure. Figure 4.9 shows the interfaces of five pitches with the coke. It is possible to differentiate pitch and coke particles. All the pitch surfaces contain solid particles. It was reported that the size of primary QI is about 1 μm [1, 9], and the size of the secondary QI particles is greater than 1 μm [18]. Both are also spherical. It can be seen that there are particles with shapes other that spherical in Figure 4.9 (a-e). Hence, the SEM images indicate that all pitches used in this study contain particles with characteristics similar to those of primary QI. However, it is difficult to arrive at a conclusion that all are QI particles.

It was observed that the particles of Pitch-5 showed agglomeration and patchy distribution compared to those in other pitches (Figure 4.9 (e)). As mentioned previously, optical microscopy results showed that Pitch-5 had large particles. The interaction between Pitch-5 and the coke was less since the pores of the coke were plugged by the particles in pitch, which consequently reduced the contact surface between coke and pitch. It can be seen that the size, distribution, and agglomeration of particles in pitches play a significant role in the wettability of coke by pitch. There are two possibilities for the agglomerated particles. First, they may be carbon black particles (5-500 μm) because of the agglomeration of small particles. Second, they may be primary QI agglomerated due to the heating process during wetting or the effect of interaction between primary QI and coke

particles. That may be the reason why the wettability of Pitch-5 was the lowest after 60 s. It is possible that it took some time to block the pores of coke and the bed of coke particles. This may explain why the wettability of Pitch-5 reduced after 60 s. The optical microscopy and SEM results show that the particle size distribution in all pitches might vary before and after heating or in the presence of coke particles (see Figure 4.6 (a-e) and Figure 4.9 (a-e)). The particle size distribution in pitch before heating and in coke-pitch mixture after heating (170 °C) varied. It is possible that heating may have changed the chemical nature of particles in pitch.

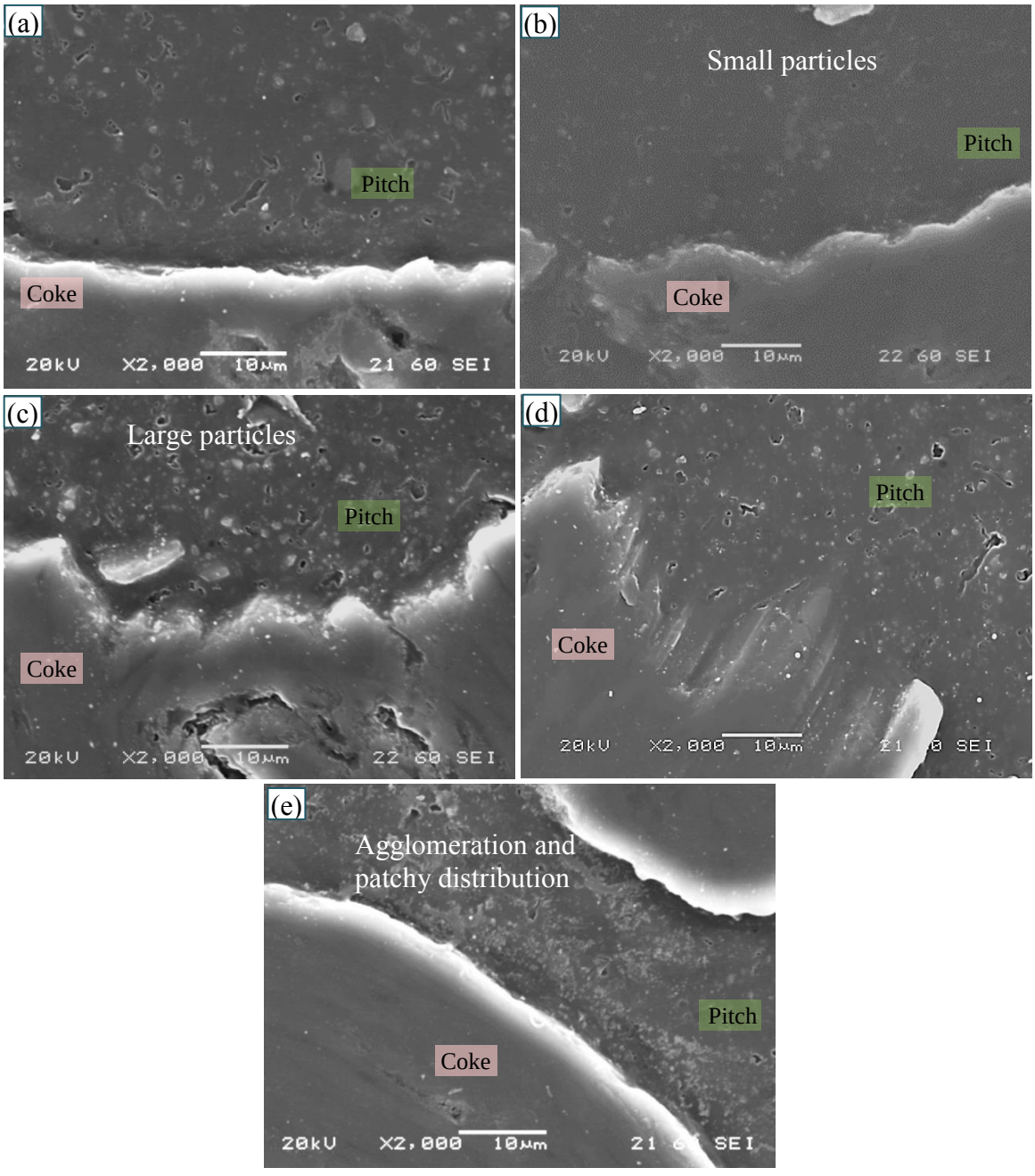

Figure 4.9: SEM images of (a) Pitch-1/Coke, (b) Pitch-2/Coke, (c) Pitch-3/Coke, (d) Pitch-4/Coke, and (e) Pitch-5/Coke Interfaces.

4.1.2 Wettability of coke by pitch blends

Sarkar et al. [36] investigated the dynamic contact angles and the interaction of different cokes by pitch. Huang et al. [39] studied the wettability of bio-coke by pitch based on initial contact angles, total wetting time, and K-values. However, there is no study on the dynamic wettability of coke by pitch blends. This study was carried out to fill this void.

Figure 4.10 shows the variation of contact angles of the blends of (a) Pitch-1/Pitch-2 and (b) Pitch-3/Pitch-5. These pitches and their blends are presented here, which show that pitches behave quite differently in blends. The results of the other pitches and their blends are presented in Appendix 2. It was observed that the contact angles decreased with increasing time, and the pitches and their blends penetrated completely through the coke bed within 300 s. However, the complete penetration time of different pitch samples are different. The complete penetration time for the blends of Pitch-1 and Pitch-2 in descending order is as follows: [Pitch-1 (25 %) and Pitch-2 (75 %)] > [Pitch-1 (75 %) and Pitch-2 (25 %)] > [Pitch-2 (100 %)] > [Pitch-1 (100 %)], and the complete penetration time for the blends of Pitch-3 and Pitch-5 in descending order is: [Pitch-5 (100 %)] > [Pitch-3 (25 %) and Pitch-5 (75 %)] > [Pitch-3 (75 %) and Pitch-5 (25 %)] > [Pitch-3 (100 %)]. Figure 4.10 also shows that the contact angles measured initially and at earlier times (up to about 40-50 s) are close, which makes the comparison of the wettability of coke by different pitches and pitch blends difficult. At later times, the differences are quite noticeable. The results also show that the wettability of coke by the blends of Pitch-1 and Pitch-2 is less than those of pure Pitch-1 and Pitch-2 (Figure 4.10 (a)). On the other hand, for blends of Pitch-3 and Pitch-5, the wettability of coke by pitch blends was

between those of pure Pitch-3 and Pitch-5 (Figure 4.10 (b)). As the same coke was used, the reason why the blends behaved differently in the two cases was explored based on the chemical functional groups of coke and pitch. The results are presented in relevant sections.

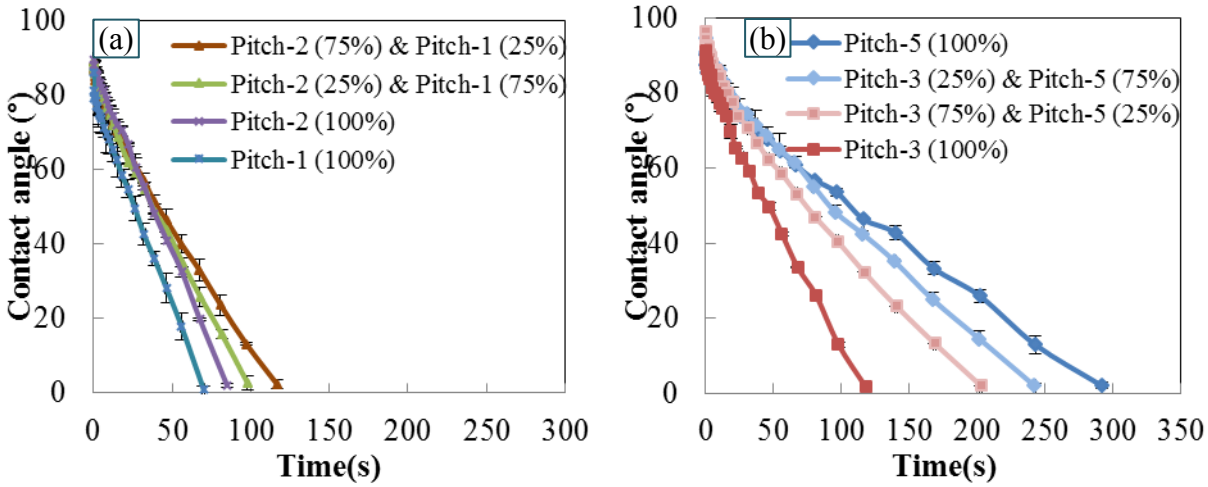

Figure 4.10: Contact angles of the blends: (a) Pitch-1and Pitch-2 (b) Pitch-3 and Pitch-5.

4.1.2.1 K-value

In order to determine the wettability trend and allow the comparison of different pitch-coke systems, the K values, which indicate how fast a liquid can spread and penetrate into a solid, were calculated. A higher K-value indicates better wetting. As discussed in the literature part (section 2.2), the K-value of a liquid-solid system can be determined by curve-fitting the experimental data using Equation (2-6).To determine the absolute value of K, it is necessary to know the equilibrium contact angle. However, there is no equilibrium contact angle in the case of pitch-coke systems when there is chemical interaction taking place. Such interaction can change the surface, and the system may not reach equilibrium; the equilibrium is possible only in liquid-solid systems with physical wetting. Another reason for not achieving equilibrium is the porous nature of the coke bed. To reach

equilibrium, the surface has to be smooth and non-porous, which does not allow the penetration of liquid. The wettability tests with porous solids are carried out with very small particle-size solids and well-packed beds to approach the ideal case. They still give results which allow the comparison of the wettability of different liquid-solid systems. In this case, the complete penetration time of different pitches into the coke bed is significantly different since better wetting pitch can also penetrate faster. The order of wettability with different pitches may also change at a certain time during the wetting process. This affects the comparison of the wettability of different samples.

Since the equilibrium contact angle does not exist for coke-pitch systems studied, a reference contact angle was used to calculate the K-value. The reference contact angle, θ_e, can be determined as the contact angle measured at an arbitrarily chosen time after the drop is placed on the coke bed for all the samples. This approach allows the calculation of K-values based on the chosen reference contact angle which help compare the wettability of different systems on a relative basis [39]. The contact angle at 60 s was used as the reference contact angle θ_e to calculate the K-value since the kneading time is usually around 60 s during the anode paste preparation. Figure 4.11 presents the graphical presentation of K-value for Pitch-5 and coke system.

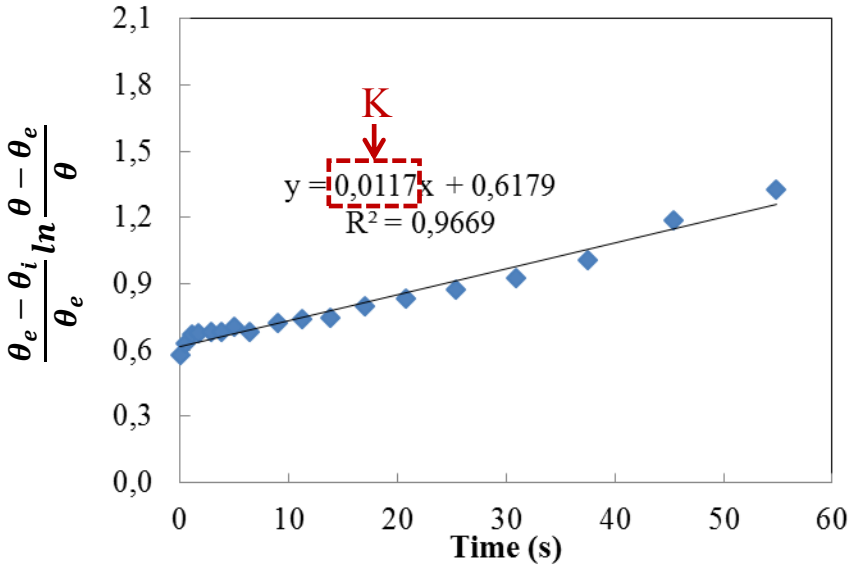

Figure 4.11: Determination of K-value for Pitch-5 and coke system.

The calculated K-values of different pure pitch and their blends on coke were presented in Table 4.3 along with initial contact angles (0 s), contact angles at 60 s, corresponding percent decrease in contact angle, and correlation coefficient R^2. R^2 values were high for all samples. The lower K-values of the blends of Pitch-1 and Pitch-2 compared to corresponding pure pitches indicate that their wettability of coke before 60 s is less than pure Pitch-1 and Pitch-2. Also, it can be seen from Table 4.3 that the K value of pitch-2 is less than that of Pitch-1. As for the blends of Pitch-3 and Pitch-4, the wettability of coke by these blends is between those of their corresponding pure pitches. These results show a trend similar to that of the previous findings of the dynamic wettability study as expected. There exists a good correlation between the percent decrease in contact angle and K-value (Figure 4.12). These results show that the above approach with K-values is another tool for the comparison of wettability.

Table 4.3: Contact angles and K-values of different pure pitch and their blends on coke.

Pitch type	Initial θ°	θ° at 60 s	θ° decrease	K-value	R^2
Pitch-1 (100 %)	85.9	1.0	98.84 %	0.0422	0.9312
Pitch-1 (75 %) and Pitch-2 (25 %)	89.0	25.8	71.03 %	0.0315	0.9226
Pitch-1 (25 %) and Pitch-2 (75 %)	88.9	33.0	62.89 %	0.0294	0.9290
Pitch-2 (100 %)	89.4	21.2	76.29 %	0.0317	0.9044
Pitch-3 (100 %)	91.0	33.5	63.21 %	0.0261	0.9390
Pitch-3 (75 %) and Pitch-5 (25 %)	96.3	53.1	44.82 %	0.0198	0.9571
Pitch-3 (25 %) and Pitch-5 (75 %)	94.5	61.4	35.01 %	0.0154	0.9427
Pitch-5 (100 %)	93.5	59.5	36.34 %	0.0117	0.9669

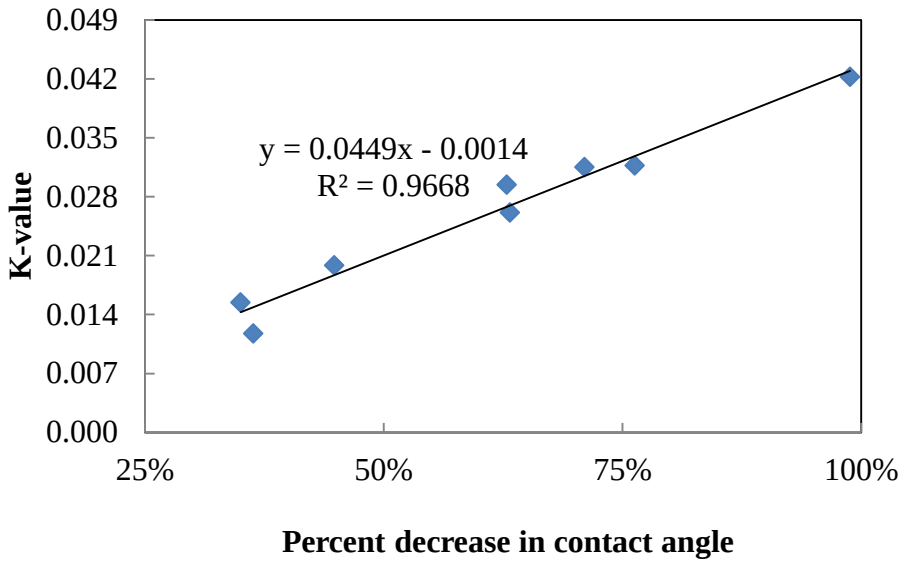

Figure 4.12: Correlation between percent decrease in contact angle and K-value.

4.1.2.2 XPS analysis

Different authors studied the chemical composition of carbon materials (coke and/or pitch) using XPS [28, 63-66]. It was found that coke and/or pitch contain mostly carbon as well as heteroatoms such as oxygen, nitrogen, and sulfur. The binding energy (BE) values

used in this work for C1s, O1s, and N1s peaks are given in Table 4.4, Table 4.5, and Table 4.6, respectively. Presence of different elements in the vicinity of an element may influence the binding energy (BE) of electrons of that element. Therefore, the ranges of BE were chosen based on published works [50, 71-74].

Table 4.4: List of functional groups and their corresponding binding energies for C1s. spectrum [28, 63-66].

Element	Binding energy (eV)	Range of BE (eV)	
		Start	End
C1s	284.3	280.5	290.0
Csp^2 (C=C)	284.3	280.5	284.6
Csp^3 (C-C)	285.1	285.0	286.0
C-N/C-O/C-S	286.0	285.5	287.0
C=O/CSO_2	287.1	287.0	288.5
COOH	289.1	289.0	290.0

Table 4.5: List of functional groups and their corresponding binding energies for O1s spectrum [28, 63-66].

Element	Binding energy (eV)	Standard deviation (eV)	
		Start	End
O1s	533.0	531.0	536.0
C=O	531.6	531.1	532.2
C-O	533.0	532.4	533.6
Adsorbed H_2O	534.7	533.6	536.8
Adsorbed O_2	535.7	534.9	536.6
$C(NH_2)COOH$	530.9	526.8	531.8

Table 4.6: List of functional groups and their corresponding binding energies for O1s spectrum [28, 63-66].

Element	Binding energy (eV)	Standard deviation (eV)	
		Start	End
N1s	400.0	398.0	406.5
Pyridine	398.9	398.3	399.5
NR_3/CN	399.5	398.8	400.2
Pyrrole	400.3	399.9	400.7
N+	401.5	401.1	401.9
-NO	403.3	402.6	404.0
NO_2	405.8	405.2	406.4

XPS analysis provides information about the distribution of different atoms on the surface based on their electronic binding energy. High-resolution spectra of XPS give an idea about the nature of bonds and elemental analysis. It can also give quantitative information about different chemical functional groups.

The XPS spectra of different pitches and the coke sample were analyzed [Appendix 1]. Figure 4.13 (a) shows an example of the survey spectra obtained by XPS scan for Pitch-2. The most prominent peak at 284.5 eV was designated as C1s, other notable peaks were the O1s peak at 533 eV, and the N1s peak at 400 eV. The relative positions of these peaks can be used to determine the chemical nature of these atoms. High resolution scans and peak fit for C1s, O1s, and N1s regions are shown in Figure 4.13 (b), (c), (d), respectively. The quantitative information about the different

functions groups can be obtained based on the deconvolution of C1s, O1s, and N1s binding energies (BE).

Deconvolution given in Figure 4.13 (b) reveals three peaks located at 284.3 eV, 285.1 eV, and 286 eV, which form the C1s peak. The dominant peak at 284.3 eV is associated with the C=C bond of aromatic structures. The 285.1 eV peak corresponds to C-C bond of aliphatic structures. The peak at higher energy position 285.5 eV is associated with CN/CO/CS/C=O/CSO_2/COOH bonds. As the BE of these bonds is slightly different [Table 4.4], it was assumed that the BE corresponding to the range of 285.5 eV to 289 eV with a peak at 286 eV corresponds to a number of functional groups C-N/C-O/C-S/C=O/C-SO_2/COOH.

The O1s peak was deconvoluted and was found to be a combination of several peaks at 530.1 eV, 531.7 eV, and 532.9 eV. The 531.7 eV peak corresponds to the carbonyl functional group, and the 532.9 eV peak corresponds to alcohol/phenolic groups. The peak at 530.1 eV is likely to be due to C(NH_2)COOH group (Figure 4.13 (c)). It was reported that nitrogen in pitch or coke was found to be present predominantly in pyrrolic and pyridinic forms. Since the proportion of pyrrolic is greater than pyridinic form in coal, the predominant form of nitrogen in coal tar pitch is also pyrrolic nitrogen [63]. The N1s in coal tar pitch can be deconvoluted to peaks at 400.3 eV, 398.7 eV, and 399.6 eV. The 400.3 eV peak corresponds to the pyrrolic nitrogen, and the 398.7 eV peak corresponds to pyridinic groups. The peak at 399.6 eV is likely to be amines group (Figure 4.13 (d)). The N1s in coke was deconvoluted based on the peaks described earlier (Table 4.6). The peak at 401.5 eV in coke was likely to be quaternary N-type (N+). In Pitch-3 and Pitch-4, the peaks

for N1s could not be deconvoluted because of the noise and the detection limit of the XPS equipment.

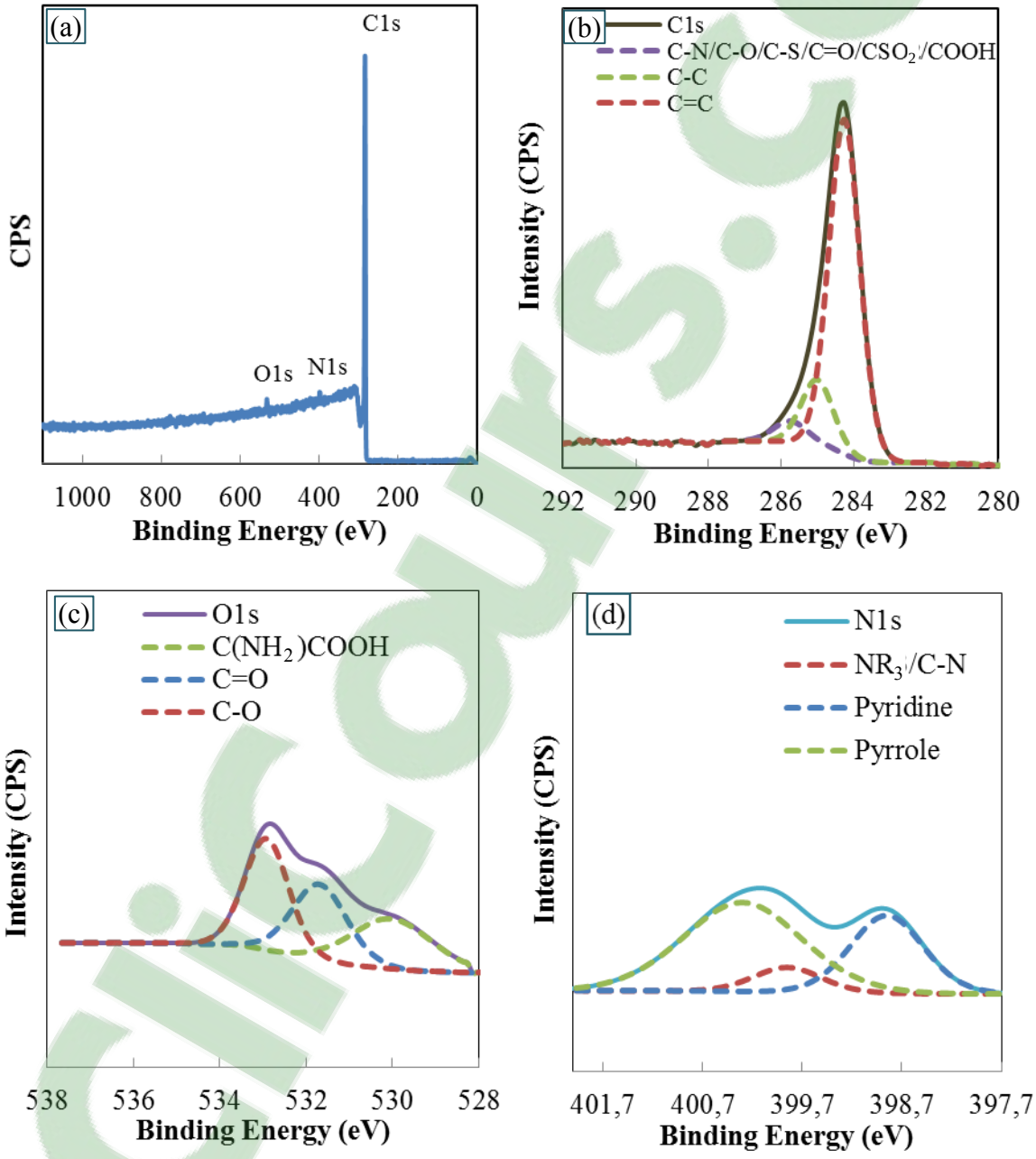

Figure 4.13: XPS spectra of pitch-2 (a) Survey spectra, (b) De-convoluted C1s spectra, (c) De-convoluted O1s spectra, (d) De-convoluted N1s spectra.

Table 4.7 shows the carbon (C1s) functional groups of different pitches and coke. This result is in good agreement with the previous findings of the present study. The atomic percentages of carbon (C1s) functional groups with elements (O, N, and S) in different samples: Pitch-1 > Pitch-2 > Pitch-5 > Pitch-3> Pitch-4. As the percentages of carbon (C1s) functional groups with elements (O, N, and S) increase, the possibility for the formation of covalent bonds between the functional groups of coke and pitch increases. Pitch-5 did not follow this trend because of the agglomeration of the particles in the pitch sample. Table 4.8 shows that Pitch-2 has the highest percentage of carboxylic acid group (COOH). From Table 4.9, the NR_3/-CN % in Pitch-1 can be attributed to the higher concentration of amine group which is basic in nature. When Pitch-1 and Pitch-2 were mixed, the wettability of coke by pitch mixture decreased significantly. The carboxylic acid COOH of Pitch-2 could react with the amine group of Pitch-1. Thus, the active functional group left in the mixture which can react with coke is greatly reduced. The presence of COOH and NR_3 groups may lead to an interaction in the pitch blends. It may be noted that, in pitch, COOH and pyrrole are acidic. Amine and pyridine are basic. Acid base reaction is not limited to only COOH and amine. That might be the reason why the wettability of coke by the blends of Pitch-1 and Pitch-2 were less than those by pure Pitch-1 and Pitch-2. Except for Pitch-2, other pitches contained similar amounts of COOH (Table 4.8). Pitch-1 had a high amount of amines (Figure 4.9) compared to the other pitches. This probably reinforced the acid-base reaction between Pitch-1 and Pitch-2. Thus, the extent of COOH in pitch might have controlled the wettability of coke by pitch blends.

The results show that both chemical and physical properties of pitches contribute to their wetting capacity on a particular coke bed.

Table 4.7: Atomic percentages of different components and carbon (C1s) functional groups in different pitch samples and coke.

Material	C (%)	Carbon (C1s) functional groups (%)			O (%)	N (%)	S (%)
		C=C	C-C	CN/CO/CS/C=O/CSO_2/COOH			
Pitch-1	96.6	81.42	13.00	5.58	1.89	1.21	0.29
Pitch-2	96.9	78.66	15.96	5.38	1.74	1.07	0.25
MP12	96.8	79.19	15.46	3.35	1.76	1.16	0.29
Pitch-3	98.1	75.01	21.03	3.69	1.21	0.51	0.20
MP35	97.8	79.52	16.47	4.01	1.19	0.79	0.25
Pitch-5	97.6	81.29	14.42	4.29	1.18	0.94	0.27
Coke	95.9	80.54	12.21	7.25	2.53	0.60	0.98

Table 4.8: Atomic percentages of oxygen and oxygen (O1s) functional groups in different pitch samples and coke.

Material	O (%)	Carbon (O1s) functional groups (%)		
		C=O	C-O	$C(NH_2)COOH$
Pitch-1	1.89	44.94	40.93	14.64
Pitch-2	1.74	31.73	37.49	30.78
MP12	1.76	40.48	41.42	18.10
Pitch-3	1.21	43.84	54.81	10.35
MP35	1.19	43.46	47.10	9.44
Pitch-5	1.18	42.05	46.32	11.63
Coke	2.53	49.63	39.99	10.37

Table 4.9: Atomic percentages of nitrogen and nitrogen (N1s) functional groups in different pitch samples and coke.

Material	N (%)	Nitrogen (N1s) functional groups (%)			
		Pyridinic (Py)	NR_3/CN	Pyrrolic (PR)	N+
Pitch-1	1.21	28.68	21.38	49.94	-
Pitch-2	1.07	31.59	9.47	58.93	-
MP12	1.16	24.00	-	68.92	7.09
Pitch-3	0.51	-	-	-	-
MP35	0.79	24.60	7.84	52.37	15.20
Pitch-5	0.94	14.97	5.26	58.69	21.09
Coke	0.60	39.84	-	47.75	12.41

4.1.3 Effect of pitch softening point on wettability of coke

As shown in Figure 4.14 (a) and Table 3.1, Pitch-6 has a softening point about 10 °C higher than those of the other pitches. The temperature of coke and pitch was around 170 °C in the wetting study for Pitches 1 to 5. In this part, the effect of the temperature of pitch on wetting was studied by performing the wetting tests at 170 ºC and 180 ºC for Pitch-2 (standard softening point) and Pitch-6 (high softening point). Figure 4.14 (b) shows the change in contact angle as a function of time for Pitch-2 and Pitch-6 at 170 °C and 180 °C. The contact angles for both the pitches at 180 ℃ were found to be lower (better wetting) than those at 170 °C. As it can be seen from the contact angle results, increasing temperature has a favorable effect on the wetting behavior of pitch due to the decrease in pitch viscosity, which leads to better spreading and penetration of pitch through

the coke bed. However, the change in the wettability of pitch-coke system with temperature seems to affect Pitch-6 more than Pitch-2. At 170 ºC, Pitch-6 wetted the coke less compared to Pitch-2. However, at 180 ºC, the reverse trend was observed. The effect of softening point on the wettability of coke by pitch is complex, and further work involving the study of the relation between the softening point and the viscosity of pitch is needed to understand the mechanism.

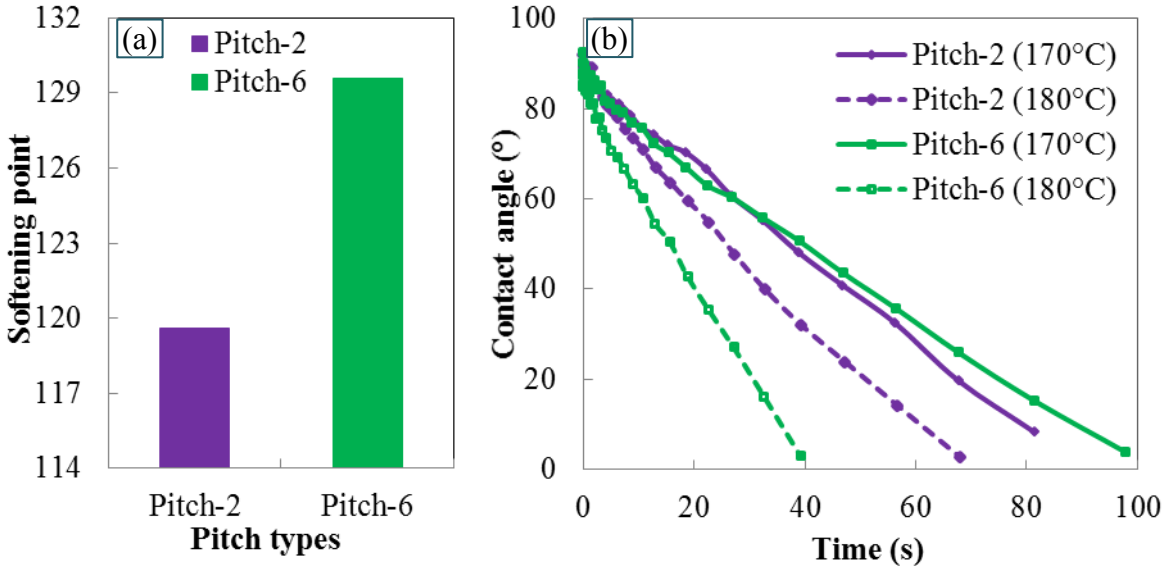

Figure 4.14: (a) Softening points of Pitch-2 and Pitch-6, (b) Dynamic contact angles of Pitch-2 and Pitch-6 on coke at 170 °C and 180 °C.

4.1.4 Effect of coke particle size distribution on wettability of pitch-coke system

Although the as received coke particles of +100 µm/-125 µm size were used in this study for the wetting tests, it was reported that some studies were carried out with coke particles which were first ground and then sieved to have the same particle size for the tests [34]. There does not seem to be any published work on the effect of preparation techniques of coke samples on the wettability of coke by pitch. The objective of this part

was to investigate the wetting of coke, which was prepared using two different techniques, by different pitches. As mentioned earlier, one coke sample was prepared by sieving the coke "as received", and +100 μm -125 μm size fraction was collected. This sample has been referred to as "as received". To prepare the second sample, the same coke was first crushed and then sieved. The same size fraction was used (+100 μm -125 μm), and this coke sample was referred to as "crushed". Thus, this wetting study shows the effect of crushing on the wettability of coke by pitch. Figure 4.15 shows the change in contact angle with time for five different pitches on the two coke samples (as received and crushed) prepared from the same source. The contact angles for both pitch/coke systems decreased with the increasing time. The results also showed that the contact angles were different for the coke samples although their wettability by five pitches, in general, followed a similar trend; Pitch-1 was the best-wetting and Pitch-5 was the least-wetting for both coke samples. The complete penetration time into the coke bed for the pitches (time at which the contact angle is zero) was significantly shorter for the "as received" coke sample than that for the "crushed" coke sample. The "as received" coke sample was completely wetted by all the pitches within 300 s as shown in Figure 4.15 (a). On the other hand, four of the five did not penetrate completely into the crushed coke bed even after 1200 s as shown in Figure 4.15 (b).

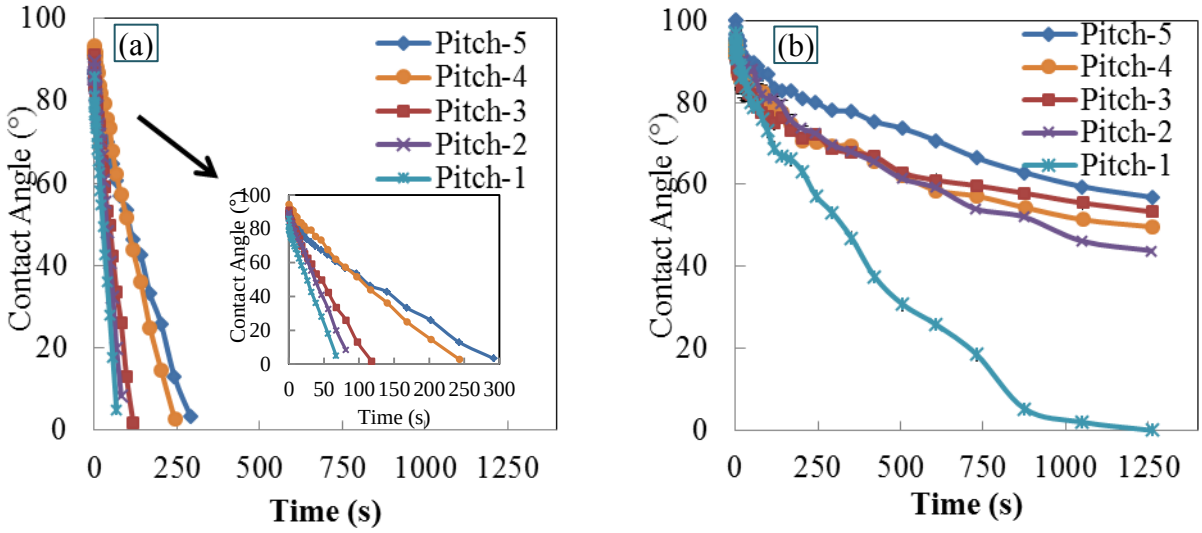

Figure 4.15: Dynamic contact angles of five different pitches on coke samples prepared using two different procedures (a) As received, (b) Crushed.

The contact angles measured at the initial time and at 60 s are shown in Figure 4.16, respectively, for all the pitches and the coke samples ("as received" and "crushed"). The initial time was taken as 5 s since it takes some time for the sessile-drop to stabilize on the coke bed. The initial contact angles of all pitches on the "as received" coke sample were slightly less compared to those of the crushed coke sample (Figure 4.16 (a)). However, the contact angles measured at 60 s for these two coke samples were significantly different (Figure 4.16 (b)). The contact angles were much greater with the "crushed" coke sample showing that it was wetted less by all the pitches compared to the "as received" coke sample. In order to understand the difference in wettability between the two coke samples by different pitches, the image analysis of both samples was carried out using SEM. The coke-pitch interfaces of the sessile-drops obtained from the wetting experiments were also investigated using optical microscopy to understand the wetting mechanism.

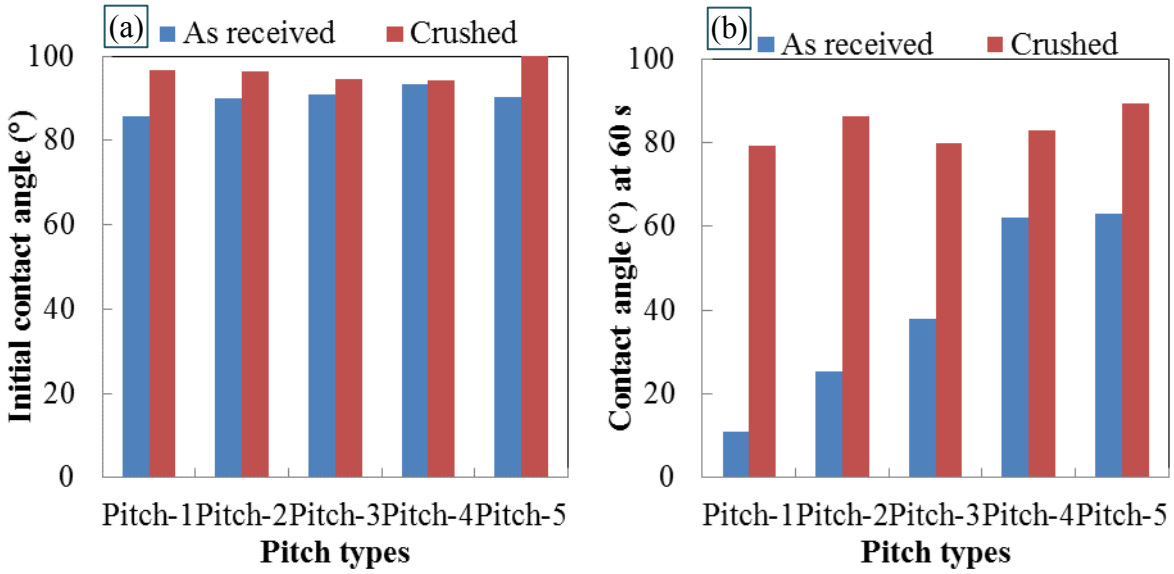

Figure 4.16: (a) Initial contact angle (at 5 s) and (b) Contact angle at 60 s for five different pitches on two coke samples.

4.1.4.1 SEM analysis

SEM is a useful tool to visualize the shape and the distribution of coke particles. It was found that there was no notable difference in the surface texture between the "as received" and "crushed" coke particles for the same size range (Figure 4.17). The SEM images of "as received" coke sample presented in Figure 4.17 (a) show that the particle size distribution is narrower, which means that the sizes of the particles were similar. However, the crushed coke particles appear to have a wider particle size distribution (Figure 4.17 (b)). Crushed coke sample contains finer particles of less than 100 µm generated during crushing even though they were prepared by the same sieving procedure as the one used for the preparation of "as received" coke sample. The finer particles fill the space between the larger particles. The mixture of coarse and fine particles of the crushed coke sample resulted in a more compact coke bed than that of the as received coke sample, and this

reduced the pitch penetration into the crushed coke bed. This is discussed in the following section.

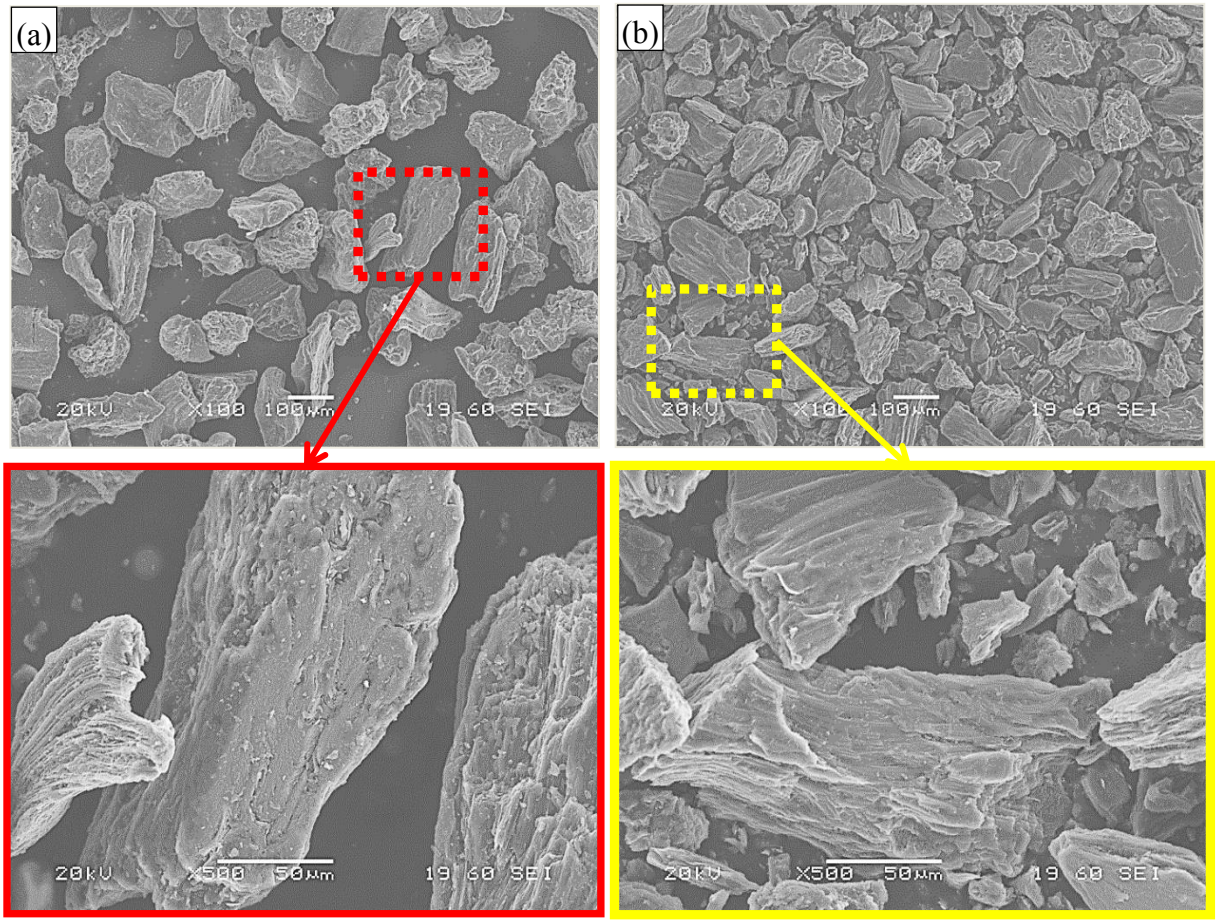

Figure 4.17: SEM Images of (a) As received, (b) Crushed coke samples

4.1.4.2 Optical microscopy analysis

Figure 4.18 presents the optical microscopy images of the pitch-coke interfaces in the sessile-drops for both coke samples. Coke, pitch, and pitch solid particles can be seen on these images. Figure 4.18 (a) shows that pitch penetrated into the bed of “as received” coke sample homogenously. Moreover, the solid particles of pitch are distributed homogenously in pitch around the coke particles. The bed of crushed coke sample,

however, displays different characteristics. Solid particles of pitch seem to form layers during wetting (Figure 4.18 (b)). Some of the solid particles of pitch were blocked by the finer crushed coke particles, which prevented them from entering into the coke bed. Consequently, a layer of solid particles of pitch was formed on the surface of the crushed coke bed. This layer acted as a filter and reduced the pitch penetration into the coke bed. This explains the lower wettability of crushed coke particles by the same pitches compared to the wettability of the "as received" coke particles. It can also explain the differences in contact angles observed at initial times and at 60 s. It takes some time for the filter-like layer to form. Until the formation of this layer, the contact angles of both coke samples were similar. Later, the difference became more pronounced.

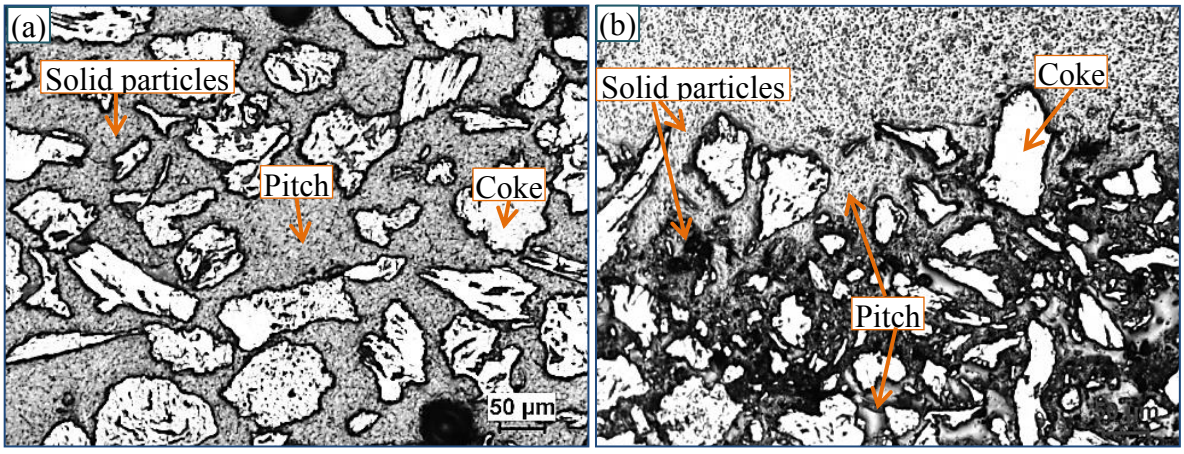

Figure 4.18: Optical microscope images of Pitch-3 with (a) As received and (b) Crushed coke samples.

4.2 Effect of pitch properties on anode properties

4.2.1 Calibration of the thermogravimetric analyzer

To find the temperature in different regions of the furnace, a calibration was carried out at the beginning of the study. Nitrogen gas was passed through the furnace, and the furnace was heated to 600 ºC. When the temperature stabilized at 600 ºC, a thermocouple was used to measure the temperature at different positions inside the furnace. Figure 4.19 (a) shows the furnace calibration data. The uniform region in the furnace was found to be between 24 cm and 55 cm from the top of the furnace (Figure 4.19 (b)). In TGA experiments, the anode sample was placed in the region where the temperature was uniform.

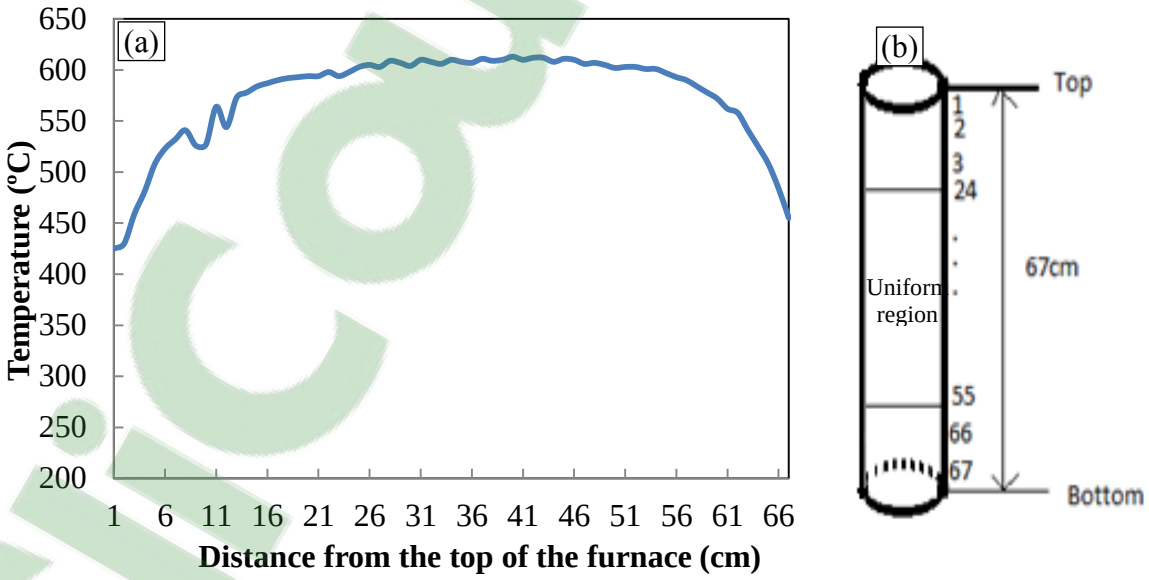

Figure 4.19: (a) Furnace calibration curve, (b) Distance from the top of the furnace.

4.2.2 Effect of pitch percentage on anode properties

The effect of pitch content on anode properties was studied by making anodes under the same conditions with four different percentages (13 %, 15 %, 17 %, and 20 %) of Pitch-2 using the standard recipe. Then, these anodes were cored, and the cores were baked to 1100 ºC using the standard heating rate in the laboratory. The density and electrical resistivity of the cores were measured before and after baking. Figure 4.20 (a) and (b) show the results in dimensionless form. In this study, the dimensionless value was calculated by dividing a given quantity by the average value of that quantity for all samples. It can be seen that the green anode density (GAD) increases with increasing pitch percentage up to 17 %, above which the GAD remains almost constant (Figure 4.20 (a)). This is expected since increase in pitch content after the optimum value has an adverse effect on GAD (and baked anode density). As the coke apparent density is greater than the pitch density, excess pitch increases the anode volume, and this increased volume is filled with pitch, a lower density material. Normally, with further increase in pitch content (above 20 %), a decrease in GAD would be expected [1]. The results also show that the value of baked anode density (BAD) is less than the value of GAD (Figure 4.20 (a)) as expected. The volatile release (hydrogen, methane, and tar) during baking creates pores, reducing density. The carbonization of pitch helps increase the baked anode density by restructuring the carbon matrix. The overall impact is always a BAD lower than a GAD. BAD is low when the pitch content is insufficient (13 %) because of the high porosity of green anode further augmented by the devolatilization. As the pitch percentage increases, the porosity decreases increasing the density. This occurs up to 17 % pitch percentage here (Figure 4.20 (a)).

Excess pitch causes a large amount of (rapid) devolatilization, again leaving a highly porous structure (possibly with a significant level of crack formation). This reduces the density as can be seen in Figure 4.20 (a).

It can be observed from Figure 4.20 (b) that the electrical resistivity of anodes decreases significantly after baking. In green anodes, the presence of a large volume of pores increases the electrical resistivity. For this reason, the green anode electrical resistivity (GER) is high for the anode containing 13 % pitch. As the pitch level increases, the pores are filled with pitch, decreasing the resistivity, up to an optimum value as seen in Figure 4.20 (b) for the anode with 17 % pitch. Excess pitch however again increases the resistivity as is the case with anodes containing 17 % and 20 % pitch. In baked anodes, the presence of a large volume of pores (either due to the lack of pitch or an excess amount of pitch which creates a large number of pores/cracks during baking) also increases the electrical resistivity, BER, (anodes with 13 % and 20 % pitch). Optimum (or close to optimum) level of pitch reduces the BER as seen in Figure 4.20 (b) for anodes with 15 % and 17 % pitch. The density and electrical resistivity results seem to indicate that the optimum level of pitch is in the 15-17 % range.

The air and CO_2 reactivity tests were also carried out for the baked anode core samples. It was found that both air and CO_2 reactivities were influenced by the pitch percentage (Figure 4.20 (c) and (d), respectively). The air reactivity mainly depends on the availability of combustible material (in this case, carbon); thus, it increases with density. This can be seen in Figure 4.20 (c) for anodes with 15 % and 17 % pitch. This is due to the increase in surface contact between air and anode because the air reactivity is mainly

reaction controlled. As the pitch content increases further, the anode becomes over-pitched and more carbonized pitch is exposed to air. Since carbonized pitch reacts more easily with air compared to coke, the air reactivity increases with increase in pitch content. As for the anode with 13 % pitch, the high volume of pores allows air to penetrate into the anode increasing the air reactivity. Thus, the surface morphology seems to have some impact as well on air reactivity. On the other hand, the CO_2 reactivity is diffusion controlled. Therefore, it is inversely proportional to the density which is strongly affected by the pitch content (Figure 4.20 (d)). As the density increases, the CO_2 reactivity decreases, and vice versa. The under-pitched anode made with 13 % pitch has the highest CO_2 reactivity. This is due to its higher porosity which, consequently, increased the diffusion of CO_2 into the anode.

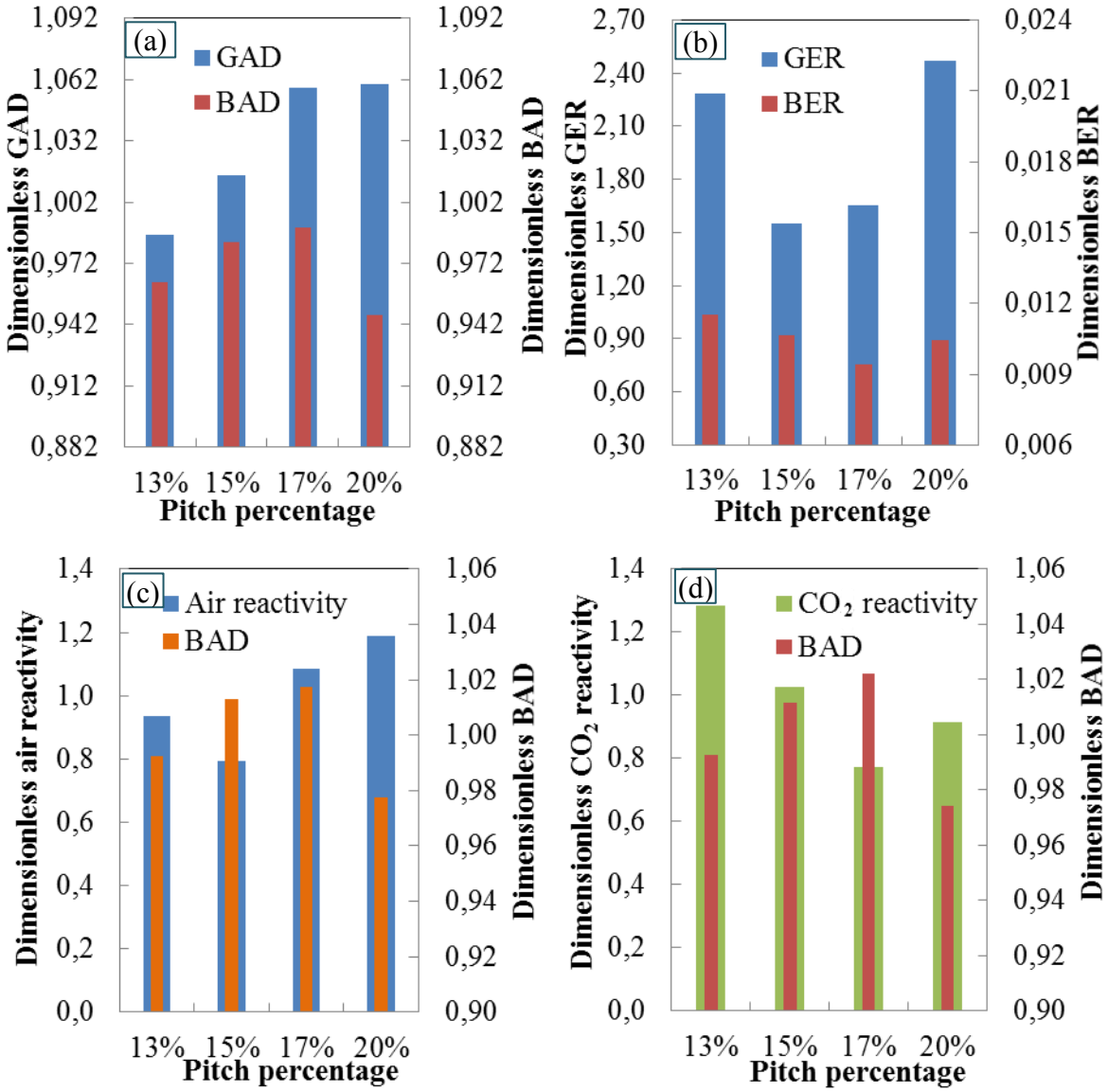

Figure 4.20: (a) Density of anode cores containing different pitch percentages before and after baking; (b) Electrical resistivity of anode cores containing different pitch percentages before and after baking; (c) CO_2 and (d) Air reactivities with baked density of anode cores containing different pitch percentages.

4.2.2.1 Optical microscopy analysis

The green and baked anode core samples were characterized using the optical microscopy. The percentages of pore, pitch, and coke in green anodes were determined by the image analysis. Figure 4.21 shows the original and treated images for the anode containing 20 % pitch. The results show that green anode with a higher pitch percentage has fewer pores, which is confirmed by the higher density of green anode core (Figure 4.20 (a)). However, it is difficult to apply this technique to baked anodes to separate coke and pitch due to the similarity of color and appearance of carbonized pitch and calcined petroleum coke after baking at high temperatures.

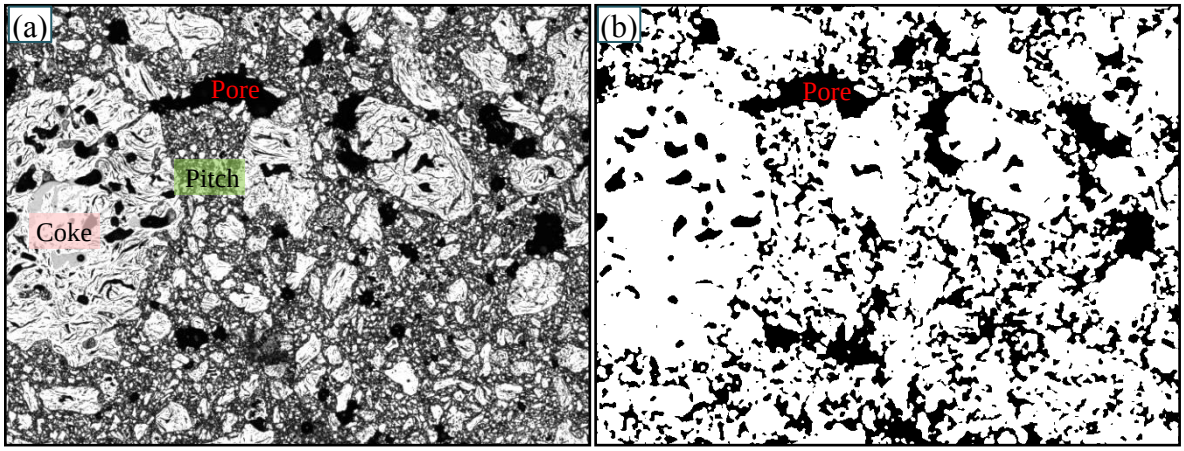

Figure 4.21: Green anode with 20 % Pitch-2: (a) Optical microscopy image, (b) Pores visualized using the image analysis.

4.2.2.2 SEM analysis

Scanning electron microscopy (SEM) with its large depth of focus is well suited to identify the topography of different percentage of pitch in the green anodes at high magnification. It can be seen in Figure 4.22 that all pitch surfaces contain solid particles, cracks, and pores. All four green anodes with different percentages of pitch show bonding

between coke and pitch as well as micro-cracks and solid particles present in the pitch. It was reported that the mesophase (> 4 µm) and mesogens (2 - 4 µm) can be present in pitch [1, 9]. Thus, the images indicate that the pitch in this study does not seem to contain mesophase and mesogens. Instead, the particles appear to be carbon black or primary QI according to their characteristics observed form the images [16]. The anode with 20 % pitch content has the most micro-cracks among these four green anodes (Figure 4.22 (d)) as expected. These different structures influence the baked anode properties such as density, air/CO_2 reactivity, and electrical resistivity.

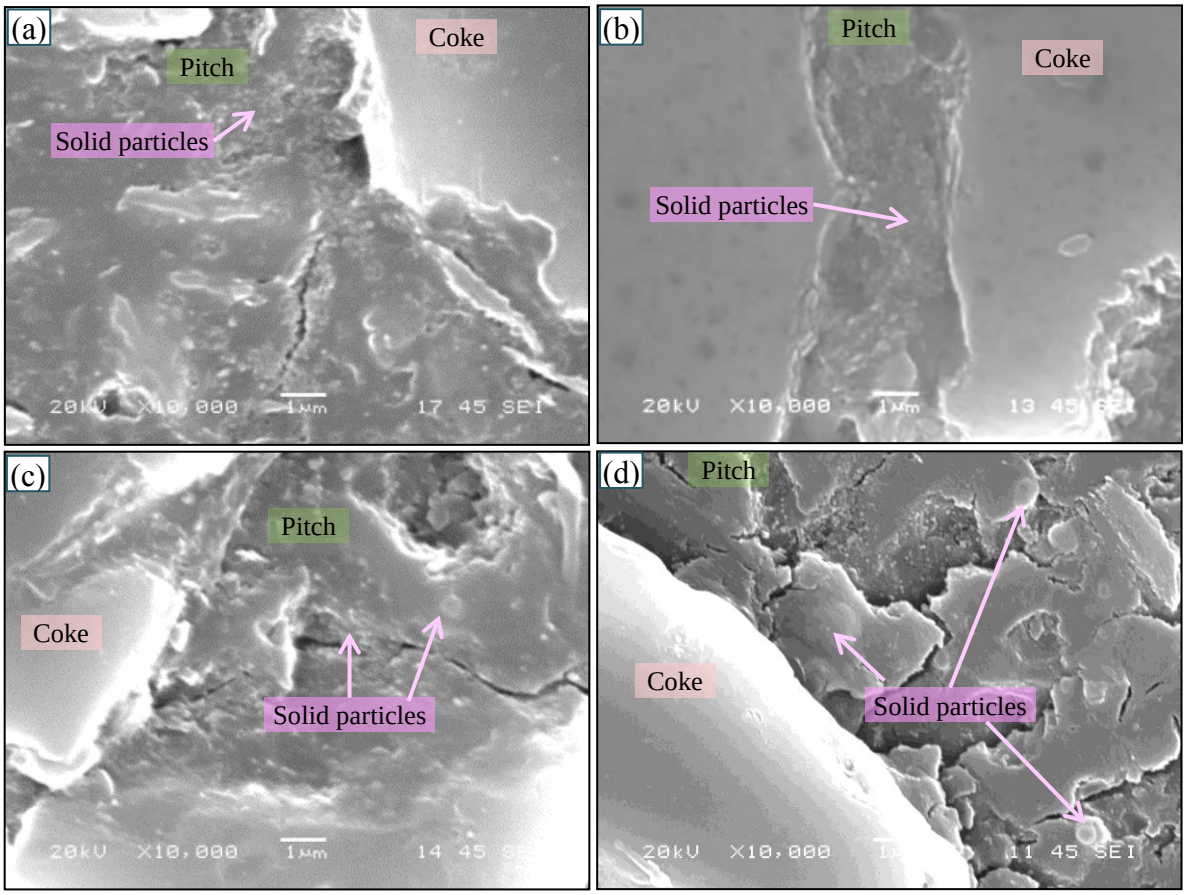

Figure 4.22: SEM images of green anode samples with different percentages of Pitch-2: (a) 13 %, (b) 15 %, (c) 17 %, and (d) 20 %.

The SEM images of baked anode samples with different percentages of Pitch-2 are shown in Figure 4.23. The surface topography which reflects the structural order of the anode sample was different in the baked anodes after etching by air at 525 °C for 20 min with a low flowrate of air. It was difficult to find the textures in carbonized pitch of the anode containing 13 % pitch due to the small quantity of pitch left after etching. Lamellar component in etched surface was observed in Figure 4.23 (b-c). It was not possible to see the textures of carbonized pitch in baked anode with 20 % pitch due to inadequate etching. Probably longer etching time was necessary for this sample.

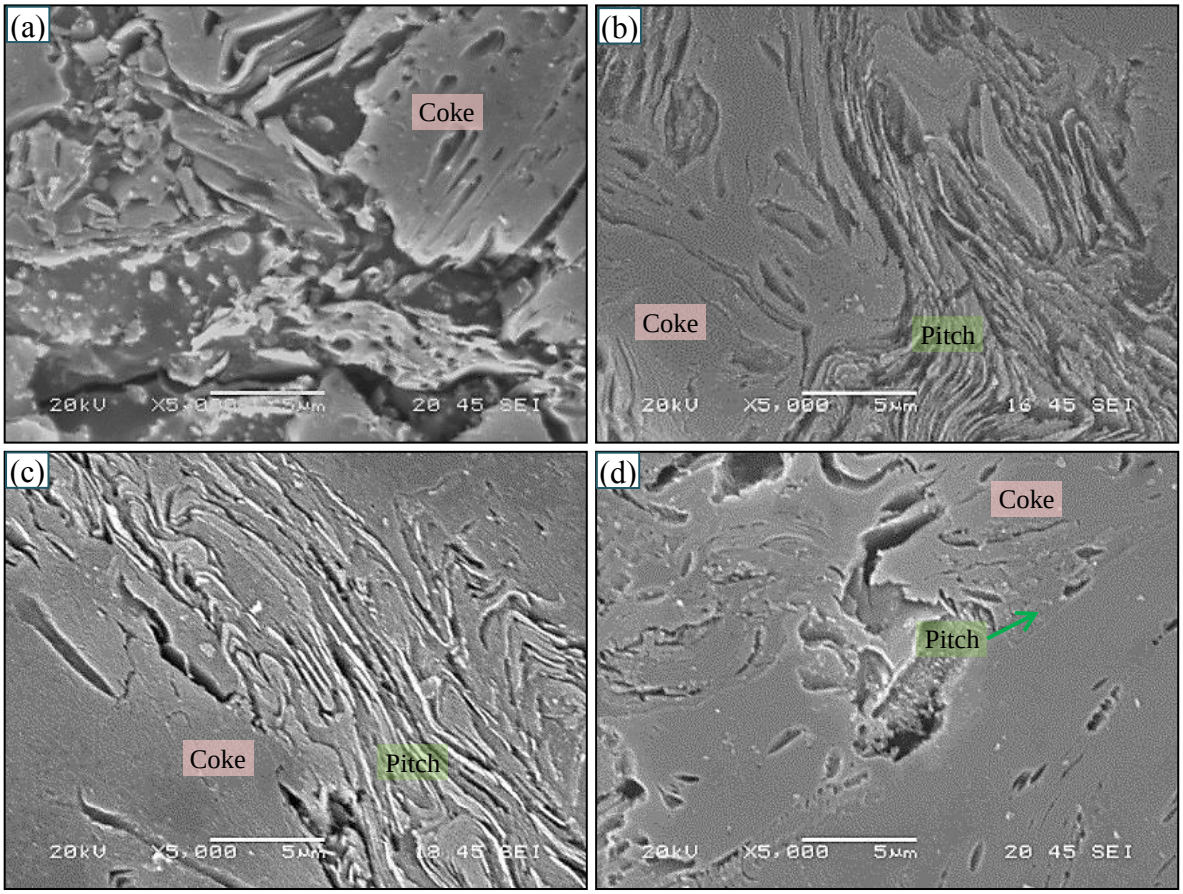

Figure 4.23: SEM images of baked anode samples with different percentages of Pitch-2: (a) 13 %, (b) 15 %, (c) 17 %, and (d) 20 %.

4.2.3 Effect of different pitches on anode properties

4.2.3.1 Relationship between green anode density and contact angle

Anodes were fabricated with six pitches with different properties and were baked using a standard procedure. The green and baked core samples were characterized as stated previously. The different properties such as green/baked density and electrical resistivity as well as air/CO_2 reactivity were analyzed and compared for different samples. It was observed that the green anode density generally increases with decreasing contact angle obtained for different pitches at 60 s (Figure 4.24). The dimensionless contact angle is the ratio of a given contact angle to the average of all contact angles. This indicates that the wettability of coke by different pitches plays an important role on anode properties. It was shown previously that the wettability of pitch by coke is a function of the coke and pitch structure as well as the chemical composition of their surfaces.

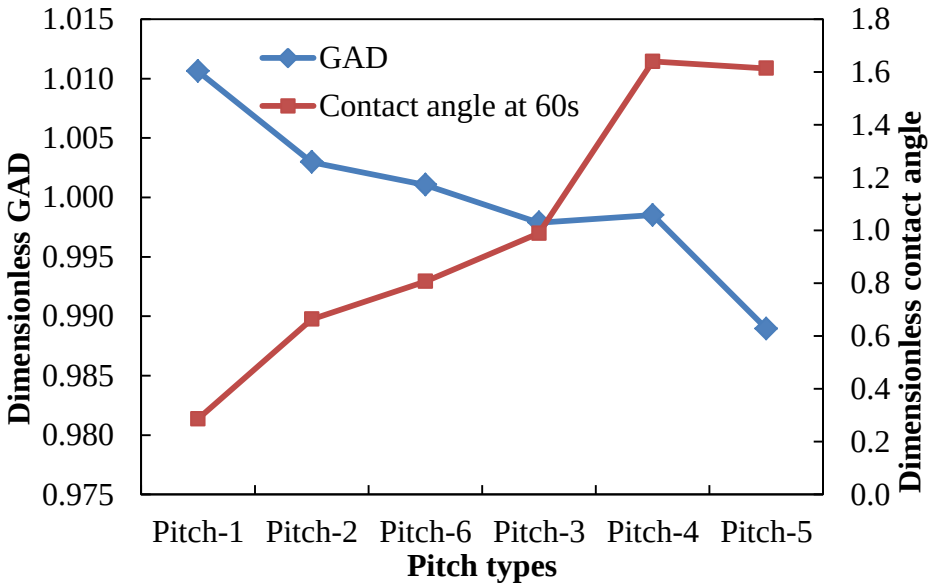

Figure 4.24: Relationship between green anode density and contact angle at 60 s.

4.2.3.2 Relationship between anode density and electrical resistivity before and after baking

Figure 4.25 (a) shows the variation in the density of the anode core samples, made with different pitches, before and after baking. The dimensionless BAD/GAD is the ratio of a given BAD/GAD to the average of all BAD/GAD. It can be observed that the density of the baked anode (BAD) is less than that of the corresponding green anode (GAD) and the green anode density generally decreases with decreasing wettability (increasing contact angle) as discussed previously. However, the density of baked anodes does not show the same trend as that of the green anodes made with the same pitches; however, the variation in baked anode density is not significant (0.979 to 0.988). This slight variation might be due to the different chemical components present in different pitches, which affect the amounts of volatiles released during the baking process, and consequently resulting in slightly different baked densities.

Figure 4.25 (b) shows the variation in BER/GER of the anode core samples, made with different pitches, before and after baking. The dimensionless BER/GER is the ratio of a given BER/GER to the average of all BER/GER. As mentioned previously, the electrical resistivity of baked anodes (BER) is significantly smaller than those of green anodes (GER) because pitch, before baking, is electrically non-conducting. During the anode baking process, the pitch in anode is carbonized and binds the dry aggregates together, yielding a strong coke structure in baked anodes. As seen in Figure 4.25 (b), BER generally follows a trend similar to GER (except for Pitches 5 and 6). Higher GER results in higher BER after baking, and vice versa.

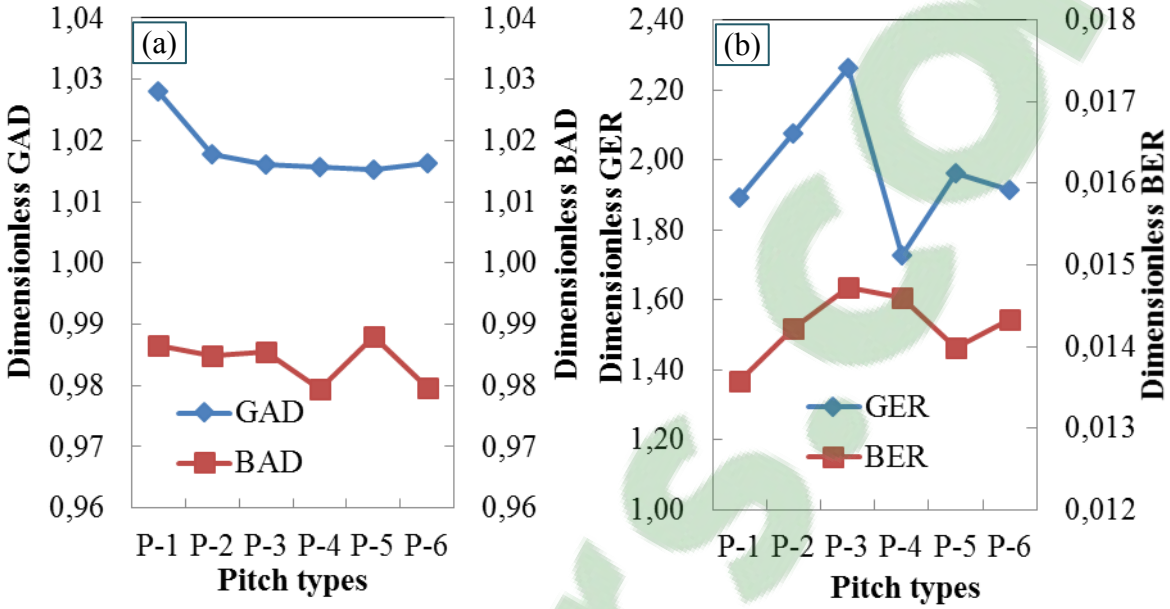

Figure 4.25: (a) Density of anodes (cores) with different pitches before and after baking, (b) Electrical resistivity of anodes (cores) with different pitches before and after baking.

4.2.3.3 Relationship between electrical resistivity and density of baked anode

Figure 4.26 shows the variation in baked anode electrical resistivity (BER) with the baked anode density (BAD). It can be seen that there exists a good correlation between BER and BAD. As BAD increases, BER decreases. As the density of an anode sample increases, there is less porosity, which helps reduce the electrical resistivity.

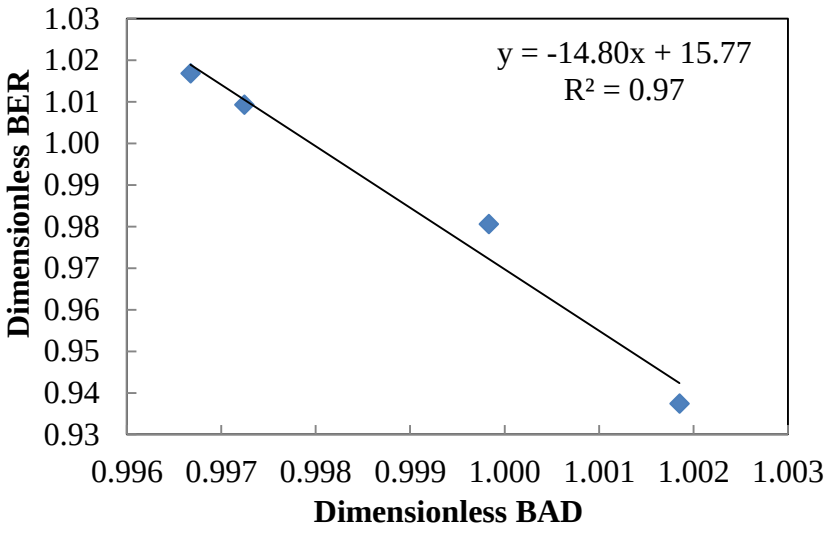

Figure 4.26: Correlation between baked electrical resistivity and baked density of anode core samples.

4.2.3.4 Relationship between baked anode density and reactivities

The air reactivity increases with increase in BAD (with an R^2 value of 0.56 Figure 4.27 (d)); but the CO_2 reactivity shows the opposite trend, it decreases with increase in BAD (with the R^2 value of 0.97 Figure 4.27 (b)). As explained previously, these results show that air and CO_2 reactivities follow different mechanisms. Air reactivity is fast and mainly reaction controlled. It can react with any carbon compound. Thus, with increase in density, air is in contact with more carbon leading to more reaction. On the other hand, CO_2 reactivity is slow and diffusion controlled. It increases with increasing anode porosity. Anodes which have low baked density are more porous. Thus, lower density anodes have higher CO_2 reactivity.

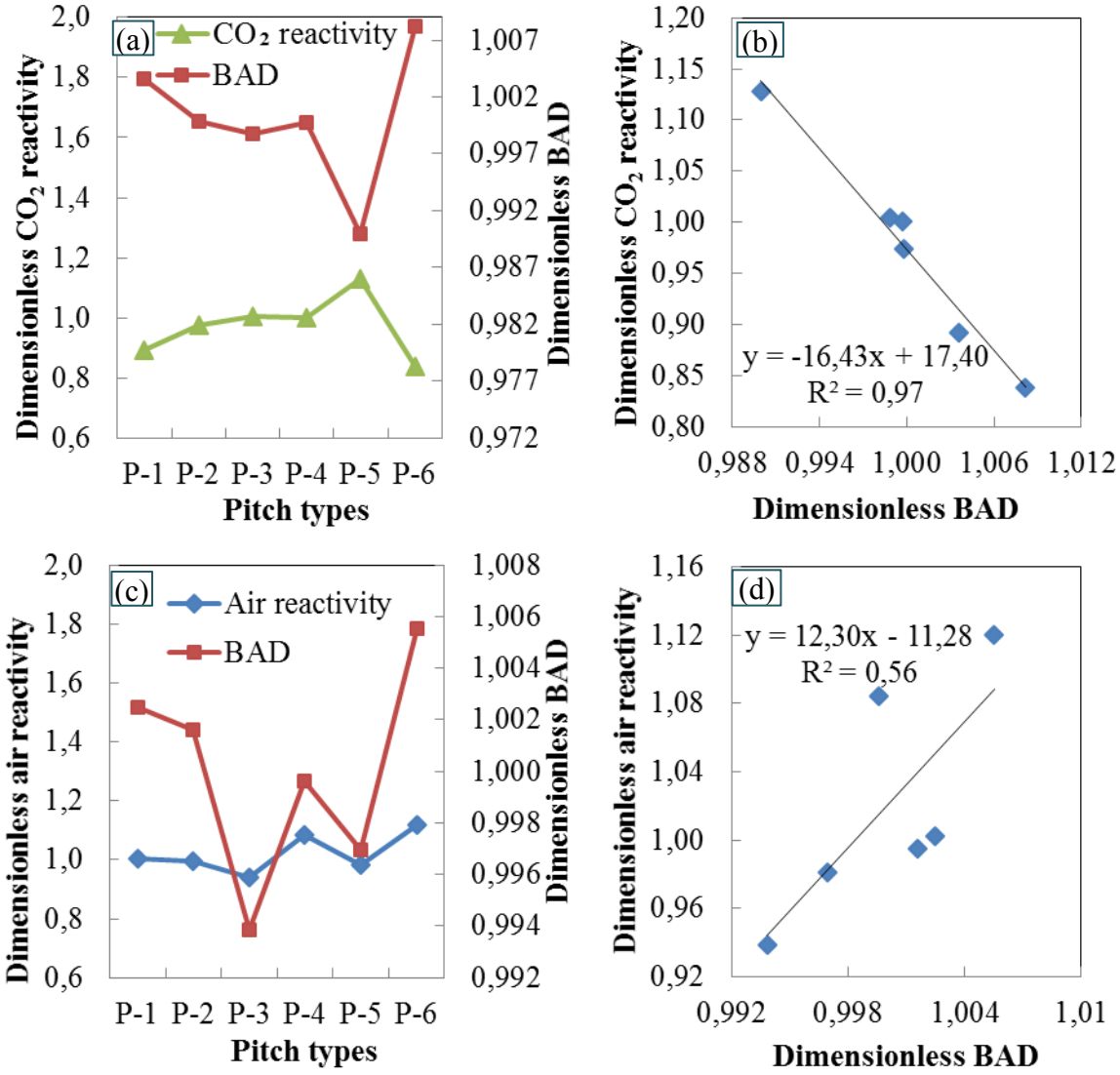

Figure 4.27: (a) Relationship between density and CO_2 reactivity of baked anodes (cores) made with different pitches, (b) Correlation between CO_2 reactivity and baked anode (cores) density, (a) Relationship between density and air reactivity of baked anodes (cores) made with different pitches, (b) Correlation between air reactivity and baked anode (cores) density.

4.2.3.5 Image analysis of green anodes made with different pitches

The optical microscopy provides some information on the distribution of the coal tar pitch in green anode samples (Figure 4.28). Pitch and the coke particles can be seen on all

images. However, the differences among the different pitches are not obvious in the optical microscopy images at low magnification. Therefore, the scanning electron microscope (SEM) was used to understand the topography of pitch and the interfaces between pitch and coke particles in green anodes. The SEM images are presented in Figure 4.29.

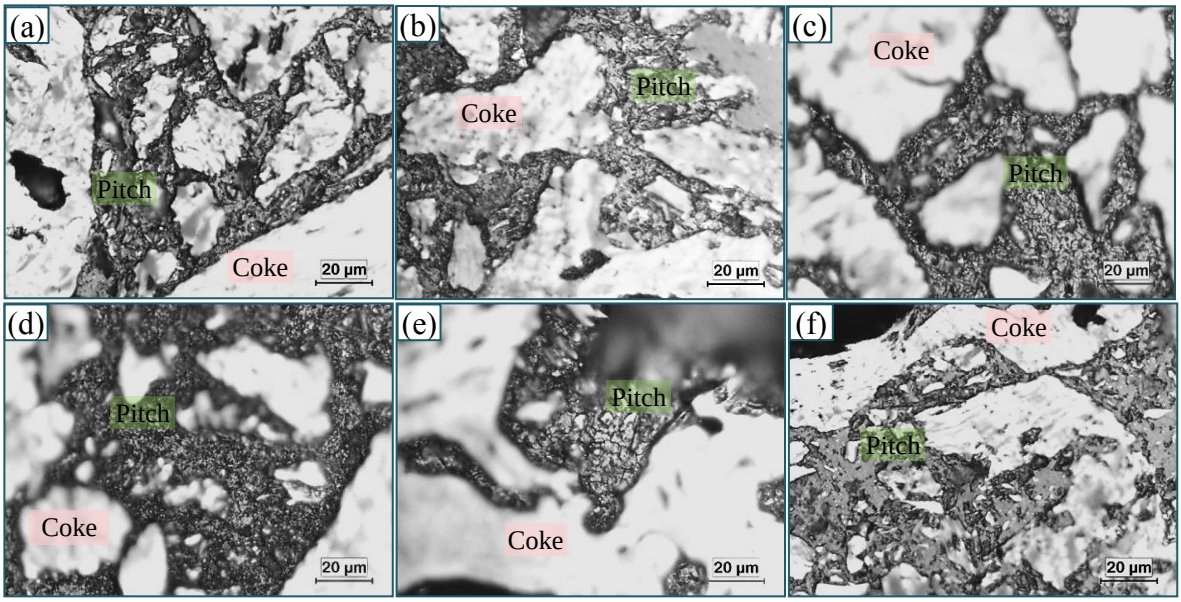

Figure 4.28: Optical microscopy images of green anode cores with different pitches (a) Pitch-1, (b) Pitch-2, (c) Pitch-6, (d) Pitch-3, (e) Pitch-4, and (f) Pitch-5.

As can be seen in Figure 4.29, all pitches show good bonding with coke. While some cracks are present at these interfaces, those of Pitch-4 are quite pronounced (Figure 4.29 (e)). The cracks of Pitch-6 are also fairly noticeable (Figure 4.29 (e)). On SEM images, it is possible to differentiate pitch and coke particles. All pitch surfaces contain solid particles, cracks, and pores. It was reported that the mesophase particles are > 4 µm and mesogens are 2 - 4 µm [1, 9]. Thus, these images indicate that the pitches used in this study do not contain mesophase and mesogens. An SEM image illustrating the appearance of agglomerated submicron particles is shown in Figure 4.29 (b). These particles appear to

be carbon black according to their characteristics. Pitch-3 has the most solid particles, and Pitch-1 has the least solid particles. The solid particles in Pitch-2 display a patchy distribution, and the size of solid particles in Pitch-5 seems to be larger than those of the other pitches. These different structures may contribute to the wetting behaviour and the formation of carbonized pitch during the anode baking process. This needs further study.

In order to study the chemical composition of anodes before and after baking, the XPS results of green and baked anodes (with Pitch-2 and/or Pitch-4) were analyzed [Appendix 3].

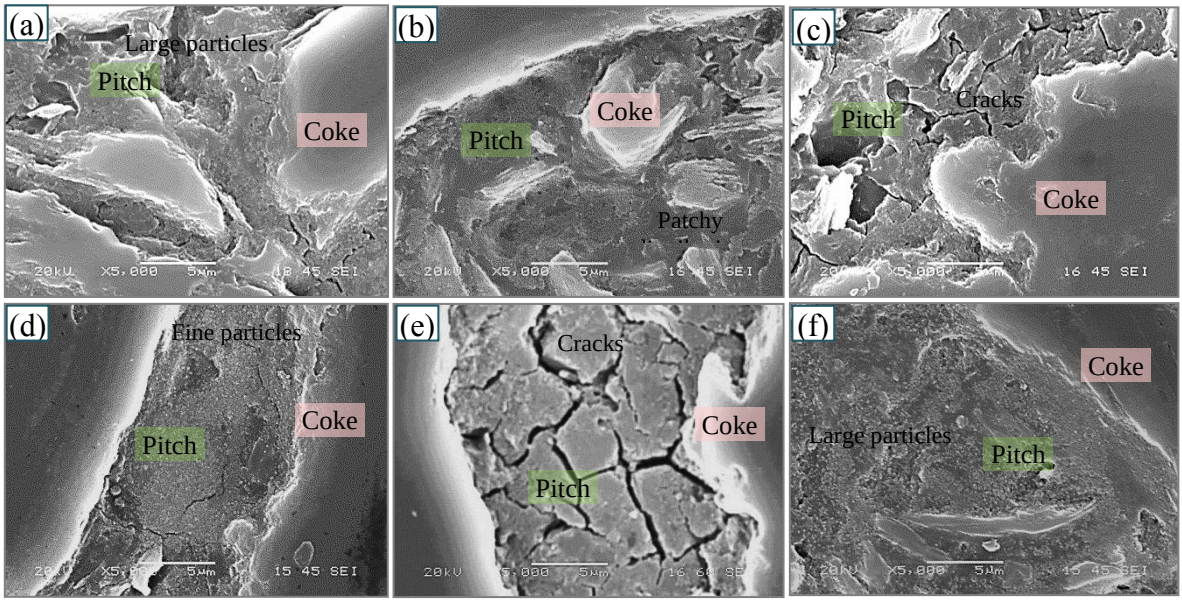

Figure 4.29: SEM images of green anode samples with different pitches:
(a) Pitch-1, (b) Pitch-2, (c) Pitch-6, (d) Pitch-3, (e) Pitch-4, and (f) Pitch-5.

4.2.3.6 Different structures of carbonized pitch in baked anodes

Figure 4.30 (a) shows an optical microscopy image of a baked anode sample made with Pitch-2 before etching. Due to the similar hardness and appearance of coke and carbonized pitch in baked anodes, it is difficult to identify coke, carbonized pitch, and their

interface after polishing the surface. A new method to etch the anodes has been developed in this study as explained in the methodology section. The images of baked anodes samples etched under different conditions are shown in Appendix 4. As shown in Figure 4.30 (b), it is possible to differentiate carbonized pitch, coke, and their interface in optical microscopy images of baked anodes after etching.

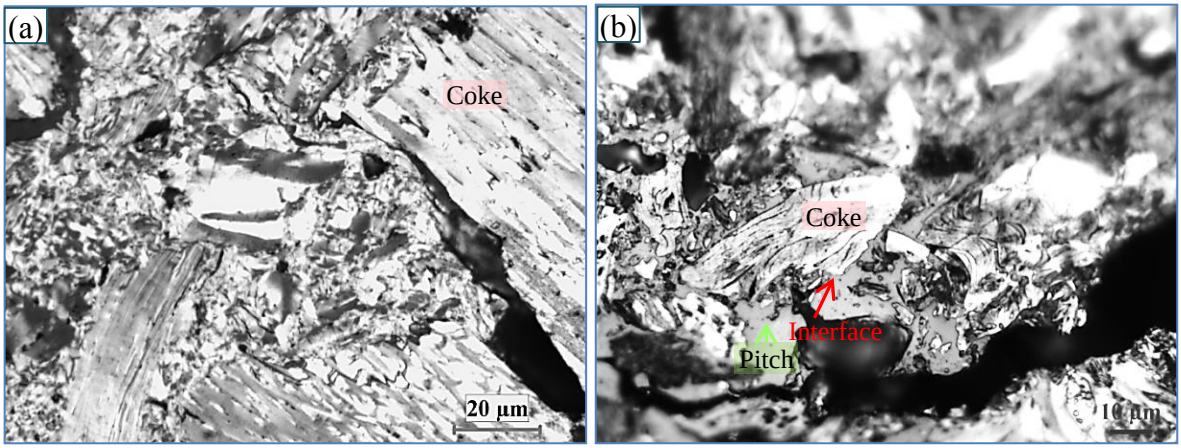

Figure 4.30: Optical microscopy images of a baked anode sample (made with Pitch-2): (a) before etching, (b) after etching.

Figure 4.31 (a) shows an SEM image of a baked anode sample (made using Pitch-2) before etching. It is difficult to identify coke, carbonized pitch, and their interface after polishing the surface. Figure 4.31 (b) shows an SEM image of a baked anode sample after etching. It can be seen that the carbonized pitch could be distinguished from the coke and could be characterized in terms of its different textural components, namely, granular (see Figure 4.31 (b1)) and lamellar (Figure 4.31 (b2)). Figure 4.31 (b1) shows the presence of parallel arrangements of short ridges and channels broken by pits. Figure 4.31 (b2) shows that the basal layer alignment is poor and random. The method is safe, simple, and effective

for etching such samples which makes the identification of anode constituents possible (see Figure 4.30 (b) and Figure 4.31 (b), (b1), (b2)).

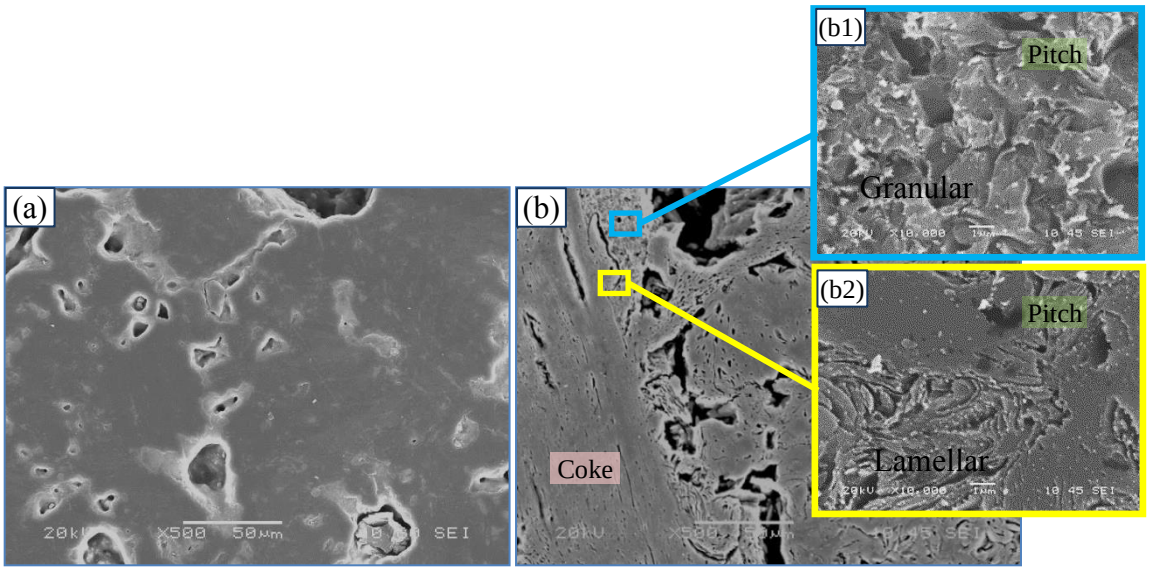

Figure 4.31: SEM image of a baked anode sample (made with Pitch-2) (a) before etching, (b) after etching.

Figure 4.32 shows six different textures that can be found in the same binder pitch (Pitch-5) in an anode, and these textures can be characterized in terms of the three components: lamellar (Figure 4.32 (a) and (d)), intermediate (Figure 4.32 (b) and (e)), and granular (Figure 4.32 (c) and (f)) [16]. Figure 4.32 (a) reveals the presence of smooth river patterns; Figure 4.32 (d) presents small distorted lamellar structures. The structure presented in Figure 4.32 (b) is like sponge with short ridges and channels often branched with pits. Figure 4.32 (e) displays parallel arrangements of ridges and channels broken by pits. Figure 4.32 (c) shows poor and random basal layer alignment. The structure shown in Figure 4.32 (f) is arranged like rays or in circular pattern. The formation of pores or pits displayed in Figure 4.32 (b) and Figure 4.32 (e) might be due to the loss of particles during

the oxidation process. It is difficult to measure the proportion of different components of the carbonized pitch in an anode because of the small percentage of pitch and the interference of approximately 65 % petroleum coke, 20 % recycled anode and butt particles with a wide range of size distribution. Further study is needed to correlate the anode properties with the proportion of various structural components in different binder pitches.

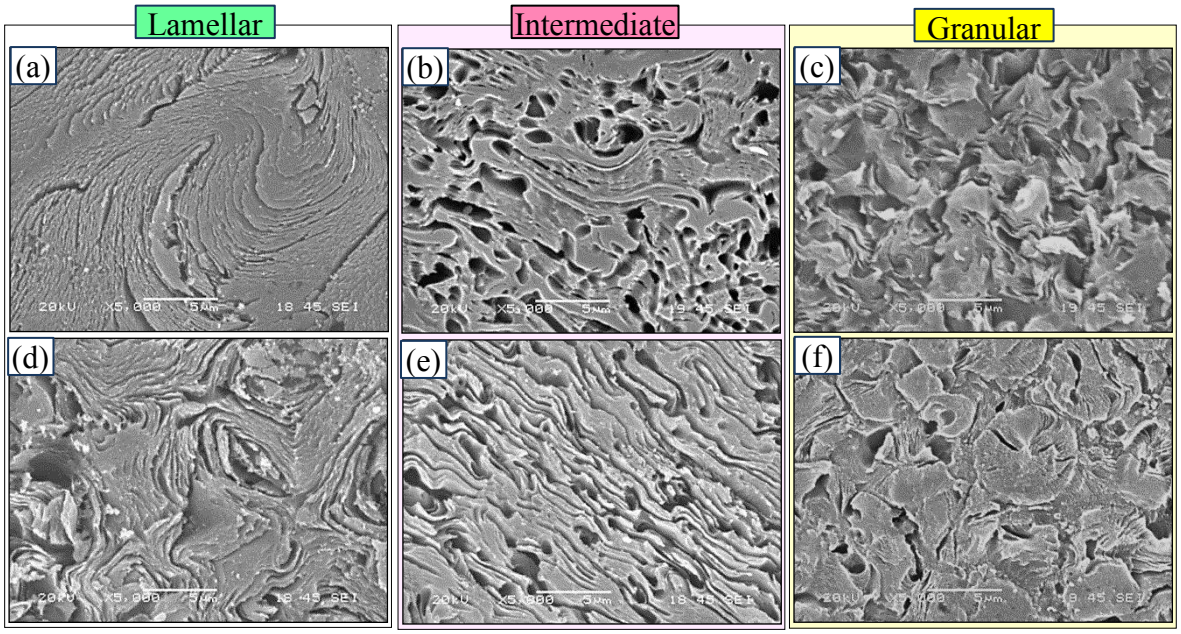

Figure 4.32: Components visible on the etched surface of binder pitch (Pitch-5) in anode: (a) Lamellar: smooth river pattern, (b) Intermediate: sponge with short ridges pattern, (c) Granular: random basal layer alignment pattern, (d) Lamellar: small distorted lamellar pattern, (e) Intermediate: parallel arrangements of ridges and pits pattern, (f) Granular: rays or in circular pattern.

4.2.3.7 Pore images in green and baked anodes

Coke contains pores and cracks, and the presence of very small pores prevents the penetration of pitch into the coke particles. In general, there are two kinds of pores in coke particles: open pore and closed pore. Figure 4.33 (a) shows a nearly empty (E) coke pore

and a pitch filled (F) coke pore in a green anode. Figure 4.33 (b) shows a relatively empty (E) coke pore formed and some solid particles (F) found in a coke pore after baking. The solid particles inside the pores may be the carbonized pitch. It is possible that the redistribution of pitch in the void space between the particles and further pitch impregnation into the pores of the coke particles occur during baking at low temperatures when pitch becomes fluid. Furthermore, the thermal decomposition of binder pitch results in the release of volatiles and formation of carbonized pitch and pores [17, 18].

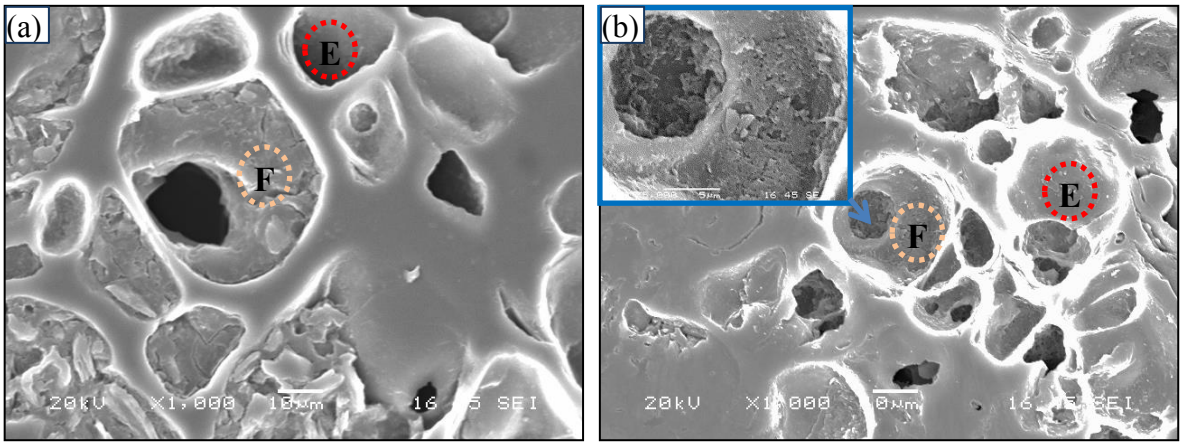

Figure 4.33: SEM images of pores of coke in (a) green anode and (b) baked anode.
(E: empty pore, F: Pore filled with particles/pitch.)

4.2.3.8 Image analysis of baked anodes produced with different pitches

As shown in Figure 4.34, it is possible to differentiate carbonized pitch, coke, and pores in optical microscopy images of baked anodes after etching with air at 525 °C. The coke appears to have various surface textures (anisotropic, isotropic) (Figure 4.34). It was reported in the literature that petroleum coke with an isotropic structure has a detrimental influence on anode thermo-mechanical properties [50]. It is difficult to obtain the proportion of the three different coke textures in industrial anodes due to the large range of

coke particle sizes and the small area analyzed with optical microscope and SEM. Also, it is not easy to see the basic structural units present in carbonized pitch of anode in the images taken with the optical microscope. SEM with its large depth of focus is better-suited for such studies; therefore, SEM was also used to understand the topography of carbonized pitch and the interface between carbonized pitch and petroleum coke in anodes.

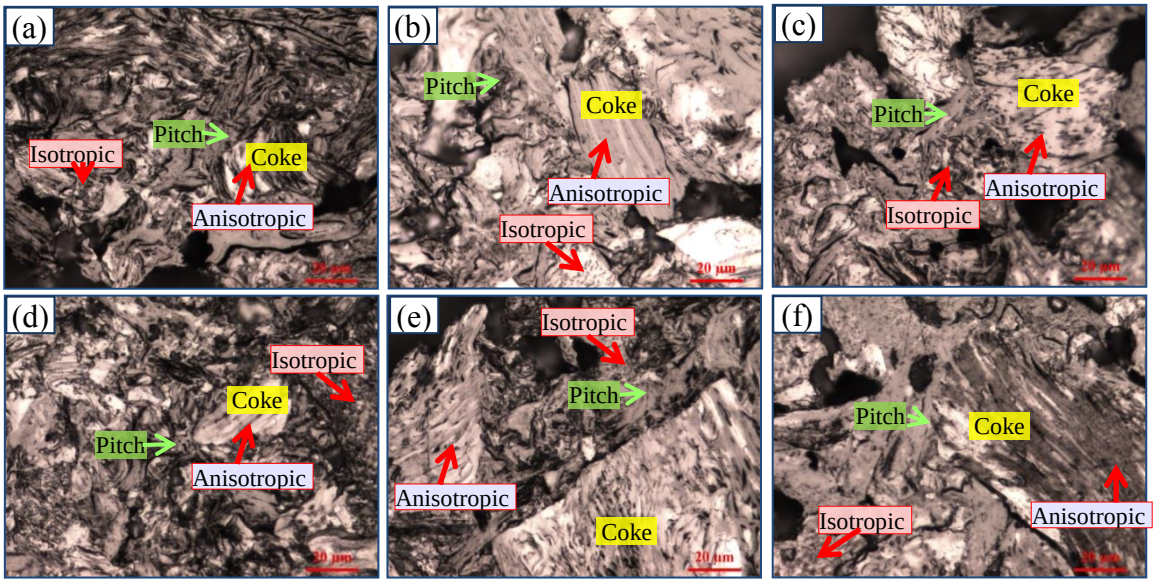

Figure 4.34: Optical microscopy images of baked anode cores with different pitches (a) Pitch-1, (b) Pitch-2, (c) Pitch-6, (d) Pitch-3, (e) Pitch-4, and (f) Pitch-5.

Figure 4.35 shows the appearance of interfaces between coke and carbonized pitch with different surface textures, namely lamellar, intermediate, and granular. Lamellar component in etched surface is observed as alternate arrangement of ridges and channels (Figure 4.35 (a)). Granular component exhibits poor and random basal-layer alignment (Figure 4.35 (c)). This is not in agreement with the results reported in the literature. The granular component of carbonized pitch in laboratory anodes was found to have a uniformly pitted texture [16]. Intermediate component (Figure 4.35 (b)) is the mixture of

the lamellar and granular components. It has small distorted lamellar structure with short ridges. However, there are no elongated grains observed in this component, which is in agreement with literature [16]. The lamellar and intermediate components of carbonized pitch bond well with coke while there are cracks present at the interface of granular carbonized pitch component and coke (see Figure 4.35 (c)).

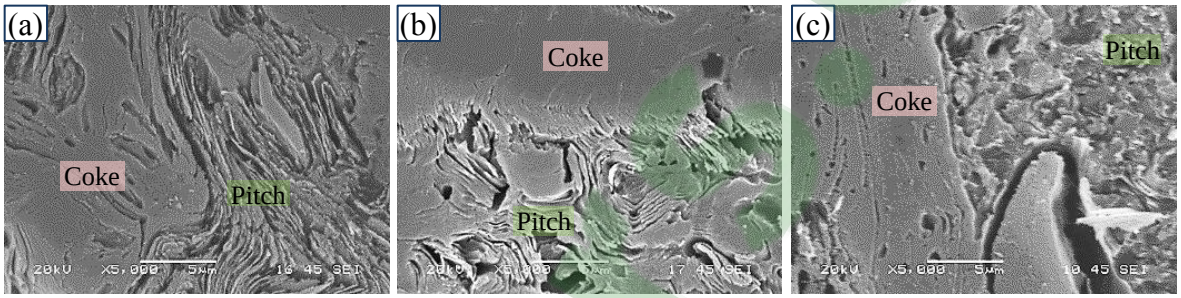

Figure 4.35: Components visible on etched surfaces of the interface between carbonized pitch and coke in a baked anode: (a) Lamellar, (b) Intermediate, and (c) Granular.

As mentioned in section 4.2.2.6, these three different textures (lamellar, intermediate, and granular) are found in the carbonized pitch of all the anodes produced in this study. However, it is difficult to measure the proportion of the different components of the carbonized pitch in an anode because of the small percentage of pitch and the interference of small coke particles. Further study is needed to develop the method to measure the proportion of these three different components for the carbonized pitch in an anode and correlate the anode properties with the components in different carbonized pitches.

4.2.4 Image analysis of anodes baked at different temperatures (evolution of anode structure during baking)

The anodes were produced using Pitch-2 and baked to different temperatures as explained in the methodology section. After baking, they were examined using the optical microscopy (see Figure 4.36) in order to study the evolution of anode structure (structure of carbonized pitch and pitch-coke interface). The results show that Pitch-2 in anode was carbonized and bound the coke particles during the anode baking process as expected. It was found that pitch, coke, and pores are easily identifiable for anodes baked to temperatures less than 400 ºC. The differences in pitch structure of the anodes are evident as can be seen from the optical microscopy images. The anodes baked to higher temperatures (≥ 600 ºC) are more porous compared to those baked to lower temperatures. This is due to the release of pitch volatiles (hydrogen, methane, and tar), which was confirmed by the kinetic study. The solidification of pitch and the formation of carbon bridges between coke and pitch occur at higher temperatures. However, due to the similar hardness and composition of calcined coke and carbonized pitch in baked anodes, it is difficult to identify coke, pitch, and their interface after polishing the surface. The polished surfaces of baked anode samples were etched in air at 525 ºC to see the details of the carbonized pitch-coke interface and the pitch structure. The SEM results show that there are three different surface textures in carbonized pitch for anodes baked at higher temperatures (≥ 600 ºC) (Figure 4.35) as discussed previously.

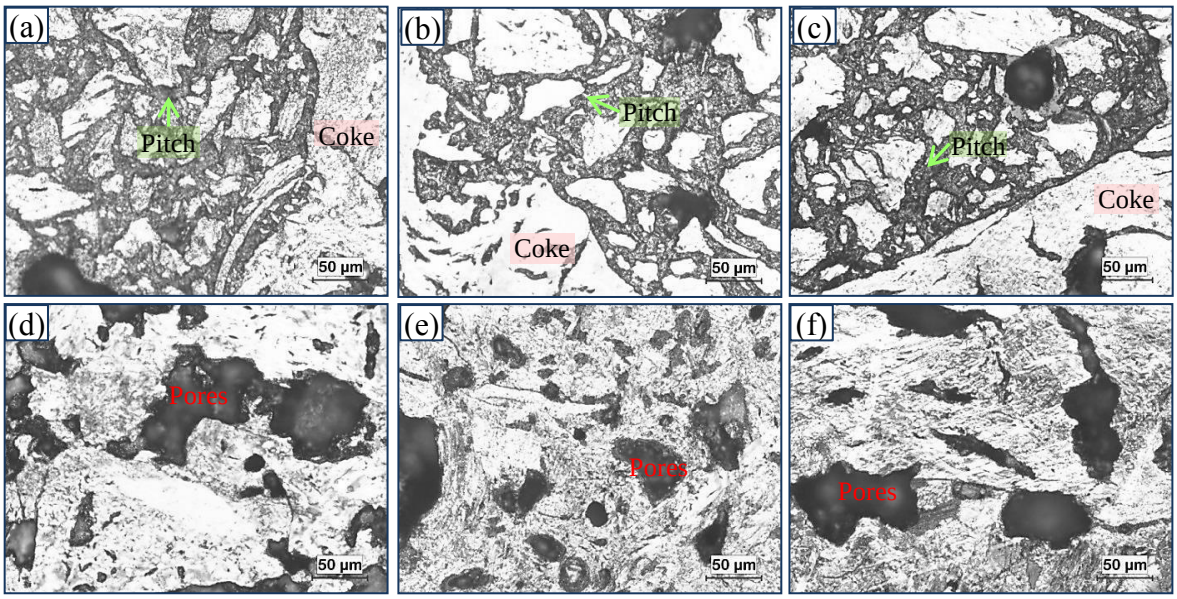

Figure 4.36: Optical microscopy images of anode cores baked to:
(a) 200 ºC, (b) 300 ºC, (c) 400 ºC, (d) 600 ºC, (e) 800 ºC, and (f) 1050 ºC.

4.2.5 Effect of pitch softening-point on anode properties

The effect of the utilization of Pitch-6, which has a 10 ℃ higher softening point than those of the other pitches, on the carbonized pitch structure in anodes was studied. Three anodes were produced using this pitch and the standard anode recipe. First anode was produced under standard condition (CS). For the second anode (C1), the pitch and mixing temperatures were increased by 10 °C. For the third anode (C2), only the pitch temperature was increased by 10 ºC. All the other anode production conditions for C1 and C2 were kept the same as those of the standard anode (CS). The green and baked core samples with pitch-6 were characterized as stated earlier.

Figure 4.37 shows the BAD and BER as well as air/CO_2 reactivity and dusting for CS, C1, and C2. It can be seen that as BAD increases BER decreases (Figure 4.37 (a)). This figure also indicates that BAD of C1 is the highest, which shows the effect of using

10 ºC higher pitch temperature and mixing temperature. C2 also had higher BAD compared to the standard anode but its resistivity was also higher showing that increasing only pitch temperature was not enough to efficiently use the high softening point pitch. Figure 4.37 (b) shows the reactivity and the BAD of these anodes. C1 has higher density, reduced CO_2 reactivity, and dusting due to this reactivity compared to other two anodes. This is in agreement with the previous results: baked anode density is inversely proportional to the CO_2 reactivity. Normally, higher densities increase the air reactivity. The air reactivity and dusting results somewhat follow this trend with C1 air reactivity which is slightly higher than that of SC. The results show that it is necessary to increase both pitch and mixing temperatures while handling high softening point pitch, which is in good agreement with the literature [12]. As the high density anodes are less porous; this in turn, reduces the CO_2 reactivity. The non-homogeneity of the anodes can result in slight differences. This indicates that the anode production conditions need to be adjusted according to pitch properties to have good quality anodes.

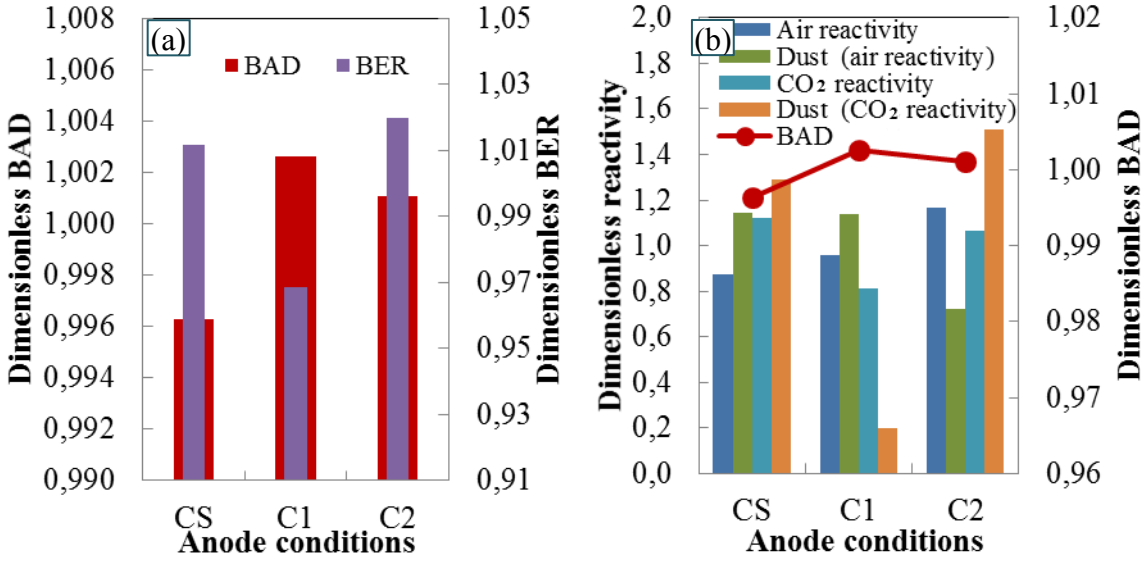

Figure 4.37: (a) BAD and BER and (b) Reactivities and BAD of anode core samples with Pitch-6 under conditions of different pitch preheating and mixing temperatures.

4.2.6 Effect of using pitch blends on anode properties

Anodes were made using the standard recipe with pitch blends that gave best (MP12: 75 % Pitch-1 (P1) and 25 % Pitch-2 (P2)) and least (MP35: 75 % Pitch-5 (P5) and 25 % Pitch-3 (P3)) wetting under the standard conditions among the blends studied. The green and baked anode core samples were characterized as described earlier.

Figure 4.38 shows the different properties such as baked density and electrical resistivity as well as air/CO2 reactivity for the baked anodes produced using different pure pitches and their blends. It was observed that as the baked anode density (BAD) increased, the baked anode resistivity (BER) decreased. Anodes made with the pitch blends have higher anode density and lower electrical resistivity compared to corresponding anodes made with pure pitch (Figure 4.38 (a) and (c)). In general, good wettability improved anode properties when pure pitches were used [1]. As discussed in Section 4.1.2, Pitch-1 and

Pitch-2 interact; therefore, the wettability of the coke by this blend (MP12) is less than the wettability of the same coke by parent pitches. Thus, it would be expected that the anode produced with this pitch blend (MP12) has lower density and higher resistivity compared to those of the anodes made with Pitch 1 and Pitch-2. However, this trend was not observed. On the other hand, the blends of Pitch-3 and Pitch-5 wetted the coke more than Pitch-5 but less than Pitch-3. Nevertheless, the anode made with the blend of these pitches (MP35) also had better properties compared to those of the anodes made with the pure pitches. It must be noted that only one anode was made with each pitch blend (MP12, MP35). The coke-pitch wettability is one of the criteria which affect the anode properties. These results show that there are other parameters affecting the anode quality in addition to wettability of coke by pitch, especially in the case of blends. The effect of blending pitches on anode properties has to be studied further.

Figure 4.38 (b) shows the reactivities and BAD of anodes with pure pitches (P1, P2) and their blend (M12, best wetting). It can be seen that the air reactivity and dusting due to air reactivity increased for the blend. The increase in air reactivity may be attributed to increase in density as explained before. The CO_2 reactivity and corresponding dusting decreased for the blend. The decrease in CO_2 reactivity is also due to increase in density. The decrease in CO_2 reactivity is very small compared to that of Pitch-1 (P1), but appreciable compared to that of Pitch-2 (P2). Dusting due to CO_2 reactivity decreased significantly compared to those of both pitches. Dusting is one of the major problems in plants, and appropriate pitch blending may remedy this situation. Figure 4.38 (d) shows the reactivities and BAD of anodes with pure pitches (P3, P5) and their blend (MP35, least

wetting). Unlike the best wetting blend, in this case, the air reactivity and corresponding dusting decreased. On the other hand, CO_2 reactivity decreased with respect to that of Pitch-3 (P3) but increased with respect to that of Pitch-5 (P5). However, the dusting due to CO_2 reactivity is increased, which is not desired. This study shows that the reactivities and dusting not only depends on the density of baked anodes, but also on the type of pitches used. It was shown previously that the wettability of coke by pitch blends is due to the combined effect of the structure of coke and pitch and the chemical components of pitch and coke surfaces. This indicates that the pitch blends plays an important role on anode properties. However, the complete mechanism of pitch blends impact on anode properties is complex, and further work involving the chemical and physical interactions of anodes with pure pitch and their blends is needed.

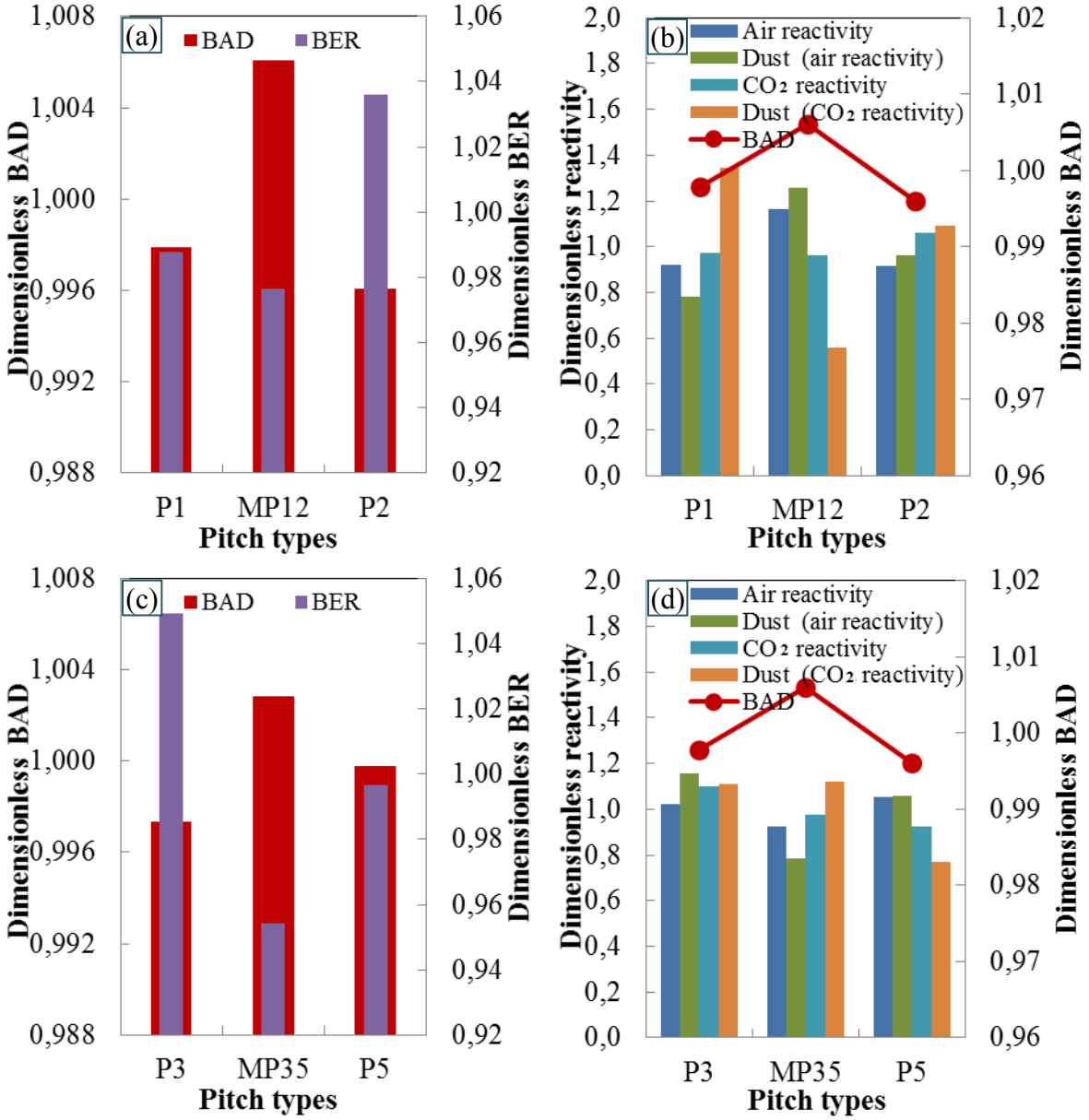

Figure 4.38: (a) BAD and BER and (b) Reactivities and BAD of anode core samples with P1, P2, and MP12; (c) BAD and BER and (d) Reactivities and BAD of anode core samples with P3,P5 and MP35.

4.2.7 Effect of vibro-compaction time on anode properties

The effect of vibro-compaction time on anode properties was studied with anodes made using Pitch-5 and the standard anode recipe, at two different vibro-compaction times.

One anode (CS) was made under the standard conditions. A second (C3) anode was produced using a vibro-compaction time of 5 s less than that of the standard, keeping all other conditions similar to that for CS.

Figure 4.39 shows the different properties, BAD and BER as well as air/CO_2 reactivity of the anodes produced at two different vibro-compaction times. It was observed that the BER decreases with increasing BAD (Figure 4.39 (a)). The density of the anode decreased with decrease in compaction time for the cases studied. This shows that, for the same anode recipe and fabrication conditions, higher compaction time was beneficial since the anode was better compacted in this case. However, further increase in compaction time (over-compaction) might cause cracking, consequently, the anode density might decrease. It can be observed (Figure 4.39 (b)) that the air reactivity slightly decreased and CO_2 reactivity increased when the compaction time was reduced. This can be explained in terms of the anode density. As discussed earlier, lower anode density reduces air reactivity and increases CO_2 reactivity. Dusting also followed the same trend as the reactivities.

This indicates that the vibro-compaction time plays an important role on anode properties. In this study, only two anodes were compared and the analysis was limited only to the cases studied. A detailed study can help understand the effect of compaction time on anode properties.

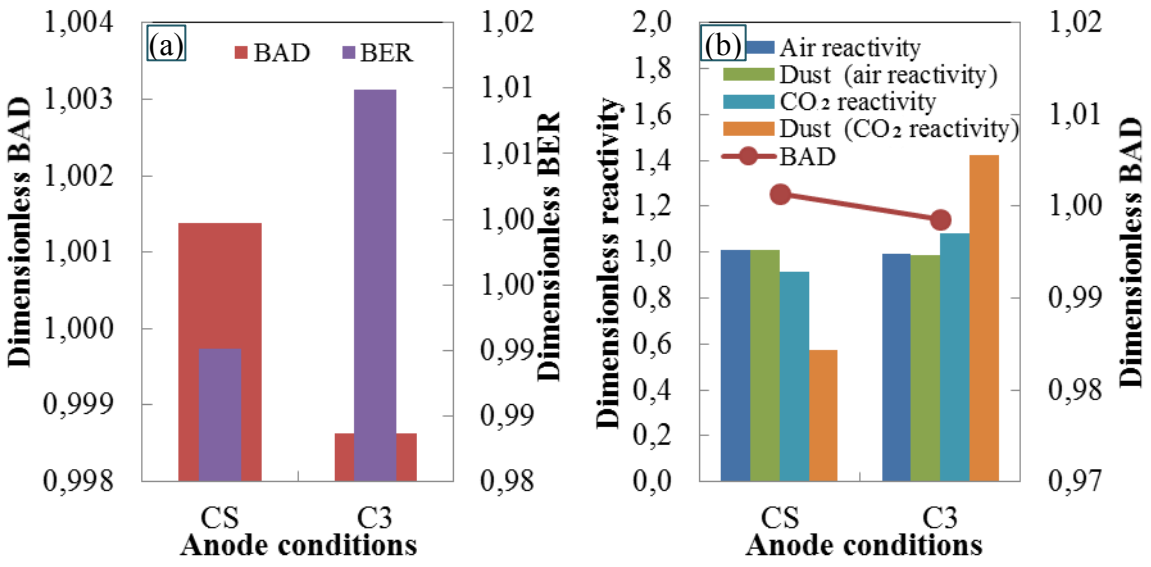

Figure 4.39: (a) BAD and BER and (b) Reactivities and BAD of anodes with Pitch-5 at two different vibro-compaction times.

4.2.8 The relationship between different anode properties

4.2.8.1 Correlation between the density and the resistivity of green anodes and green core samples with 15 % pitch

Figure 4.40 (a) and (b) shows that the relationship between the density and the resistivity of green anodes and corresponding cores made with 15 %. It can be seen that there exists a correlation between the density and the electrical resistivity for both green anodes as well as cores from these anodes. Figure 4.40 (a) shows that the electrical resistivity (GER) of green anode decreases with increasing density (GAD). Similar trend is observed for the resistivity (GER) and density (GAD) of the cores of the same green anodes. With an increase in density, the porosity decreases resulting in a decrease in electrical resistivity.

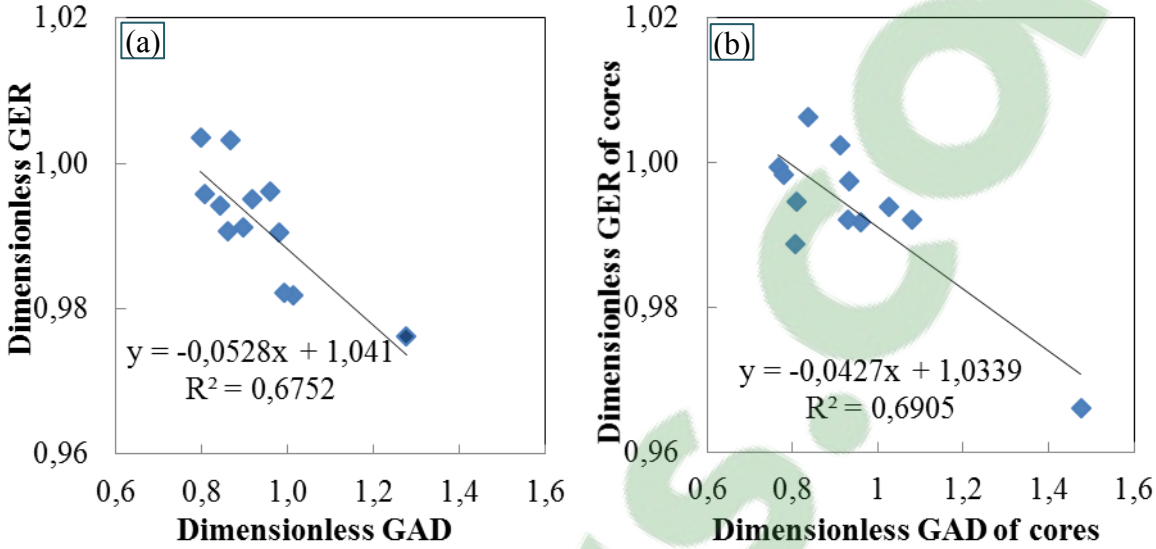

Figure 4.40: Correlation between density and resistivity for (a) green anodes and (b) green anode core samples with 15 % pitch.

4.2.8.2 Correlation between the density and the resistivity of baked anode core samples with 15 % pitch

Figure 4.41 shows that the relationship between the density and the electrical resistivity of baked anodes cores made with 15 % pitch. It can be seen that there exists a correlation between density and resistivity for baked anodes. The electrical resistivity (BER) of baked anode decreases with increasing density (BAD). With an increase in density, the porosity decreases resulting in a decrease in resistivity.

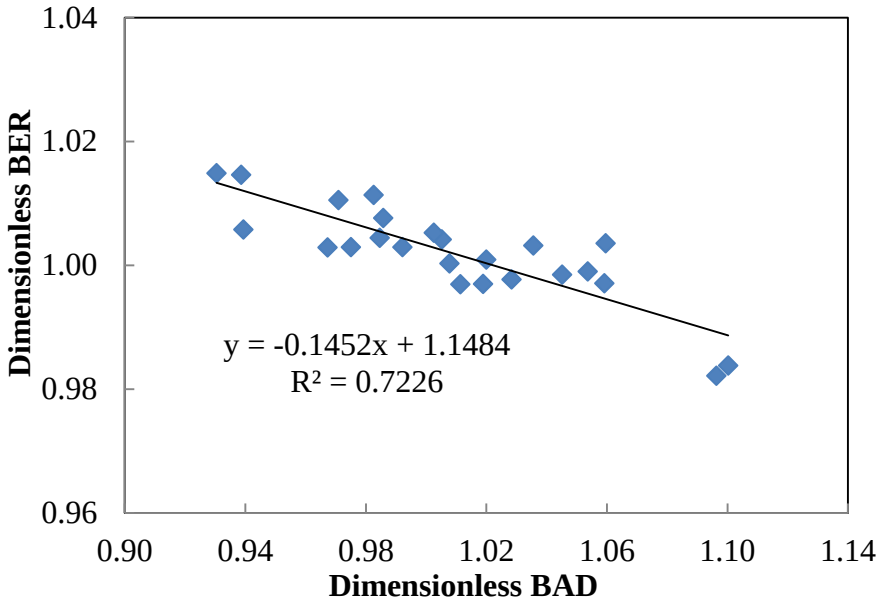

Figure 4.41: Correlation between density and resistivity of baked anode core samples with 15 % pitch.

4.2.8.3 Correlation between CO_2/air reactivity and dusting (CO_2/air reactivity) of baked anode samples

For different baked anode samples (cores), CO_2 and air reactivities as well as dusting due to CO_2 and air reactivities were determined.

Figure 4.42 (a) shows the variation of the CO_2 reactivity with corresponding dusting due to CO_2 reactivity of the core samples. It can be seen that there is a good correlation between them with an R^2 of 0.76. The results show that as the CO_2 reactivity increases, the dusting (CO_2 reactivity) increases. However, it was difficult to find a correlation between the air reactivity and the corresponding dusting due to air reactivity of these anode samples (R^2=0.25) (see Figure 4.42 (b)).

Dusting occurs due to the difference in the rate of oxidation of the carbonized pitch and the dry aggregate by the reacting gas. If the carbonized pitch gets consumed due to reaction, the aggregate particles cannot remain intact and fall; this is known as dusting.

The rate of air reaction is much faster compared to that of CO_2 reaction. Depending on the granulometry and surface composition, air can react with either carbonized pitch and/or coke, which makes it difficult to find a correlation between the air reactivity and its dusting. On the other hand, CO_2 preferentially attacks carbonized pitch. Thus, dusting increases with increase in CO_2 reactivity.

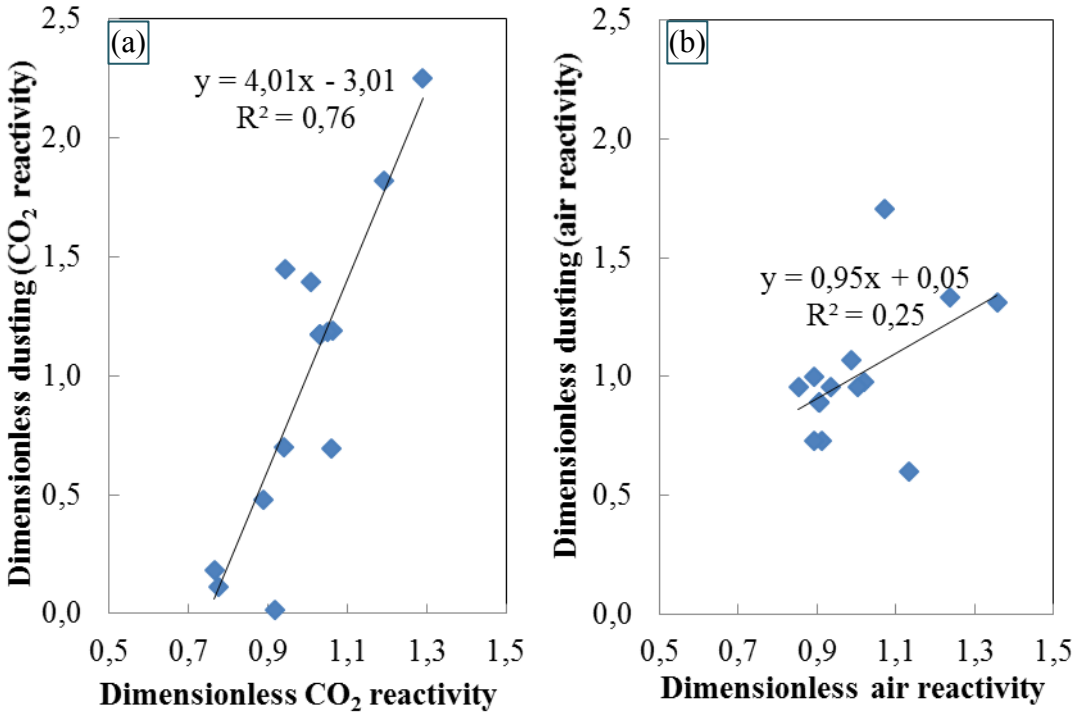

Figure 4.42: (a) Correlation between CO_2 reactivity and dusting (CO_2 reactivity) of cored anode samples, (b) Correlation between air reactivity and dusting (air reactivity) of cored anode samples.

Air-burn, carboxy attack, and selective oxidation results in excess anode consumption, which is detrimental to the production of aluminium. In this study, it was found that the density of carbon anode affects the anode reactivity. The detailed mechanism of reactivities is complex, and further work involving the chemical and physical interactions of the reacting gas with anodes is needed.

4.2.9 Thermogravimetric study on devolatilization kinetics of anodes

4.2.9.1 Effect of pitch percentage on devolatilization kinetics of anodes

Figure 4.43 (a) shows the green anode densities (GAD) of the core samples with different percentages of Pitch-2 and corresponding baked anode densities (BAD) of the same core samples. The dimensionless BAD/GAD is calculated by dividing a given BAD/GAD by the average of all BAD/GAD. Both GAD and BAD increased with increasing Pitch-2 percentage (17 % > 15 % > 13 %) within the range studied here. It should be noted that further increase in pitch content does not necessarily give higher densities as discussed previously. The densities of anode samples decreased after baking as expected. In this study, all anode samples were baked using the same baking parameters in TGA, and the weight loss of samples due to volatile release was continuously recorded with respect to temperature and time. Figure 4.43 (b) shows the weight loss curves of the anode samples with different percentages of Pitch-2. It can be seen that the weight loss was the highest for the anode with 17 % pitch compared to those of the anodes with 13 % and 15 % pitch. The weight loss increased with increasing Pitch-2 percentage (17 % > 15 % > 13 %). Higher pitch content gave greater amount of volatile release, resulting in higher weight

loss. This shows that the weight loss of pitch in green anodes depends on the green anode density and pitch percentage.

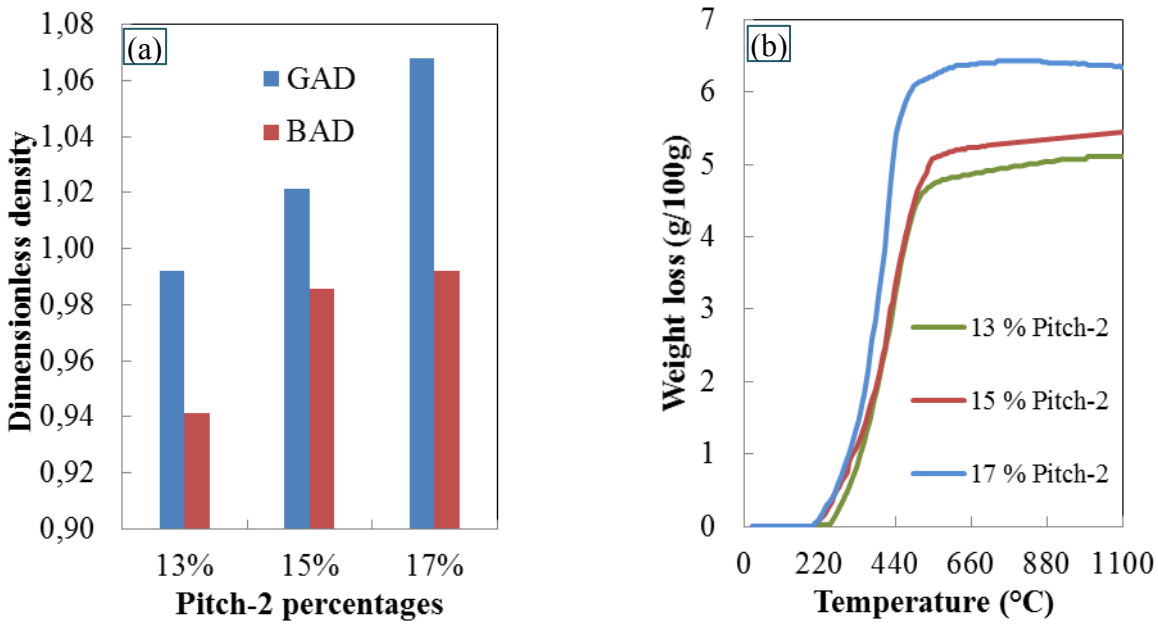

Figure 4.43: (a) The GAD and BAD of the anode core samples with different Pitch-2 percentages, (b) The weight loss (g/100g) of the anode core samples with different Pitch-2 percentages as a function of temperature.

Figure 4.44 (a), (b), and (c) compare the instantaneous release rate of hydrogen, methane, and condensable volatiles, respectively, with respect to temperature for anodes with different percentages of pitch.

During the anode baking process, first, the relatively low molecular weight condensables (tar) are released from pitch. At higher temperatures, the volatiles with large molecules in pitch undergo cracking reactions producing hydrogen and methane. Figure 4.44 (a) and (b) shows that the instantaneous rate of hydrogen and methane release started slowly around 350ºC and reached a maximum value at a certain temperature, and

then the rate started to decrease again. For hydrogen, the maximum was reached within the range of 650 ºC to 700 ºC. For methane, the maximum was reached within the range of 470 ºC to 505 ºC. Depending on the percentages of pitch, the maximum point varied.

Figure 4.44 (a) shows that the instantaneous rate of hydrogen released reached maximum at 653 ºC, 669 ºC, and 696.5 ºC for pitch percentages of 13, 15 and 17 %, respectively. At these temperatures, the instantaneous rate of release of hydrogen was highest for the anode with 15 % pitch, whereas it was lowest for the anode with 17 % pitch. The instantaneous rate of hydrogen release at this condition by anode with 13% pitch was slightly lower than that of the anode with 15 % pitch. However, the cumulative amount of hydrogen (Table 4.10) shows that the maximum amount of hydrogen was released by the 13 % pitch and minimum amount by the 17 % pitch during the baking process. The 15 % pitch released slightly less hydrogen than that released by the anode with the 13 % pitch.

Figure 4.44 (b) shows that the instantaneous rate of release for methane reached the maximum at 471 ºC, 504 ºC, and 471 ºC for pitch percentages of 13, 15 and 17 %, respectively. At these temperatures, the instantaneous rate of methane release by the anodes with 13 % and 17 % pitch was maximum whereas it was minimum for the anode with 15 % pitch. The instantaneous methane release at this condition by the anode with 13 % pitch was nearly the same as that of the anode with 17 % pitch. However, the cumulative amount of methane (Table 4.10) shows that the maximum amount of methane was released by the anode with 13 % pitch and the minimum amount by the anode with 17 % pitch during the baking process. The anode with 15 % pitch released slightly less methane than the anode with 13 % pitch.

Figure 4.44 (c) shows that the instantaneous rate of release of condensables reached maximum at 443.5 ºC, 432.5 ºC, and 394.0 ºC for pitch percentages of 13, 15, and 17 %, respectively. At these temperatures, the instantaneous rate of condensable release by the anode with 17 % pitch was maximum followed by the anode with 15 % pitch, and the rate was minimum for the anode with 13 % pitch. The cumulative amount of condensables (Table 4.10) shows the same trend.

Table 4.10 shows also that the maximum total amount of volatiles was released by the anode with 17 % pitch followed by 15 % pitch, and the minimum total amount was released by the anode with 13 % pitch.

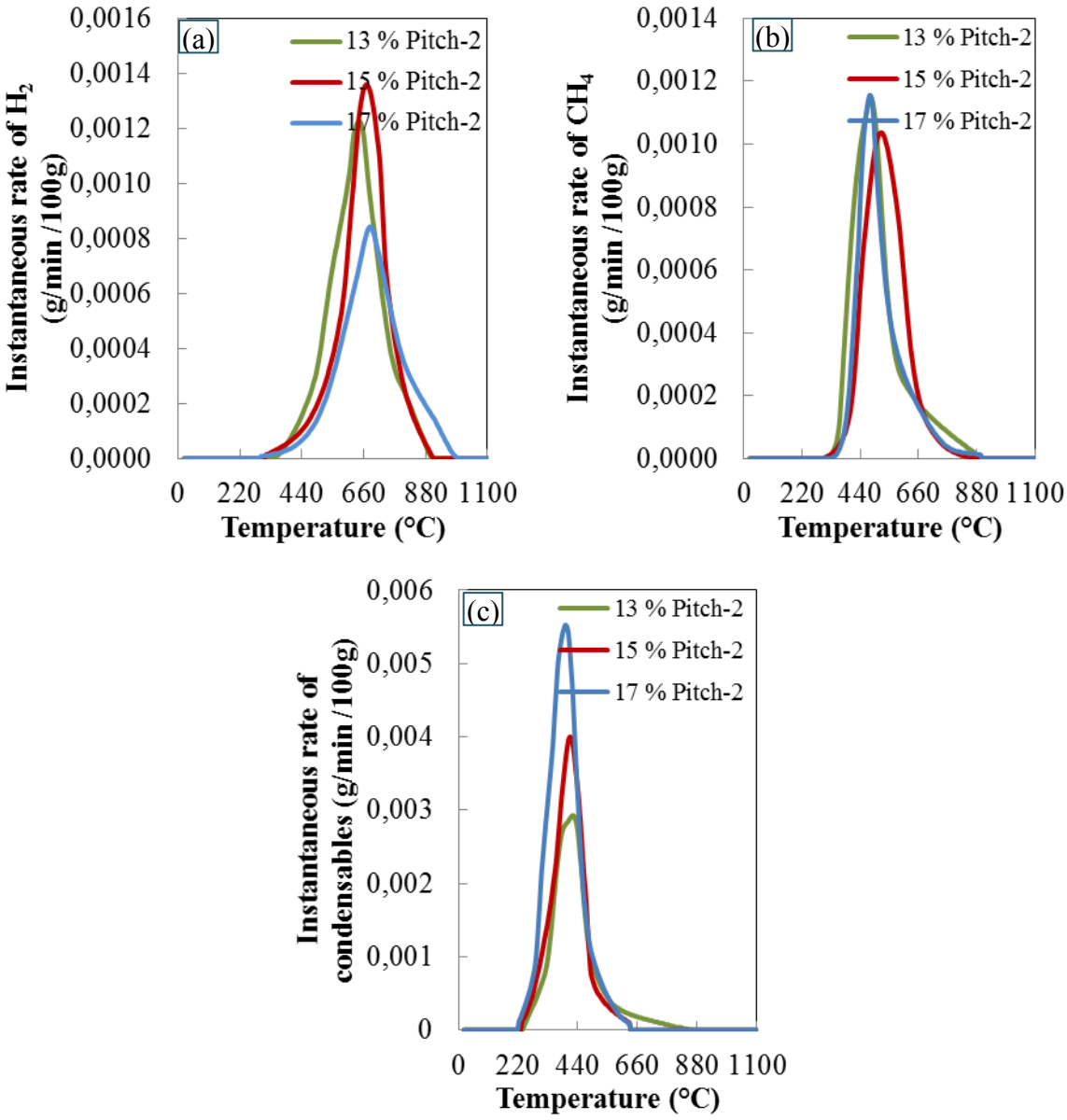

Figure 4.44: Comparison of the instantaneous rates of (a) hydrogen, (b) methane, and (c) condensables for anodes with different pitch percentages as a function of temperature.

Figure 4.45 (a) shows the instantaneous release rates of hydrogen, methane, and condensables from the anode with 15 % Pitch-2. The kinetic results for anodes with different pitch percentages (13 % and/or 17 % Pitch-2) and with different pitches (15 %

Pitch-3 and/or Pitch-4) are presented in Appendix 5. During baking, first the heavy components such as polycyclic aromatic hydrocarbons (PAH) are evolved. Then, at higher temperatures, hydrogen and methane are evolved. It can be seen from this Figure 4.45 (a) that the release of condensables started at around 218 °C and its instantaneous rate increased rapidly reaching a maximum value at around 400 °C. Then, it started to decrease and became negligible after 625 °C. Methane started to evolve at around 340 °C, reached a maximum around 500 °C, and decreased to negligible levels when 900 °C was reached. Hydrogen release started at around 340 °C, the rate of release reached a maximum at around 660 °C, and decreased to negligible levels after 900 °C. Experiments with other anodes showed similar tendencies except for some slight differences in the temperature ranges and the quantities released. The cumulative weight loss due to the condensables, hydrogen, and methane were obtained by integrating the instantaneous rate of volatile components released with respect to time for the anode with 15 % Pitch-2 (Figure 4.45 (b)). The conversions of all three components were calculated and are shown in Figure 4.45 (c). Figure 4.45 (d) gives an example of the plot for the determination of the kinetic parameters. The slope and the intercept of the linear trend line were used to calculate these parameters. The method was described earlier in Section 3.3.8.

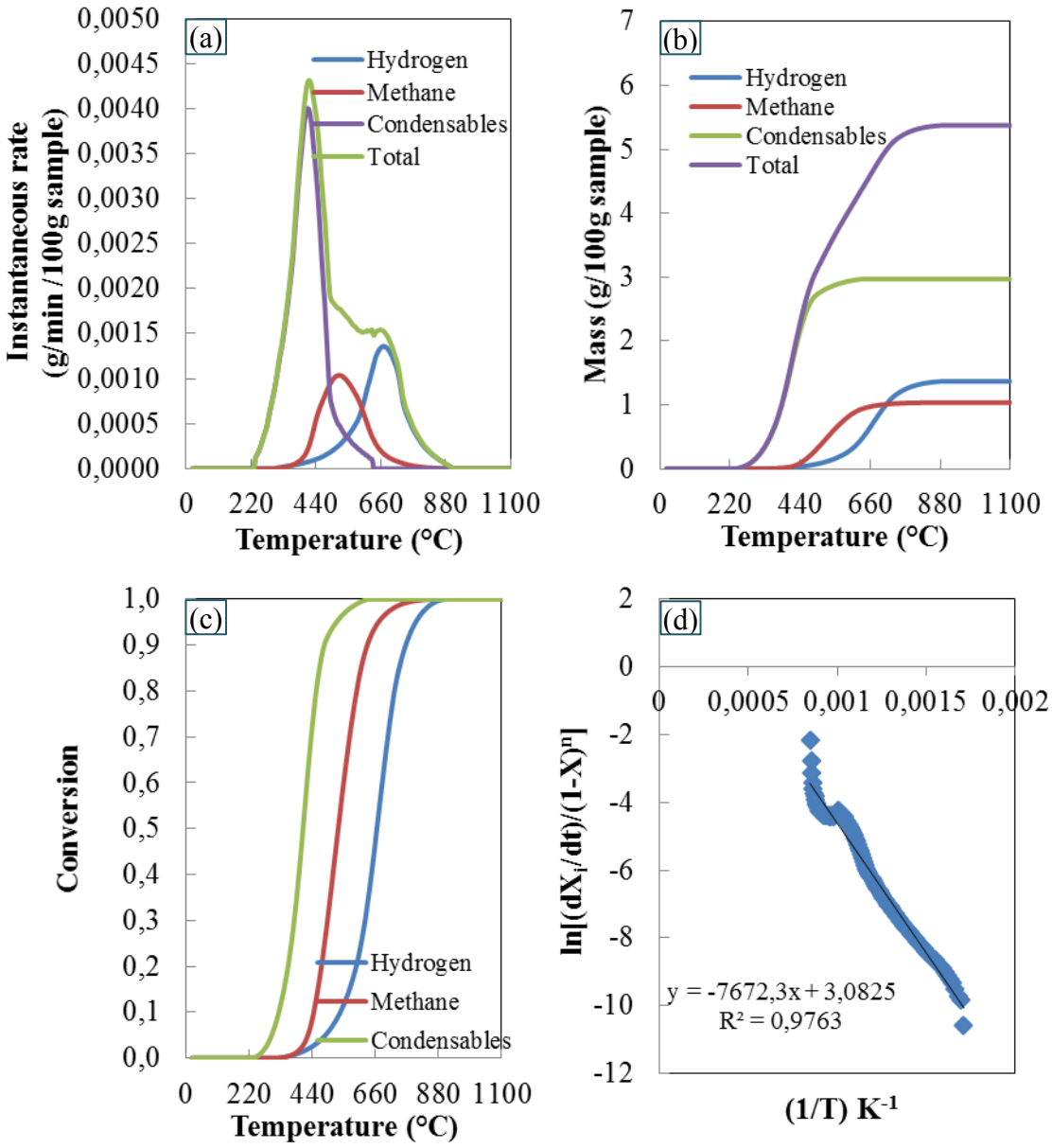

Figure 4.45: (a) Instantaneous rate of devolatilization, (b) Cumulative weight loss, (c) Conversions for hydrogen, methane, and condensables, and (d) Determination of kinetic parameters of hydrogen for anode with 15 % Pitch-2.

4.2.9.2 Effect of different pitches on devolatilization kinetics of anodes

Figure 4.46 (a) shows the value of green (GAD) and baked anode (BAD) densities of core samples made of pitches with different QI contents. The dimensionless BAD/GAD

is calculated by dividing a given BAD/GAD by the average of all BAD/GAD. The densities varied with the type of pitch. Pitch-2 gave the highest density and Pitch-4 the lowest. It seems that there is a relation with the wettability; the better the wettability is, the higher the density is. Figure 4.46 (b) shows the weight loss curves of the anode samples with different pitches. It can be observed that the weight loss for the anode with Pitch-4 was the highest whereas Pitch-2 was the lowest. The weight loss for anodes made with Pitch-3 and Pitch-2 were close. The weight loss depends on the type of pitch and its constituents (Table 4.10 and Figure 4.48). Again, it seems that the better wetting pitch lost relatively less volatiles.

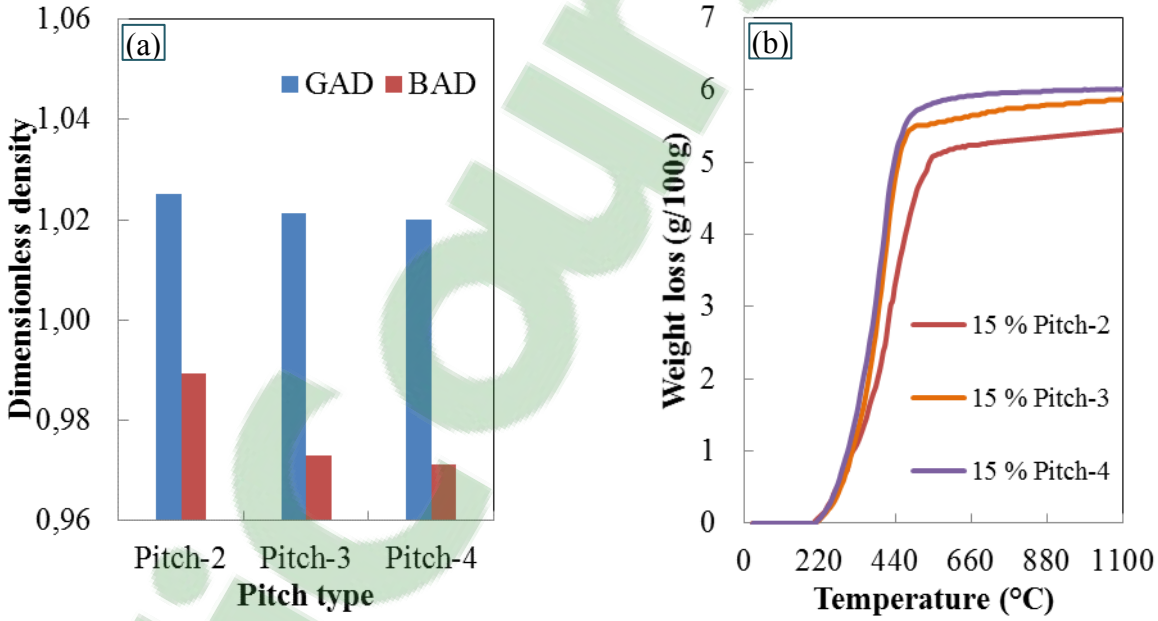

Figure 4.46: (a) The GAD and BAD of the anode core samples with different pitches, (b) The weight loss (g/100g) of the anode core samples with different pitches as a function of temperature.

Figure 4.47 (a), (b), and (c) compare the instantaneous amount of hydrogen, methane, and condensables released, respectively, for anodes with different pitches as a

function of temperature. In all these anodes, 15 % pitch was used.

Figure 4.47 (a) and (b) show that the instantaneous rate of release for hydrogen and methane started slowly around 350 ºC and reached maximum at a certain temperature, and then the rate started decreasing. For hydrogen, the maximum was reached within the range of 585 ºC to 650 ºC. For methane, the maximum was reached within the range of 415 ºC to 500 ºC. Depending on the type of pitch, the maximum point varied. Figure 4.47 (a) shows that the rate of hydrogen release reached maximum at 647 ºC, 636 ºC, and 587 ºC for Pitch-2, Pitch-3, and Pitch-4, respectively. The maximum rate of hydrogen release was observed for the anode with Pitch-3 whereas the minimum was observed for the anode with Pitch-4, and the Table 4.10 also shows that maximum total amount of hydrogen was released by Pitch-3 and minimum amount by Pitch-4 during the baking process.

Figure 4.47 (b) shows that the instantaneous rate of release for methane reached maximum at 499 ºC, 449 ºC, and 416 ºC for Pitch-2, Pitch-3, and Pitch-4, respectively. Table 4.10 shows that the maximum total amount of methane was released by the anode with Pitch-2 and the minimum amount by the anode with Pitch-3 during the baking process. The anode with Pitch-4 released slightly less than that by the anode with Pitch-2.

Figure 4.47 (c) shows that the instantaneous rate of release for condensables reached maximum at 400 ºC, 377 ºC, and 373 ºC for Pitch-2, Pitch-3, and Pitch-4, respectively. Table 4.10 shows that the maximum total amount of condensables was released by the anode with Pitch-4, followed by the one with Pitch-2, and the minimum total amount was released by the anode with Pitch-4 during the baking process.

Since the baking parameters are the same for all anodes, the variations in pitch appear to affect the release of hydrogen, methane, and condensables. A compilation of the overall results are given in Figure 4.48 (a) and (b).

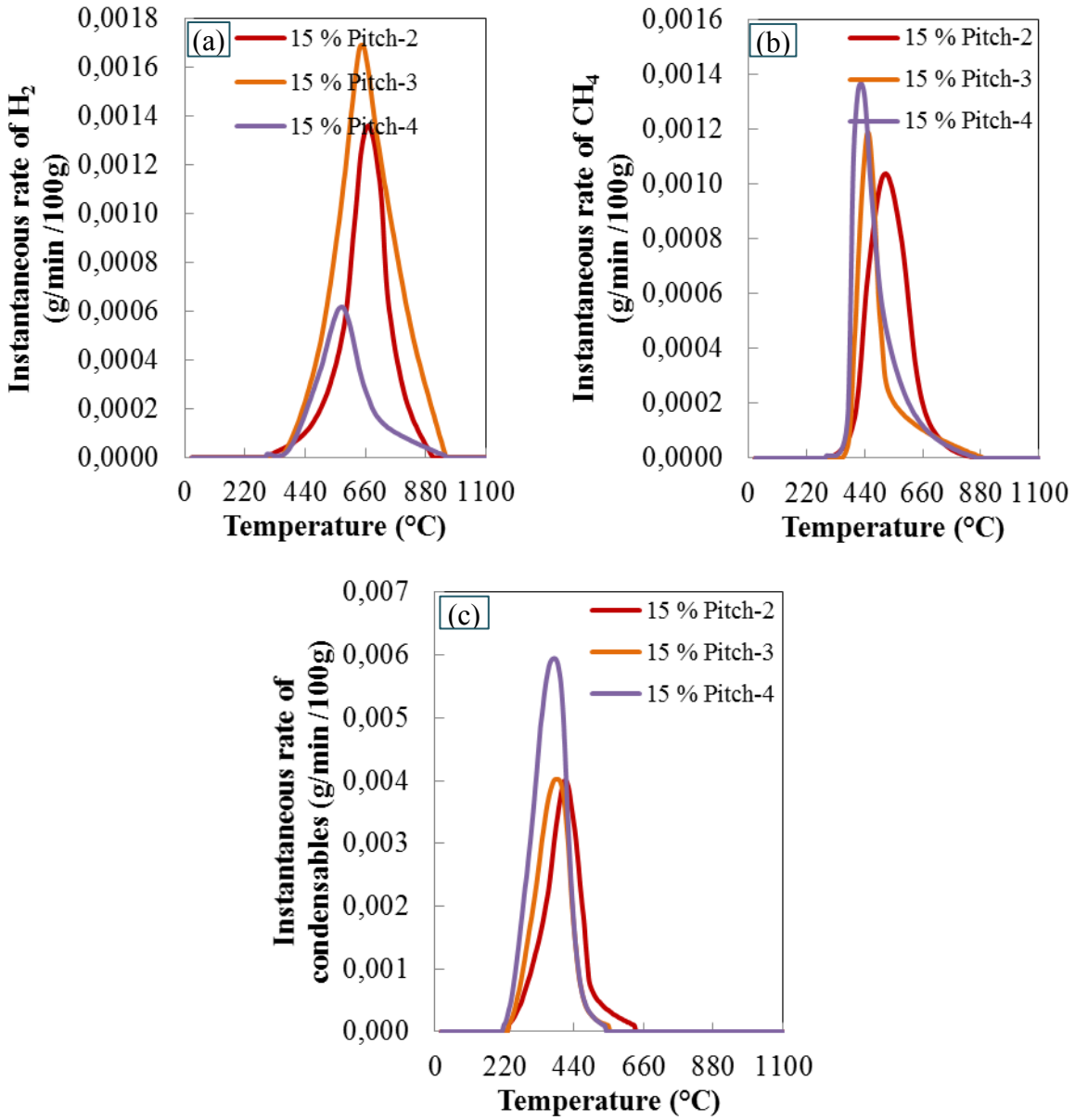

Figure 4.47: Comparison of the instantaneous rates of release of (a) hydrogen, (b) methane, and (c) Condensable gas for anodes with different pitches.

Table 4.10: Total amount of volatile components released during baking from anodes made with different pitches and pitch concentrations.

Anode	Experimental total weight loss (g/100 g sample)	Total (g/100 g sample)	Hydrogen (g/100 g sample)	Methane (g/100 g sample)	Condensables (g/100 g sample)
13 % Pitch-2	5.11	5.09	1.40	1.09	2.60
15 % Pitch-2	5.45	5.38	1.37	1.04	2.97
17 % Pitch-2	6.34	6.28	1.10	0.90	4.29
15 % Pitch-3	5.88	5.94	2.29	0.73	2.92
15 % Pitch-4	6.01	6.05	0.71	1.00	4.35

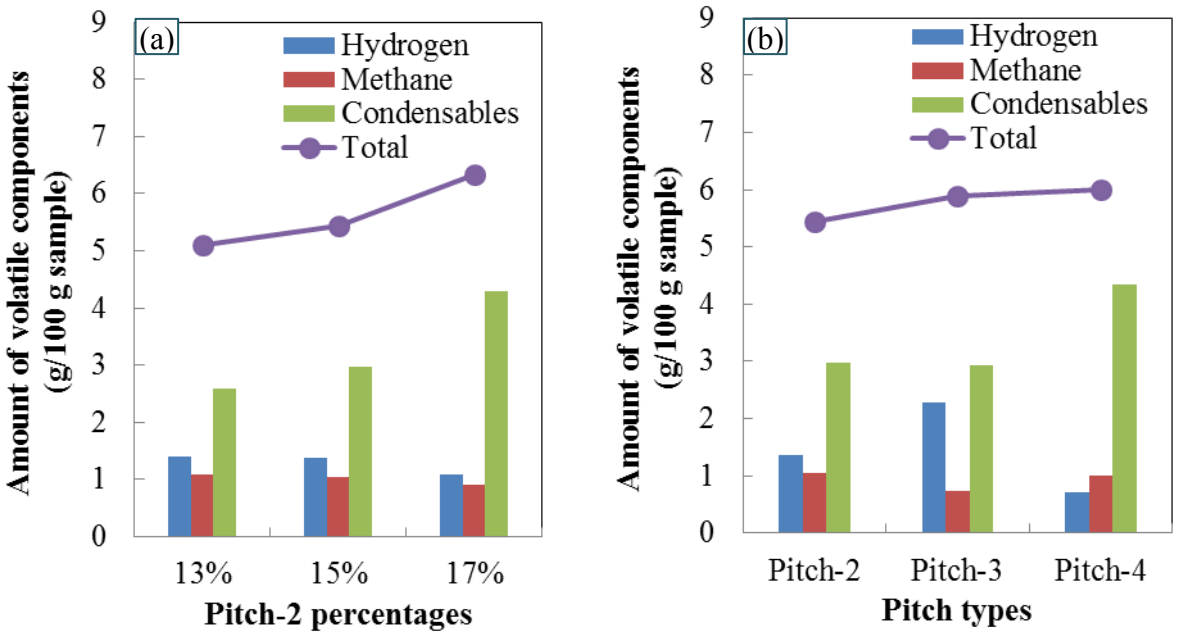

Figure 4.48: (a) Amount of volatile components released during baking from anodes made with different pitch concentrations. (b) Amount of volatile components released during baking from anodes made with different pitches.

Table 4.11 shows the values of the kinetic parameters found for the anodes with different pitch types and pitch contents. Pitch types and pitch content influence the devolatilization kinetics during anode baking. As pitch is a mixture of a number of chemical components, the kinetics for each component is supposed to be different. However, it is difficult, rather impossible, to calculate the kinetics of all the components during the baking process. In this analysis, the kinetic data of the devolatilization of the major components (condensables, hydrogen, and methane) were determined representing the overall devolatilization during the anode baking process. The kinetic parameters are useful to calculate the amount of volatiles released from anodes made with coke and pitch used in the study. These kinetic data help determine the heat release due to the combustion of volatiles in the baking furnace. The kinetic parameters can also be used in baking furnace models.

Table 4.11: Summary of kinetic analysis results.

Anode	Hydrogen			Methane			Condensable Gas		
	n	E, kJ/mol	$K_{0,app,}$ 1/min	n	E, kJ/mol	$K_{0,app,}$ 1/min	n	E, kJ/mol	$K_{0,app,}$ 1/min
13 % Pitch-2	1.1	86.2	1.5E+02	2.0	114.8	1.7E+05	1.5	63.1	5.5E+02
15 % Pitch-2	0.8	62.8	4.0E+00	1.5	108.3	2.8E+04	1.8	84.8	8.6E+04
17 % Pitch-2	0.8	58.7	1.4E+00	2.4	150.5	6.3E+07	1.4	72.4	1.4E+03
15 % Pitch-3	1.1	78.5	3.6E+01	2.9	183.0	2.2E+10	1.5	93.1	1.5E+05
15 % Pitch-4	1.4	78.7	1.1E+02	1.9	119.8	5.6E+05	1.3	80.8	1.5E+04

4.3 Study of air/CO_2 reactivity of industrial anodes

The air and CO_2 reactivities of cylindrical (Ø 50 mm×50 mm) industrial baked anode samples were measured, and the results were analyzed. Four samples (samples S-1, S-2, S-3, and S-4) from 4 industrial anodes fabricated in 2011 were used for air reactivity tests, and four others (samples I-1, I-2, I-3, and I-4) were used for CO_2 reactivity tests (see section 3.1 for details). Samples from five industrial anodes fabricated in 2013 (Anode 18, Anode 27, Anode 28, Anode 31, Anode 32), which were produced with different vibro-compactors (Vibro-C and Vibro-D) using different compaction times and baked at different positions in the baking furnace, were also used for air and CO_2 reactivity tests (see section 3.1 for details). Thus, for each reactivity test, there were 9 samples: 4 from the anodes fabricated in 2011 (Table 3.2) and 5 from the anodes fabricated in 2013 (Table 3.3). The weight loss was recorded at every minute during the tests. The average rate of percentage weight loss (%/min) for CO_2 and air reactivity tests of all the nine industrial anode samples are shown in Figure 4.49. It can be seen that the rate of weight loss (%/min) for the air reactivity is higher compared to that for the CO_2 reactivity. This indicates that the rate of reaction for air reactivity is much faster than that for CO_2 reactivity as expected. The correlations between reactivities (CO_2/air) of industrial anodes are presented in Appendix 6.

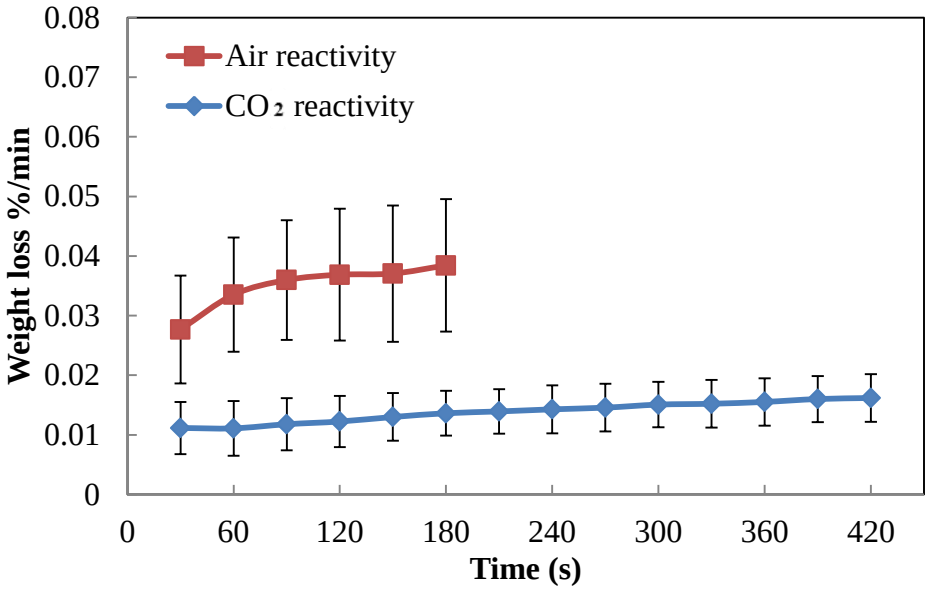

Figure 4.49: The average rate of percentage weight loss (%/min) for CO_2 and air reactivities of all industrial anode samples (nine samples).

4.3.1 SEM analysis of air/CO_2 reacted industrial anode samples

The reacted samples S-4 (air reactivity) and I-4 (CO_2 reactivity), obtained from the anode produced by Vibro-D in 2011, were cut vertically into small thin slices (5 mm) in order to analyze the depth of reaction region using SEM (Figure 4.50).

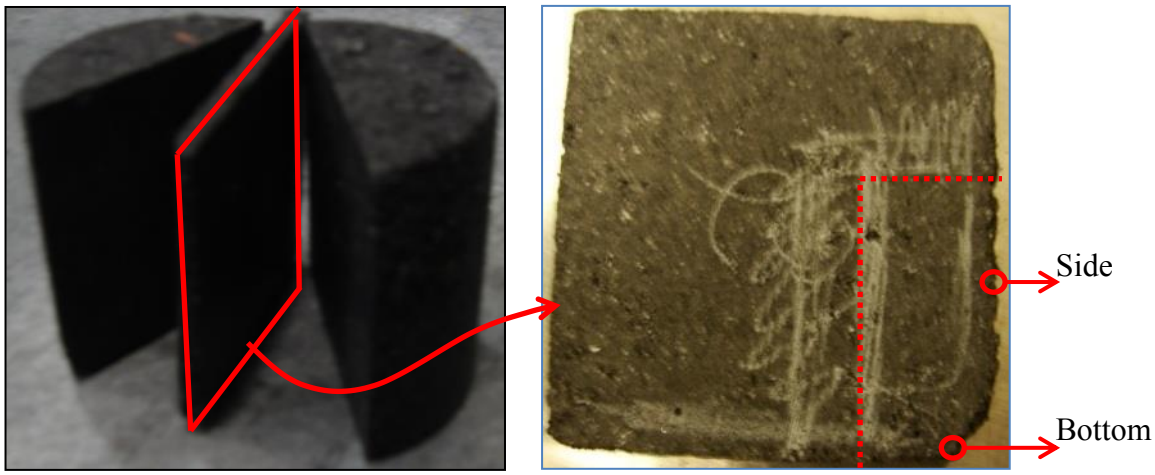

Figure 4.50: The CO_2 /air reacted anode sample preparation for SEM.

Figure 4.51 shows the SEM images of the reacted surface of anode samples S-4 and I-4 for two different positions (bottom and side). It was found that there is big difference in the depth of CO_2 and air-reacted regions. The SEM image of the air-reacted area (bottom) in Figure 4.51 (a) shows that the reaction zone covers a region of 640 µm to 1040 µm. However, Figure 4.51 (c) shows a larger region of CO_2 reaction (bottom) ranging from 800 µm to 1350 µm. It can be also seen that the depth of air reacted region (side) is in the range of 430 µm to 760 µm in Figure 4.51 (b) and the depth of CO_2-reacted region (side) is in the range of 760 µm and 1300 µm in Figure 4.51 (d). The measurements at both positions indicate that the depth of the reaction zone for air reactivity is always smaller (reaction controlled) than that for the CO_2 reactivity (diffusion controlled). It may be noted that the samples were collected after the completion of the reactivity tests. As air reacts faster compared to CO_2, air might have consumed most of the surface leaving behind a smaller reaction zone. CO_2 selectively reacts with carbonized pitch and diffuses slowly into the matrix. Thus, it takes longer time to consume the material on the surface and inside the pores and cracks. Therefore, the CO_2 reactivity test is longer than the air reactivity test according to ASTM standards. The reaction zones for the same gas for the side and the bottom of the samples did not differ much, which shows a good contact of the gas with the sample surfaces.

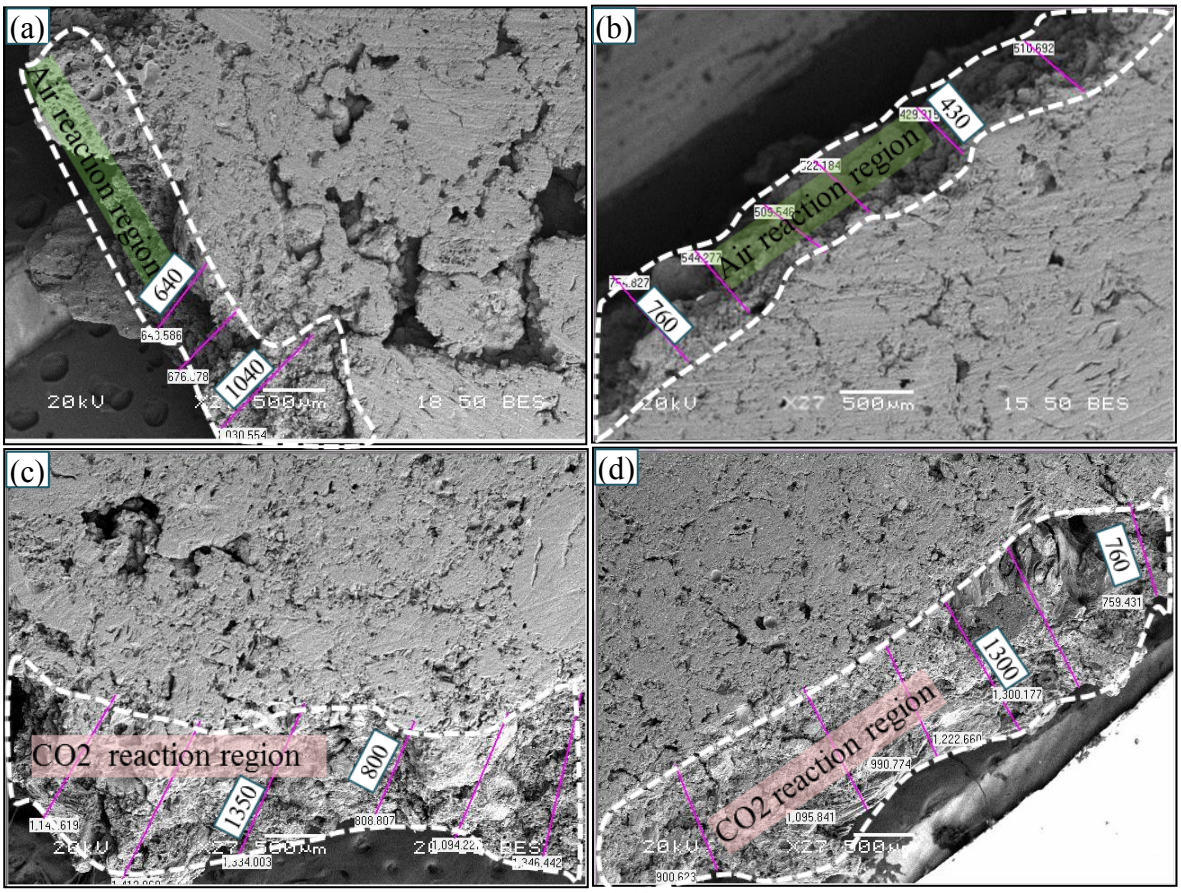

Figure 4.51: SEM images of air-reacted region on anode (S4) surface: (a) Bottom, (b) Side; SEM images of CO_2-reacted region on anode (I4) surface: (c) Bottom, (d) Side.

4.3.2 Effect of vibro-compactors on anode air/CO_2 reactivity

In this study, four samples (S-1, S-2, S-3 and S-4) were used for air reactivity and four samples (I-1, I-2, I-3, and I-4) were used for CO_2 reactivity study from the four anodes produced by four vibro-compactors in 2011 (Figure 3.3). As fabrication conditions and recipes were similar, this study gives an idea of the effect of the different vibro-compactors on anode reactivities.

Figure 4.43 shows the air and CO_2 reactivities and the densities of the cores. The baked anode density (BAD) was the highest for the cores obtained from anode produced by

vibro-D. The air reactivity and CO_2 reactivity were the lowest for vibro-C; the air reactivity for vibro-C is almost the same as that for vibro-D (Figure 4.52). It is difficult to find a correlation between anode reactivity and BAD of these anode samples (Figure 4.52). Even though the densities are similar, the reactivities vary significantly. This might be due to the non-homogeneous nature of industrial anode samples.

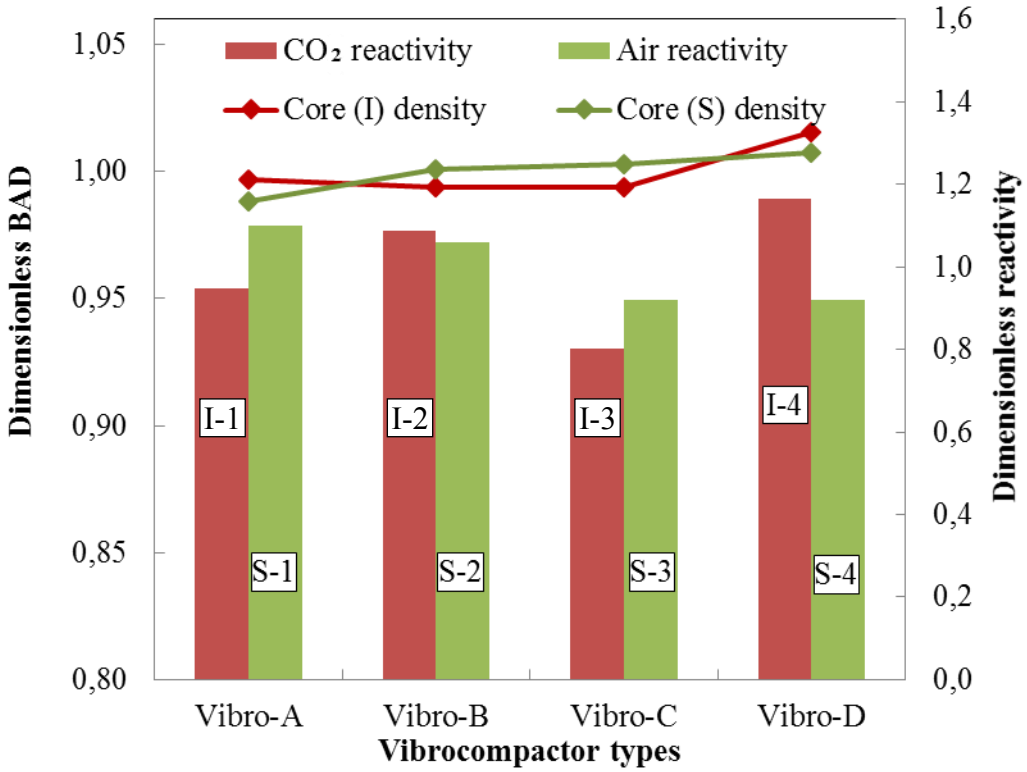

Figure 4.52: CO_2 reactivity, air reactivity, and baked anode density (BAD) of the cores obtained from anodes fabricated using different vibro-compactors.

Figure 4.53 (a) shows the variation in air reactivity for core samples (S1, S2, S3, S4) of baked anodes for corresponding dusting due to the air reactivity. It can be observed that there exists a good correlation between air reactivity and dusting (air reactivity) of these anode samples with an R^2 value of 0.8241. Dusting increases with increase in air reactivity.

It can also be observed that there exists a good correlation between CO_2 reactivity and dusting (CO_2 reactivity) for the anode samples (I1, I2, I3, I4) with an R^2 value of 0.8044. Figure 4.53 (b) shows that dusting increases with increase in CO_2 reactivity.

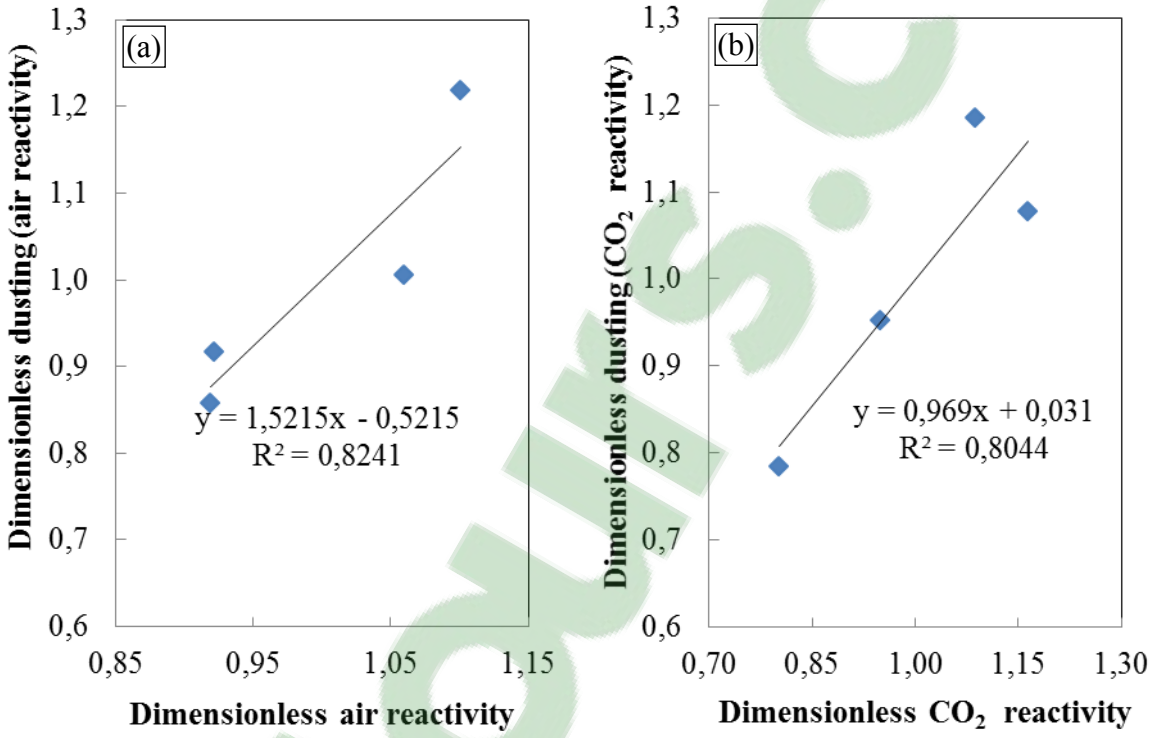

Figure 4.53: Correlation between (a) air reactivity and dusting (air reactivity) and (b) CO_2 reactivity and dusting (CO_2 reactivity) of anode core samples from anodes produced using different vibro-compactors.

4.3.3 Effect of anode position in the baking furnace on its air/CO_2 reactivity

Air and CO_2 reactivities of the cores (cylindrical cores of Ø 50 mm×50 mm) taken from industrial anodes (Anode 18, Anode 27, Anode 28, Anode 31, Anode 32) were measured and analyzed.

Out of the five industrial anodes produced in 2013, Anode-27 and Anode-28 were fabricated by Vibro-C. Similarly Anodes-31 and Anode-32 were fabricated by Vibro-D.

The compaction times were the same for these cases (Table 3.3). Anode-27 and Anode-28 were compared to study the effect of top and bottom rows in the pit of the baking furnace. Anode-31 and Anode-32 were compared to study the effect of placing the anodes in the corner and center positon of the pit in the baking furnace (Figure 3.4). The positons of baked anode cores (11, 25, 12, and 24) are shown in Figure 3.5. Cores 11 and 25 were used for air reactivity, and cores 12 and 24 were used for CO_2 reactivity study.

Air/CO_2 reactivity and dusting (due to air/CO_2 reactivity) of baked anode cores (11, 25, 12, and 24) from Anode 27 and Anode 28 are shown in Figure 4.54 (a) and (b), respectively. Figure 4.54 (a) shows that the values of air/CO_2 reactivity of Anode 27 and Anode 28 are similar. It can be observed in Figure 4.54 (b) that dusting (due to air/CO_2 reactivity) for the cores of the two anodes is different. Anodes 27 and 28 were placed at the top and bottom, respectively, in the same pit along the same vertical line. The results show that the reactivities did not vary significantly for these positions. However it is difficult to correlate the anode position in the pit with dusting.

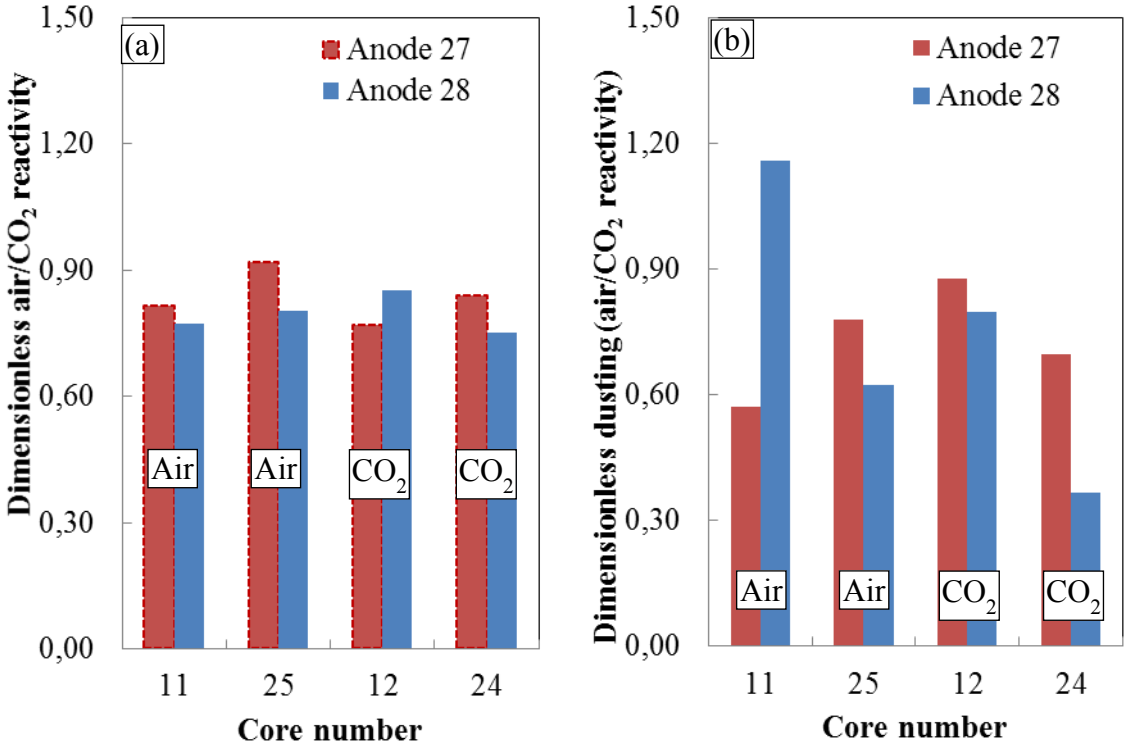

Figure 4.54: (a) Air/CO_2 reactivity and (b) Dusting (air/CO_2 reactivity) of anode core samples from Anode 27 and Anode 28.

Figure 4.55 (a) and (b) show that all the cores of Anode 31 have higher reactivities and dusting compared to those of Anode 32. Anode 31 was placed at the top corner whereas Anode 32 was placed at the center in the pit of the baking furnace. This indicates that the anodes positions (corner and center) in the baking furnace can influence the anode reactivity and dusting.

Following the investigation to identify the reasons for the observations above, it was found that the average temperature of the two anodes produced by vibro-C (Anode 27 and Anode 28) were the same. Thus, it is likely that similar baking temperatures resulted in similar reactivities. On the other hand, Anode 32 was baked at a higher temperature than

Anode 31. Thus, the lower baking temperature of Anode 31 gave higher reactivities compared to that of Anode 32.

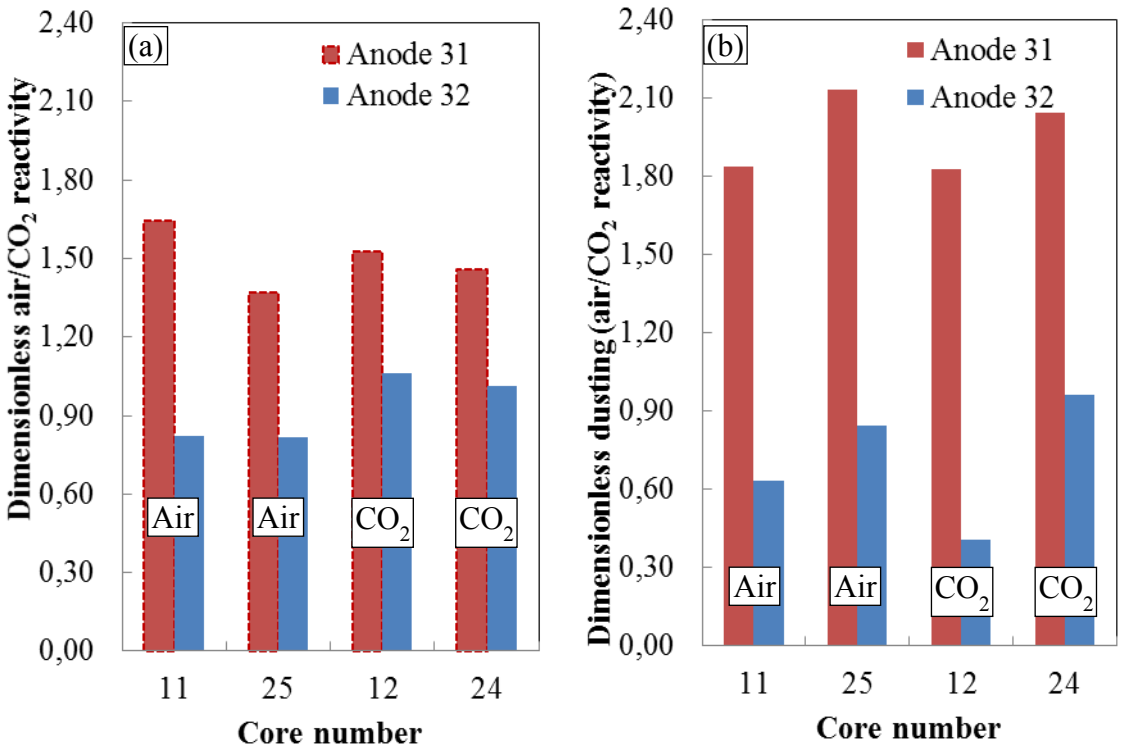

Figure 4.55: (a) Air/CO_2 reactivity and (b) Dusting (air/CO_2 reactivity) of anode core samples from Anode 31 and Anode 32.

The study shows that the temperature distribution in the baking furnace can influence anode reactivities. Dusting, however, does not always correlate well with the baking temperature.

4.3.4 Effect of vibro-compaction times on air/CO_2 reactivity

The effect of compaction times on reactivities were studied using Anode-18 and anode-31 (both fabricated in 2013). They were produced using the same recipe and vibro-compactor (Vibro-D). They were even baked at similar positions (the top-right

corners of two pits) in the pit of the baking furnace. The baking conditions were supposed to be same, but the measurements showed that the final baking temperatures were slightly different. It was found that the baking temperature of Anode 18 was slightly higher than that of Anode 31 in spite of similar positions in the baking furnace. The main difference between these two anodes was the compaction time. Anode-31 was compacted 7 s longer than Anode-18. Cores 11 and 25 were used for air reactivity, and cores 12 and 25 were used for CO_2 reactivity tests.

Figure 4.56 (a) and (b) show that the reactivities and dusting of the anode produced using Vibro-D in a shorter vibration time have lower reactivities and dusting. The reduced reactivities and dusting may be the combined effect of vibration time and baking temperature.

It is difficult to find a relationship between anode density, electrical resistivity, and reactivity for industrial anodes probably due to their non-homogeneity.

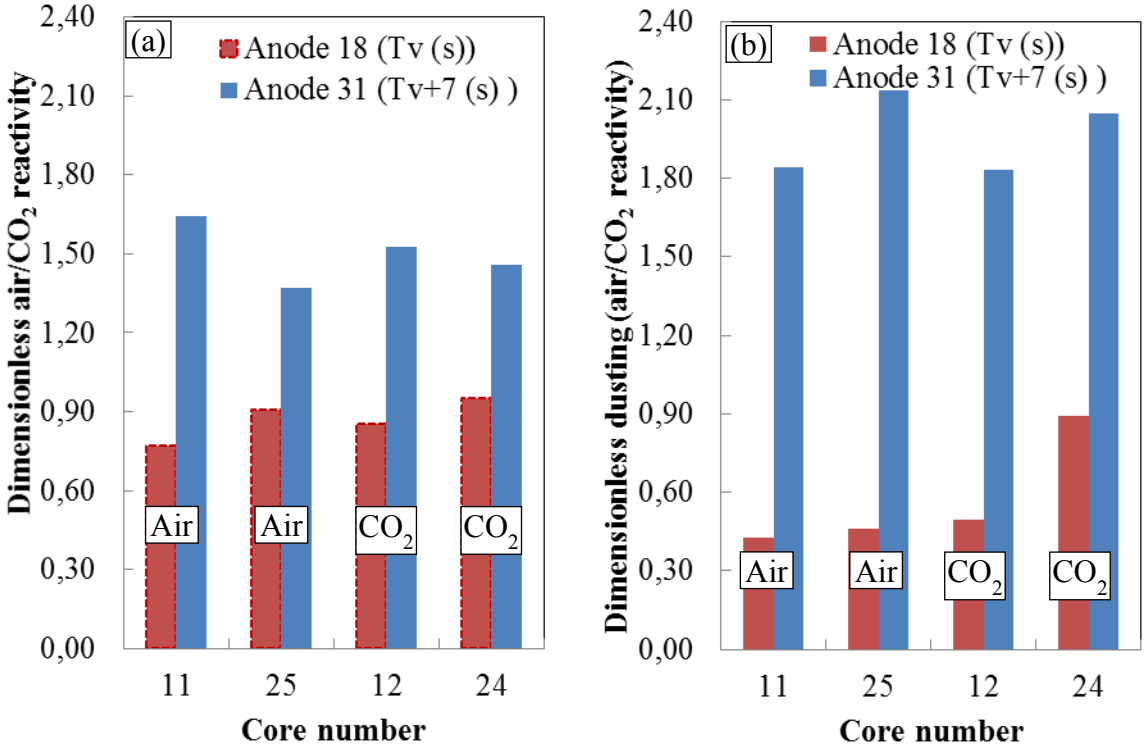

Figure 4.56: (a) Air/CO_2 reactivity and (b) Dusting (air/CO_2 reactivity) of anode core samples at two compaction times.

CHAPTER 5

CONCLUSIONS AND RECOMMENDATIONS

5.1 Conclusions

Improving the quality of carbon anodes used in aluminum production increases the productivity and decreases the energy consumption, the production cost of the process, and the emission of greenhouse gases. There are many factors affecting the anode quality. In this project, the effect of pitch properties on anodes properties was studied. More specifically, wettability of coke by pitches, some pitch chemical and physical properties, anode pitch content, kinetics of devolatilization during baking, some of the anode forming and baking parameters, and structure of anode (coke and carbonized pitch) were the elements examined in detail. The major conclusions of this work are presented below.

1. The wettability results confirmed that both the chemical and physical properties of pitches contribute to the wettability of coke by pitch. The presence of complimentary functional groups on the surfaces of coke and pitch likely induce chemical interaction between them and, hence, promote wetting. Chemical interactions can be through the formation of hydrogen bonds, acid-base interactions as well as the formation of electrostatic bonds.

2. The wettability results showed that the size distribution of solid pitch particles affects the wetting. Large particles may accumulate and form a barrier, which prevents the pitch penetration into the coke. Blending different pitches also influences the wettability of coke by pitch.

3. In addition, wettability is affected also by the particle size distribution of coke. The coke containing finer particles is wetted less by a given pitch than the same coke containing larger particles within the same particle size range since fines can block the pitch penetration.

4. High softening point pitches can wet coke better due to their lower viscosity at higher temperature. As it is well-known, they also have lower PAH content, which means lower gas emissions. The results for anodes made using higher softening point pitch showed that it is necessary to increase both pitch temperature and mixing temperature while handling this pitch. It should be noted that their utilization would require certain modifications in the plant.

5. The green anode density increased with decreasing contact angle. This indicates that the wettability of coke by pitch plays an important role on green anode properties. However, further research is needed to study the effect of wettability on baked anode properties.

6. It was observed that the pitches used in this study do not contain mesophase and mesogens. This is due to the fact that pitches used in North America are not subjected to heat treatment.

7. A new method, which involves the etching of anodes sample surfaces by hot air, developed during this study made the visualization of different baked anode components possible. The analyses showed that the carbonized pitch and the coke-pitch interface have three possible textures: lamellar, granular, and intermediate (mixture of

lamellar and granular). Coke has also three surface textures: anisotropic, isotropic, and amorphous.

8. As BAD increases, BER decreases. Dense anodes are less porous, which helps reduce the electrical resistivity. If the density is too high (over-compacted anodes), cracks might form, which reduce the BER.

9. The results of the reactivity tests carried out with anodes made with different pitches showed that the air and CO_2 reactivities have different mechanisms. The air reactivity and dusting due to air reactivity increase with increasing BAD while the trend is opposite for CO_2 reactivity and dusting due to CO_2 reactivity. Air reactivity is fast and reaction controlled. Since dense anodes have higher carbon content at the surface, air reactivity is higher. On the other hand, CO_2 reactivity is slow and diffusion controlled. CO_2 reacts preferentially with carbonized pitch causing dusting. Since the contact area is higher between this gas and coke in porous anodes, low density anodes have higher CO_2 reactivities.

10. Pitch particles were also observed in green anodes during the image analysis using optical microscopy and SEM of green anodes, which gives information on the pitch solid content and pitch distribution. These may affect the wetting of coke and the carbonization of pitch during the anode baking process.

11. The optical microscopy images of anodes baked at different temperatures indicated that the pitch, coke, and pores can be easily visualized in anodes baked at temperatures less

than 400 ºC. Etching had to be used for the anodes baked at higher temperatures since it is difficult to differentiate carbonized pitch and coke.

12. It was found that pitch blends behave differently than the pure pitches. To evaluate the impact of a pitch blend on anode properties, it needs to be tested separately because it is difficult to predict its behavior from its parent pure pitches.

13. The experiments carried out with two different vibro-compaction times showed that the density of the anode decreased with decreasing compaction time. This indicates that the compaction time has to be long enough to have good compaction of anodes. However, further increase in compaction time (over-compaction) might cause cracking, consequently, the anode density might decrease.

14. To have a good quality anode, the pitch content has to be well adjusted. Anodes with higher and lower pitch contents than required result in lower quality anodes. When the pitch content is higher, pores and cracks form due to the release of volatiles resulting in low density and high resistivity anodes. When the pitch content is lower, there is not enough pitch to fill the existing pores, cracks and the void volume between the particles. This again results in in low density and high resistivity anodes.

15. The thermogravimetric analyser is a useful tool to study the kinetics of devolatilization taking place during anode baking. This allows the determination of kinetic expressions which can be used to calculate the position and the quantity of volatile evolution in baking furnace. Such information can be used to determine the energy available from

the volatiles and to control the volatile combustion to improve the energy use. Type and quantity of pitch influences the quantity of volatiles released.

16. The rate of weight loss for the air reactivity was higher compared to that for the CO_2 reactivity. However, the depth of the reaction zone observed for air reactivity was smaller than that for the CO_2 reactivity. As air reacts faster compared to CO_2, air burns most of the surface that it is in contact with, leaving behind a smaller reaction zone. CO_2 diffuses slowly into the matrix, which results in a larger reaction zone.
17. It was found that the anode reactivities did not vary significantly with the position of anodes in the pit of the baking furnace with the exception of the one at the corner. The results indicate some relation between the maximum temperature of an anode and its reactivity; but, the factors affecting dusting are not clear.

5.2 Recommendations

The study on the wettability of coke by higher softening point pitch was carried out using two different temperatures during the wetting test. The results show that increasing temperature had a favorable effect on the wetting behavior of this pitch. Pitch viscosity decreases with increasing temperature, which leads to better spreading and penetration of pitch through the coke bed. However, the complete mechanism of the impact of softening point on wettability is complex, and further work involving the softening point and the viscosity of pitch is needed to understand the mechanism.

Anodes made with the pitch blends (best and least wetting) have higher anode density and lower electrical resistivity compared to the ones made with pure pitches in this

study. This study showed that the pitch blends play an important role on anode properties. More blends need to be tested in order to understand the behavior of pitch blends and their impact on anode properties.

In the project, an attempt was made to correlate the nature of the carbonized pitch with the characteristics of the original pitch, especially with its QI content. The impact on anode properties was also investigated. Three different textures (lamellar, intermediate, and granular) were found in the same carbonized pitch. However, it is difficult to measure the proportion of different components of the carbonized pitch in an anode because of the small percentage of pitch. Further study is needed to develop a method to measure the proportion of these three different components of the carbonized pitch in an anode and correlate them with anode properties.

References

1. K.L. Hulse, *Anode manufacture : Raw materials, formulation and processing parameters (*Sierre [Suisse]: R & D Carbon Ltd., 2000), xxxv, 416 p.

2. R. Menéndez, M. Granda, and J. Bermejo, *Introduction to carbon technologies (*1997), 461.

3. R.C. Perruchoud, M.W. Meier, and W. Fischer, *Worldwide pitch quality for prebaked anodes*, in *TMS (The Minerals, Metals & Materials Society) Annual Meeting and Exhibition*, P.N. Crepeau, Editor. 2003, Light Metals: San Diego, California. p. 509-518.

4. J.W. Stadelhofer, W. Gemmeke, and M. Zander, *Characterization of binder pitches (iii),* in *AIME Annual Meeting*. 1983, Light Metals: Atlanta, Ga, USA. p. 1211-1221.

5. B.J. Mason, and P.M. Najjar, *Laboratory assessment of binder pitch performance,* in *TMS (The Minerals, Metals & Materials Society) Annual Meeting and Exhibition*, E. Rooy, Editor. 1991, Light Metals 1991: New Orleans, LA, USA. p. 585-590.

6. H.Marsh, *Introduction to carbon science (*Butterworth-Heinemann, 1989), vii.

7. A. Alscher, R. Wildfoerster, and J.A. Sharp, *Performance of binder pitches with decreased qi-content in anode making formation - nature - properties and substitution of quinoline insolubles*, in *TMS (The Minerals, Metals & Materials Society) Annual Meeting and Exhibition*, C.M. Bickert, Editor. 1990, Light Metals: San Diego, California. USA. p. 232-236.

8. J.A. Branscomb, Dr.V.L.Bullough, and H.A.Morrissey *The relationship of pitch properties to anode properties*. 1966. 115-123.

9. M. Sakai, Y. Wang, T. Fukuoka, and H. Hatano, *Importance of primary quinoline insoluble in binder pitch for anode*, in *TMS (The Minerals, Metals & Materials Society) Annual Meeting and Exhibition*, C.E. Suarez, Editor. 2012, Light Metals: Orlando, FL. p. 1223-1228.

10. A. Alscher, W. Gemmeke, F. Alsmeier, and W. Boenigk. *Evaluation of electrode binder pitches for the production of prebaked anodes using a bench scale process*. in *AIME Annual Meeting*. 1987. Warrendale, PA, USA. Denver, CO, USA: Light Metals.

11. D. Belitskus, and W. Hill, *Properties of bench scale anodes produced using binder pitches varying in primary and secondary qi contents*, in *TMS (The Minerals, Metals & Materials Society) Annual Meeting and Exhibition*, C.M. Bickert, Editor. 1990, Light Metals: Anaheim, CA, USA. p. 577-581.

12. T.A. Golubic, S.A. McKinney, and R.H. Wombles, *High softening point coal tar pitch as anode binder pitch*, in *TMS (The Minerals, Metals & Materials Society) Annual Meeting and Exhibition*, J.A. Johnson, Editor. 2010, Light Metals: Seattle, WA. p. 909-911.

13. S.M. Hume, *Anode reactivity : Influence of raw material properties (*Sierre [Suisse]: R & D Carbon Ltd., 1999), xi, 433 p.

14. A. Sarkar, D. Kocaefe, Y. Kocaefe, D. Bhattacharyay, B. Morais, and M. Pouliot. *Characterization of petroleum coke and butts used in anode manufacturing in*

aluminum industry. in *Materials Science and Technology Conference and Exhibition 2013, MS and T 2013*. 2014. Montreal, QC.

15. E.R. McHenry, J.T. Baron, and W.E. Saver, *Effect of thermal treatment on industrial pitch and carbon anode properties-part 2*, in *TMS (The Minerals, Metals & Materials Society) Annual Meeting and Exhibition*, U. Mannweiler, Editor. 1994, Light Metals: Warrendale, PA. p. 525-533.

16. D. Hays, J.W. Patrick, and A. Walker, "Sem study of binder coke in electrode carbon," *Fuel*. 62(8) (1983), p. 946-952.

17. R. H.Wombles, and B. Sadler. *The effect of binder pitch quinoline insolubles content on aluminum anode physical properties*. in *Australasian Aluminium Smelting Technology Conference*. 2004. Queensland, AU: Coke oven managers' year book.

18. S.S. Jones, and R.D. Hildebrandt, *Electrode binder pyrolysis and bond-coke microstructure (*John Wiley and Sons, Vol. 4. 2013).

19. E.A. Heintz, "Influence of coke structure on the properties of the carbon-graphite artefact," *Fuel*. 64(9) (1985), p. 1192-1196.

20. N. Turner, *Influence of pitch qi particle type and size on anode quality. The volatiles emitted from bench-scale anodes during bake*, in *TMS (The Minerals, Metals & Materials Society) Annual Meeting and Exhibition*, E. Cutshall, Editor. 1992, Light Metals: San Diego, CA. p. 571-580.

21. W. Boenigk, A. Niehoff, and R. Wildfoerster, *Influence of qi content on binder pitch performance*, in *TMS (The Minerals, Metals & Materials Society) Annual*

Meeting and Exhibition, E. Rooy, Editor. 1991, Light Metals: New Orleans, LA. p. 615-619.

22. S.S. Jones, and E.F. Bart, *Role of primary quinoline-insolubles in pitch-coke bond formation in anode carbon*, in *TMS (The Minerals, Metals & Materials Society) Annual Meeting and Exhibition*, E. Rooy, Editor. 1991, Light Metals: New Orleans, LA. p. 609-613.

23. J.L. Saint Romain, P. Lagassie, R. Bertau, and B. Souffrey, *Qi in coal tar pitches part. 1: Investigation of coke oven parameters acting on tar characteristics*, in *TMS (The Minerals, Metals & Materials Society) Annual Meeting and Exhibition*, C.M. Bickert, Editor. 1990, Light Metals: Warrendale, PA, United States,Anaheim, CA, USA. p. 591-595.

24. P.J. Rhedey, *Laboratory evaluation of a low quinoline insolubles coal-tar pitch as anode binder*, in *TMS (The Minerals, Metals & Materials Society) Annual Meeting and Exhibition*, C.M.Bickert, Editor. 1990, Light Metals: Warrendale, PA,Anaheim, CA. p. 605-608.

25. A.N. Adams, J.P. Mathews, and H.H. Schobert, *The use of image analysis for the optimization of pre-baked anode formulation*, in *TMS (The Minerals, Metals & Materials Society) Annual Meeting and Exhibition*, W. Schneider, Editor. 2002, Light Metals: Seattle, WA. p. 547-552.

26. N.R. Turner, *Improvements in anode binder pitches by advances in raw materials handling, manufacturing and transportation*, in *TMS (The Minerals, Metals & Materials Society) Annual Meeting and Exhibition*, C.M.Bickert, Editor. 1990, Light Metals: Warrendale, PA,Anaheim, CA. p. 629-638.

27. Anon, *Year-book of the coke oven managers' association 1984 (*Coke Oven Managers' Association (Year Book) Ltd, Mexborough, 1984), 247p.

28. K.N. Tran, A.J. Berkovich, A. Tomsett, and S.K. Bhatia, "Influence of sulfur and metal microconstituents on the reactivity of carbon anodes," *Energy and Fuels*. 23(4) (2009), p. 1909-1924.

29. P. Couderc, P. Hyvernat, and J.L. Lemarchand, "Correlations between ability of pitch to penetrate coke and the physical characteristics of prebaked anodes for the aluminium industry," *Fuel*. 65(2) (1986), p. 281-287.

30. V.G. Rocha, C. Blanco, R. Santamaría, E.I. Diestre, R. Menéndez, and M. Granda, "The effect of the substrate on pitch wetting behaviour," *Fuel Processing Technology*. 91(11) (2010), p. 1373-1377.

31. M.B. Dell, and R.W. Peterson, "Wettability of petroleum cokes by pitch," *Industrial and Engineering Chemistry Product Research and Development*. 9(2) (1970), p. 190-194.

32. J. Lahaye, J.P. Aubert, and A. Buscailhon, "Interaction between a coke and a tar. 2. Limit of tar penetration in coke porosity," *Fuel*. 56(2) (1977), p. 188-191.

33. S.S. Jones, and E.F. Bart, *Binder for the ideal anode carbon*, in *TMS (The Minerals, Metals & Materials Society) Annual Meeting and Exhibition*, C.M.Bickert, Editor. 1990, Light Metals: Anaheim, CA, USA. p. 611-627.

34. D. Hays, J.W. Patrick, and A. Walker, "A scanning electron microscope study of fractured and etched metallurgical coke surfaces," *Fuel*. 61(3) (1982), p. 232-236.

35. V.G. Rocha, C. Blanco, R. Santamaría, E.I. Diestre, R. Menéndez, and M. Granda, "An insight into pitch/substrate wetting behaviour. The effect of the substrate processing temperature on pitch wetting capacity," *Fuel*. 86(7-8) (2007), p. 1046-1052.

36. A. Sarkar, D. Kocaefe, Y. Kocaefe, D. Sarkar, D. Bhattacharyay, B. Morais, and J. Chabot, "Coke-pitch interactions during anode preparation," *Fuel*. 117(PART A) (2014), p. 598-607.

37. E.A. Heintz, "Wetting of filler by binder-a simple apparatus for determining wetting temperatures," *Carbon*. 24(2) (1986), p. 131-134.

38. S.Q. Shi, and D.J. Gardner, "Dynamic adhesive wettability of wood," *Wood and Fiber Science*. 33(1) (2001), p. 58-68.

39. X. Huang, D. Kocaefe, Y. Kocaefe, and D. Bhattacharyay, "Wettability of bio-coke by coal tar pitch for its use in carbon anodes," *Colloids and Surfaces A: Physicochemical and Engineering Aspects*. 490 (2016), p. 133-144.

40. X. Huang, D. Kocaefe, Y. Boluk, Y. Kocaefe, and A. Pichette, "Effect of surface preparation on the wettability of heat-treated jack pine wood surface by different liquids," *European Journal of Wood and Wood Products*. 70(5) (2012), p. 711-717.

41. A. International, *Standard test method for apparent density by physical measurements of manufactured anode and cathode carbon used by the aluminum industry (d5502-00)*. 2005.

42. A. International, *Standard test method for electrical resistivity of anode and cathode carbon material at room temperature (d6120-97)*. 2007.

43. W.K.Fischer, and R.Perruchoud, "Determining prebaked anode properties for aluminum production," *Journal of metals*. 39(11) (1987), p. 43-45.

44. A. International, *Standard test method for determination of tga co_2 reactivity of baked carbon anodes and cathode blocks (d6558-00a)*. 2010.

45. A. International, *Standard test method for determination of tga air reactivity of baked carbon anodes and cathode blocks (d6559-00a)*. 2010.

46. X.Y. Kocaefe.D, Kocaefe.Y, Liu.W, Zou.S, Wu.A, "Thermogravimetric study on devolatilization kinetics of chinalco anodes during baking," *Journal of Materials Science Research*. 2(2) (2013), p. 22-34.

47. A. Charette, D. Kocaefe, J. Ferland, and P. Couderc, *Kinetic study of the pyrolysis of impregnated carbon electrodes*, in *TMS (The Minerals, Metals & Materials Society) Annual Meeting and Exhibition*, P.G. Campbell, Editor. 1989, Publ by Metallurgical Soc of AIME: Warrendale, PA,Las Vegas, NV. p. 489-494.

48. M.R.J. Tosta, and E.M. Inzunza, *Structural evaluation of coke of petroleum and coal tar pitch for the elaboration of anodes in the industry of the aluminum*, in *TMS (The Minerals, Metals & Materials Society) Annual Meeting and Exhibition*, D.H. Deyoung, Editor. 2008, Light Metals: New Orleans, LA. p. 887-892.

49. K. Neyrey, L. Edwards, J. Anthony Ross, and F. Vogt, *A tool for predicting anode performance of non-traditional calcined cokes*, in *TMS (The Minerals, Metals & Materials Society) Annual Meeting and Exhibition*, H. Kvande, Editor. 2005, Light Metals: San Francisco, CA. p. 607-612.

50. A. Innus, A. Jomphe, and H. Darmstadt, *A method for the rapid characterization of petroleum coke microstructure using polarized light microscopy*, in *TMS (The Minerals, Metals & Materials Society) Annual Meeting and Exhibition*, B. Sadler, Editor. 2013, Light Metals: San Antonio, TX. p. 1069-1073.

51. D. Hays, J.W. Patrick, and A. Walker, "Sem characterization of cokes and carbons," *Fuel*. 62(9) (1983), p. 1079-1083.

52. R. Menéndez, M. Granda, and J. Bermejo, "Relationships between pitch composition and optical texture of cokes," *Carbon*. 35(4) (1997), p. 555-562.

53. E.R. McHenry, J.T. Baron, and K.C. Krupinski, *Development of anode binder pitch laboratory characterization methods*, in *TMS (The Minerals, Metals & Materials Society) Annual Meeting and Exhibition*, B.J. Welch, Editor. 1998, Light Metals: San Antonio, TX, USA. p. 769-774.

54. S. Rørvik, A.P. Ratvik, and T. Foosnæs, *Characterization of green anode materials by image analysis*, in *TMS (The Minerals, Metals & Materials Society) Annual Meeting and Exhibition*, T.J. Galloway, Editor. 2006, Light Metals: San Antonio, TX. p. 553-558.

55. H. Marsh, M. Forrest, and L.A. Pacheco, "Structure in metallurgical cokes and carbons as studied by etching with atomic oxygen and chromic acid," *Fuel*. 60(5) (1981), p. 423-428.

56. S. Amrani. "The effect of anode baking conditions on anode crack formation," (PhD, Université du Québec à Chicoutimi, 2015),

57. K.D. Lu.Y, Kocaefe.Y, Bhattacharyay.D, Huang.X, Morais.B, *Study of the wetting of coke by different pitches*, in *TMS (The Minerals, Metals & Materials Society) Annual Meeting and Exhibition*, E. Williams, Editor. 2016, Light Metals: Nashville, TN. p. 871-876.

58. Y. Kocaefe, D. Kocaefe, and D. Bhattacharyay, *Quality control via electrical resistivity measurement of industrial anodes*, in *TMS (The Minerals, Metals & Materials Society) Annual Meeting and Exhibition*, M. Hyland, Editor. 2015, Light Metals: Orlando, FL. p. 1097-1102.

59. D. Kocaefe, Y. Kocaefe, and D. Bhattacharyay, *Measurement of anode electrical resistivity for quality control in aluminum industry*, in *COM (Conference of Metallurgists)*. 2014: Vancouver,BC.

60. D. Kocaefe, A. Charette, and L. Castonguay, "Green coke pyrolysis: Investigation of simultaneous changes in gas and solid phases," *Fuel*. 74(6) (1995), p. 791-799.

61. O. Levenspiel, "Chemical reaction engineering," *Industrial and Engineering Chemistry Research*. 38(11) (1999), p. 4140-4143.

62. M.D. Guillén, M.J. Iglesias, A. Domínguez, and C.G. Blanco, "Semiquantitative ftir analysis of a coal tar pitch and its extracts and residues in several organic solvents," *Energy & Fuels*. 6(4) (1992), p. 518-525.

63. A.N. Buckley, "Nitrogen functionality in coals and coal-tar pitch determined by x-ray photoelectron spectroscopy," *Fuel Processing Technology*. 38(3) (1994), p. 165-179.

64. J.M. Jiménez Mateos, and J.L.G. Fierro, “X-ray photoelectron spectroscopic study of petroleum fuel cokes,” *Surface and Interface Analysis*. 24(4) (1996), p. 223-236.

65. H. Estrade-Szwarckopf, “Xps photoemission in carbonaceous materials: A “defect” peak beside the graphitic asymmetric peak,” *Carbon*. 42(8–9) (2004), p. 1713-1721.

66. R.I.R. Blyth, H. Buqa, F.P. Netzer, M.G. Ramsey, J.O. Besenhard, P. Golob, and M. Winter, “Xps studies of graphite electrode materials for lithium ion batteries,” *Applied Surface Science*. 167(1–2) (2000), p. 99-106.

Appendix 1

XPS analysis of different pitches and coke

Table A.1.1: Atomic percentages of elements in different samples.

Pitch type	C (%)	O (%)	N (%)	S (%)
Pitch-1	96.62	1.89	1.21	0.29
Pitch-2	96.93	1.74	1.07	0.25
MP12	96.80	1.76	1.16	0.29
Pitch-6	97.16	1.59	0.96	0.29
Pitch-3	97.98	1.05	0.7.0	0.26
MP35	97.80	1.19	0.79	0.25
Pitch-5	97.61	1.18	0.94	0.27
Pitch-4	98.01	1.25	0.53	0.21
Coke	95.89	2.53	0.60	0.98

Table A.1.2: Carbon (C1s) functional groups of different samples.

Pitch type	C=C	C-C	CN/CO/CS/C=O/CSO_2/COOH
Pitch-1	81.42	13.00	5.58
Pitch-2	78.66	15.96	5.38
MP12	79.19	15.46	3.35
Pitch-6	79.04	15.62	5.34
Pitch-3	79.41	16.74	3.85
MP35	79.52	16.47	4.01
Pitch-5	81.29	14.42	4.29
Pitch-4	75.01	21.03	3.69
Coke	80.54	12.21	7.25

Table A.1.3: Oxygen (O1s) functional groups of different samples.

Pitch type	C=O	C-O	$C(NH_2)COOH$
Pitch-1	44.94	40.93	14.64
Pitch-2	31.73	37.49	30.78
MP12	40.48	41.42	18.10
Pitch-6	48.64	41.96	9.40
Pitch-3	43.84	54.81	10.35
MP35	43.46	47.10	9.44
Pitch-5	42.05	46.32	11.63
Pitch-4	40.20	47.46	12.34
Coke	49.63	39.99	10.37
Coke-2*	44.71	45.70	9.59

Table A.1.4: Nitrogen (N1s) functionality of different samples.

Pitch type	Pyridine	NR_3/CN	Pyrrole	N+
Pitch-1	28.68	21.38	49.94	-
Pitch-2	31.59	9.47	58.93	-
MP12	24.00	-	68.92	7.09
Pitch-6	27.19	7.91	54.94	9.96
Pitch-3	-	-	-	-
MP35	24.60	7.84	52.37	15.20
Pitch-5	14.97	5.26	58.69	21.09
Pitch-4	-	-	-	-
Coke	39.84	-	47.75	12.41

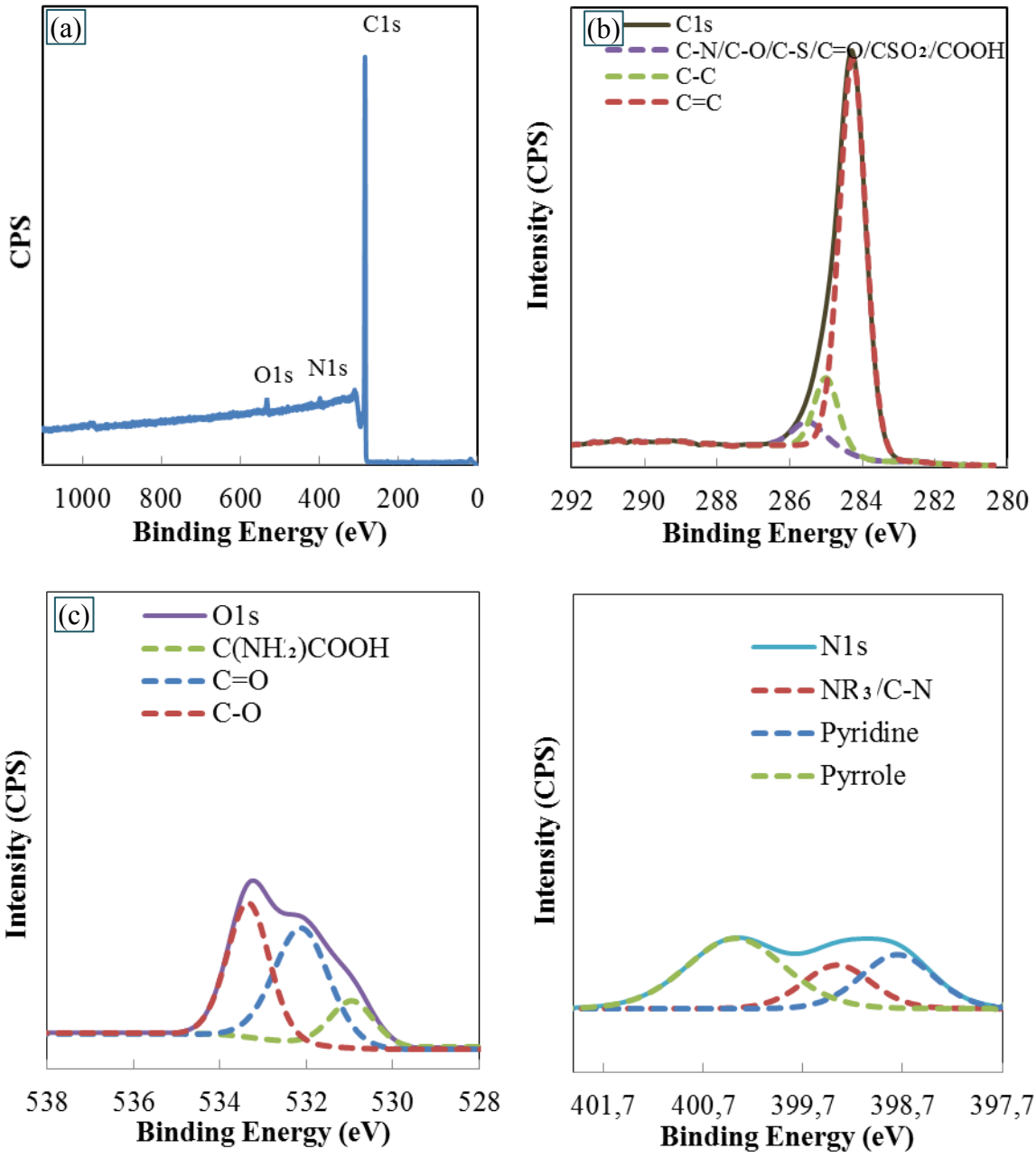

Figure.A.1.1: XPS spectra of Pitch-1 (a) Survey spectra, (b) De-convoluted C1s spectra, (c) De-convoluted O1s spectra, (d) De-convoluted N1s spectra.

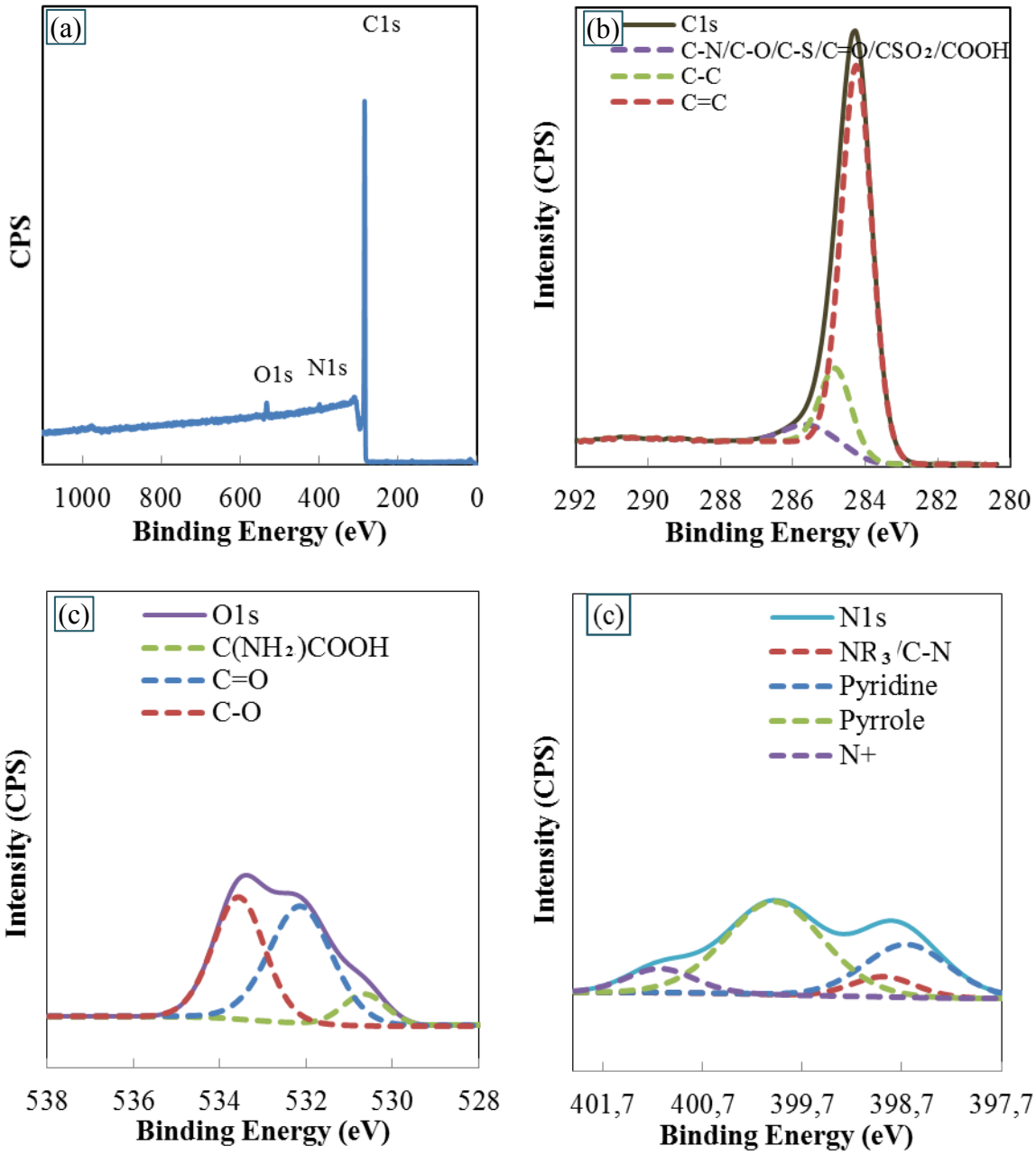

Figure.A.1.2: XPS spectra of Pitch-6 (a) Survey spectra, (b) De-convoluted C1s spectra, (c) De-convoluted O1s spectra, (d) De-convoluted N1s spectra.

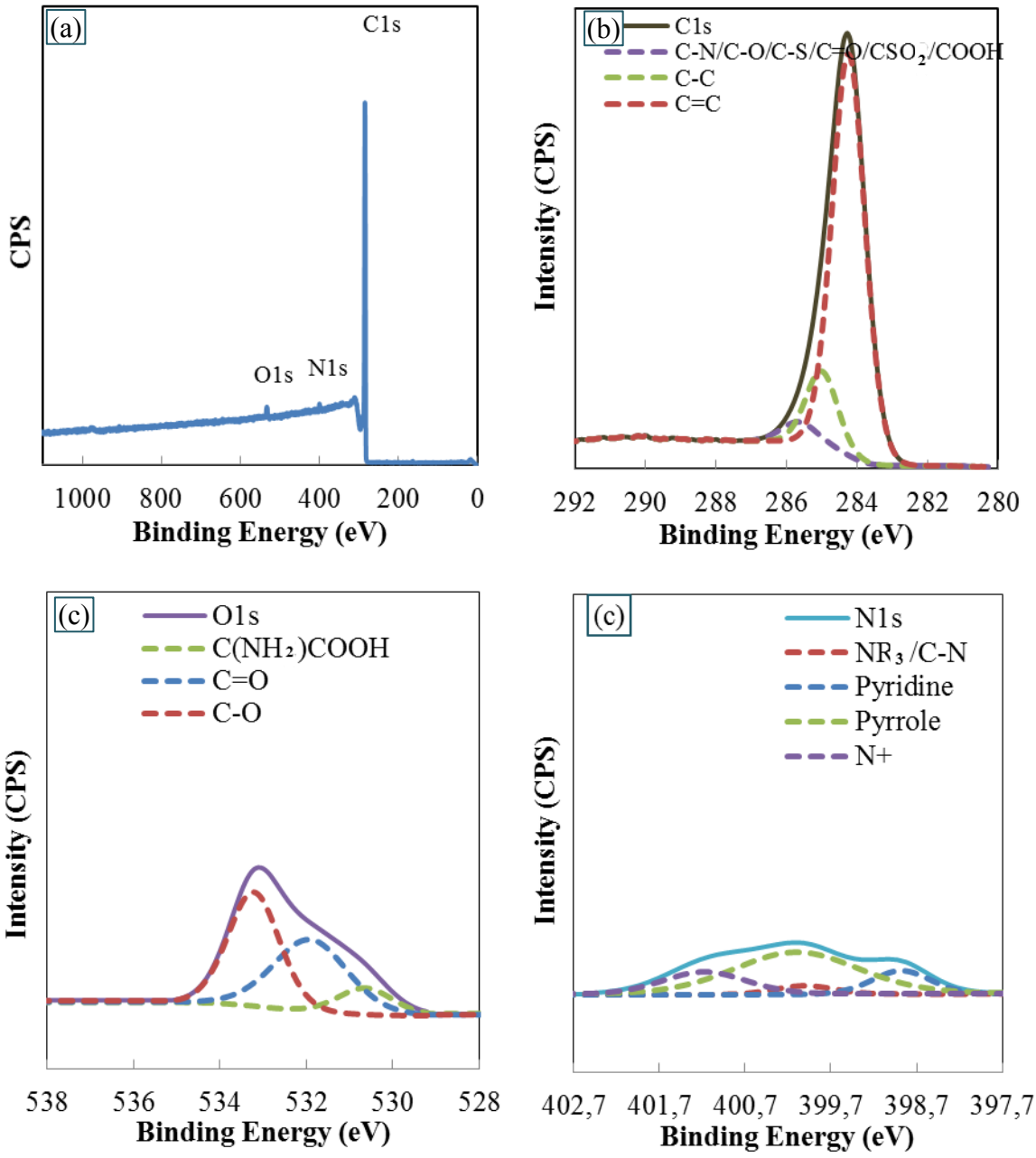

Figure.A.1.3: XPS spectra of Pitch-5 (a) Survey spectra, (b) De-convoluted C1s spectra, (c) De-convoluted O1s spectra, (d) De-convoluted N1s spectra.

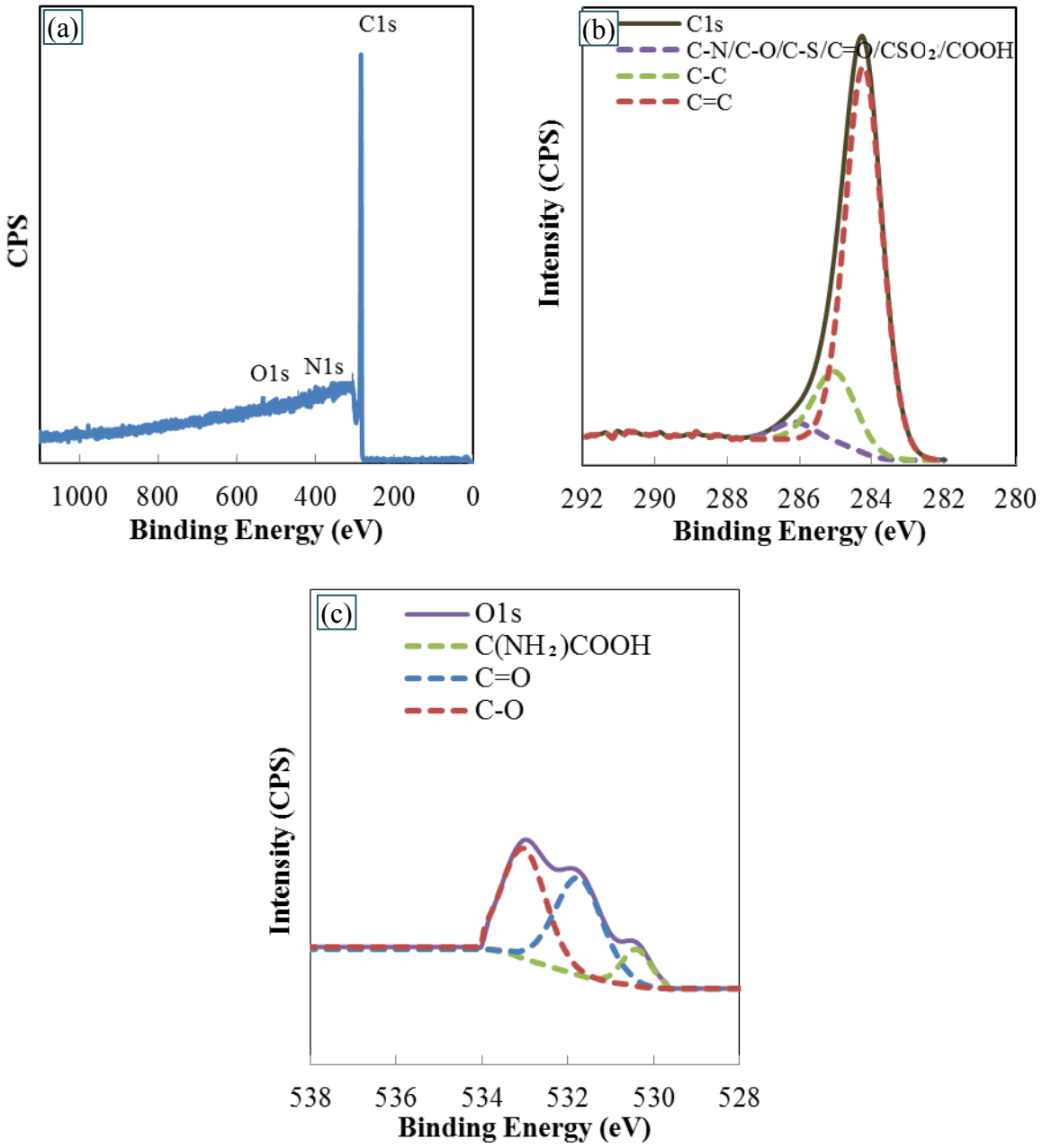

Figure.A.1.4: XPS spectra of Pitch-3 (a) Survey spectra, (b) De-convoluted C1s spectra, (c) De-convoluted O1s spectra, (d) De-convoluted N1s spectra.

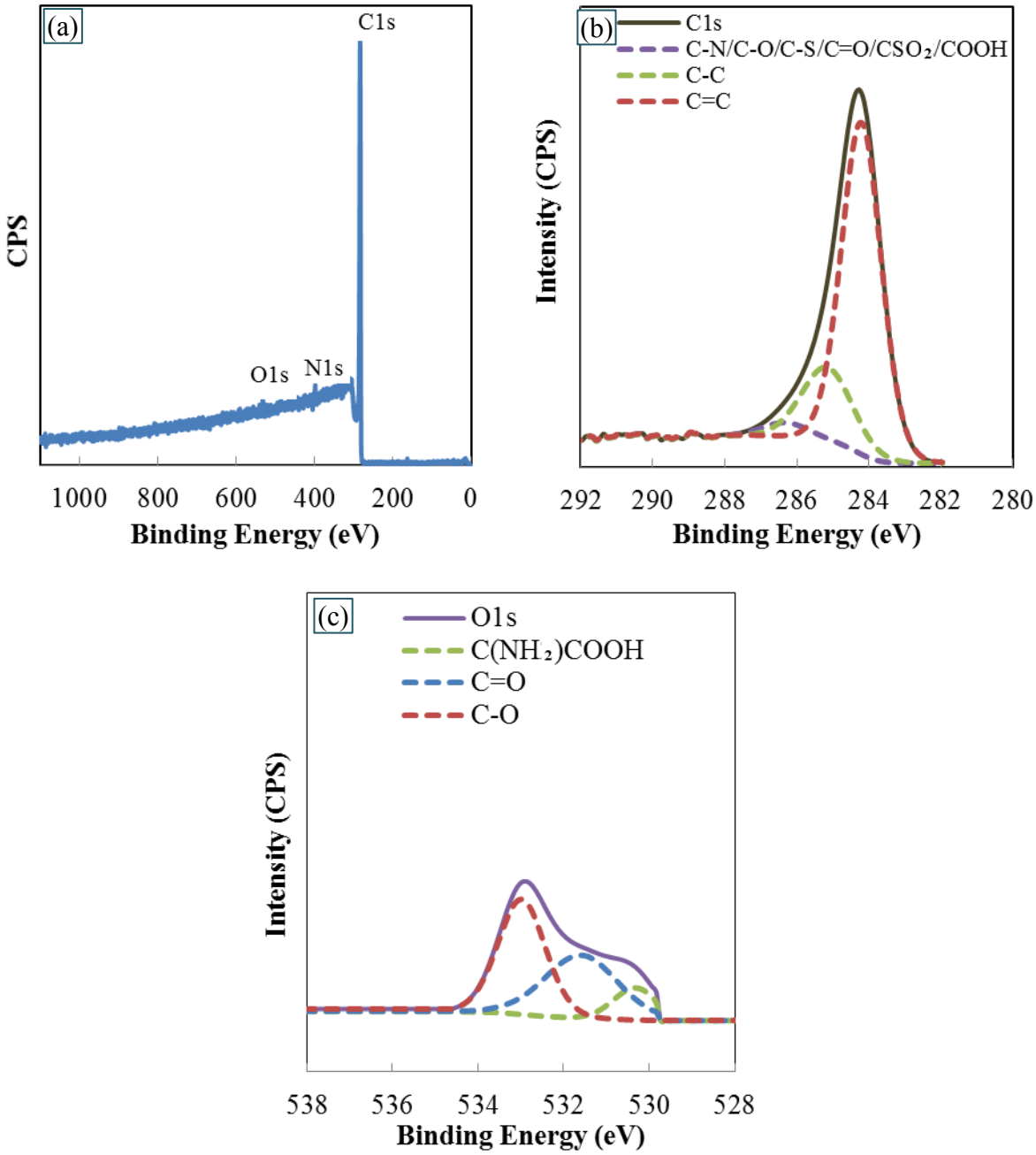

Figure.A.1.5: XPS spectra of Pitch-4 (a) Survey spectra, (b) De-convoluted C1s spectra, (c) De-convoluted O1s spectra, (d) De-convoluted N1s spectra.

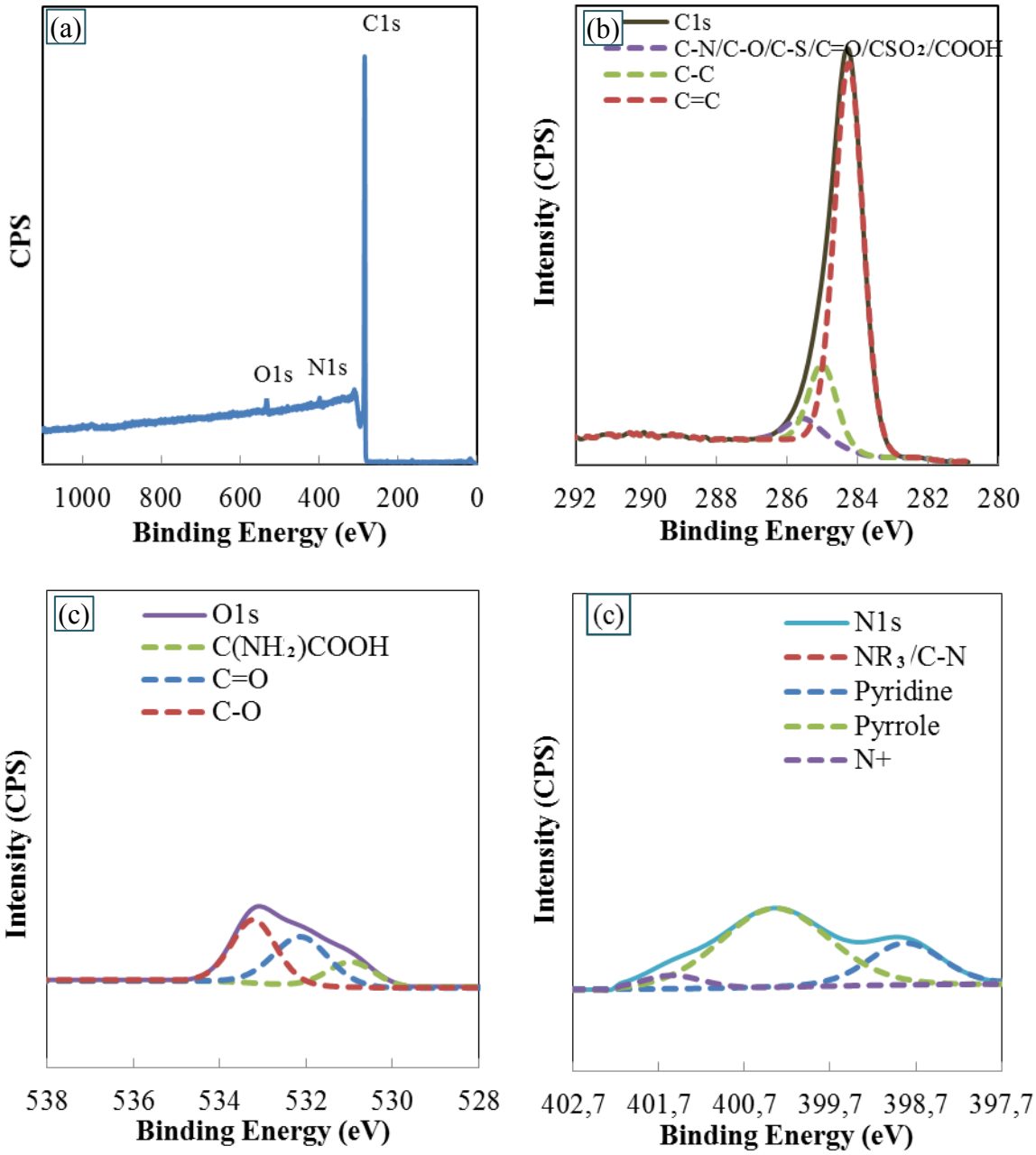

Figure.A.1.6: XPS spectra of MP12 (a) Survey spectra, (b) De-convoluted C1s spectra, (c) De-convoluted O1s spectra, (d) De-convoluted N1s spectra.

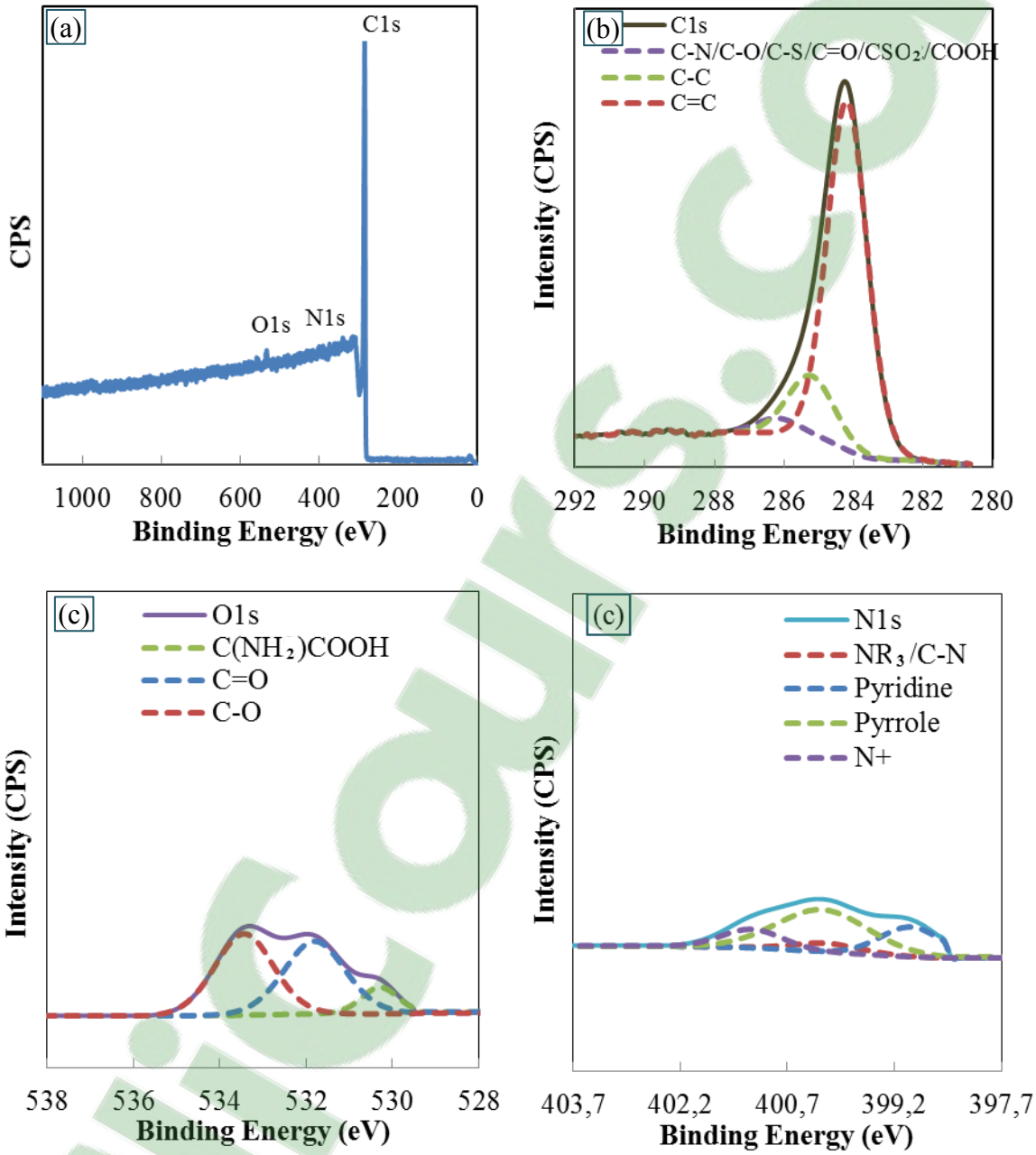

Figure.A.1.7: XPS spectra of MP35 (a) Survey spectra, (b) De-convoluted C1s spectra, (c) De-convoluted O1s spectra, (d) De-convoluted N1s spectra.

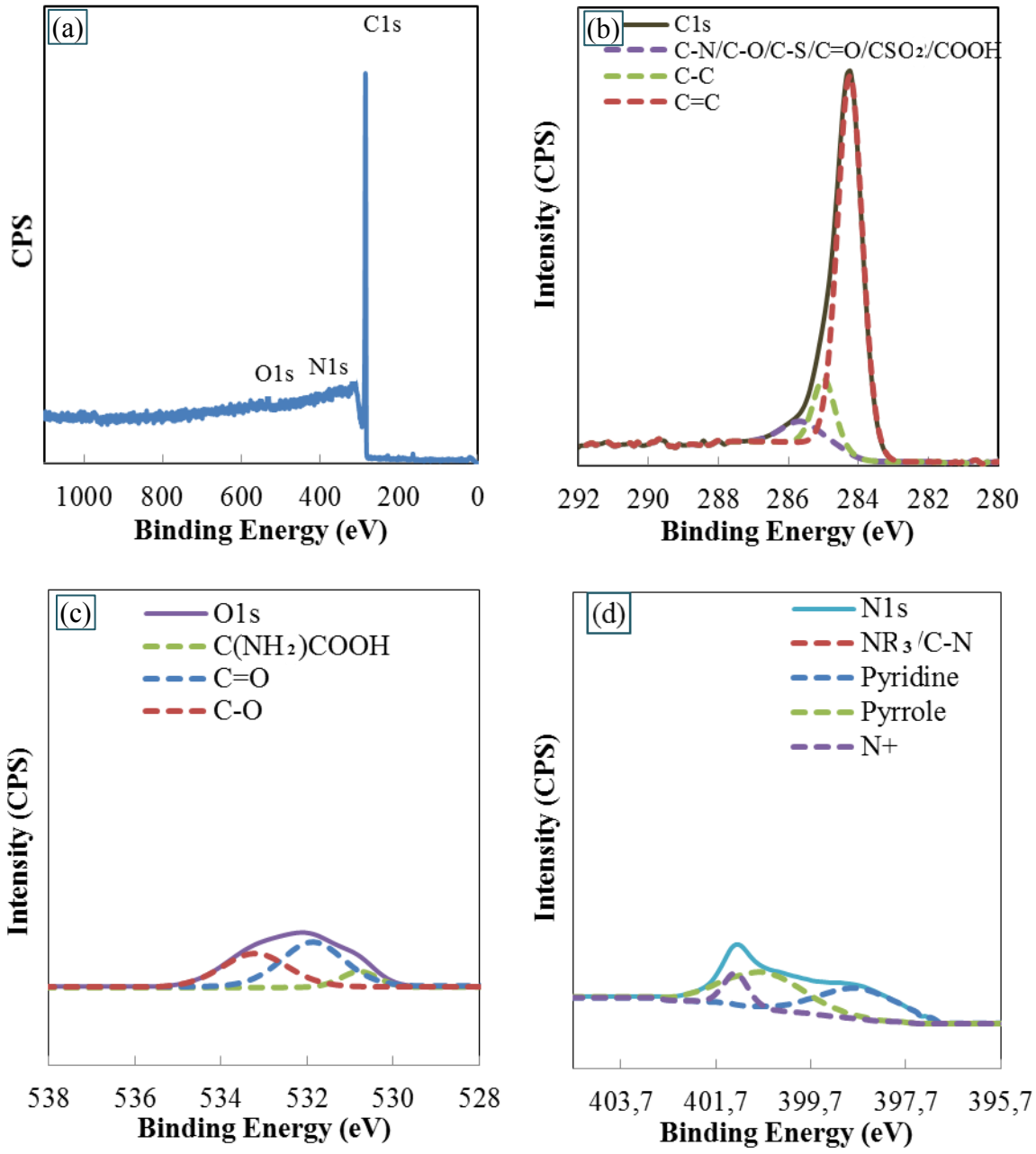

Figure.A.1.8: XPS spectra of Coke (a) Survey spectra, (b) De-convoluted C1s spectra, (c) De-convoluted O1s spectra, (d) De-convoluted N1s spectra.

Appendix 2

Wettability of different pure pitches and their blends

Table A.2.1: Contact angles and K-values of different pure pitch and their blends on coke.

Pitch type	Initial θ°	θ° at 60 s	θ° decrease	K-value	R2
Pitch-1 (100%)	85.9	1.0	98.84%	0.0422	0.9312
Pitch-1 (75%) & Pitch-2 (25%)	89.0	25.8	71.03%	0.0315	0.9226
Pitch-1 (25%) & Pitch-2 (75%)	88.9	33.0	62.89%	0.0294	0.9290
Pitch-2 (100%)	89.4	21.2	76.29%	0.0317	0.9044
Pitch-1 (100%)	85.9	1.0	98.84%	0.0422	0.9312
Pitch-1 (75%) & Pitch-3 (25%)	91.6	36.9	59.73%	0.0315	0.9200
Pitch-1 (25%) & Pitch-3 (75%)	89.8	35.6	60.38%	0.0296	0.9119
Pitch-3 (100%)	91.0	33.5	63.21%	0.0261	0.9390
Pitch-2 (100%)	89.4	21.2	76.29%	0.0317	0.9044
Pitch-2 (75%) & Pitch-3 (25%)	91.6	22.8	75.12%	0.0304	0.9131
Pitch-2 (25%) & Pitch-3 (75%)	90.8	36.9	59.40%	0.0252	0.9226
Pitch-3 (100%)	81.4	33.5	58.84%	0.1927	0.9475
Pitch-2 (100%)	89.4	21.2	76.29%	0.0302	0.9239
Pitch-2 (75%) & Pitch-4 (25%)	90.3	52.9	41.44%	0.0123	0.9109
Pitch-2 (25%) & Pitch-4 (75%)	93.9	60.2	35.93%	0.0135	0.9370
Pitch-4 (100%)	93.3	62.1	33.40%	0.0094	0.9591
Pitch-2 (100%)	89.4	21.2	76.29%	0.0317	0.9044
Pitch-2 (75%) & Pitch-5 (25%)	93.9	40.1	57.27%	0.0210	0.9125
Pitch-2 (25%) & Pitch-5 (75%)	89.4	51.2	42.76%	0.0151	0.9445
Pitch-5 (100%)	83.8	59.5	28.92%	0.0255	0.9705
Pitch-2 (100%)	89.4	21.2	76.29%	0.0317	0.9044
Pitch-2 (75%) & Pitch-6 (25%)	92.9	39.8	57.21%	0.0242	0.9221
Pitch-2 (25%) & Pitch-6 (75%)	91.1	27.8	69.43%	0.0295	0.9111
Pitch-6 (100%)	92.3	25.8	72.05%	0.0303	0.9422
Pitch-3 (100%)	91.0	33.5	63.21%	0.0261	0.9390
Pitch-3 (75%) & Pitch-5 (25%)	96.3	53.1	44.82%	0.0198	0.9571
Pitch-3 (25%) & Pitch-5 (75%)	94.5	61.4	35.01%	0.0154	0.9427
Pitch-5 (100%)	93.5	59.5	36.34%	0.0117	0.9669
Pitch-3 (100%)	91.0	33.5	63.21%	0.0261	0.9390
Pitch-3 (75%) & Pitch-6 (25%)	94.4	34.4	63.58%	0.0294	0.9131
Pitch-3 (25%) & Pitch-6 (75%)	92.7	25.5	72.46%	0.0352	0.9177
Pitch-6 (100%)	92.3	25.8	72.05%	0.0303	0.9422

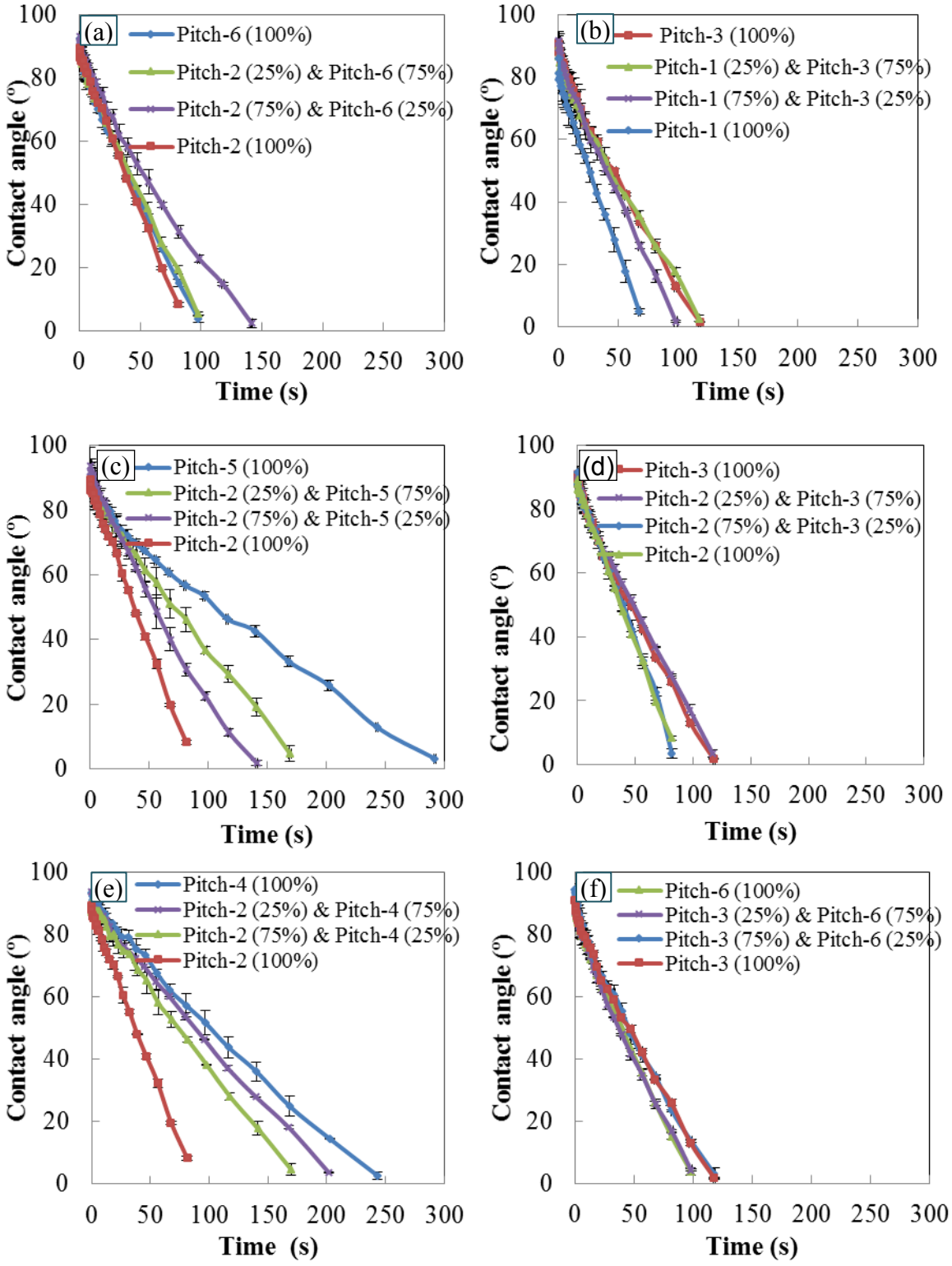

Figure.A.2.1: Contact angles of different pure pitches and their blends.

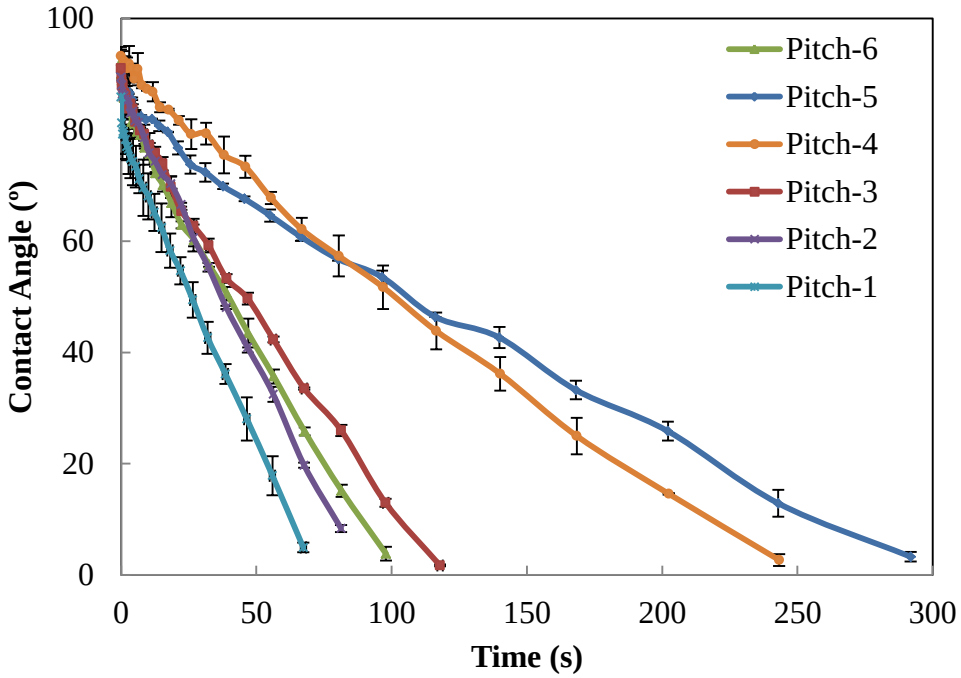

Figure.A.2.2: Contact angles of different pure pitches.

Appendix 3

XPS analysis of green and baked anodes

Table A.3.1: Atomic percentages of elements in different samples.

Anodes	C (%)	O (%)	N (%)	S (%)
Green anode (Pitch-2)	95.73	3.38	0.62	0.27
Green anode (Pitch-4)	94.44	2.22	2.79	0.55
Baked anode (Pitch-2)	93.07	5.41	1.36	0.16
Baked anode (Pitch-4)	94.59	2.64	2.44	0.33

Table A.3.2: Carbon (C1s) functional groups of different samples.

Anodes	C=C	C-C	CN/CO/CS/C=O/CSO_2/COOH
Green anode (Pitch-2)	44.62	47.71	7.67
Green anode (Pitch-4)	60.03	30.79	9.18
Baked anode (Pitch-2)	46.81	43.29	9.89
Baked anode (Pitch-4)	68.16	22.72	9.12

Table A.3.3: Oxygen (O1s) functional groups of different samples.

Anodes	C=O	C-O	$C(NH_2)COOH$
Green anode (Pitch-2)	36.71	15.29	48.01
Green anode (Pitch-4)	38.46	14.11	47.43
Baked anode (Pitch-2)	27.57	8.98	63.45
Baked anode (Pitch-4)	37.09	15.45	47.46

Table A.3.4: Nitrogen (N1s) functionality of different samples.

Anodes	Pyridine	NR_3/CN	Pyrrole	N+
Green anode (Pitch-2)	26.87	39.62	17.95	15.55
Green anode (Pitch-4)	17.20	15.82	32.66	34.33
Baked anode (Pitch-2)	21.70	31.45	26.71	20.14
Baked anode (Pitch-4)	14.32	15.73	34.06	35.88

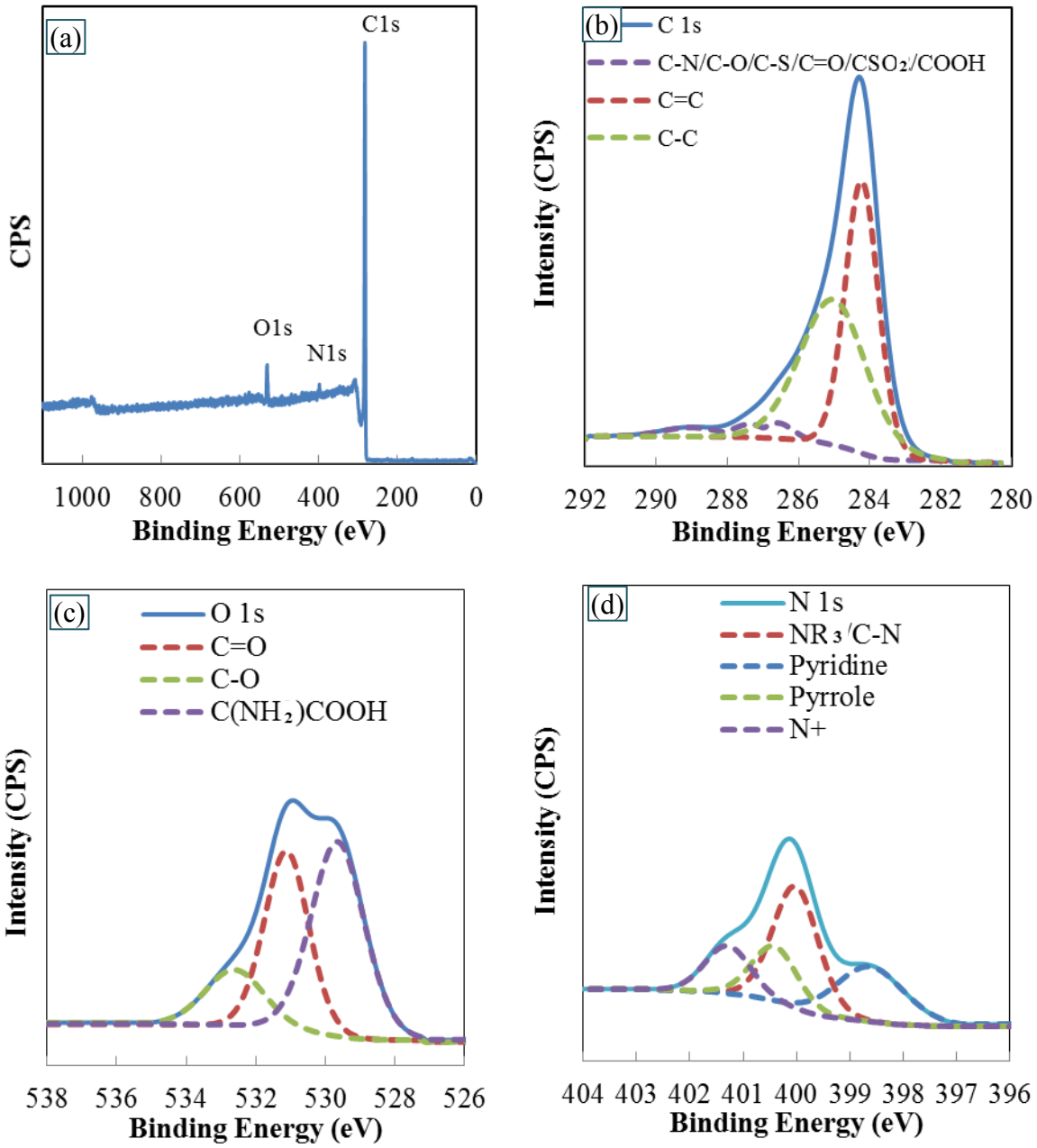

Figure.A.3.1: XPS spectra of green anode (Pitch-2) (a) Survey spectra, (b) De-convoluted C1s spectra, (c) De-convoluted O1s spectra, (d) De-convoluted N1s spectra.

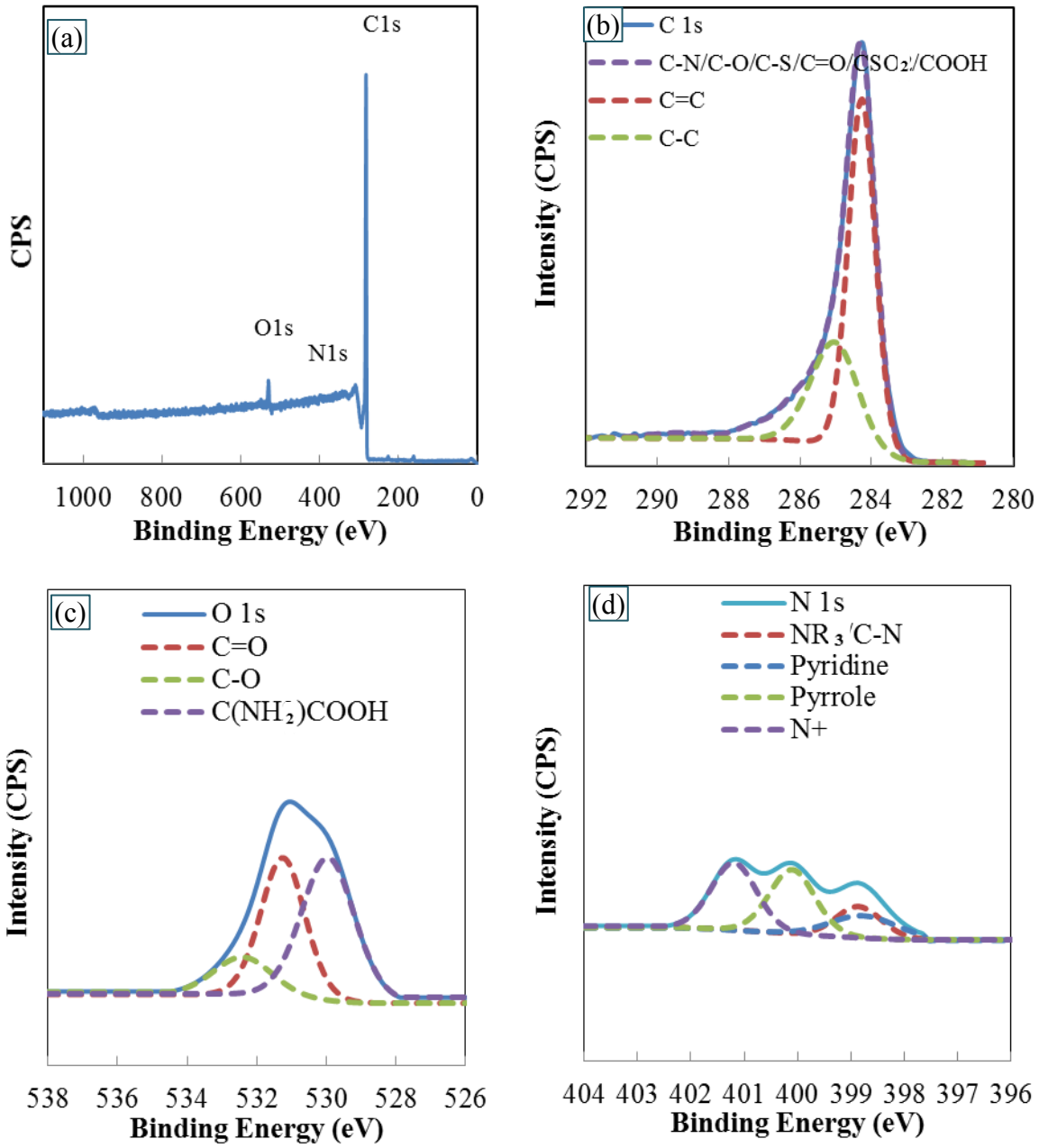

Figure.A.3.2: XPS spectra of green anode (Pitch-4) (a) Survey spectra, (b) De-convoluted C1s spectra, (c) De-convoluted O1s spectra, (d) De-convoluted N1s spectra.

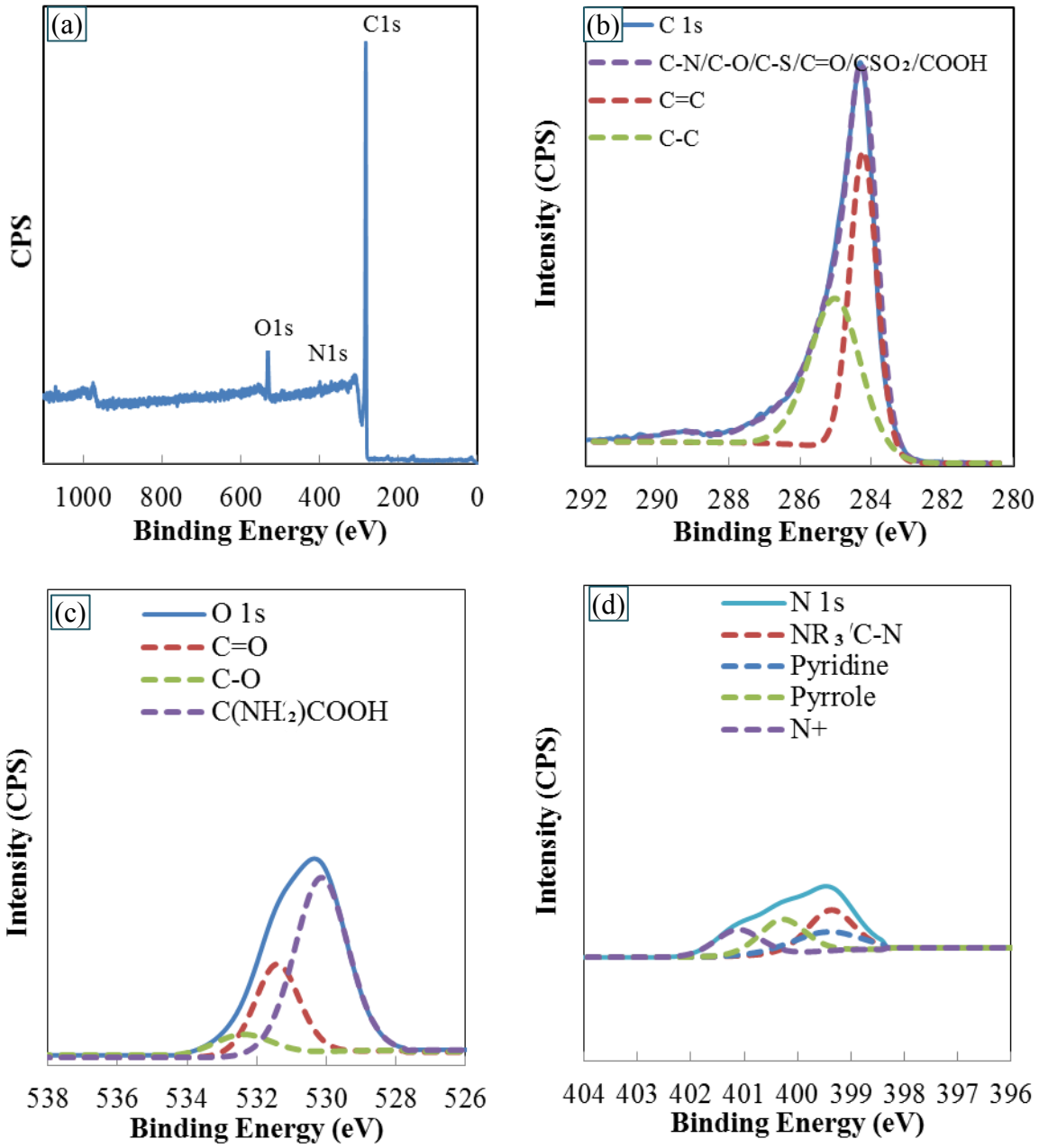

Figure.A.3.3: XPS spectra of baked anode (Pitch-2) (a) Survey spectra, (b) De-convoluted C1s spectra, (c) De-convoluted O1s spectra, (d) De-convoluted N1s spectra.

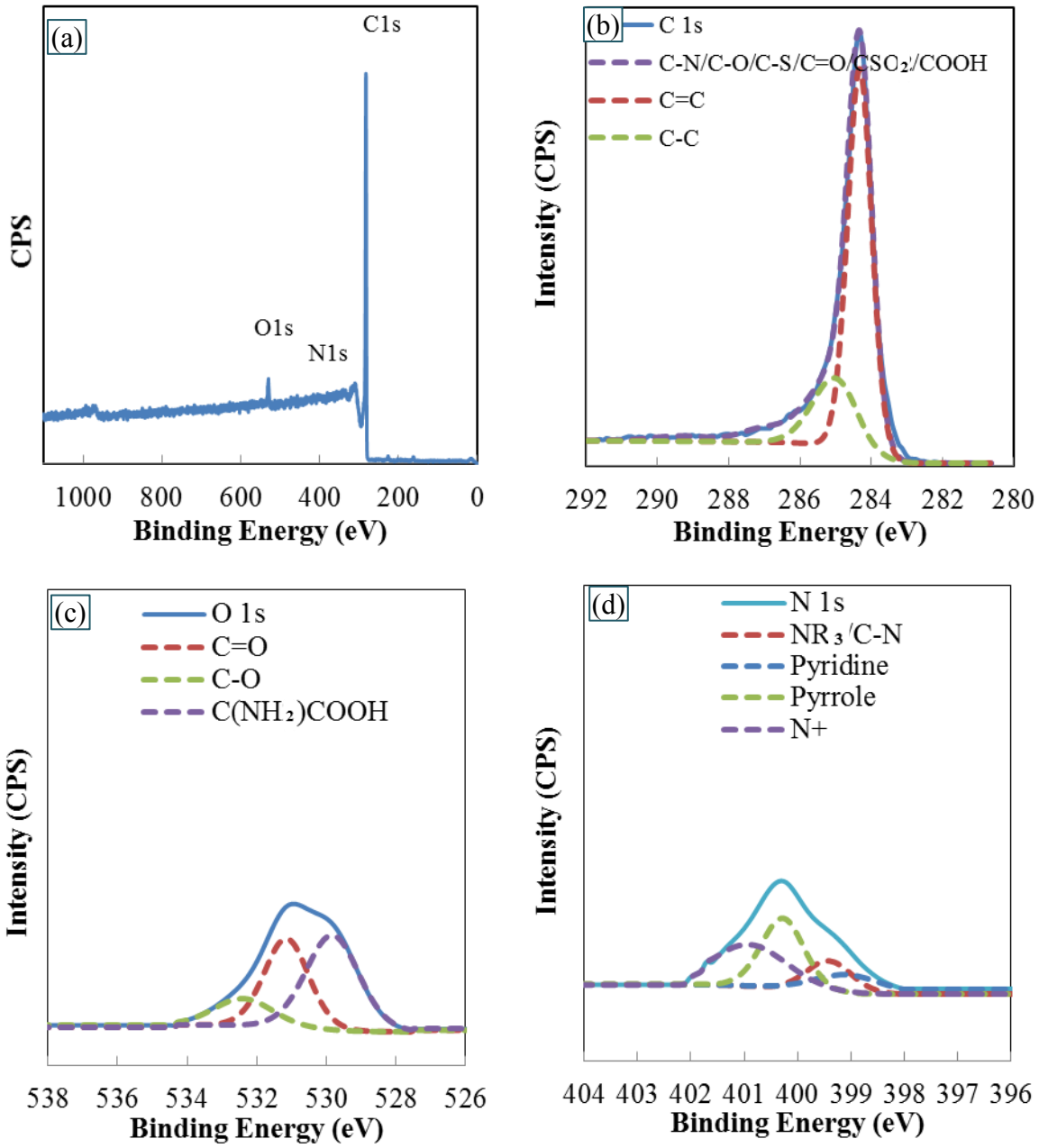

Figure.A.3.4: XPS spectra of baked anode (Pitch-4) (a) Survey spectra, (b) De-convoluted C1s spectra, (c) De-convoluted O1s spectra, (d) De-convoluted N1s spectra.

Appendix 4

Images of baked anodes samples etched under different conditions

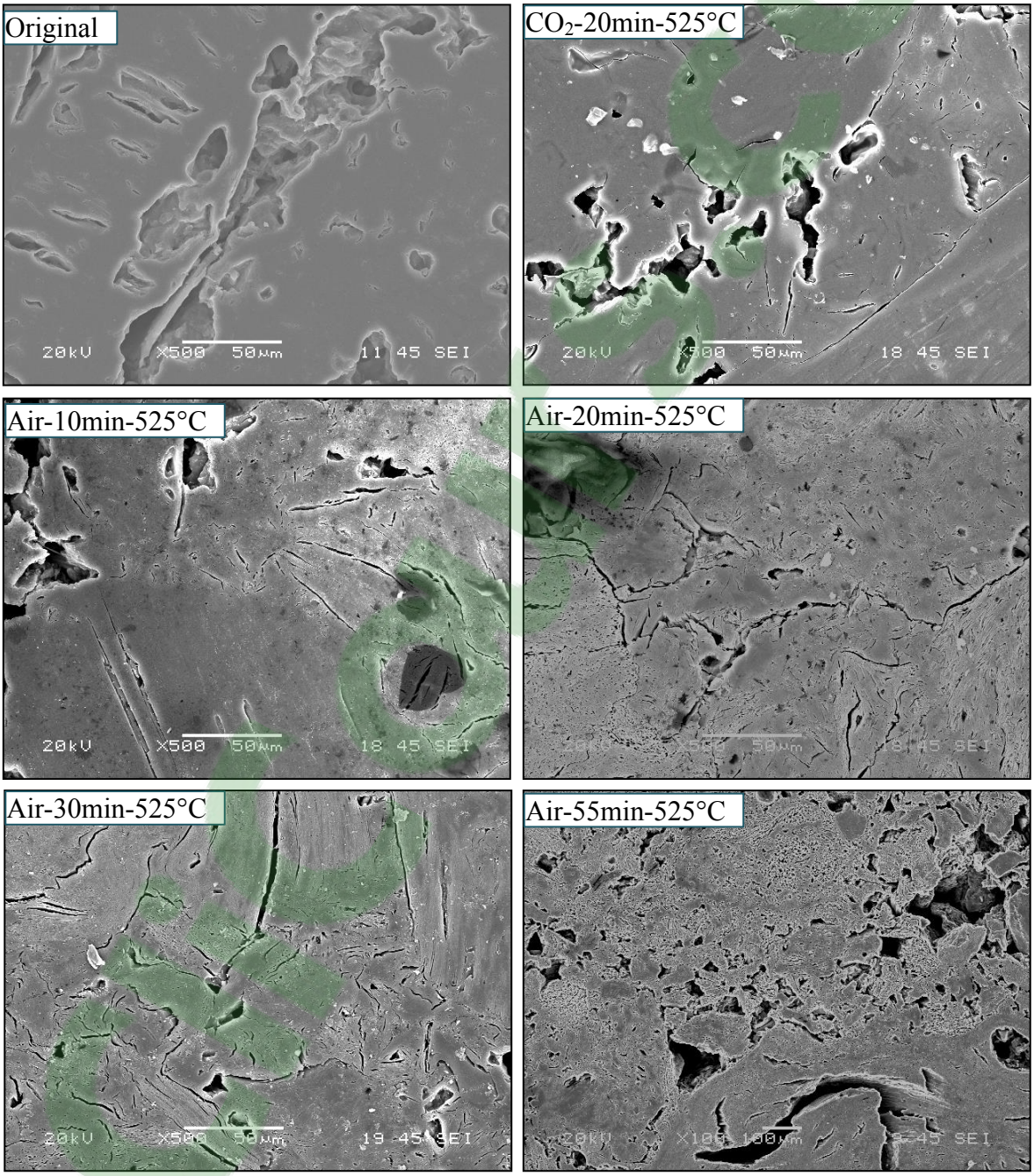

Figure.A.4.1: Images of baked anodes etched under different conditions.

Appendix 5

Kinetic results for anode samples

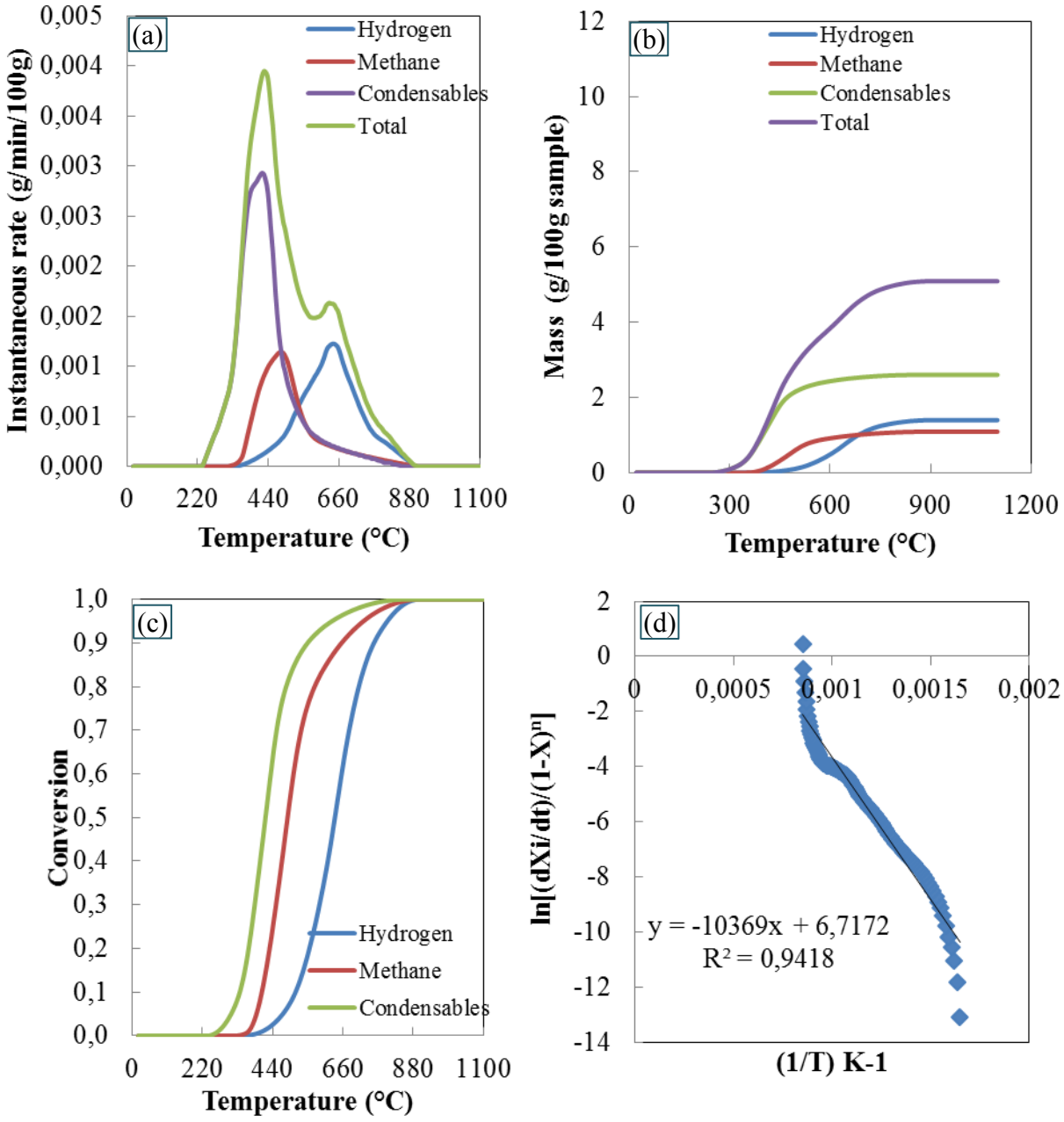

Figure.A.5.1: (a) Instantaneous rate of devolatilization, (b) Cumulative weight loss, (c) Conversions for hydrogen, methane, and condensables, and (d) Determination of kinetic parameters of hydrogen for anode with 13 % Pitch-2.

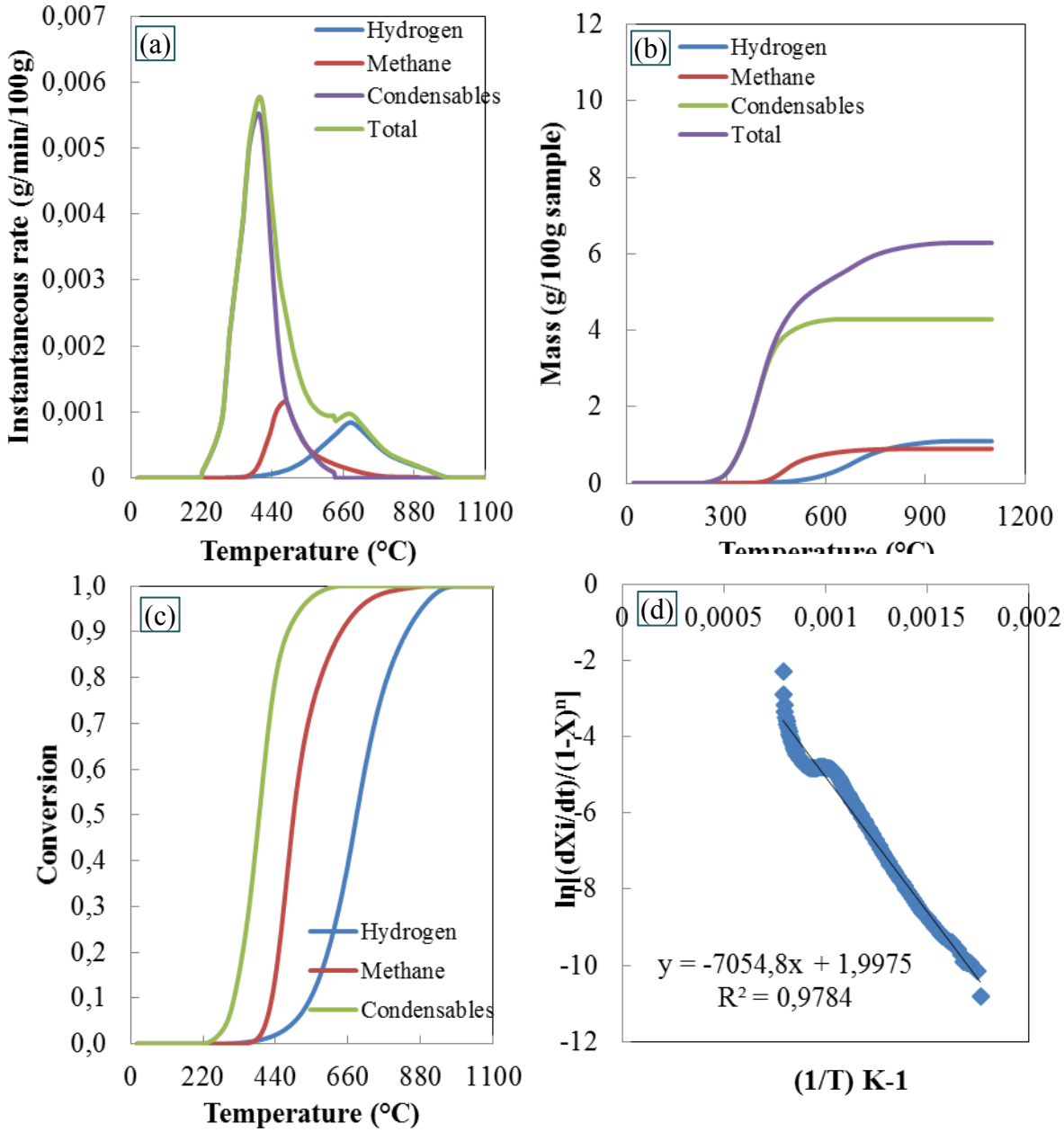

Figure.A.5.2: (a) Instantaneous rate of devolatilization , (b) Cumulative weight loss, (c) Conversions for hydrogen, methane, and condensables, and (d) Determination of kinetic parameters of hydrogen for anode with 17 % Pitch-2.

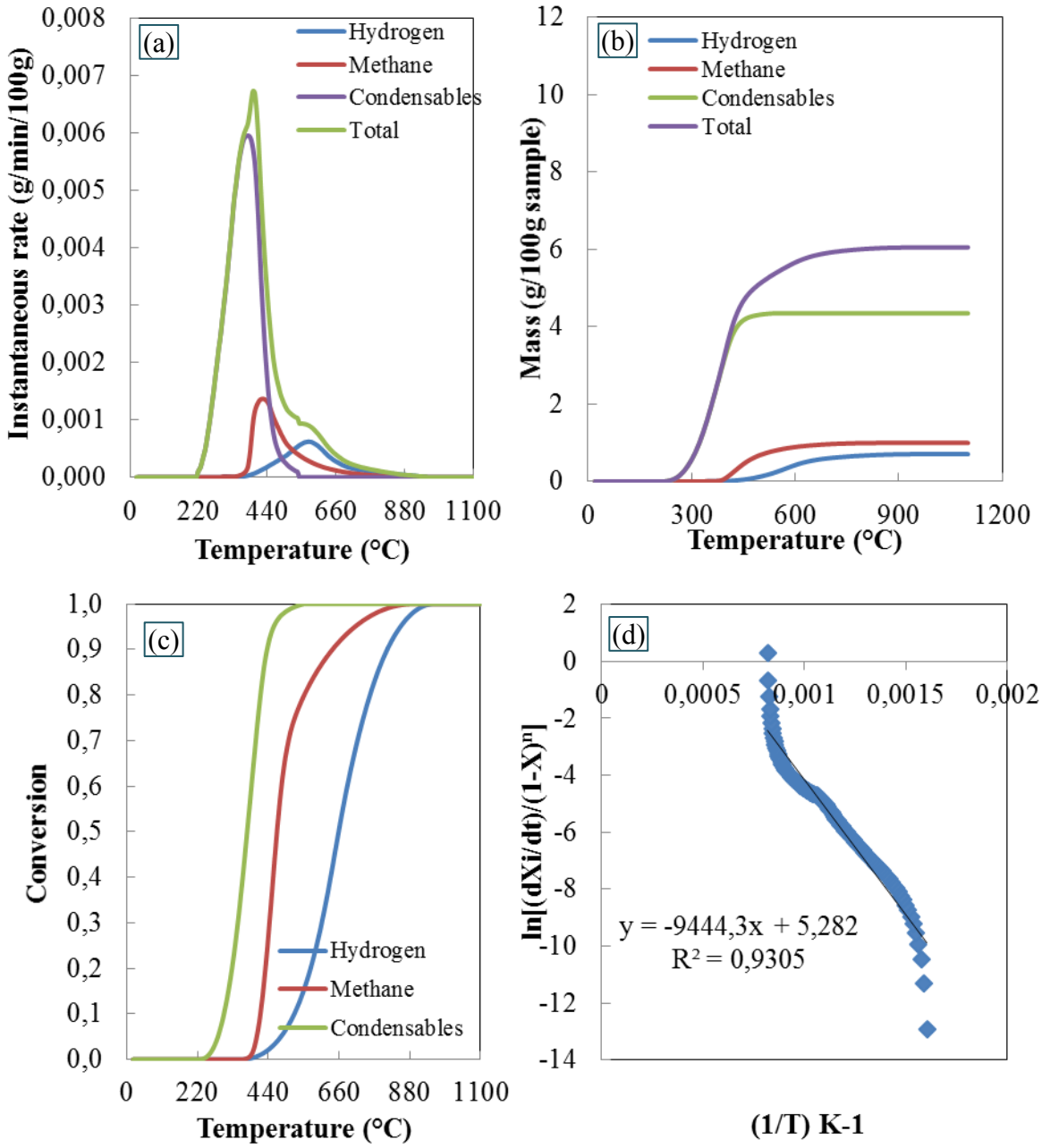

Figure.A.5.3: (a) Instantaneous rate of devolatilization, (b) Cumulative weight loss, (c) Conversions for hydrogen, methane, and condensables, and (d) Determination of kinetic parameters of hydrogen for anode with 15 % Pitch-4.

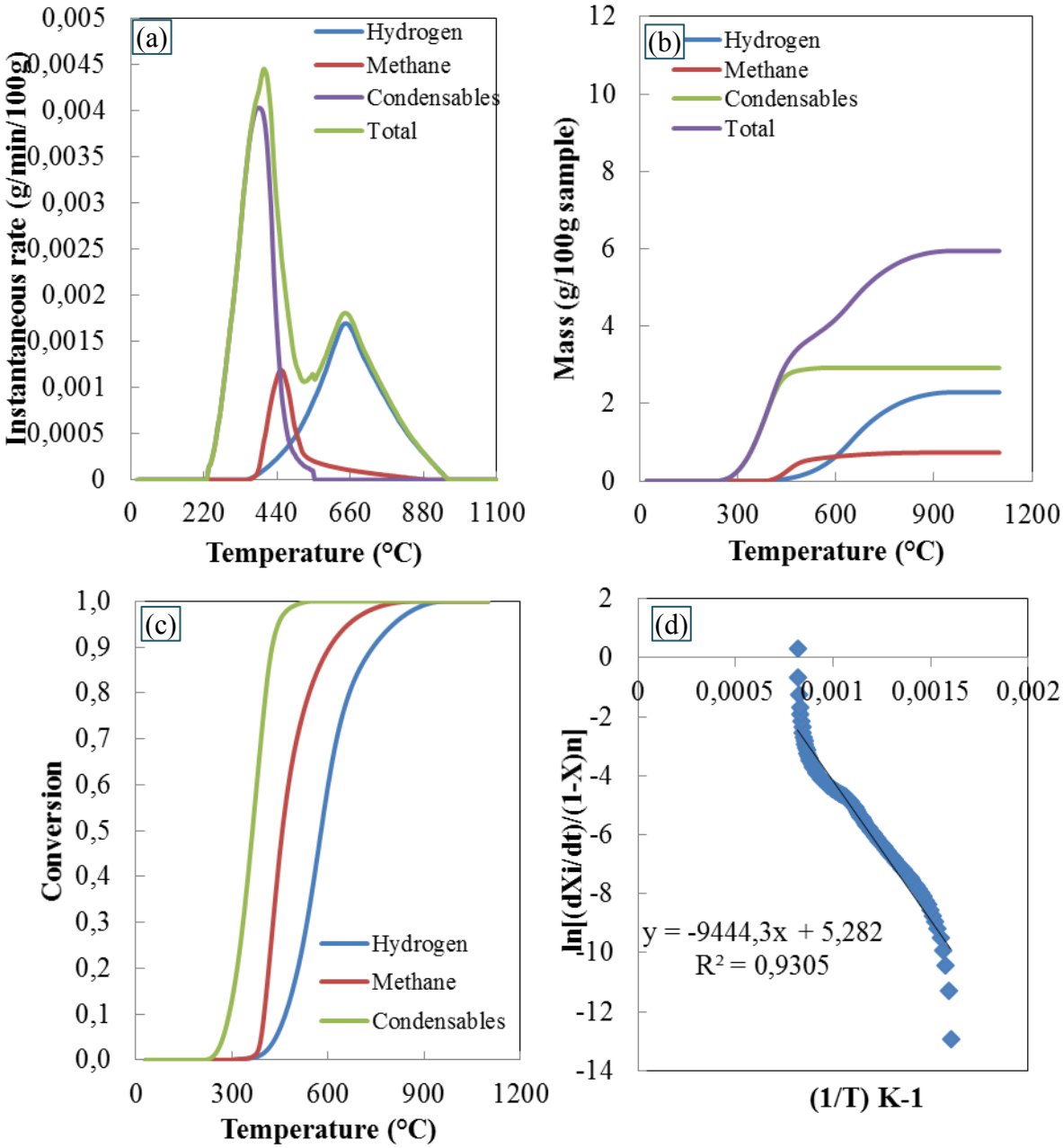

Figure.A.5.4: (a) Instantaneous rate of devolatilization, (b) Cumulative weight loss, (c) Conversions for hydrogen, methane, and condensables, and (d) Determination of kinetic parameters of hydrogen for anode with 15 % Pitch-3.

Appendix 6

Correlation between reactivities (CO_2/air) of anodes

For different baked anode samples, the rate of weight loss when in contact with air or CO_2, initial (first 30 min), final (last 30 min), and total air and CO_2 reactivities were determined.

Figure.A.6.1 (a) and (b) shows the correlation between the final reactivity and the total reactivity of anodes. It can be seen that the final reactivity is well correlated with the total reactivity. The R^2 value for the final CO_2 reactivity vs. the total CO_2 reactivity of anode was found as 0.62 and for the final air reactivity vs. the total air reactivity as 0.92. However, the total reactivity does not correlate well with the initial reactivity of anodes (Figure.A.6.1 (c) and (d)). The R^2 value for the initial CO_2 reactivity vs. the total CO_2 reactivity of anode was found as 0.22 and for the initial air reactivity vs. the initial air reactivity as 0.32.

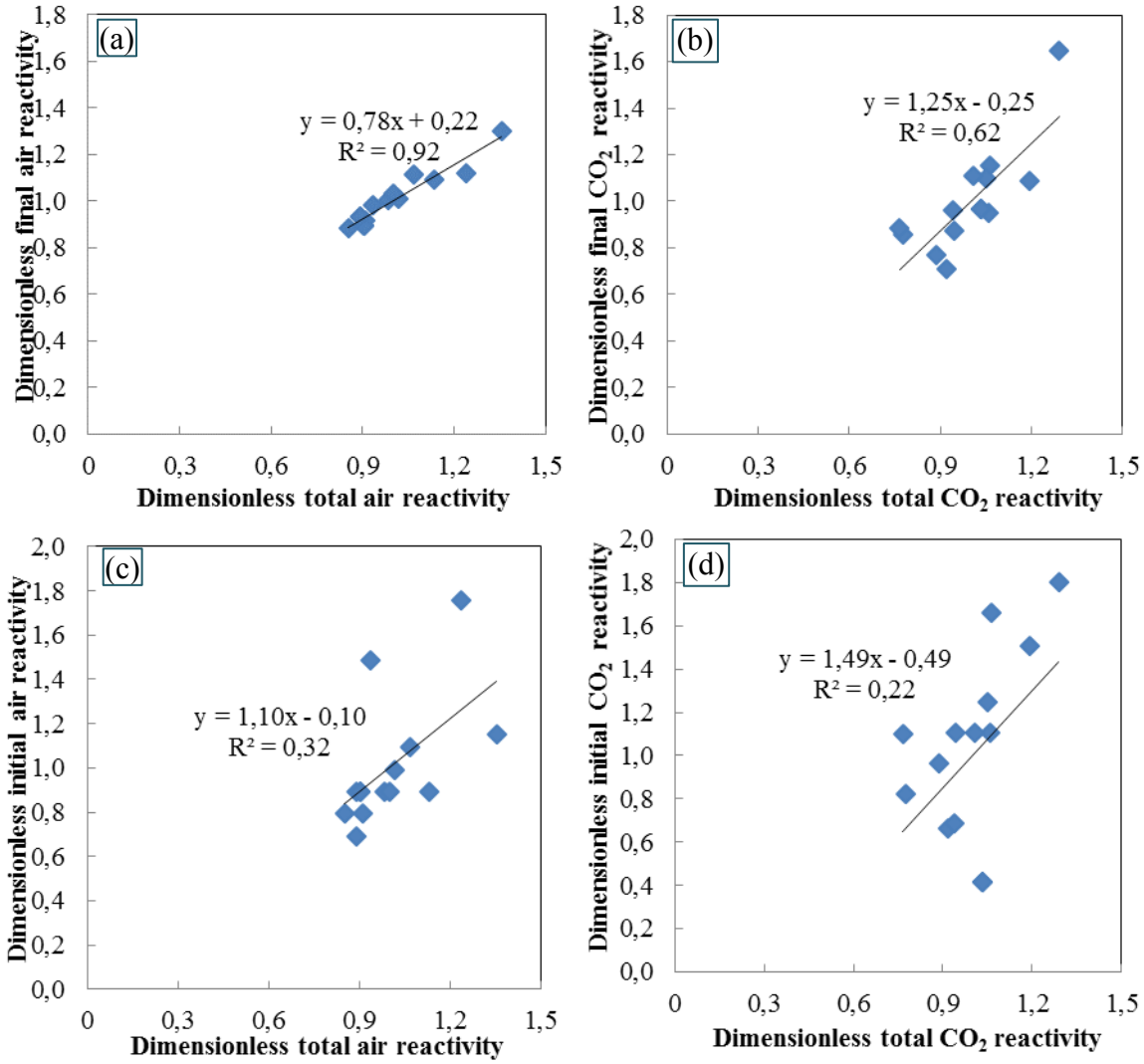

Figure.A.6.1: (a) Correlation between final air reactivity and total air reactivity of anodes, (b) Correlation between final CO_2 reactivity and initial CO_2 reactivity of anodes, (c) Correlation between initial air reactivity and total air reactivity of anodes, (d) Correlation between initial CO_2 reactivity and total CO_2 reactivity of anodes.